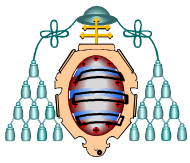

UNIVERSIDAD DE OVIEDO

PROGRAMA DOCTORADO

CIENCIAS DE LA SALUD

CARACTERIZACIÓN ELECTROFISIOLÓGICA DE LAS FIBRAS SENSORIALES DE LA CÓRNEA EN RATONES JÓVENES Y ENVEJECIDOS Y SU PAPEL EN LA SENSIBILIDAD OCULAR.

AUTOR: **Omar González González**

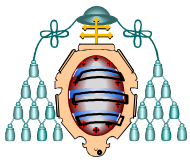

UNIVERSIDAD DE OVIEDO

PROGRAMA DOCTORADO

CIENCIAS DE LA SALUD

CARACTERIZACIÓN ELECTROFISIOLÓGICA DE LAS FIBRAS SENSORIALES DE LA CÓRNEA EN RATONES JÓVENES Y ENVEJECIDOS Y SU PAPEL EN LA SENSIBILIDAD OCULAR.

AUTOR: **Omar González González**

Universidad de Oviedo
Universidá d'Uviéu
University of Oviedo

RESUMEN DEL CONTENIDO DE TESIS DOCTORAL

1.- Título de la Tesis	
Español/Otro Idioma: "Caracterización electrofisiológica de las fibras sensoriales de la córnea en ratones jóvenes y envejecidos y su papel en la sensibilidad ocular".	Inglés: "Electrophysiological recordings of corneal sensory fibers in young and aged mice and their influence in ocular sensitivity".

2.- Autor	
Nombre: Omar González González	DNI/Pasaporte/NIE:
Programa de Doctorado: CIENCIAS DE LA SALUD	
Órgano responsable: CENTRO INTERNACIONAL DE POSTGRADO	

RESUMEN (en español)

La córnea es la superficie tisular más densamente inervada del cuerpo (600 terminaciones/mm^2). Estas terminaciones corresponden a neuronas del ganglio trigémino (GT) y están especializadas en la detección de diferentes estímulos ambientales. Se ha postulado que la expresión de diferentes canales TRP en las neuronas corneales confiere a éstas su diferente capacidad de transducción sensorial. Así, el canal TRPM8, miembro de la superfamilia de los TRP y presente, entre otros lugares, en las terminaciones nerviosas de la córnea, se considera el principal canal transductor de las neuronas termorreceptoras de frío corneales, que participan en la regulación de la lagrimación basal y el parpadeo, y están involucradas en el síndrome de ojo seco (SOS)

Mediante el registro electrofisiológico de estas terminaciones en la córnea de ratón, se han descrito en esta tesis tres tipos de terminaciones nerviosas sensoriales corneales: mecano-nociceptores, nociceptores polimodales y termorreceptores de frío. Los primeros responden únicamente a indentaciones de la córnea; los segundos lo hacen frente a estímulos nocivos de calor, estimulación mecánica o estimulación química; y los terceros pueden dividirse en dos tipos diferenciados, según su frecuencia de disparo basal y como sea su respuesta ante los descensos de temperatura, siendo clasificados como HB-LT (aquellos termorreceptores que presentaron una elevada frecuencia de disparo espontáneo y respondían ante pequeñas bajadas de temperatura) y LB-HT (con una frecuencia de disparo basal muy baja y que necesitan una bajada de temperatura de al menos 4 ºC para iniciar su respuesta).

Morfológicamente, se estudiaron expresamente las neuronas termorreceptoras de frío que expresaban TRPM8 e inervaban la córnea de ratones jóvenes de la línea TRPM8^{BAC}-EYFP. Aproximadamente, el 50 % de esas neuronas termorreceptoras de frío del GT eran intensamente fluorescentes, daban lugar a axones también intensamente fluorescentes y arrosariados, y a terminaciones nerviosas corneales complejas que posiblemente se corresponden funcionalmente con las HB-LT. El resto de los axones corneales TRPM8$^+$ fueron de débil fluorescencia, no arrosariados (lisos) y con terminales escasamente ramificadas, correspondiéndose con los termorreceptores LB-HT.

Las alteraciones funcionales y morfológicas de las neuronas somatosensoriales

periféricas que ocurren durante el envejecimiento dan lugar a una disminución de la percepción somatosensorial. En esta tesis analizamos también los cambios que tienen lugar con la edad en el GT y en los termorreceptores de frío que inervan la córnea del ratón. Así, en ratones viejos, el número de neuronas de fluorescencia débil del GT era más elevado que en los animales jóvenes, representando un 89% de las neuronas y los axones TRPM8^{+}, que también eran no ramificados y a menudo finalizaban en el epitelio basal. Funcionalmente, se la proporción de termorreceptores HB y LB aparece alterada con la vejez, con un incremento notable de los segundos y además se detectan termorreceptores de frío que presentaban características mixtas entre los dos grupos.
Estos cambios morfo-funcionales se desarrollaron en paralelo con un incremento de la tasa de lagrimación basal y de la osmolaridad de la misma, lo que sugiere que el flujo de información sensitiva anormal que viaja hacia el cerebro desde los termorreceptores de frío periféricos dañados, contribuye a la lagrimación anormal desarrollada con la edad y a la elevada incidencia del SOS en personas ancianas.

RESUMEN (en Inglés)

The cornea is the most richly innervated tissue of the body (600 terminals/mm^2). Corneal nerve terminals belong to neurons with their cell body located in the trigeminal ganglion (TG) and are specialized in the detection of environmental stimuli of different modality. It has been proposed that the expression of different TRP channels in the corneal neurons give them their capacity for sensory transduction. The TRPM8 channel, member of the TRP superfamily, that it is express, among other tissues, in the corneal nerve terminals, is the main channel involve in the transduction of the corneal cold thermoreceptors.
In mouse, three functionally distinct populations of nerve terminal were identified with electrophysiological recording of the cornea: mechano-nociceptors, polymodal nociceptors and cold thermoreceptors. Mechano-nociceptor terminals responded phasically and only to mechanical stimuli; polymodal nociceptor terminals were tonically activated by heat and chemical stimuli, responding too to mechanical stimulation; and the cold thermoreceptors can be divided in two different populations, according to the basal activity and the cooling threshold; those with high background activity and low cooling threshold were called HB-LT thermoreceptors, and those with a low background activity and high threshold were called LB-HT thermoreceptors.
The termoreceptor neurons, expressing TRPM8, of corneal young TRPM8^{BAC}-YYFP mice, were morphologically analyzed. About 50 % of the cold thermoreceptor neurons were intensely fluorescence (IF) likely providing strongly fluorescence axons and complex corneal nerve terminals with an activity and threshold corresponding to HB-LT thermoreceptors; The remaining TRPM8^{+} corneal axons were weakly fluorescence (WF) with nonbeaded axons,

sparsely ramified nerve terminals and exhibit functional characteristics corresponding to LB-HT thermoreceptors.

The functional and morphological alterations observed with aging in the somatosensory neurons gives place to a reduction of the somatosensory perception. In aged (24 months) mice the number of WF TG neurons was strikingly high while the morphology of $TRPM8^{+}$ corneal axons changed drastically; 89 % were weakly fluorescent, unbranched and often ending in the basal epithelium. Functionally, the proportion of HB and LB thermoreceptors was also altered, with a remarkable increased in the LB-HT population, some of them showing abnormal responsiveness to cooling pulses.
The morpho-functional changes develop in parallel with an enhancement of tear`s basal flow and osmolarity, suggesting that the aberrant sensory inflow to the brain from impaired peripheral cold thermoreceptors contributes to age-induced abnormal tearing and to the high incidence of DED in elderly people.

SR. PRESIDENTE DE LA COMISIÓN ACADÉMICA DEL PROGRAMA DE DOCTORADO EN CIENCIAS DE LA SALUD

Agradecimientos

Quiero empezar agradeciendo este trabajo a mis padres, sin cuyo apoyo y cariño nada de esto hubiera sido posible. También a Martín y a Ela por estar ahí ayudándome a sobrellevar los momentos de mayor estrés y trabajo.

También agradecer a mis directores de tesis: a Jesús, por depositar su confianza y apostar por mí para iniciar esta aventura en la ciencia, y a Carlos por ser una fuente inagotable de enseñanza, un ejemplo a seguir y un padre científico.

No me quiero olvidar tampoco de aquellos compañeros que siempre estuvieron a mi lado y que me ayudaron a empezar en ciencia, haciendo más fácil el camino que me ha traído hasta aquí: tanto a mis compañeros de Oviedo (Héctor, Carlos, Ana, Enol, Joana… y todos los demás que compartieron mi día a día), como los de Alicante (que hicieron la llegada a un nuevo laboratorio mucho más fácil y llevadera de lo esperado).

Por último, también agradecer a mi compañero de viaje durante estos cinco años de tesis, Federico, que compartió todos los momentos de estrés y desesperación (también hubo alguno bueno) que conlleva hacerse doctor.

Listado de Abreviaturas

ABC: avidina-biotina-peroxidasa

Ag: plata

AgCl: cloruro de plata

AITC: isotiocianato de alilo

BCTC: 4-(3-cloro-2-piridinil)-N-[4-(1,1-dimetiletil) fenil]-1piperazincarboxamida

BSA: albumina bovina fetal

Ca^{2+}: calcio

$CaCl_2$: cloruro de calcio

CGRP: péptido relacionado con el gen de la calcitonina

CMR1: receptor de mentol 1

CO_2: dióxido de carbono

DAPI: 4', 6'-diamidino-2-phenylidole

DMSO: dimetil-sulfóxido

DRG: ganglios raquídeos

EDTA: ácido etilendiaminotetraacético

EGFP: proteína fluorescente verde aumentada

GFP: proteína verde fluorescente

HB-HT: high background-high threshold

HB-LT: high background-low threshold

HB: high background

HCN: hyperpolarization-activated, cyclic-nucleotide-modulated

Ig: inmunoglobulina

Ins: coteza insular

K^+: potasio

K_{2P}: canales de potasio de dominio de dos poros

Kir: canales de potasio rectificadores

KO: knock-out

Kv: canales de potasio dependientes de voltaje

LB-HT: low background-high threshold

LB-LT: low background-low threshold

LB: low background

LH: hipotálamo lateral

$MgCl_2$: cloruro de magnesio

Na^+: sodio

NaCl: cloruro de Sodio

NaH_2PO_4: sodio di-hidrógeno fosfato

$NaHCO_3$: sodio hidrógeno carbonato

NTIs: impulsos nerviosos en terminaciones

NTS: núcleo del tracto solitarius

O_2: oxígeno

PAG: substancia gris periaqueductal

PBS: tampón fosfato salino

PO: grupo nuclear posterior del tálamo

PRK: queratectomía fotorrefractiva

TBNC: complejo nuclear trigeminal espinal

TG: ganglio trigémino

TRP: transient receptor potential

TRPA1: transient receptor potential ankyrin 1

TRPM8: transient receptor potential melastatin 8

TRPV1: transient receptor potential vailloid 1

TRPV4: transient receptor potential vailloid 4

Vi/C1: subnúcleos caudalis y alta médula espinal cervical

Vi/Vc: subnúcleos caudalis e interpolaris

Vm: potencial de membrana plasmática

VPM: núcleos talámicos ventrales posteromediales

WT: silvestre (wild type)

Índice

I. Introducción

1. Sistema nervioso somatosensorial.

1.1. Sistema Nervioso Somatosensorial Periférico.

El sistema nervioso somatosensorial es el encargado de detectar los cambios de energía que tienen lugar tanto en el medio externo como el interno, en concreto los más relevantes para la supervivencia y la reproducción. Es el responsable de la transducción sensorial, es decir, la transformación de los distintos estímulos en señales eléctricas que serán las encargadas de transmitir al cerebro la información acerca de la naturaleza, localización e intensidad de esos estímulos (Adrian, 1926). Tal información es procesada por una red compleja de neuronas sensoriales especializadas, circuitos y vías que, en su conjunto, constituyen la división somatosensorial del sistema nervioso. El sistema engloba la percepción consciente del tacto, la presión, el dolor y la temperatura, la posición de las extremidades y su movimiento así como un amplio número de respuestas motoras no conscientes. Su objetivo, junto con el sistema nervioso autónomo, es mantener el equilibrio del medio interno (homeóstasis) frente a los continuos cambios energéticos en el mundo exterior e interior (Revisión de Mountcastle, 1968).

Los receptores somatosensoriales están formados por terminaciones periféricas de neuronas sensoriales primarias (receptores primarios) o por células especializadas encargadas de la transducción de los estímulos, transmitiendo esa información a los axones periféricos de las neuronas sensoriales primarias (receptores secundarios). Los somas de estas neuronas somatosensoriales primarias están localizadas en los ganglios espinales (ganglios raquídeos) (DRG, del inglés *Dorsal Root Ganglia*) cuando reciben información del tronco y extremidades y cefálicos (trigémino y nodoso, petroso y genicular), cuando reciben información de cabeza y cuello. Las neuronas aferentes somatosensoriales de primer orden son células pseudo-monopolares, cuyo cuerpo celular, mediante un proceso único de división de su axón, da lugar a una rama periférica y a otra central. El axón periférico viaja hasta alcanzar piel, mucosas, músculos, tendones, huesos y articulaciones, y el axón central finaliza en el sistema nervioso central (Figura I.1).

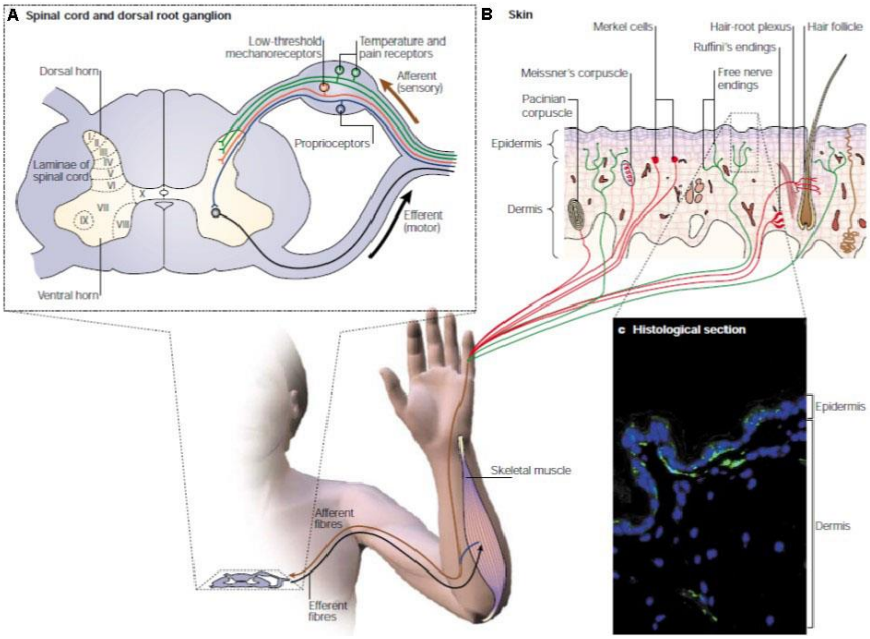

Figura I.1. ***Esquema general de la organización anatómica y funcional del sistema somatosensorial***. ***A***. *Los nervios espinales formados por la unión de raíces aferentes (sensitivas) y eferentes (motoras) proporcionan inervación periférica a la piel, músculo esquelético, vísceras y glándulas. Las flechas marcan la dirección de los impulsos sensoriales, entrantes y los motores, salientes. Los cuerpos celulares de las neuronas motoras están localizados en el asta ventral (lámina VII-IX) de la médula espinal. Los cuerpos celulares de las neuronas sensitivas que inervan el cuerpo están localizadas en los ganglios raquídeos o de la raíz dorsal (DRG) (estructura oval azulada del recuadro ampliado). Las neuronas sensitivas que inervan la cabeza están localizados en el ganglio trigémino (GT) de cada lado. En los DRG hay varios sub-tipos de neuronas sensoriales; neuronas propioceptivas (azul), mecanosensoras de bajo umbral (rojo) y neuronas sensoriales de temperatura y dolor (verde). Estas neuronas proyectan centralmente a neuronas del asta dorsal (lámina I-VI de la médula espinal) o directamente a núcleos del tronco cerebral, mientras que la otra rama del axón se ramifica en los tejidos periféricos. Las neuronas propioceptivas (fibras azules) proyectan a estructuras especializadas periféricas diana como el músculo, y son sensores del estiramiento muscular.* ***B***. *Las neuronas mecanosensoras de bajo umbral (fibras rojas) proyectan hacia órganos especializados que transmiten los estímulos mecánicos a la terminación nerviosa. Hay cinco subtipos de mecanosensores descritos, representados en la figura. Las neuronas sensitivas de temperatura y dolor (verde) no poseen órganos especializados terminales; en su lugar,*

finalizan como terminaciones nerviosas libres en la piel y mucosas, próximas a vasos sanguíneos y folículos pilosos. ***C****. Sección de la piel que muestra terminaciones nerviosas libres (verde) teñidas con el marcador de pan-neuronal PGP9.5. Los núcleos de las células de la piel se han teñido de azul con 4.6.diamino-2-phenylindole (DAPI). Tomado de* (Patapoutian *et al.*, 2003).

1.1.1. Generación del impulso nervioso en los receptores somatosensoriales.

La descripción de los procesos que llevan a la generación del potencial del receptor y del potencial de acción en los receptores somatosensoriales de mamíferos se llevó a cabo por vez primera en los corpúsculos de Pacini, un mecano-sensor fásico localizado en la dermis profunda (GRAY and SATO, 1953).

De modo general, en los receptores sensoriales las diferentes formas de energía estimulante son transducidas por moléculas específicas en una despolarización local de la membrana plasmática, que genera lo que denominamos indistintamente potencial del receptor o generador. Si el cambio de potencial es de magnitud suficiente, alcanza el umbral para la generación del potencial de acción conducido en el axón aferente. Este es el proceso general conocido como transducción sensorial (Belmonte, 1996), similar en todas las aferencias somatosensoriales.

El proceso de transducción implica un cambio conformacional en las proteínas de membrana (proteína receptora o canal iónico) que conducen directamente, o indirectamente a través de vías de señalización intracelular, a la apertura o cierre de los diferentes canales iónicos de la membrana receptora y, de este modo, al potencial del receptor (Widmaier, Raff and Strang, 2006). Con un circuito de registro apropiado, es posible medir el cambio de voltaje debido al flujo de corriente en la terminal sensorial. (GRAY and SATO, 1953). El punto de iniciación del potencial de acción no está localizado físicamente en la misma zona de la terminación donde se genera el potencial del receptor, sino que tiene lugar en una zona específica más central del axón, denominada zona de iniciación del potencial de acción. Esta región se caracteriza por una elevada expresión de canales de sodio dependientes de voltaje. Una vez la corriente generada por el potencial del receptor alcanza esta zona de iniciación, se produce el potencial de acción como una rápida respuesta eléctrica de todo o nada (GRAY and SATO, 1953). La frecuencia de disparo de potenciales de acción depende del nivel de despolarización que alcanza la terminación nerviosa y su duración. La tasa de disparo es logarítmicamente proporcional a la intensidad del estímulo. Los receptores fásicos no muestran este comportamiento debido a la rápida adaptabilidad de su potencial del receptor (Patton, 1965).

Las características de la codificación de los estímulos específicos en descargas de impulsos nerviosos en los diversos tipos funcionales de receptores sensoriales se definieron especialmente durante la segunda mitad de siglo XX [para revisión ver (Mountcastle, 1968)Mountcastle, 1968]. En los años siguientes se lograron avances significativos en la comprensión de los mecanismos moleculares implicados en la transducción de foto-receptores y quimio-receptores (Lamb, 2009; DeMaria and Ngai, 2010). Sin embargo, el conocimiento de estos procesos en los mecanorreceptores, nociceptores y termorreceptores somatosensoriales ha sido más lento (Belmonte, 1996). Esto se debe, al menos en parte, al pequeño tamaño de las terminaciones periféricas en las que tienen lugar los procesos de transducción en estos receptores, lo que ha imposibilitado el uso en las terminaciones nerviosas sensitivas, de los métodos biofísicos convencionales de registro usualmente aplicados a los somas neuronales, aunque el registro del cuerpo celular en cultivos de neuronas sensoriales ha paliado en parte este problema. Además, la identificación y el clonaje de las proteínas de los canales iónicos asociados a la transducción de distintas fuerzas por los receptores somatosensitivos, como ha ocurrido con algunos miembros de la súper-familia de canales iónicos TRP, ha proporcionado nueva información para una mejor comprensión del proceso de transducción por los receptores somatosensoriales de fuerzas mecánicas, cambios de temperatura o estímulos químicos.

A pesar de los avances logrados en años recientes, los mecanismos moleculares implicados en la transducción y la codificación de los estímulos en una descarga de impulsos nerviosos para cada modalidad de sensación son todavía conocidos de modo incompleto, en particular en el caso de las neuronas somatosensoriales primarias implicadas en la detección de estímulos térmicos, químicos y mecánicos inocuos o nocivos y que conducen finalmente a las sensaciones de temperatura y dolor.

La caracterización de las corrientes extracelulares asociadas a la activación individual de una terminación somatosensorial receptora libre en los mamíferos fue lograda por vez primera en la córnea del ojo del cobaya (Brock, McLachlan and Belmonte, 1998; Brock, Pianova and Belmonte, 2001). Mediante el registro extracelular en terminaciones receptoras polimodales, mecánicas y de frío, de la actividad espontánea o evocada por su estímulo específico, se consiguió registrar impulsos nerviosos aislados, generados en la terminación (NTIs, del inglés *Nerve Terminal Impulse*s).

2. La Córnea.

La córnea es un tejido único en el sistema visual por su transparencia, esencial para llevar a cabo su papel de permitir el paso de la luz. Esta transparencia se deriva de su particular

estructura anatómica, compuesta por células epiteliales muy ordenadas, un tejido conectivo con patrón regular y definido en el estroma, y la ausencia de vasos sanguíneos y nervios mielinizados (Saude, 1993; Nishida, 2008).

Otra característica especial de la córnea es que está cubierta por una película de lágrima que mantiene su humedad, protege al epitelio corneal transparente, facilita el intercambio de gases y lava la superficie externa, protegiéndola de la invasión de partículas, virus o bacterias (Walcott, 1998). Además de transmitir la luz, la córnea actúa de barrera entre el medio externo y la cámara anterior del ojo (Nichols, Dawson and Togni, 1983), proporcionando un campo inmunogénico para luchar contra microorganismos invasores y sustancias exógenas.

2.1. Anatomía.

Salvo pequeñas diferencias, la estructura, inervación y papel fisiológico de la córnea son comunes en los animales superiores en los que han sido estudiados (WHITEAR, 1960; Payrau *et al.*, 1967; Nichols, Dawson and Togni, 1983). La córnea está compuesta por cinco capas (de la más externa a la más interna): epitelio, membrana de Bowman (identificada solo en humanos, primates, pájaros y reptiles), estroma, membrana de Descemet y endotelio (Figura I.3). El espesor de la córnea no es homogéneo. En humanos, es de unos 0.52 mm en la parte central, mientras que la zona más próxima al limbo es de 0.67 mm, aproximadamente, Centrándonos en el ratón, el espesor medio de la córnea es de unas 100 μm, de las que unas 30 μm son el epitelio y unas 65 μm el estroma (WHITEAR, 1960).

El epitelio corneal humano se apoya en la membrana de Bowman (ausente de muchos animales, incluyendo el ratón) situada entre el estroma y el epitelio y compuesta por fibrillas de colágeno dispuestas de manera irregular, de unas 12 μm de espesor (Saraux *et al.*, 1985; Saude, 1993). El epitelio corneal está formado por 5-8 capas de células, con un espesor que ronda las 50 μm de media y se divide en tres regiones, si atendemos a la forma y la tasa metabólica de sus células (revisado por (Saude, 1993)). En general, el metabolismo de las células epiteliales es bajo y disminuye a medida que nos acercamos a capas más superficiales, donde las células se van descamando (Nichols, Dawson and Togni, 1983). Las células basales de la capa epitelial más profunda, unidas firmemente a la membrana basal subyacente por hemi-desmosomas, que la atraviesan. llegando incluso a penetrar en el estroma (Saraux *et al.*, 1985; Saude, 1993), son células columnares y tienen una tasa metabólica elevada. A través de mitosis se generan nuevas células, que irán migrando a capas más externas, cambiando gradualmente su forma. Así, por encima de las *células basales* hay tres capas de *células aladas* con una forma más aplanada; las *células escamosas* de la superficie de la córnea son poligonales planas, lo que otorga a la córnea una superficie lisa.

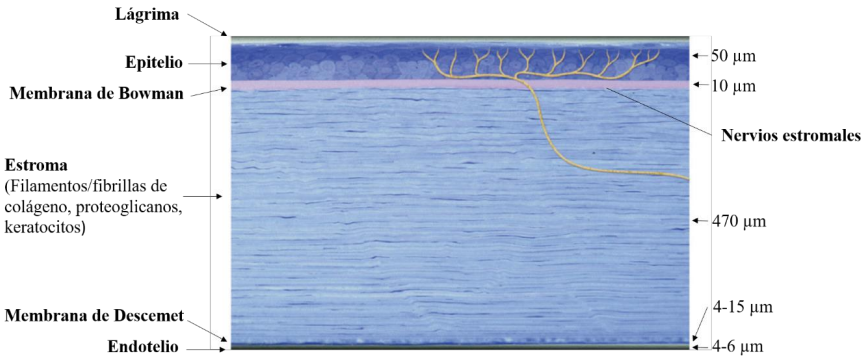

Figura I.3. ***Estructura de la córnea****. Sección histológica de córnea humana con sus cinco capas principales teñidas (Azul de toluidina). Tomada de* (Dawson, Ubels and Edelhauser, 2011) .

El estroma ocupa aproximadamente el 90 % del grosor total de la córnea (WHITEAR, 1960) (Figura I.3). Ultraestructuralmente, contiene tres elementos: láminas de fibras de colágeno regularmente orientadas, dispuesta en paralelo unas a otras formando un patrón definido; una matriz extracelular de mucopolisacáridos incrustados entre las láminas, que las mantiene unidas y keratocitos planos y finos, situados entre las fibras de colágeno. Se trata de un estructura avascular y transparente, gracias a su patrón regular (Dawson, Ubels and Edelhauser, 2011).

El endotelio es la capa más profunda de la córnea. Tiene entre 4-6 µm de espesor y está formado por células hexagonales, con su cara apical en contacto con el humor acuoso a través de estructuras ciliares y microvillis, en la que se realiza un intercambio continuo de sustancias. Y una cara basal, que contiene la membrana de Descemet, una membrana fina (entre 8-10 µm de espesor), elástica y resistente que actúa como membrana basal del endotelio corneal (Figura I.3). El contorno lateral de la células endoteliales presenta las uniones intracelulares típicas, que le proporcionan la elasticidad y resistencia que el endotelio necesita (Dawson, Ubels and Edelhauser, 2011)

2.2. Inervación sensitiva.

La inervación sensitiva de la superficie ocular, y del párpado superior e inferior, procede de los axones periféricos de las neuronas sensoriales del ganglio trigémino que inervan todos los tejidos del globo ocular, a excepción del cristalino y la retina y los anejos oculares. La córnea es el tejido más densamente inervado de todas las estructuras oculares (además de ser la superficie epitelial con mayor densidad de inervación del cuerpo humano), aunque el resto de tejidos oculares también poseen una densa inervación (Belmonte, Tervo and Gallar, 2011).

Las neuronas sensoriales que inervan la superficie ocular tienen sus cuerpos celulares en las regiones maxilar y oftálmica del ganglio trigémino (GT). Los axones de las neuronas pseudounipolares del TG se dividen, como en los DRG en una rama que proyecta hacia los tejidos diana periféricos y otra rama central que penetra en el tronco cerebral hasta alcanzar el complejo sensitivo trigeminal (Belmonte, Tervo and Gallar, 2011). La mayoría de las neuronas sensitivas oculares (alrededor de un 1.5 % del total de neuronas del GT (Marfurt, Kingsley and Echtenkamp, 1989)) inervan la córnea.

La rama oftálmica del GT se ramifica en los nervios nasociliares (Figura I.4), frontales y lagrimales. El nervio nasociliar da varias ramas que inervan el ojo y áreas adyacentes: dos nervios ciliares largos (Figura I.4), que constituyen el mayor output sensitivo del ojo; el nervio infratroclear que inerva tejidos alrededor del ojo y el saco lagrimal; el nervio nasal externo y la rama que comunica con el ganglio ciliar (Belmonte, Tervo and Gallar, 2011). El ganglio ciliar da lugar a los nervios ciliares cortos, que contienen fibras tanto sensitivas como autónomas (Figura I.4). Los nervios ciliares, largos y cortos, penetran la esclera en la parte posterior del ojo y corren hacia el segmento anterior en el espacio supracoroidal (May, 1997). Los nervios ciliares se dividen dando lugar a múltiples ramificaciones que alcanzan el limbo corneal a intervalos equidistantes alrededor de su circunferencia, donde forman el *plexo pericorneal* o *limbal* en disposición de anillo. Parte de estos troncos nerviosos que llegan por el *plexo limbal* entran en el estroma corneal, dando lugar a los nervios corneales estromales (ZANDER and WEDDELL, 1951) (Revisado en (Belmonte, Tervo and Gallar, 2011)).

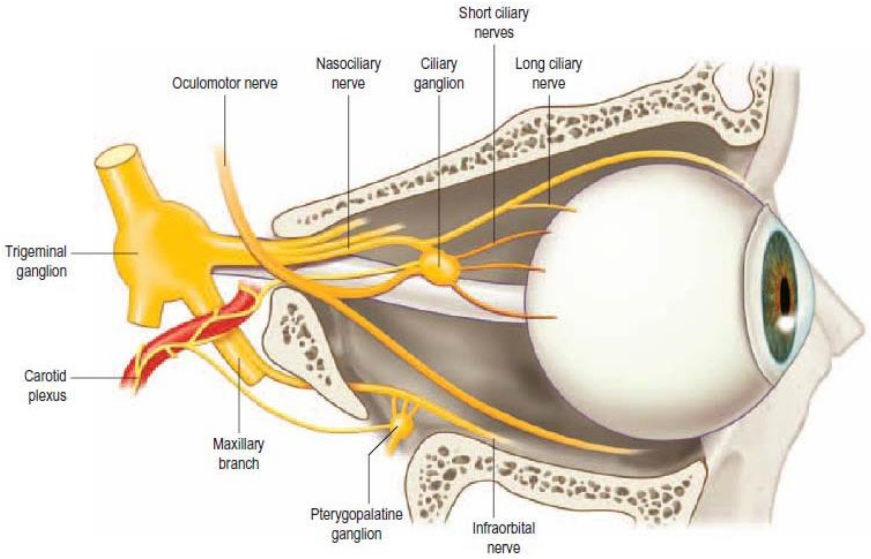

Figura I.4. ***Inervación del ojo****. Vista media de la órbita ocular, que muestra los nervios sensitivos y autónomos que inervan el ojo. La rama oftálmica del ganglio trigémino da lugar al nervio nasociliar que envía nervios ciliares largos y cortos hacia el globo ocular, éstos últimos a través del ganglio ciliar. Los nervios frontales y lagrimales no se muestran en este esquema. La rama trigeminal maxilar da lugar al nervio infraorbital que inerva parte del ojo y del párpado inferior. Las fibras simpáticas del ganglio cervical superior, que viajan en el plexo carotídeo y las ramas parasimpáticas del ganglio ciliar y del ganglio pterigopalatino, se unen a los nervios ciliares cortos. Tomado de* (Belmonte, Tervo and Gallar, 2011).

Entre el 20 y el 30 % de los axones que inervan la córnea son ligeramente mielinizados (Aδ) mientras que el resto son amielínicos (Felipe *et al.*, 1999). Sin embargo, las fibras mielinicas pierden su vaina de mielina aproximadamente 1 mm después de su entrada al estroma corneal (ZANDER and WEDDELL, 1951). Los nervios corneales poseen diversas funciones, como la transducción térmica y de los estímulos químicos o mecánicos que evocan sensaciones dolorosas; el mantenimiento de la integridad de la córnea evitando los estímulos lesivos, así como efectos tróficos sobre la córnea, que parecen estar mediados por neuropéptidos contenidos en terminaciones nerviosas periféricas (Gallar *et al.*, 1990). Estos factores tróficos contribuyen a mantener la integridad del epitelio celular, modulando la proliferación celular y la mitosis, estimulando el transporte de iones y regulando el proceso de cierre de heridas después de lesiones corneales (Marfurt, 2000).

2.2.1. Arquitectura de los axones y terminales.

Los axones sensoriales forman haces nerviosos que llegan a la córnea desde el anillo nervioso que forma el plexo nervioso limbal. Esos haces nerviosos se distribuyen uniformemente y se extienden radialmente dentro de la córnea, inervando primero la periferia y luego el conjunto del estroma. Los nervios estromales profundos proporcionan la inervación de casi toda la superficie corneal, mientras los nervios más superficiales, que entran por el estroma más cercano al epitelio, inervan principalmente la periferia (Belmonte, Tervo and Gallar, 2011)(Figura I.5).

Los nervios corneales no son estructuras estáticas. Los fascículos de fibras nerviosas del estroma profundo mantienen una posición y configuración relativamente constante en la córnea, mientras que el plexo nervioso sub-basal, y especialmente las terminaciones nerviosas intraepiteliales, están sujetas a elongaciones y reorganizaciones continuas a lo largo de la vida (Harris and Purves, 1989; Dvorscak and Marfurt, 2008; Wang *et al.*, 2012).

Anatómicamente, la inervación corneal se organiza en cuatro niveles de nervios desde las penetraciones de paquetes nerviosos estromales, procedentes del plexo nervioso limbal, hasta las terminaciones nerviosas intraepiteliales (Figura I.5).

2.2.1.1. Nervios corneales estromales.

La anatomía de los paquetes nerviosos que entran en el estroma corneal es muy similar dentro de los mamíferos, variando únicamente en su número (Müller, Pels and Vrensen, 1996). Aproximadamente un milímetro después de entrar en el estroma, los axones mielinizados de los nervios estromales pierden su capa de mielina. Poco después de penetrar en el estroma corneal, los paquetes nerviosos se ramifican y anastomosan con los fascículos nerviosos vecinos para formar el *plexo nervioso estromal* anterior, en el primer tercio del estroma (Marfurt *et al.*, 2010).

El plexo estromal es una red compleja de haces nerviosos de tamaño pequeño y medio que se cruzan, y de axones individuales situados en el 25-50 % del estroma anterior, dependiendo de la especie, siendo más denso en las capas más anteriores. Por el contrario, la mitad posterior del estroma en humanos, así como el endotelio corneal, carecen de fibras nerviosas sensitivas.

La mayoría de los axones que llegan al estroma corneal lo abandonan penetrando a través la membrana de Bowman desde el plexo subepitelial y terminando como terminaciones nerviosos no encapsulados en el epitelio corneal (Müller, Pels and Vrensen, 1996) (Figura

I.5). Sin embargo, una pequeña proporción de los axones finaliza en el estroma y algunos establecen relaciones anatómicas con los keratocitos y macrófagos estromales (Marfurt *et al.*, 2010).

2.2.1.2. Plexo nervioso subepitelial.

En humanos y mamíferos superiores, la capa más superficial del *plexo nervioso estromal* anterior, localizado justo bajo la membrana de Bowman, está densamente inervada y se conoce como *plexo nervioso subepitelial* (Figura I.5). Su densidad nerviosa es mayor en la periferia que en el centro de la córnea. Hay dos tipos diferenciados de haces nerviosos en el *plexo subepitelial*. Uno forma una malla altamente anastomosada de fascículos nerviosos axonales únicos y delgados, situados inmediatamente debajo de la membrana de Bowman, que no llegan a penetrar hacia el epitelio corneal. El segundo grupo está formado por unos 400-500 ramilletes curvilíneos de tamaño medio que penetran la membrana de Bowman, principalmente en la zona periférica e intermedia de la córnea, perdiendo la cubierta de células de Schwann, doblándose en un ángulo de 90 º y dividiéndose, cada uno en 2-20 fascículos nerviosos más finos que continúan en el epitelio corneal formando allí el *plexo nervioso sub-basal* (Belmonte, Tervo and Gallar, 2011) (Figura I.5).

En el centro de la córnea penetra un número relativamente bajo de los nervios estromales, por lo que esta región recibe una parte importante de su inervación desde nervios sub-basales largos que penetran en la periferia de la córnea directamente desde el *plexo limbal*.

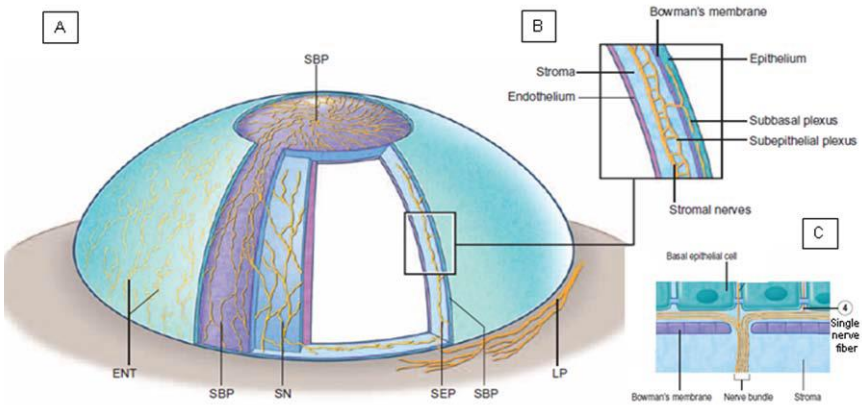

Figura I.5. ***Esquema de la distribución de los nervios en la córnea. A****. Desde el plexo limbal (LP), los troncos de nervios estromales (SN) penetran en el estroma radialmente y se dividen dicotómicamente para formar el plexo subepitelial (SEP). Las ramas de este plexo ascienden hasta el epitelio, atravesando la membrana de Bowman y formando el plexo sub-basal (SBP) entre la capa basal del epitelio y su lámina basal, donde las ramas nerviosas corren horizontalmente como familias de nervios paralelos largos (leashes), que acaban dando lugar a las terminaciones nerviosas intraepiteliales (ENT).* ***B.*** *Imagen aumentada de las capas y la inervación de la córnea intermedia, La imagen se centra en los nervios estromales y el plexo nervioso estromal, mostrando los haces que penetran la membrana de Bowman para formar los leashes del plexo nervioso sub-basal.* ***C****. Gran aumento del plexo nervioso sub-basal y las terminaciones nerviosas únicas que ascienden perpendicularmente hacia la superficie epitelial. Tomado de* (Belmonte, Tervo and Gallar, 2011).

2.2.1.3. Plexo nervioso sub-basal.

En humanos, está formado por unos 5000-7000 nervios, en un área aproximada de 90 mm^2. Un ramillete de nervios sub-basales da varias ramas laterales, cada una de ellas conteniendo de 3 a 7 axones individuales. Por todo ello, una estimación del número total de axones en el plexo sub-basal varía entre los 20.000 y los 44.000 (Müller *et al.*, 2003).

Los axones sub-basales viajan en paralelo entre las células basales del epitelio y la lámina basal durante hasta 6 mm. La estructura compuesta por un haz nervioso estromal que penetra y se ramifica en paralelo en múltiples fascículos nerviosos hijos, paralelos (denominados leashes de "correa" o "cinta" en inglés), constituye una estructura neuroanatómica única de la córnea (Figura 5). Los *leashes* epiteliales los forman hasta 40 fibras nerviosas individuales y no mielinizadas rectas o arrosariadas (*beaded*) de diámetro variable (entre 0.05 y 2.5

micras). Los axones de *leashes* adyacentes están interconectados repetidamente de manera que ya no pueden ser diferenciados individualmente, formando un plexo nervioso relativamente homogéneo (Belmonte, Tervo and Gallar, 2011).

Espacialmente, el *plexo sub-basal* agrupa sus fibras nerviosas en un patrón en espiral cuyo centro se denomina *vórtex*. En humanos, este punto está localizado unos 2-3 mm en la zona nasal inferior del centro de la córnea. Los mecanismo de formación y mantenimiento de este patrón estructural son desconocidos hasta la fecha. (Belmonte, Tervo and Gallar, 2011).

2.2.1.4. Terminaciones nerviosas intraepiteliales.

Desde los nervios sub-basales que corren horizontalmente a lo largo del epitelio basal, hay fibras individuales que se separan y giran 90 º de manera vertical dando terminaciones axónicos ascendentes, finos, cortos y arrosariados que suben entre las células epiteliales, a menudo con ramificaciones adicionales, hasta llegar a las capas más superficiales del epitelio corneal (Figura 5) (Müller *et al.*, 2003; Marfurt, 2010). Las fibras intraepiteliales finalizan como terminaciones nerviosas libres, con una expansión terminal prominente y bulbosa, de aspecto morfológicamente homogéneo al microscopio óptico o electrónico, si bien mediante tinciones inmunohistoquímicas se aprecian entre ellas diferencias en la expresión de neuropéptidos y otros neurotransmisores, sugestivas de diferencias funcionales (Müller *et al.*, 2003).

Las terminaciones epiteliales están localizadas a lo largo de todas las capas del epitelio corneal, llegando hasta unas pocas micras de la superficie, pero siendo especialmente numerosas en las capas celulares basales y aladas. En ocasiones, las terminaciones nerviosas se invaginan en la membrana de las células epiteliales, llegando a rodear completamente la terminación nerviosa (Marfurt, 2000, 2010; Müller *et al.*, 2003). Esta estrecha relación suscita la posible existencia de un intercambio bidireccional de sustancias difusibles entre ambas estructuras, además de sugerir la capacidad de las terminaciones nerviosas de detectar cambios en la forma o volumen de la célula epitelial, como los generados por la sequedad o la hinchazón.

La inervación del epitelio corneal es, probablemente, la de mayor densidad de cualquier otro epitelio superficial del organismo. Se calcula que el centro de la córnea posee, aproximadamente, entre 3500 y 7000 terminaciones nerviosas por mm^2. Esta densa inervación otorga a la córnea un sistema de detección sensitivo muy eficaz, por lo que puede aventurarse que el daño de una única célula epitelial podría ser suficiente para disparar impulsos nerviosos generadores de una percepción dolorosa consciente (Marfurt, 2000). Además, la densidad de terminaciones nerviosas es mayor en el centro que en la periferia de

la córnea. Tanto la densidad nerviosa como la sensibilidad corneal decrece progresivamente con la edad, además de con otras patologías (Belmonte, Tervo and Gallar, 2011).

Un axón estromal individual que entra por el limbo esclerocorneal experimenta ramificaciones repetidas, viajando a través de hasta tres cuartas partes de la córnea antes de finalizar. Como resultado, el rango de cobertura espacial de las fibras sensitivas individuales varía desde menos de 1 mm^2 hasta los 50 mm^2 y puede cubrir hasta el 25 % de la superficie de la córnea (Marfurt, 2010).

2.2.2. Características Morfo-funcionales de la inervación sensitiva corneal.

Gracias a los registros electrofisiológicos de las fibras nerviosas sensitivas únicas que inervan la córnea, se tiene constancia de la existencia de distintos tipos funcionales de neuronas sensitivas oculares. Estas se pueden clasificar en tres grandes grupos, atendiendo a su habilidad específica para detectar cambios en el ambiente externo: neuronas mecano-nociceptoras, nociceptoras polimodales y termorreceptoras de frío (Belmonte, 1996; Belmonte *et al.*, 2004). Hay evidencias de que los tres tipos funcionales pueden ser identificados también atendiendo a su fenotipo molecular y a su morfología (Ivanusic, Wood and Brock, 2013; Bron *et al.*, 2014; Alamri *et al.*, 2015). Esta heterogeneidad morfológica ha sido observada tanto a nivel de las terminaciones nerviosas del epitelio corneal como a nivel del soma de las neuronas sensitivas del TG.

Los estudios electrofisiológicos de las neuronas sensitivas corneales se han centrado, principalmente, en el registro extracelular de la actividad del impulso nervioso propagado en el axón periférico de neuronas del GT, bien en su trayecto en los nervios periféricos o bien en las terminaciones corneales donde se registra el llamado impulso nervioso terminal (NTI ver arriba) (Brock, McLachlan and Belmonte, 1998).

2.2.2.1. Mecano-nociceptores.

Alrededor del 15-20 % de las fibras nerviosas que inervan la córnea responden únicamente ante estímulos mecánicos próximos a intensidades nocivas. Los axones periféricos de neuronas mecano-nociceptoras de la córnea aparentemente finalizan como terminaciones simples o escasamente ramificadas localizadas en las capas celulares más elevadas del epitelio corneal (Alamri *et al.*, 2018) (Figura I.6). Todos los axones de esta clase de receptores son Aδ ligeramente mielinizados. Sus campos receptivos son redondeados y de

tamaño medio, cubriendo alrededor de un 10 % de la superficie de la córnea. La fuerza requerida para activar los mecano-nocicpetores, su umbral a la estimulación mecánica es de aproximadamente, 0.6 mN, diez veces menor que la fuerza necesaria para activar los receptores equivalentes de la piel. Esta diferencia de umbral posiblemente sea debida a la proximidad de las terminaciones a la superficie y a la falta de queratinización del epitelio corneal.

Cuando se aplica un estímulo mecánico que alcanza el umbral, los mecano-nociceptores responden con una descarga fásica de corta duración (Figura I.6). Parece que la sensibilidad mecánica de estos receptores está mediada principalmente por los canales iónicos Piezo 2 (Coste *et al.*, 2010; Fernández-Trillo *et al.*, 2020), aunque no se pueden descartar la contribución de otros canales como el TRPA1 (Gallar *et al.*, 2017). También cabe destacar que una parte de las neuronas corneales expresan el transportador vesicular de glutamato 3 (VBLUT3) también encontrado en mecanorreceptores de bajo umbral de neuronas de la piel (Huang *et al.*, 2018).

2.2.2.2. Nociceptores polimodales.

La mayoría de las fibras nerviosas sensitivas que inervan la córnea (alrededor del 70%) son nociceptores polimodales, llamados así por activarse ante una amplia variedad de estímulos, que incluyen energías mecánicas nocivas o próximas a ello, así como calor intenso e irritantes químicos, respondiendo con una descarga irregular y continua. También presentan sensibilidad frente a mediadores químicos endógenos liberados por el tejido corneal dañado y por células inflamatorias residentes o migrantes, que se filtran desde los vasos sanguíneos limbales (Belmonte and Giraldez, 1981; Belmonte *et al.*, 1991; Gallar *et al.*, 1993; MacIver and Tanelian, 1993). Los axones periféricos de neuronas polimodales nociceptoras de la córnea finalizan como terminaciones simples o escasamente ramificadas (Figura I.6).

La mayoría de estos nociceptores polimodales son fibras C no mielinizadas, mientras que una pequeña parte de ellos pueden ser fibras Aδ ligeramente mielinizadas. Su campo receptivo es redondeado u ovalado, normalmente amplio y que ocupa un cuarto o más de la superficie corneal, pudiendo extenderse hasta zonas adyacentes del limbo y de la conjuntiva bulbar (Belmonte and Giraldez, 1981). Este solapamiento de los campos receptivos adyacentes, junto con mecanismos de convergencia a nivel del sistema nervioso central, explica por qué los estímulos de la superficie corneal son tan pobremente localizados conscientemente.

Los nociceptores polimodales tienen un umbral para la estimulación mecánica ligeramente inferior al umbral de los mecano-nociceptores puros (descritos anteriormente) y generan una descarga sostenida en respuesta a una indentación mecánica prolongada (Belmonte, 1996).

Cuando se les estimula con calor, comienzan a responder a temperaturas por encima de los 37 ºC (Gallar *et al.*, 1993). Soluciones ácidas de pH entre 5.0-6.5 o chorros de aire con CO2 (que genera ácido carbónico en la superficie ocular) también activan los nociceptores polimodales (Belmonte and Giraldez, 1981; Belmonte *et al.*, 1991; Gallar *et al.*, 1993; Chen *et al.*, 1995; Acosta, Belmonte and Gallar, 2001), así como los mediadores químicos capaces de activar nociceptores polimodales de otros tejidos (capsaicina, prostaglandinas, bradikininas…) (Belmonte *et al.*, 1991; Gallar *et al.*, 1993; MacIver and Tanelian, 1993; Chen *et al.*, 1995; Chen, Belmonte and Rang, 1997; Parra *et al.*, 2014) (Figura I.6). Repetidas estimulaciones con calor lesivo o con mediadores inflamatorios (Belmonte and Giraldez, 1981; Belmonte *et al.*, 1991; Gallar *et al.*, 1993) sensibilizan los nociceptores polimodales corneales, lo que ocurre también en animales con queratoconjuntivitis alérgica (Acosta *et al.*, 2013). En córneas de gato, los nociceptores polimodales responden a veces ligeramente a estímulos de frío por debajo de los 29 ºC (Belmonte and Giraldez, 1981; Gallar *et al.*, 1993; Acosta, Belmonte and Gallar, 2001).

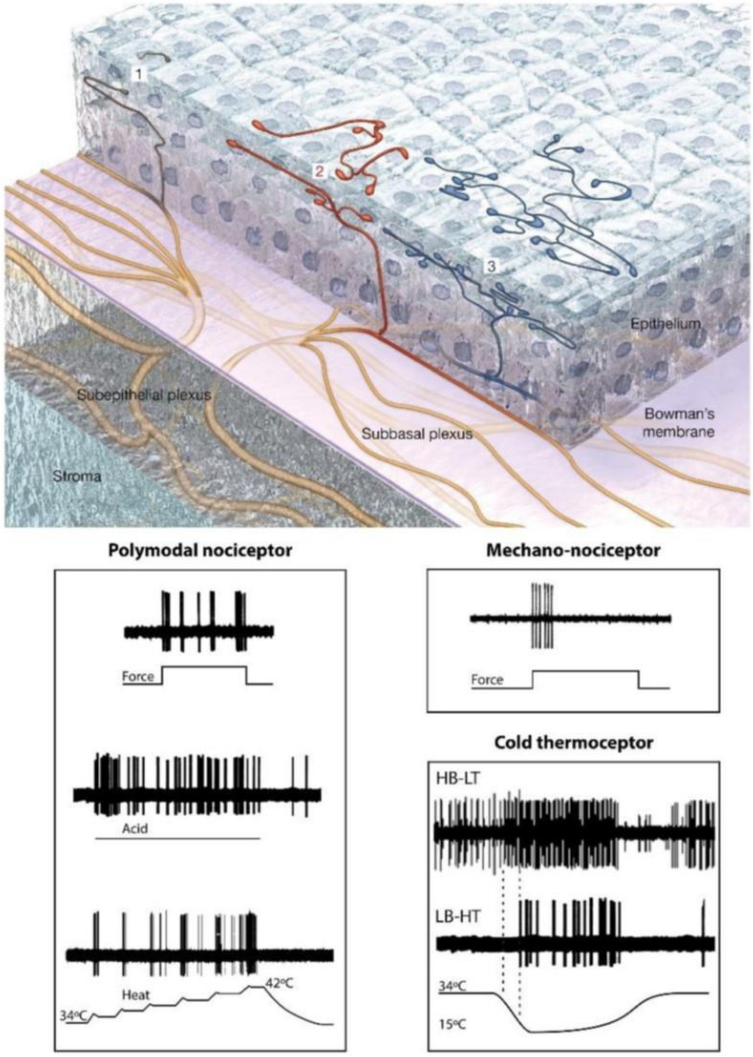

Figura I.6. ***Reconstrucción de las terminaciones superficiales en el epitelio corneal de ratón,*** *mostrando ejemplos de terminaciones simples (1, negro), ramificadas (2, rojo) y complejas (3, azul), y de las descargas de impulsos registradas en los diferentes tipos funcionales de terminaciones nerviosas, en respuesta a sus estímulos específicos (tomada de* (Belmonte *et al.*, 2017)*).*

El canal iónico más relevante para la transducción sensorial de los nociceptores polimodales es el canal catiónico de la familia de los TRP, subfamilia V, miembro 1 (TRPV1), considerado el "transductor molecular del dolor" (Julius and Basbaum, 2001), que por ello es usado como marcador molecular para este tipo celular. El canal TRPV1 se activa por capsaicina, pH bajo (~pH 6), calor nocivo (>42 ºC) e hiperosmolaridad (Caterina *et al.*, 1997; Tominaga M. *et al.*, 1998; Clapham *et al.*, 2000; Straub, 2014). La capsaicina activa los nociceptores polimodales de la córnea (Belmonte *et al.*, 1991; Chen, Belmonte and Rang, 1997; Gover, Kao and Weinreich, 2003) y su aplicación en el ojo en humanos provoca dolor (Dupuy, Thompson and Beuerman, 1988; Zollman, Bragg and Harrison, 2000). La activación del canal TRPV1 por calor, mediadores inflamatorios y protones, intensifica la excitabilidad de los nociceptores polimodales (Immke and Gavva, 2006). Además, ratones *knock out* para el canal TRPV1 mostraron respuestas alteradas frente a estos estímulos y redujeron la hipersensibilidad termal en condiciones de inflamación (Belmonte *et al.*, 1991; Chen, Belmonte and Rang, 1997; Straub, 2014). En el GT de rata y cobaya, aproximadamente un 25-45 % de las neuronas aferentes corneales expresan TRPV1 (Guo *et al.*, 1999; Murata and Masuko, 2006; Alamri *et al.*, 2015).

Otro canal transductor presente en una parte de las neuronas polimodales corneales es el TRPA1, activado por irritantes químicos exógenos, toxinas naturales, LPS bacteriano, agentes pruritogénicos, fuerzas mecánicas intensas y temperaturas frías en el rango nocivo (Cabanes, Viana and Belmonte, 2006; Brierley *et al.*, 2009; Meseguer *et al.*, 2014). El contacto de estos agonistas con la córnea produce la activación de neuronas corneales del tronco cerebral del GT, que se intensifica en modelos animales con un *síndrome del ojo seco* (SOS) experimental. No obstante, la contribución del canal TRPA1 al incremento de excitabilidad de los nociceptores polimodales en condiciones inflamatorias parece ser bastante más modesta que la del canal TRPV1 (Acosta *et al.*, 2013).

Otros canales presentes en los nociceptores polimodales son los ASICs (Callejo *et al.*, 2015), que se abren ante soluciones ácidas y mediadores endógenos como lo demuestra el que una parte de los nociceptores polimodales corneales mantienen su sensibilidad a estímulos ácidos, a pesar de tener el canal TRPV1 bloqueado con su antagonista, capsacepina (Acosta *et al.*, 2013).

Los neuropétidos que contienen algunos receptores polimodales (sustancia P y péptido relacionado con el gen de la calcitonina, CGRP) contribuyen a la respuesta inflamatoria (*inflamación neurogénica*) (Mantelli *et al.*, 2010) y estimulan el mantenimiento del epitelio corneal y la renovación fisiológica mediante la activación de vías celulares que estimulan la proliferación de células epiteliales, su migración, adhesión y diferenciación (Reid *et al.*, 1993; Garcia-Hirschfeld, Lopez-Briones and Belmonte, 1994; Tran *et al.*, 2000). Por ello, los

nociceptores polimodales peptidérgicos probablemente jueguen un papel importante en el mantenimiento de la integridad corneal.

Finalmente cabe señalar que hay evidencia de la existencia de varias subpoblaciones de nociecptores polimodales corneales con diferentes fenotipos moleculares, diferentes morfologías en su terminación nerviosa y diferente distribución en el epitelio corneal. Por ejemplo, en el epitelio corneal de cobaya las terminaciones nerviosas que expresan TRPV1 pueden dividirse en 3 poblaciones (Alamri *et al.*, 2015). Una presenta terminaciones con morfología ramificada en la capa celular escamosa, no contienen CGRP, pero sí expresan el factor neurotrófico derivado de la línea celular glial de la familia del receptor alpha3 (GFRα3). Las otras dos poblaciones finalizan en terminaciones simples, una en la capa de células aladas, que expresan tanto CGRP como GFRα3, y la otra en el plexo sub-basal expresando CGRP pero no GFRα3. Estos fenotipos moleculares se mantienen tanto a nivel de las terminaciones nerviosas epiteliales como en los somas del GT (Alamri *et al.*, 2015). Si esta heterogeneidad molecular de los nociceptores polimodales se refleja en diferencias funcionales está todavía por determinar.

2.2.2.3. Termorreceptores de frío.

Alrededor de un 10-15 % de las fibras nerviosas corneales son termorreceptores de frío (Belmonte *et al.*, 2004), localizadas superficialmente y en general profusamente ramificadas, que presentan generación de potenciales de acción espontáneos a temperaturas basales próximas a las de la superficie corneal (unos 34 ºC) e incrementan su tasa de disparo cuando esa temperatura disminuye, silenciándose de manera transitoria cuando se le aplica calor (Tanelian and Beuerman, 1984; Belmonte *et al.*, 1991; Gallar *et al.*, 1993; Brock, McLachlan and Belmonte, 1998; Carr *et al.*, 2003; Brock *et al.*, 2006), semejándose a los termorreceptores de frío canónicos encontrados en otros tejidos. Las fibras receptoras de frío corneales poseen campos receptivos pequeños, de 1 mm aproximadamente, distribuidos por toda la superficie corneal, aunque son más abundantes en la periferia (Figura I.6).

Las terminaciones termorreceptoras de frío cambian la frecuencia de disparo de su actividad basal a diferentes temperaturas estáticas, pero responden mucho más enérgicamente a los cambios dinámicos de la temperatura (Gallar *et al.*, 1993; Fern *et al.*, 2016). Tanto con estímulos de frío como de calor, la magnitud del cambio en la generación de potenciales de acción de los termorreceptores de frío depende altamente de la magnitud y velocidad del cambio de temperatura (Carr *et al.*, 2003; Brock *et al.*, 2006). Estos termorreceptores son capaces de detectar y codificar en su frecuencia de impulsos, de manera muy precisa, la intensidad de la variación en temperatura, pudiendo responder a descensos de temperatura de incluso 0.5 ºC o menos (Gallar *et al.*, 1993; Hirata and Meng, 2010; Parra *et al.*, 2010), lo

que explica la percepción de frío evocada por reducciones en la temperatura de la superficie corneal de 1-2 ºC (Acosta, Belmonte and Gallar, 2001; Parra *et al.*, 2010).

Las bajas temperaturas externas pueden evocar una amplia variedad de sensaciones, desde sensaciones frías placenteras hasta desagradables, incluido el dolor (Hensel, 1981; Morin and Bushnell, 1998; Davis and Pope, 2002). De manera general, se postula que las sensaciones de frío evocadas por temperaturas no nocivas y las dolorosas evocadas por un enfriamiento fuerte implican la activación de dos grupos de fibras diferentes: fibras de frío de alto y de bajo umbral (revisado por (Green, 2004; Reid, 2005; Dhaka *et al.*, 2007)). Se ha postulado que la diferencia entre estos dos tipos de fibras viene marcada por el distinto balance de expresión de los canales TRPM8 y Kv1, responsables de las corrientes I_{COLD} y la I_{KD}, respectivamente, con poca o nula implicación del canal TRPA1 en esta discriminación. Así, las neuronas termorreceptoras de frío de bajo umbral presentarán una mayor expresión de canales TRPM8 y una baja o nula de los canales Kv1; por el contrario, las neuronas termorreceptoras de frío de alto umbral tendrían una menor expresión de TRPM8 y mayor expresión de los canales Kv1 (Madrid *et al.*, 2009).

Aparte de los cambios en temperatura, los termorreceptores corneales de frío detectan también cambios pequeños y moderados en la osmolaridad (Gallar *et al.*, 1993; Hirata and Meng, 2010; Kurose and Meng, 2013b; Parra *et al.*, 2014; Quallo *et al.*, 2015). A temperaturas constantes, un incremento de la osmolaridad acelera la generación de potenciales de acción en estos receptores (Parra *et al.*, 2014). Este incremento de actividad evocado por un aumento de la osmolaridad se ha observado tanto si la solución hiperosmótica empleada estaba elaborada por adición de NaCl (Hirata and Meng, 2010; Hirata and Rosenblatt, 2014; Parra *et al.*, 2014) o por adicción de manitol o sacarosa (Hirata and Meng, 2010; Hirata and Oshinsky, 2012; Hirata *et al.*, 2015; Quallo *et al.*, 2015), lo que sugiere que es el cambio en la osmolaridad, más que en la carga electrostática de los iones de la solución, lo que modula la actividad nerviosa, aunque un efecto adicional generado por la alta concentración de iones de Na^+ no puede ser excluido. Por el contrario, soluciones hipo-osmóticas inhiben la actividad de los termorreceptores de frío (Quallo *et al.*, 2015). Estos efectos explican que, en condiciones basales, la osmolaridad de la lágrima representa un estímulo para los termorreceptores de frío que contribuye al mantenimiento de su actividad basal (Parra *et al.*, 2014; Olivares *et al.*, 2015).

El canal TRPM8, un canal catiónico de la familia de los TRP, subfamilia M y miembro 8, es considerado el canal más importante para la transducción del frío (McKemy, Neuhausser and Julius, 2002; Peier *et al.*, 2002; Parra *et al.*, 2010), incluido el frío doloroso (Knowlton *et al.*, 2013). El canal TRPM8 se expresa en neuronas del DRG y GT y en fibras C y Aδ de pequeño diámetro. Es un canal no selectivo de apertura por voltaje, activado por enfriamiento y por mentol, además de por los incrementos en la osmolaridad desde, aproximadamente, 200

$mOsm.L^{-1}$. Además, la sensibilidad de las células que expresan TRPM8 a los cambios en osmolaridad es muy similar a la encontrada en los termorreceptores corneales de frío en la córnea de ratón (Quallo *et al.*, 2015).

En ratones k*nock out* para el canal TRPM8, no han sido detectados termorreceptores de frío corneales con la actividad característica de los termorreceptores de frío canónicos (Parra *et al.*, 2010). Más aún, el bloqueo del canal TRPM8 mediante su antagonista, BCTC (N-(4-tertiarybutylphenyl)-4-(3-chloropyridin-2-yl) tetrahydropy-razine-1(2H)-carbox-amide) reduce de manera significativa (incluso silencia) la actividad basal de los termorreceptores de frío, inhibiendo también sus respuestas ante el enfriamiento (Parra *et al.*, 2010). Todo ello indica que los canales TRPM8 son los transductores del frío y la osmolaridad en los termorreceptores corneales de frío, y también los responsables de la corriente despolarizante (I_{COLD}) que determina su actividad nerviosa basal.

Aproximadamente un 6 % de la población de neuronas aferentes corneales que expresan TRPV1 también co-expresan el canal TRPM8, (Alamri *et al.*, 2015). La co-expresión de estos dos canales puede ser la responsable de las respuestas paradójicas a calor observadas en una porción de las neuronas termorreceptoras de frío (Hirata, Fried and Oshinsky, 2012).

Los canales de potasio "de fuga" se cierran por el frío, tendiendo a despolarizar inespecíficamente a las neuronas. La corriente I_{KD} es una corriente de potasio que actúa en general como un freno contra esa despolarización inespecífica de las neuronas sensoriales por los descensos de temperatura. En las neuronas termorreceptoras de frío la densidad de la corriente I_{KD} ayuda a definir los umbrales de los termorreceptores de frío siendo muy pequeña en los termorreceptores de frío con gran sensibilidad (Viana, De la Peña and Belmonte, 2002; Madrid *et al.*, 2009).

Efectivamente, se ha observado una correlación negativa general entre la I_{KD} y la sensibilidad al frío de las neuronas del GT (Viana, De la Peña and Belmonte, 2002). Algunas de las neuronas trigeminales insensibles al frío se volvieron sensibles al aplicarles el bloqueante de canales de potasio 4-AP (4-aminopiridina). Los canales de potasio Kv1.1 y Kv1.2 han sido identificados como los responsables de la corriente I_{KD} (Madrid *et al.*, 2009). Así pues, la sensibilidad final de los termorreceptores de frío depende de la densidad de canales TRPM8, responsables de la I_{COLD} despolarizante y de la expresión de los canales de potasio encargados de la corriente I_{KD} que tiende a reducir la sensibilidad al frío.

En las neuronas termorreceptoras de frío se ha señalado también la presencia de canales activados por hiperpolarización y nucleótidos cíclicos (HCN) (Patricio Orio *et al.*, 2012), responsables de la corriente activada por hiperpolarización I_h, un importante modulador de la frecuencia de disparo del potencial de acción en muchas células excitables (Momin *et al.*, 2008). Se han descrito varios bloqueantes orgánicos para la corriente I_h, como el ZD-7288 (Gasparini and DiFrancesco, 1997), o el S-16527 (Ivabradina) (Bois *et al.*, 1996), aunque no

son totalmente específicos, pudiendo alterar la transmisión sináptica independientemente del bloqueo de la I_h.

También se han encontrado los canales de potasio K_{2p} (TREK-1 y TRAAK), cuya apertura está regulada por la estimulación mecánica y térmica (Maingret *et al.*, 1999, 2000; Kang, Choe and Kim, 2005). Pertenecen a la familia de canales de dominio de dos poros (K_{2p}).

2.2.2.4. *Nociceptores Silentes*.

La presencia en la córnea de fibras nociceptoras que, en condiciones fisiológicas, permanecen inactivas pero que cuando el tejido sufre un proceso de inflamación se vuelven excitables ante estímulos mecánicos, químicos o térmicos (los conocidos como *nociceptores silentes*) fue sugerida por MacIver & Tanelian [(MacIver and Tanelian, 1993) Aunque no hay evidencias directas de su presencia en la córnea, los nociceptores silentes han sido descritos en muchos tejidos somáticos, sobre todo en humanos, donde parecen jugar un papel importante en el dolor inflamatorio (Schaible and Schmidt, 1983; Tanelian and Beuerman, 1984; Belmonte *et al.*, 2004).

2.2.3. Vías centrales.

Las neuronas del GT que proveen la inervación de la superficie ocular y los tejidos circundantes, envían ramas centrales que finalizan en diversos niveles rostrocaudales del complejo trigeminal del tronco cerebral (TBNC) (Marfurt, 1981; Marfurt and Del Toro, 1987; Marfurt and Echtenkamp, 1988; Panneton, Hsu and Gan, 2010). El TBNC está compuesto por el núcleo trigeminal principal (Vp) en la protuberancia (pons) y el núcleo trigeminal en el bulbo que está subdividido en el *subnucleus oralis* (Vo), *interpolaris* (Vi) y *caudalis* (Vc), y las neuronas del asta posterior en el nivel C1 de la médula espinal alta.

.Las neuronas de segundo orden que responden ante estímulos de la superficie ocular se encuentran en diversos niveles del TBNC, una organización única del sistema trigeminal (Bereiter, Hirata and Hu, 2000). La mayoría de las neuronas del GT que responden ante estímulos de la superficie corneal finalizan en dos regiones del TBNC bajo: la región de transición entre el Vi y el Vc (transición Vi/Vc) y en la unión del Vc/medula espinal cervical (región Vc/C1). Por otro lado, una pequeña porción de estas fibras aferentes finalizan en Vp y Vo (Marfurt and Echtenkamp, 1988; Panneton, Hsu and Gan, 2010). Las neuronas trigeminales que inervan los párpados (May and Porter, 1998; Gong, Zhou and LeDoux, 2003), glándula lagrimal (Simons and Smith, 1994; Baljet and VanderWerf, 2005) y las glándulas de Meibonio (Panneton and Burton, 1981; Kirch, Horneber and Tamm, 1996) muestran un patrón terminal semejante en el TBNC. El hecho de que el ojo esté representado

en diversas regiones del TBNC puede reflejar una redundancia para preservar las funciones del ojo, o que las distintas áreas son responsables de diferentes funciones oculares (Bereiter, Hirata and Hu, 2000). La evidencia actual sugiere que este último es el caso de las neuronas de la región de transición Vi/Vc y de la región Vc/C1

2.2.3.1. Neuronas oculares de la transición Vi/Vc.

Las neuronas oculares registradas en la transición Vi/Vc codifican la intensidad de estimulaciones químicas, térmicas y mecánicas de la superficie ocular (Meng *et al.*, 1997; Hirata, Hu and Bereiter, 1999; Kurose and Meng, 2013a). Las neuronas de esta región se excitan con luz intensa (Okamoto *et al.*, 2010) y también son sensibles al status de humedad de la superficie corneal, característica no encontrada en ninguna otra región del TBNC (Hirata and Rosenblatt, 2014). El campo receptivo para la mayoría de las neuronas de la transición Vi/Vc incluye el total de la superficie ocular. Muchas de las neuronas de esta región también responden a estimulaciones inocuas y nocivas de la piel preorbital, aunque cerca del 50 % de las neuronas de la transición Vi/Vc responden solo ante estimulación de la superficie ocular (Pozo and Cervero, 1993; Meng *et al.*, 1997). Tanto las fibras nerviosas corneales Aδ poco mielinizadas como las fibras C no mielinizadas finalizan en la región de transición Vi/Vc. Estimulaciones repetitivas de la superficie ocular causan, a menudo, una desensibilización o fatiga en las neuronas de la transición Vi/Vc, mientras que la administración sistémica de morfina potencia las respuestas evocadas de la córnea en cerca del 30 % de las neuronas registradas, una característica que puede contribuir al picor ocular inducido por la analgesia opioide (Meng, Hu and Bereiter, 1998).

Las neuronas de la transición Vi/Vc proyectan hacia las regiones cerebrales encargadas del control de la lagrimación (*nucleo salivar superior*) y el parpadeo (*nucleo motor del facial*), y también al tálamo sensorial (Pellegrini, Horn and Evinger, 1995; Hirata *et al.*, 2000) (Figura I.7). El bloqueo de la actividad sináptica de las neuronas de la transición Vi/Vc evita la lagrimación refleja evocada por luz intensa (Okamoto *et al.*, 2012) y reduce el parpadeo evocado por aplicación tópica de solución salina hiperosmótica (Rahman *et al.*, 2014). En conjunto, las neuronas de la transición Vi/Vc parecen jugar un papel relevante en el mantenimiento de la homeóstasis ocular y no tanto en los aspectos derivados del dolor ocular.

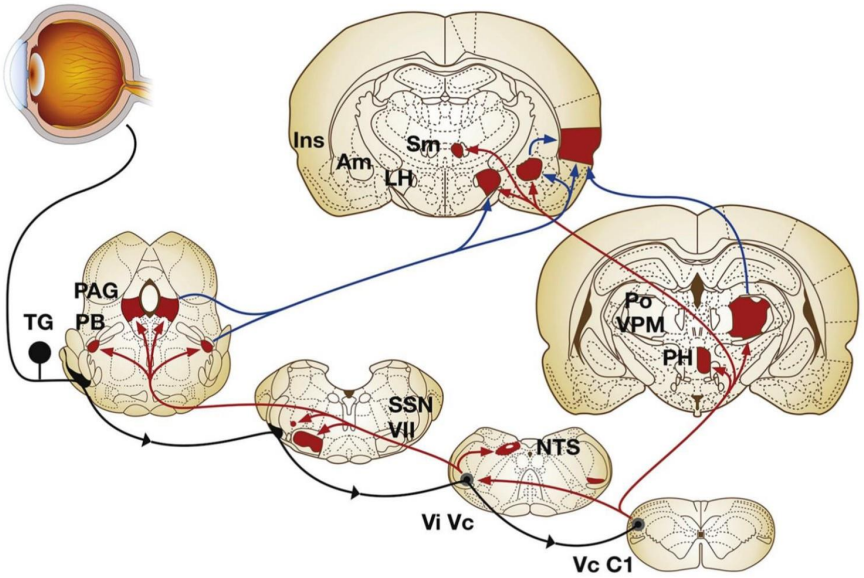

Figura I.7. ***Principales vías ascendentes cerebrales de las fibras sensitivas trigeminales que inervan el ojo****. Los somas celulares de las fibras sensitivas se encuentran en el ganglio trigémino y proyectan centralmente hacia dos regiones concretas del complejo del tronco cerebral, la zona de transición entre el subnucleo interpolaris y caudalis (Vi/Vc) y la región de transición entre el subnucleus caudalis espinotrigeminal y la médula espinal (Vc/C1). Las neuronas de segundo orden en Vi/Vc y Vc/C1 proyectan a regiones cerebrales que median el parpadeo (facial motor nucleus, VII), lagrimación (Superior salivatory nucleus, SSN), y reflejos cardiovasculares (nucleus tractus solitarius, NTS). Proyecciones hacia centros mayores como el periaqueductal grey (PAG), PBA (PB), hipotálamo lateral (LH), hipotálamo posterior (PH), y amígdala (Am) contribuyen a los aspectos afectivo y modulador del dolor ocular, mientras que proyecciones al tálamo posterior (grupo posterior nuclear, Po; núcleo ventral posteromedial, VPM) y córtex insular (Ins) median los aspectos sensitivos discriminativos. Nótese que un pequeño grupo de neuronas de respuesta ocular también se encuentran en el Vi/Vc contralateral; la fuente de entrada a este grupo no está bien definida. Las fibras aferentes primarias están dibujadas en negro; las proyecciones de segundo orden en rojo; y las de tercer orden en azul. (Tomado de* (Belmonte *et al.*, 2017)*). (Para la interpretación de las referencias al color en la leyenda de esta figura, remitimos al lector a la versión web del artículo).*

2.2.3.2. Neuronas oculares de la región Vc/C1.

Las neuronas oculares de la región Vc/C1 codifican la intensidad de la estimulación mecánica y térmica la superficie ocular, con umbrales similares a los encontrados en las neuronas de Vi/Vc (Meng *et al.*, 1997; Hirata, Hu and Bereiter, 1999), respondiendo también a varios tipos de substancias químicas irritantes (Carstens, Kuenzler and Handwerker, 1998; Bereiter *et al.*, 2005). Sin embargo, existen diferencias significativas entre las neuronas oculares de estas dos regiones. Al contrario de lo que sucedía con las neuronas de la transición Vi/Vc, las neuronas de la región Vc/C1 incluyen solo una parte de la superficie ocular, y todas las neuronas se activan con la estimulación nociva de la piel periorbital (Meng *et al.*, 1997; Hirata, Hu and Bereiter, 1999). Muchas de las neuronas de la región Vc/C1 reciben información convergente desde la córnea y desde la dura, indicando un papel en el dolor de cabeza (Ebersberger *et al.*, 1997; Schepelmann *et al.*, 1999). La estimulación repetitiva de la superficie ocular sensibiliza las neuronas de la región Vc/C1, mientras que la administración de morfina sistémica inhibe su actividad de manera dosis-dependiente (Meng, Hu and Bereiter, 1998). Mientras que las neuronas oculares de la región Vc/C1 son activadas por luz brillante, el bloqueo sináptico de esta región no altera la lagrimación evocada por luz brillante (Okamoto *et al.*, 2010). Las proyecciones eferentes de las neuronas oculares de la región Vc/C1 incluyen el *núcleo motor del facial, el núcleo parabraquial pontino*, el tálamo sensorial y el hipotálamo (Meng *et al.*, 1997; Meng, Hu and Bereiter, 1998; Hirata *et al.*, 2000; Malick, Strassman and Burstein, 2000) (Figura I.7). El bloqueo sináptico de la región Vc/C1 genera una reducción transitoria del parpadeo evocado por luz y las soluciones hipertónicas (Rahman *et al.*, 2014). Todo esto indica que las neuronas oculares de la región Vc/C1 presentan un comportamiento similar al de las neuronas nociceptoras del asta posterior de la médula espinal, probablemente jugando un papel clave en aspectos discriminativos de la sensibilidad del dolor ocular.

Algunas lesiones de la protuberancia lateral y la médula observadas en pacientes tras un infarto, se acompañan de sensaciones paroxísticas (sensaciones de "sal y pimienta") en el ojo, que cuadran con el papel adscrito a la región Vp/Vo en las sensaciones oculares (Chen *et al.*, 2012). También se han descrito neuronas de las regiones Vp y Vo que responden a estimulación periocular (Greenwood and Sessle, 1976; Davis and Dostrovsky, 1988). Sin embargo la el papel de estas regiones en las funciones oculares humanas se desconoce todavía en gran medida.

Las regiones caudal y rostral del TBNC están conectadas a través de un denso sistema de fibras longitudinales (Warren and May, 2013). Se ha propuesto que tales vías intersubnucleares tienen una función de retroalimentación en situaciones como el dolor dental agudo (Chiang *et al.*, 2002), las migrañas (Davis and Dostrovsky, 1988) o el parpadeo evocado (Henriquez and Evinger, 2007).

3. Lagrimación.

En animales terrestres vertebrados la superficie anterior del ojo está cubierta por una película líquida, la película lagrimal, que mantiene húmeda la córnea y permite el intercambio de gases entre el aire y el epitelio. También limpia de detritus la superficie corneal y protege de la invasión por virus o bacterias, además de proporcionar metabolitos esenciales, factores de crecimiento y enzimas. Así pues, la película lagrimal es esencial para el mantenimiento de la salud y transparencia de la córnea (Dartt, 2011).

La película lagrimal es una mezcla compleja de secreciones de varios tejidos. Está formada por cuatro capas: la más interna es un glicocálix que recubre la superficie del epitelio corneal; la segunda es una capa mucosa sobre el gliocálix; la tercera es una capa acuosa y la última la capa lipídica (Holly and Lemp, 1977; Dartt, 2011) (Figura I.8).

la secreción de los componentes de las capas acuosa y mucosa está regulada por reflejos nerviosos. Los nervios sensoriales en la córnea y en la conjuntiva se activan mediante estímulos mecánicos, térmicos o químicos, que a su vez activan nervios aferentes simpáticos y parasimpáticos que inervan la glándula lagrimal y las células caliciformes conjuntivales, generando la secreción de mucosa y fluido. En el caso de la capa lipídica, el parpadeo regula la liberación por los conductos de las glándulas de Meibomio de lípidos pre-secretados. La secreción lagrimal está balanceada entre el drenaje y la evaporación (Dartt, 2011).

3.1. Composición y secreción de la lágrima.

La osmolaridad de la lágrima es de unos 300 mOsm, semejante a la del plasma pero con concentraciones de iones diferentes: la lágrima posee menor concentración de sodio y mayor concentración de potasio y sobre todo, de cloro. Esta diferencia es relevante debido a que las células acinares de la glándula lagrimal controlan la secreción de agua a través de su potencial de su membrana, por lo que pequeños cambios en la concentración de iones modifica la secreción de agua (Walcott, 1998).

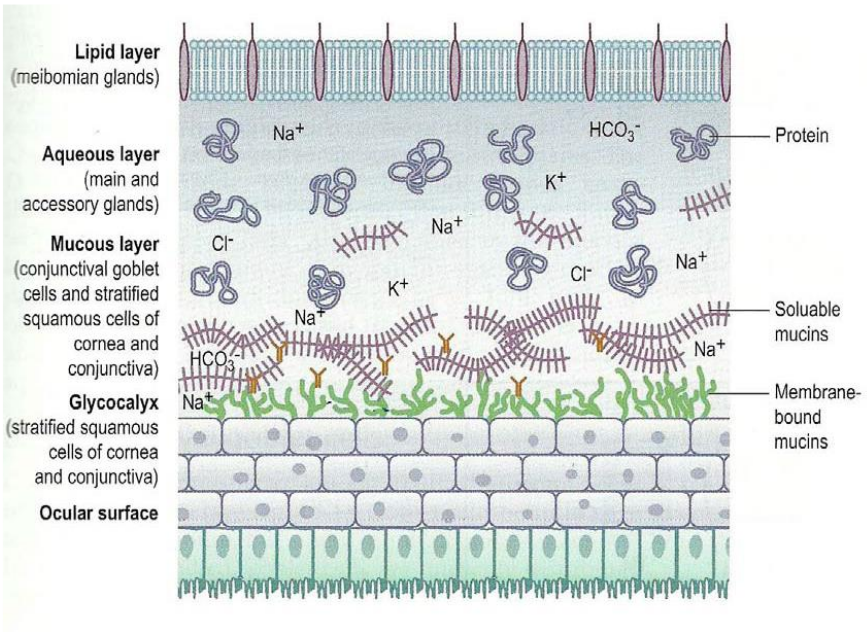

Figura I.8. ***Representación de las cuatro capas de la película lagrima pre-corneal****. El glicocálix está formado por mucinas unidas a membrana producidas por células escamosas estratificadas del epitelio corneal y conjuntivo. La capa mucosa interna está formada por MUC5AC, proteínas, electrolitos y agua, secretado por las células cúbicas conjuntivales. La capa acuosa contiene electrolitos, agua, proteínas y pequeñas mucinas solubles producidas por las glándulas lagrimales y el epitelio conjuntival. La capa lipídica, más externa, está secretada por las glándulas de Meibomio. La película lagrimal cubre la superficie ocular. Tomada de* (Dartt, 2011).

La capa más interna de la película lagrimal,el glicocálix, está formada por una red de polisacáridos que sobresale de la porción apical de los microvilli de la capa celular superficial de células escamosas estratificadas de córnea y conjuntiva (Nichols, Dawson and Togni, 1983; Corfield *et al.*, 1997; Gipson and Argüeso, 2003). Uno de sus componentes principales son las mucinas. La función del glicocálix es la de hidratar la superficie ocular y funcionar como barrera contra patógenos. Las mucinas unidas a membrana aparecen alteradas en algunos casos de ojo seco (Danjo *et al.*, 1998; Imbert *et al.*, 2006, 2009).

La columna vertebral de la capa mucosa es la mucina MUC5AC en forma de gel, secretada por las células cúbicas de la conjuntiva (Nichols, Dawson and Togni, 1983). Las mucinas

tienen un papel importante en la lubricación de la superficie ocular, anclando los componentes acuosos, estabilizando la capa lipídica y funcionando como un filtro molecular que permite el paso solo a pequeñas moléculas como aminoácidos y glucosa, bloqueando el paso de moléculas mayores (McNabb and Tomasi, 1981) (Figura I.8).

El componente acuoso de la película lagrimal contiene tanto agua como numerosos electrolitos, proteínas (incluyendo factores de crecimiento peptídicos), vitaminas, substancias químicas anti-microbianas, citoquinas, inmunoglobulinas y hormonas que, en conjunto ayudan a mantener un ambiente trófico protector en la superficie ocular (Johnson and Murphy, 2004). El componente acuoso de la película lagrimal es secretado por las glándulas lagrimales, principales y accesorias, aunque tanto la córnea como la conjuntiva pueden transportar fluido de la película lagrimal hacia dentro o hacia afuera, dependiendo de las condiciones (Johnson and Murphy, 2004; Dartt, 2009) (Figura I.8).

La capa lipídica más externa de la película lagrimal minimiza la evaporación de la lágrima en el periodo entre parpadeos, ayuda a la lubricación de los párpados durante éstos y proporciona a la córnea una superficie óptica lisa y regular. Es secretada principalmente por las glándulas de Meibomio y también por las glándulas de Moll (Bron *et al.*, 2004) (Figura 8). Una alteración o reducción en la secreción de las glándulas de Meibomio puede generar ojo seco evaporativo.

En la película lagrimal también se encuentran elementos celulares del sistema inmune, así como los agentes químicos que liberan. Además de las células hacinares de la glándula lagrimal, las células plasmáticas segregan inmunoglobulinas a la lágrima (IgA, IgG e IgM) que ayudan a proteger la superficie ocular de infecciones (Walcott, 1998).

3.2. Regulación de la lagrimación.

La estabilidad de la película lagrimal requiere que su secreción esté regulada por un sistema capaz de modificar su composición y flujo de acuerdo con los parámetros ambientales. Con el fin de asociar los diferentes componentes de esta regulación, se acuñó el concepto de unidad funcional lagrimal (Stern *et al.*, 1998), que postulaba que las células corneales y las glándulas lagrimales, junto con el input sensorial nervioso aferente y el output autónomo eferente, son interdependientes y ajustan de manera coordinada la composición y el flujo de la película lagrimal (Figura I.9).

Dependiendo de las condiciones ambientales, se propusieron dos posibles estados funcionales de esta unidad funcional lagrimal. El primero sería en condiciones normales, en las que la inervación sensorial de la superficie ocular genera un input hacia el sistema nervioso que mantiene el flujo lagrimal basal en la superficie ocular. La segunda situación se presentaría cuando algún estímulo nocivo activa las fibras sensoriales aferentes,

proporcionando al sistema nervioso un input diferente, que a su vez activaría el output reflejo, que incrementaría la lagrimación para proteger al ojo de un daño potencial (Stern *et al.*, 2004); (Figura I.9 y I.10).

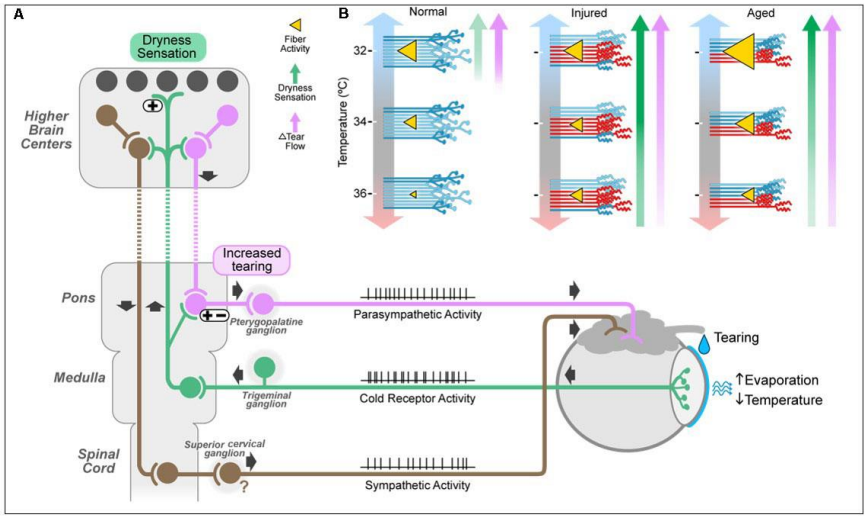

Figura I.9. ***Diagrama esquemático de los mecanismos neurales implicados en el mantenimiento de la lagrimación basal en condiciones normales por los termorreceptores de frío y la generación de sensaciones de sequedad y las alteraciones en lagrimación que suceden tras los cambios en la señal de los termorreceptores de frío tras una lesión o con el envejecimiento****. (A) Mecanismos neurales implicados en el mantenimiento de la lagrimación basal y la producción de las sensaciones de sequedad por la actividad de los termorreceptores de frío. Con niveles de humedad y temperatura ambiente confortables, la actividad basal en los termorreceptores de frío puede oscilar ligeramente entre parpadeos, pero no llega a representar una señal sensorial de amplitud temporal y espacial suficientemente elevada como para evocar sensaciones conscientes. Sin embargo, esta actividad de los termorreceptores de frío sirve para mantener un input excitatorio tónico sobre las neuronas parasimpáticas del núcleo salivatorio, que proyectan a través del ganglio pterigopalatino a las glándulas lagrimales, manteniendo así la tasa de lagrimación basal. La activación simpática también puede estar involucrada en este proceso, contribuyendo a determinar la composición y el volumen final de la lágrima. (**B**) Mecanismo hipotético que determinaría el cambio en la tasa de lagrimación y la aparición de sensaciones de sequedad conscientes durante una evaporación lagrimal en la superficie corneal, en personas jóvenes, en ancianos y en pacientes con daño en los nervios sensitivos corneales (por ejemplo, como*

consecuencia de la cirugía foto-refractiva). Normal: En individuos sanos en condiciones de humedad y temperatura ambiental normales, la actividad continua a 34ºC de los termorreceptores corneales de frío evocada por la continua evaporación, que enfría ligeramente la superficie del ojo, estimula el flujo lagrimal basal pero no evoca sensaciones de sequedad. El frío intenso evoca frecuencias de disparo de potenciales de acción en los termorreceptores de frío más elevadas y un incremento del flujo de lágrima basal, que si recluta termorreceptores de alto umbral puede paradójicamente evocar sensaciones de molestia/sequedad. Injured: las terminaciones nerviosas corneales de todo tipo dañadas muestran una actividad anormal incluyendo a nociceptores y termorreceptores de frío; esa actividad mantiene o incluso aumenta el flujo lagrimal pero es interpretada por el cortex cerebral como un mensaje de sequedad ocular. Aged: en individuos ancianos, el número total de terminaciones decrece con la edad en cerca de un 50 %; lo que previsiblemente reduce el input sensitivo aferente total a los centros parasimpáticos, tendiendo a decrecer así el flujo de lágrima basal. La excesiva evaporación que tiene lugar con un película lagrimal escasa, sin embargo puede generar una actividad aumentada en las fibras de frío que sobreviven, algunas con actividad anormal, lo que puede evocar lagrimación irritativa (epifora) acompañada paradójicamente de sensaciones de sequedad e irritación (Tomada de (Belmonte and Gallar, 2011).

Como señalamos anteriormente, se han descrito tres tipos principales de fibras sensitivas inervando la superficie corneal; mecano-nocieptores, nociceptores polimodales y termorreceptores de frío. La secreción refleja, irritativa de lágrimas parece estar determinada por la estimulación de los nociceptores polimodales y mecano-nociceptores, insensibles ante pequeños cambios de temperatura y osmolaridad en condiciones normales (Gallar *et al.*, 1993; Parra *et al.*, 2014), pero capaces de activarse por el estrés mecánico de la superficie corneal generado por la rotura y sequedad de la película lagrimal (Begley *et al.*, 2013), y también, en el caso de los nociceptores polimodales, por incrementos acusados de la osmolaridad de la película lagrimal evocados por la rotura de la misma (Liu *et al.*, 2009) (Figura I.9 y I.10).

Los termorreceptores de frío son las fibras nerviosas aferentes encargadas de la regulación de la lagrimación basal y posiblemente también del mantenimiento del parpadeo tónico (Hirata and Meng, 2010; Parra *et al.*, 2010; Belmonte and Gallar, 2011; Quallo *et al.*, 2015). Los termorreceptores de frío incrementan su actividad de disparo ante pequeños descensos de temperatura en la película lagrimal generados por la evaporación (Kimball, King-Smith and Nichols, 2010) (Figura I.9 y I.10). En humanos, durante el breve cierre rítmico del parpado del parpadeo, la temperatura de la superficie de la córnea se incrementa entre 0.5-1.0 ºC en menos de un segundo para luego volver a caer tras su apertura a un ritmo de unos 0.05 ºC/s en el tiempo entre parpadeos debido, principalmente, al enfriamiento evaporativo de la lágrima (PURSLOW and WOLFFSOHN, 2007; Li *et al.*, 2015; Pattmöller *et al.*, 2015;

Versura *et al.*, 2015). Además, el incremento en la osmolaridad de la película lagrimal generado por la evaporación incrementa adicionalmente la actividad de los termorreceptores de frío (Parra *et al.*, 2014). Así pues, la actividad de los termorreceptores de frío es modulada por los cambios cíclicos en la película lagrimal generados por el parpadeo, lo que sugiere que estos termorreceptores de frío juegan un papel importante en el control del parpadeo y de la producción de lágrima basal (Figura 9 y 10). Otra prueba que apoya esta hipótesis es que, tanto el parpadeo como el nivel basal de producción de lágrima, están muy reducidos en ratones *knock out* para el canal TRPM8, en comparación con animales *wild type* (Quallo *et al.*, 2015), Además, pequeñas concentraciones del agonista del canal TRPM 8, mentol, incrementa la producción de lágrima en ratones *wild type*, pero no en los TRPM8 *knock out* (Robbins *et al.*, 2012). El mentol también estimula la producción de lágrima en cobayas (Fern *et al.*, 2016). Cabe resaltar que las concentraciones de mentol usadas para estimular la producción de lágrima no generaron comportamientos nocifensivos en los animales, asociados a la estimulación con compuestos químicos nocivos que activan a los nociceptores polimodales. Todo ello en conjunto, apoya el papel de los termorreceptores de frío corneales en proporcionar información acerca de los niveles de sequedad de la superficie del ojo, para la regulación refleja del parpadeo y de la tasa de producción de lágrima basal (Figura I.9 y I.10). Además, cabe la posibilidad de que estos termorreceptores de frío contribuyan a la etiología del ojo seco (Parra *et al.*, 2010; Belmonte *et al.*, 2015; Fern *et al.*, 2016), aunque esto aún permanece por demostrar.

3.3. Síndrome de ojo seco (SOS).

El ojo seco ha sido definido por el TFOS DEW II como: "Una enfermedad multifactorial de la superficie ocular, que se caracteriza por una pérdida de la homeostasis de la película lagrimal y que va acompañada de síntomas oculares, en la que la inestabilidad e hiperosmolaridad de la superficie ocular, la inflamación y daño de la superficie ocular, y las anomalías neurosensoriales desempeñan papeles etiológicos." (Craig *et al.*, 2017). El SOS tiene una prevalencia del 5.3 % en los Estados Unidos, siendo la tercera afección ocular más común que lleva a los pacientes a buscar tratamiento.

Las sensaciones desagradables son el principal síntoma de este desorden. Como era de esperar, estudios clínicos y experimentales han confirmado la presencia de alteraciones morfológicas en la inervación corneal de los pacientes con SOS, junto con signos celulares y biomecánicos de inflamación epitelial (Chao *et al.*, 2015; Yamaguchi, 2018). La contribución de cada una de estas alteraciones a la génesis y evolución del SOS son, actualmente, tema de discusión (Tepelus *et al.*, 2017).

El SOS se ha conseguido reproducir con varios modelos experimentales en diversas especies animales, reduciendo la humedad de la superficie ocular bien a través del bloqueo de la

inervación colinérgica, el aumento de la evaporación de la película lagrimal mediante exposición de la superficie ocular a ambientes secos, ablación quirúrgica de las glándulas lagrimales o cirugía del nervio petroso mayor (Toshida *et al.*, 2007; Fern *et al.*, 2016; Simsek *et al.*, 2018).

El registro de la descarga de impulsos nerviosos tanto en cuerpo celular, como en axones parentales y terminaciones nerviosas corneales de neuronas del GT que inervan los ojos de cobaya y ratón, ha confirmado la correspondencia que existe entre las anomalías morfológicas en los nervios corneales y los trastornos en la función neuronal. Se han observado numerosas alteraciones en la actividad de los termorreceptores de frío periféricos, atribuidas a la sequedad, unas cuatro semanas después de la supresión de la glándula lagrimal en cobayas. Estos termorreceptores presentaron funcionalmente una actividad anormalmente elevada a temperaturas corneales basales y ante estímulos de enfriamiento, en conjunción con un incremento significativo en la excitabilidad de la membrana de los cuerpos celulares de neuronas corneales de frío (Fern *et al.*, 2016).

En definitiva, los daños nerviosos ocasionados por el SOS afectan principalmente a la actividad basal y a la respuesta al enfriamiento de las neuronas termorreceptoras de frío. Además, hay estudios que han confirmado que la sequedad crónica en la córnea de rata involucra principalmente a las neuronas termorreceptoras de frío de alto umbral, reflejando la importancia de esta subpoblación neuronal de frío en las sensaciones desagradables de sequedad en ojos con deficiencia lagrimal. También se han reportado sensaciones de sequedad desagradables y un aumento del parpadeo cuando se estimulan las terminaciones corneales de humanos con vapores de mentol o aire frío (Fern *et al.*, 2016; Corcoran *et al.*, 2017).

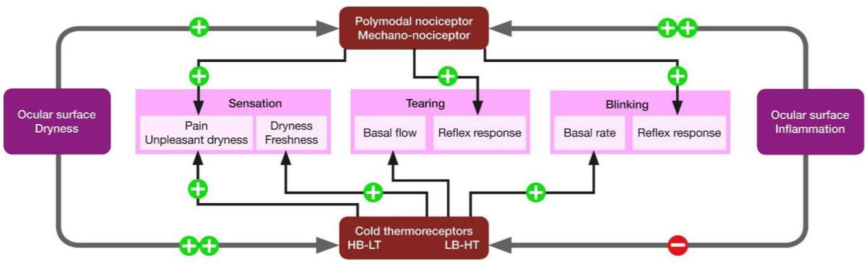

Figura I.10. ***Diagrama esquemático*** *que recoge como la inflamación ocular de etiología diversa, o la sequedad ocular en el SOS, generan s incrementos (+) o disminuciones (-) en la frecuencia de descarga de impulsos nerviosos en los nociceptores polimodales y mecano-nociceptores, y en los termorreceptores de frío de alta actividad basal y bajo umbral (HB-LT) y de baja actividad basal y alto umbral (LB-HT). En su conjunto, estos cambios evocan*

sensaciones conscientes de diversa cualidad, así como variaciones en el flujo de lágrima y en el parpadeo reflejo y espontáneo (Belmonte, 2019).

Adicionalmente, el disparo de potenciales de acción de los nociceptores polimodales de la córnea de cobayas con SOS experimental se incrementó en respuesta a la estimulación ácida, al igual que ocurrió con las corrientes de sodio en los cuerpos celulares, lo que refleja una sensibilización moderada de estos nociceptores polimodales (Fern *et al.*, 2016). Posiblemente estas observaciones sean debidas a la inflamación observada en los modelos experimentales de SOS en cobaya. Como cabría esperara, cuando estos procesos inflamatorios se vuelven más intensos, como sucede en las formas severas de SOS, el papel de los nociceptores polimodales se vuelve más relevante, aumentando el componente doloroso en las sensaciones experimentadas por los pacientes de SOS (Figura I.10).

3.4. Envejecimiento y ojo seco.

En personas ancianas, es común la aparición de sensaciones molestas de sequedad ocular La prevalencia del SOS se ve incrementada, tanto en hombres como en mujeres, cada cinco años a partir de los 50 años, siendo el envejecimiento, por tanto, un factor de riesgo para el desarrollo del SOS (revisión en (de Paiva, 2017)).

El envejecimiento genera una degeneración progresiva de las ramas periféricas distales de las neuronas sensitivas. La glándula lagrimal sufre varios cambios significativos, como atrofia de las células acinares, fibrosis periacinar o fibrosis periductal (El-Fadaly *et al.*, 2014). Los roedores han sido empleados de manera frecuente en las investigaciones del envejecimiento ya que los cambios en la glándula lagrimal relacionados con la edad son similares a los que ocurren en humanos (ver revisión (Rocha *et al.*, 2008)). También se han observado con el envejecimiento alteraciones en otras estructuras relacionadas con la lagrimación, como los párpados o la atrofia de las glándulas de Meibomian (Hykin and Bron, 1992; Alghamdi *et al.*, 2016).

Todavía existe controversia acerca de si es el envejecimiento el que conduce a la aparición de SOS o si el SOS es una dolencia que se desarrolla por mecanismos diferentes al envejecimiento *per se* (Stern, 2005; de Paiva, 2017), pero es sabido que el SOS afecta a entre el 5-30 % de la población mayor de 50 años.

Con el incremento de la población de edad avanzada por el aumento de la esperanza de vida, es esperable que el ojo seco continúe siendo una de las principales demandas en la práctica oftalmológica clínica (Pflugfelder, 2008). Por ello, es necesario una mejor comprensión de la relación SOS-edad y de las terapias adecuadas para esta población específica.

II. Justificación, hipótesis de trabajo y objetivos.

Justificación

La córnea es la superficie tisular más densamente inervada del cuerpo (600 terminaciones/mm^2). Estas terminaciones corresponden a neuronas del ganglio trigémino y están especializadas en la detección de diferentes estímulos ambientales. Se ha postulado que la expresión de diferentes canales TRP en las neuronas corneales confiere a éstas su diferente capacidad de transducción sensorial. TRPM8, TRPV1 y TRPA1 son miembros de la superfamilia de los canales TRP presentes, entre otros lugares, en las terminaciones nerviosas de la córnea, modulando su actividad.

La presente tesis persigue la caracterización electrofisiológica de los diferentes tipos funcionales de fibras sensoriales de la córnea que detectan estímulos mecánicos, químicos y térmicos (Belmonte *et al.*, 2004), analizando sus diferencias funcionales y haciendo hincapié en las dos poblaciones de fibras que presentan respuesta a frío (Gallar *et al.*, 1993).

Además de la importancia de este estudio para ampliar el conocimiento funcional de las neuronas corneales a nivel básico, es importante también para entender las disfunciones neurales ocasionadas por intervenciones quirúrgicas, así como en patologías oculares como el ojo seco.

El ratón se ha convertido en el mejor modelo experimental para el estudio de la fisiopatología de la inervación de la superficie del ojo, gracias a las posibilidades de su manipulación genética, sencillez de manejo y la abundante información científica disponible sobre sus características biológicas y semejanzas con el humano. El empleo de ratones envejecidos permitirá además comparar la respuesta de sus terminaciones nerviosas corneales con la de los ratones jóvenes, para determinar las posibles diferencias en función y su posible contribución a los trastornos de la lagrimación que se observan con la edad.

Hipótesis de Trabajo

Por ello el objetivo general de esta Tesis ha sido caracterizar en detalle las propiedades electrofisiológicas y morfológicas de la inervación corneal en ratones jóvenes y viejos y la correspondencia en esta especie entre la actividad de las fibras nerviosas oculares y la lagrimación, obteniendo nuevos datos que ayuden a mejorar la comprensión de la relación existente entre las alteraciones de dichas fibras nerviosas y los síntomas cognitivos de molestias, dolor y sequedad ocular que aparecen en los humanos con el envejecimiento.

Objetivos

Para obtener esta información proponemos los siguientes objetivos específicos:

1. Caracterizar electrofisiológicamente los distintos tipos funcionales de terminales nerviosas corneales.

2. Determinar las diferencias funcionales entre las terminales nerviosas corneales de frío de alto y bajo umbral.

3. Determinar los cambios funcionales y morfológicos de las terminaciones de frío en ratones viejos y su efecto sobre la lagrimación.

II. Materiales y Métodos

1. Animales

Para este estudio han sido utilizados un total de 614 ojos, de 307 ratones machos y hembras C57BL/6 y TRPM8^{BAC}-EYFP, de los cuales 279 fueron ratones jóvenes (edad comprendida entre los 3 y 6 meses) y 28 ratones viejos (24 meses de edad).

Todos los experimentos fueron realizados de acuerdo con las normas de ética para trabajo animal de la Universidad de Oviedo y aprobados por el comité ético de la misma y siguiendo las recomendaciones de ARVO (*Association for Research in Vision and Ophthalmology*) para la experimentación animal en las ciencias de la visión.

2. Registro electrofisiológico de la córnea de ratón.

El registro in vitro de terminaciones nerviosas corneales se realizó tal y como se ha descrito en estudios previos (Parra *et al.*, 2010). La parte posterior del globo ocular junto con el nervio óptico enucleado de ratones previamente sacrificados mediante dislocación cervical, fue colocada en el fondo de una cámara de registro rellena con solución salina fisiológica, manteniendo fijo el ojo en esta posición mediante succión, llevada a cabo por un tubo de silicona situado justo en el fondo de la cámara. El ojo era perfundido de manera continua con la solución salina, que tenía la siguiente composición (en mM): NaCl (128), KCl (5), NaH_2PO_4 (1), $NaHCO_3$ (26), $CaCl_2$ (2.4), $MgCl_2$ (1.3) y Glucosa (10). La solución se burbujeó durante todo el experimento con gas carbógeno (una mezcla de 5% CO_2 y 95% O_2) y se mantuvo a una temperatura control de 34 ºC usando un peltier de elaboración casera (Figura III.1).

Con una pipeta de cristal de borosilicaro de unas 50 μm de diámetro, llena de la misma solución salina extracelular, y en cuyo interior se colocó un electrodo Ag-AgCl, se mapeó la córnea de ratón, desplazando el electrodo por su superficie mediante un micromanipulador y realizando una ligera succión una vez que la pipeta tocaba sobre la superficie corneal (para generar un sello de alta resistencia). Los impulsos nerviosos terminales (NTIs, del inglés Nerve Terminal Impulses) fueron amplificados con un amplificador AC (Neurolog NL104; Digitimer, Welwyn, UK) y almacenados a 10 KHz en un ordenador, usando un dispositivo CED micro 1401 y el software Spike 2 (ambos de Cambridge Electronic Design, Cambridge, UK). Solo los *NTIs* con una señal homogénea y una amplitud claramente diferenciable del ruido (aproximadamente de unos 10 μV de pico a pico) y procedente de una única terminación fueron almacenados para su análisis. Para minimizar el deterioro de la preparación con el paso del tiempo, la duración total de los experimentos se limitó a un máximo de 5 horas.

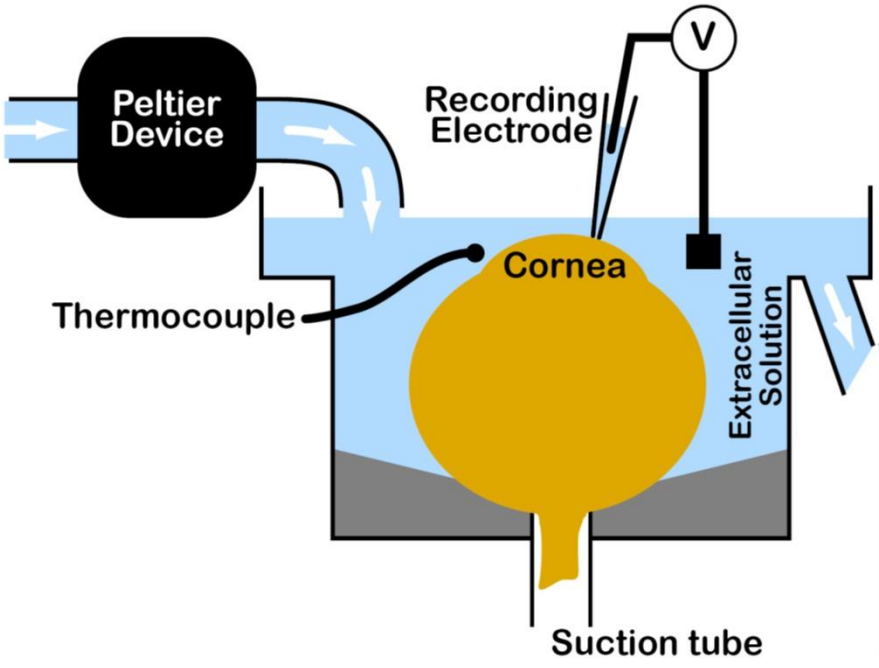

Figura III.1. ***Esquema de la cámara de registro.*** *Cámara de registro usada para el registro de las terminaciones corneales de ratón. El ojo enucleado del ratón se coloca en el interior de la cámara, donde se fija mediante una ligera succión en la parte basal de la misma. El ojo está completamente cubierto por la solución extracelular de registro, que es llevada a la temperatura deseada mediante un dispositivo peltier. El electrodo de registro, situado en el interior de una pipeta de borosilicato, se va moviendo por la superficie corneal hasta encontrar un punto en el que se detecte actividad de una terminación nerviosa, siguiendo el protocolo de búsqueda expuesto en el apartado correspondiente. Una sonda de temperatura colocada en el interior del baño y conectada a la unidad CED permite registrar la temperatura de manera continua. (Tomada de* (Parra *et al.*, 2010)*).*

2.1. Protocolo de experimentación.

Para obtener una estimación relativa de la densidad de los distintos tipos funcionales de terminaciones corneales, la pipeta de registro fue situada en una secuencia regular de puntos de la superficie corneal, separados entre sí por, aproximadamente, una distancia de unos 0.2 mm, y alineados entre sí para cubrir un espacio corneal amplio, desde el centro hasta la periferia de la misma. Una mitad de la córnea fue explorada de esta manera, y después se rotó el ojo dentro de la cámara para poder acceder a la otra mitad, en la que se repitió el procedimiento, hasta obtener un total de unas 15-20 puestas totales por ojo.

En cada puesta, una vez situada la pipeta sobre la superficie corneal y aplicada una succión, se ha mantenido la pipeta de registro en dicha posición por un periodo de, al menos, dos minutos, con el fin de determinar la presencia de actividad espontánea, lo cual, en caso de ser registrada, se tomó como un *acierto* a la hora de detectar una terminación nerviosa sensitiva en dicho punto. Si no se detectaba actividad espontánea, se procedía a realizar un estímulo mecánico (ejerciendo presión con la pipeta de registro mediante el desplazamiento del micromanipulador contra la superficie corneal) de 200 μm de desplazamiento. Si aun con todo no se evocaba actividad, se consideraba ese punto como de *no éxito* y se procedía a desplazar la pipeta de registro a la siguiente posición.

En el caso de haber observado actividad espontánea de *NTIs* en un punto, se procedió a realizar una estimulación de frío mediante rampa, consistente en disminuir la temperatura basal del baño desde 34 ºC hasta unos 14 ºC, con una tasa media de enfriamiento de 0.6 ºC.s^{-1}. Cuando se alcanzó la temperatura mínima deseada, se aplicó un calentamiento (calentamiento-control) para regresar a la temperatura basal de 34 ºC con una tasa de cambio de temperatura similar (Figura III.2).

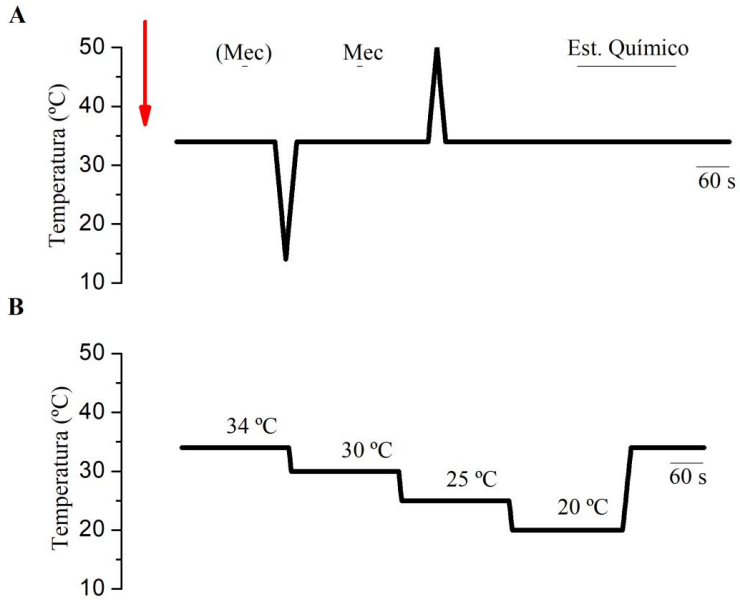

Figura III.2. ***Protocolo general de experimento. A****. Ejemplo del protocolo experimental general: una vez realizada una puesta sobre la superficie corneal (flecha roja), se mantiene la pipeta en esa posición durante dos minutos, esperando a encontrar actividad espontánea. En caso de no haberla, se realiza una estimulación mecánica con el fin de evocar una respuesta. Si aun así no se observa actividad, se sitúa la pipeta en la siguiente posición. En caso de haber observado actividad (ya sea espontánea o evocada por el estímulo mecánico)*

se procede a realizar una estimulación de frío mediante rampa (aproximadamente desde 34 hasta 14 ºC). Dos minutos después del regreso a la temperatura control, se realiza una estimulación mecánica mediante el desplazamiento de la pipeta de registro contra la superficie corneal (de unas 200 μm). Dos minutos después de la estimulación mecánica, se lleva a cabo una estimulación de calor mediante rampa (desde los 34 ºC control hasta, aproximadamente, 50 ºC). Tras un periodo de recuperación de no menos de 5 minutos, se procede a la estimulación química (normalmente de 3 minutos), en caso de haberla. ***B****. Ejemplo de escalones de temperatura llevados a cabo en algunos termorreceptores de frío corneales, unos dos minutos después de la rampa dinámica de frío inicial. Los escalones de temperatura (de 34, 30, 25 y 20 ºC) se mantuvieron por un periodo de, al menos, tres minutos, antes de iniciar el siguiente escalón.*

Tras un periodo de reposo de, al menos, 2 minutos, se realizó una estimulación mecánica de 200 μm de desplazamiento, manteniendo la presión durante 5 segundos (Figura III.2). En algunas terminaciones además de este estímulo mecánico de 200 μm, se realizó otro previo de 100 μm de desplazamiento y otro posterior de 300, μm también con 5 segundos de duración, separados entre sí por un periodo de 10 segundos.

Tras otro periodo de descanso de, al menos, 2 minutos, se procedió a realizar otro estímulo térmico, esta vez de calor. En este caso, la temperatura basal de 34 ºC se elevó hasta alcanzar unos 52 ºC, con una velocidad de calentamiento de 0.5 ºC.s^{-1} (con una duración aproximada de 30 segundo hasta alcanzar la máxima temperatura), después de lo cual se retornó la temperatura basal del baño a 34 ºC con una tasa de enfriamiento semejante (Figura III.2). En alguna de las terminaciones clasificadas como nociceptores polimodales, una segunda rampa de calor fue realizada, con unos parámetros similares, tras 10 minutos de reposo.

En algunas de las terminaciones en las que se observó una respuesta durante el estímulo térmico de rampa de frío, se realizaron escalones de frío bajando la temperatura y manteniéndola por, al menos, 2 minutos, en escalones de 34, 30, 25 y 20 ºC. Después de lo cual se regresaba a la temperatura control (34 ºC) (Figura III.2).

La estimulación química se inició unos 5 minutos después de la última estimulación térmica llevada a cabo, cambiando la perfusión con la solución salina control a otra solución salina control que contenía la droga disuelta. Todo ello a 34 ºC. La perfusión de soluciones con químicos se mantuvo, al menos, 3 minutos (Figura III.2). Después de ello, en aquellos casos en los que procediera, se realizó una rampa de frío con los mismos parámetros que las rampas de frío llevadas a cabo con la solución control. Una vez finalizado el tiempo de perfusión, se realizó un lavado con solución salina extracelular control de al menos 5 minutos.

La capsaicina se aplicó siempre al final del experimento debido al efecto inactivante de esta droga sobre las terminaciones corneales.

2.2. Soluciones.

Mentol (20 μM): preparado de una disolución stock de 20 mM en etanol, diluida a su concentración final con la solución salina extracelular control. Sigma-Aldrich Copr. St. Louis, MO, USA.

Capsaicina (1 μM): preparado de una disolución stock de 1 mM en etanol disuelta a su concentración final con la solución salina extracelular. Sigma-Aldrich Copr. St. Louis, MO, USA.

Allil isotiocinato (AITC, 100 μM): preparado de una disolución stock de 100 mM en dimetil sulfóxido (DMSO) disuelta a su concentración final con la solución salina extracelular. Sigma-Aldrich Copr. St. Louis, MO, USA.

Soluciones Hiperosmolares: fueron preparadas añadiendo NaCl (3 M) a la solución salina extracelular (310 ± 1.5 $mOsm.Kg^{-1}$) hasta alcanzar los valores de osmolaridad deseados (340,

400, 600, 800 y 1000 mOsm.Kg^{-1}). Medidos con un osmómetro al punto de congelación (OSMOSTAT OM-6020; Kyoto Daiichi, Kyoto, Japón).

Sopa Inflamatoria: contiene las siguientes sustancias, disueltas en la solución salina extracelular: Bradikinina (5 μM), Histamina (100 μM), PGE_2 (10 μM), 5-HT (100 μM) y ATP (100 μM), todas ellas de Sigma-Adrich Corp.

4-Aminioiridina (4-AP,100 μM): preparada a partir de una solución stock de 100 mM en DMSO disuelta a su concentración final con la solución salina extracelular. Sigma-Aldrich Copr. St. Louis, MO, USA.

Tacrolimus (30 μM): también conocido como FK-506 (LC Laboratorios) fue preparado de un stock de 50 mM en DMSO y disuelto en la solución salina control hasta la concentración deseada.

2.3. Análisis de la actividad de *NTIs.*

Se analizaron los siguientes parámetros de la actividad de *NTIs*:

Actividad Basal: frecuencia media (en imp.s^{-1}) de disparo de la terminación en curso, a una temperatura control de 34 ºC. Fue medida durante los 30 segundos previos al primer estímulo realizado.

Umbral de respuesta a frío: temperatura a la que una terminación supera su frecuencia media (medida los 10 segundos antes de la rampa de frío) más tres veces su desviación estándar, durante el estímulo de frío realizado mediante una rampa.

Umbral de respuesta a calor: temperatura a la que una terminación supera su frecuencia media (medida los 10 segundos antes de la rampa de calor) más tres veces su desviación estándar, durante el estímulo de calor realizado mediante una rampa.

Pico de máxima respuesta a frío: valor máximo de frecuencia por segundo de disparo (imp.s^{-1}) de la terminación alcanzado durante la respuesta a frío.

Frecuencia media en respuesta a frío: frecuencia media de disparo de *NTIs* de una terminación (imp.s^{-1}) en respuesta a frío, medido desde el valor umbral de respuesta a frío hasta el valor pico de respuesta máxima.

Temperatura de silenciamiento: temperatura necesaria para silenciar los *NTIs* de una terminación durante una rampa de frío.

3. Inmunohistoquímica.

Los ratones fueron anestesiados con una mezcla de Ketamina (80 mg/kg; Imalgène 500®, Merial; Toulouse, Francia) y Xilacina (5 mg/kg; Rompun®, Bayer, Munich, Alemania) y eutanasiados con una sobredosis de pentobarbital sódico intraperitoneal (Dolethal®, Vetoquinol, Lure, Francia). Los ojos y el ganglio trigémino (TG) fueron sustraídos con cuidado y procesados como se detalla a continuación.

3.1. Córneas completa (*Whole-mounted)*.

Método de la ABC-peroxidasa.

Se fijaron los globos oculares durante 1 hora a temperatura ambiente (RT) en paraformaldehido al 4% y ácido pícrico al 0.2 % en un búfer salino al 0.1 M (PBS, pH 7.4). Se diseccionaron las córneas y se lavaron en PBS. Pera incrementar su permeabilidad, se incubaron durante toda la noche a 37 ºC en hialuronidasa tipo IV-S al 0.01 % (Sigma-Aldrich; St- Louis, MO) y ácido etileno-diaminotetraacético al 0.1 % (EDTA; Sigma-Aldrich)

[Marfurt et al., 2010] en un búfer acetato 0.1 M (pH 6.0). Tras ello, se lavaron las córneas en PBS con triton X-100 (PBS-TX) y se incubaron durante 2 horas en solución de bloqueo, que contenía suero de albúmina bovino 1 % (BSA; Vector Laboratorios, Burlingame, CA) y suero de cabra normal al 10 % (Vector Laboratorios) en PBS-TX a RT. Después, se incubaron las córneas *por la noche* a 4 ºC con un anticuerpo policlonal de conejo anti-GFP (1:500; Molecular Probes, Eugene, OR). Tras lavar con PBS.TX, se incubaron las córneas durante 2 horas a RT con anticuerpo secundario de cabra anti-conejo IgG biotinilado (1:2000; Vector Laboratorios). Tras lavar con PBS.TX, se incubaron las córneas durante 2 horas a RT en un complejo de avidina-biotina- peroxidasa de rábano (ABC reagent; Vector Laboratorios). Se lavaron las córneas a continuación con PBS-TX y se incubaron por 2 minutos a RT en diaminobencina al 0.1 % (Sigma-Aldrich) y H_2O_2 al 0.03 %. Después de lavar con PBS, se deshidrataron las córneas en gradientes de etanol, clareadas con xilol y se montaron en portaobjetos con medio de montaje Entellan (Merck Millipore, Darmstadt, Alemania).

Inmunofluorescencia.

Se fijaron las córneas durante 2 horas a RT en metanol y DMSO (4:1), se rehidrataron y se lavaron en PBS. Se incubaron durante 1 hora en solución bloqueante que contenía BSA al 1 % (Vector Laboratorios) y suero de cabra normal al 10 % (Vector Laboratorios) en PBS-TX a RT. Después de lavarlas con PBS-TX, se incubaron durante 48 horas a 4 ºC con los anticuerpos primarios diluidos en PBS-TX: conejo anti β-tubulina clase III (1:500; Covance Research Products, Berkeley, CA) y pollo anti-GFP (1:500; Abcam, Cambridge, MA). Después de lavar las córneas con PBS-TC, se incubaron durante 2 horas a RT con los anticuerpos secundarios Alexa Fluor 594 cabra anti-conejo IgG y Alxa Fluor 488 cabra anti-pollo IgG, respectivamente (1:500; Molecular Probes) en PBS, a lo que siguió una incubación de 10 minutos a RT con *4´, 6-diamidino-2-phenylindole* (DAPI; 2 µg/mL; Molecular Probes).

3.2. Ganglio trigémino.

Ratones profundamente anestesiados, cuyos globos oculares habían sido extraídos para usar sus córneas para las técnicas de inmunohistoquímica de córneas completas (como se describe arriba), fueron perfundidos inmediatamente con salino fisiológico ascendente a través de la aorta, seguido de 15 minutos de perfusión con paraformaldehído al 4 % y ácido pícrico al 0.2 % en PBS. Después, se extrajeron los GTs y se fijaron durante 1 hora a RT con el mismo fijador, crio protegidos durante la noche a 4 ºC en sacarosa al 30 % en PBS; embebidos en medio OCT (Sakura Finetek, Torrance, CA) y congelados en nitrógeno líquido. Se almacenaron los bloques a -80 ºC hasta que fueron utilizados.

Se cortó el TG en un criostato microtomo en secciones de 7 µm de grosor y se montaron en portaobjetos *Superfrost Plus*. Se lavaron las secciones de tejido en PBS con Triton al 0.03 % durante 10 minutos y se bloquearon durante 1 hora en PBS con suero de cabra al 10 % o de asno (dependiendo de los anticuerpos secundarios utilizados) a RT y se incubaron *por la noche* a 4 ºC con anticuerpos primarios diluidos en la solución de bloqueo. Los anticuerpos polimodales de conejo usados fueron los siguientes: anti-NF200 (1:1000, Sigma-Aldrich), anti-Periferina (1:500, Millipore) y anti-TrkA (1:500, Millipore). Además, también se ha usado un anticuerpo policlonal de cabra anti-CGRP (1:500, Abcam). Tras ello, se lavaron las secciones con PBS y se incubaron durante 2 horas a RT con anticuerpos secundarios IgG de cabra anti-conejo o IgG de asno anti-cabra conjugados con una Alexa Fluor 594 (1:500, Molecular Probes) en PBS.

Para detectar la tinción de IB4, se incubaron las secciones *durante la noche* con isolectina Griffonia Simplicifolia (GS-IB_4 Alexa Fluor 594 conjugado, 1:500; Molecular Probes) en PBS a 4 ºC. Más tarde, se lavaron en PBS y se incubaron con DAPI durante 10 minutos a temperatura ambiente. Finalmente, se cubrieron las muestras con medio de montaje fluorescente (Dako, Glostrup, Dinamarca).

3.3. Caracterización de los Anticuerpos.

Los detalles de los anticuerpos y de sus diluciones se muestran en la Tabla 1.

Tabla III.1. Anticuerpos y lectinas usadas en este estudio.

Nombre	Immunógeno	Manufacter; catalog number; RRID; host species; mono/polyclonal	Dilución
Anticuerpos Primarios			
Anti-GFP	The GFP was isolated directly from the jellyfish *Aequorea victoria*	Molecular Probes; A11122; AB_221569; rabbit; polyclonal	1:500
Anti-GFP	Recombinant full length protein corresponding to GFP from *Aequorea victoria*	Abcam; ab13970; AB_300798; chicken; polyclonal	1:500
Anti-Tubulin β-III	Neuronal Class III beta tubulin	Covance Research Products; PRB-435P; AB_291637; rabbit; polyclonal	1:500
Anti-NF200	Neurofilament 200 from bovine spinal cord	Sigma Aldrich; N4142; AB_477272; rabbit; polyclonal	1:1000
Anti-Peripherin	Trp-E-peripherin fusion protein containing all but the 4 N-terminal amino acids of rat peripherin	Millipore; AB1530; AB_90725; rabbit; polyclonal	1:500
Anti-TrkA	Purified protein corresponding to the entire extracellular domain of rat TrkA receptor	Millipore; 06-574; AB_310180; rabbit; polyclonal	1:500
Anti-CGRP	Synthetic peptide corresponding to Rat CGRP (C-terminal)	Abcam; ab36001; AB_725807; goat; polyclonal	1:500
Secondary antibodies			
Biotinylated anti-rabbit IgG	Gamma Immunoglobulins heavy and light chains; IgG	Vector Laboratories; BA-1000; AB_2313606; goat; polyclonal	1:200
AF594-anti-rabbit	Gamma Immunoglobulins heavy and light chains; IgG	Molecular Probes; A11037; AB_2534095; goat; polyclonal	1:500

AF488-anti-rabbit	Gamma Immunoglobulins heavy and light chains; IgG	Molecular Probes; A11034; AB_2576217; goat; polyclonal	1:500
AF488-anti-Chicken	Gamma Immunoglobulins heavy and light chains; IgY	Molecular Probes; A11039; AB_142924; goat; polyclonal	1:500
AF594-anti-goat	Gamma Immunoglobulins heavy and light chains; IgG	Molecular Probes; A11058; AB_142540; donkey; polyclonal	1:500
Lectin stain			
GS-IB$_4$	The GS-IB$_4$ was isolated from the seeds of the *Griffonia simplicifolia*.	Molecular Probes; I21413: AB_2313921	1:500

3.4. Adquisición de imágenes.

Las imágenes de campo claro y fluorescencia fueron tomadas usando un microscopio Leica DM 6000Bm equipado con un set de filtros de fluorescencia y una cámara Laica DFC310 FX (Leica Microsystems, Alemania) y con un microscopio confocal Laser Scanning Spectral Olympus Fluoview FV1200 (Olympus Corp., Tokyo, Japón).

4. Registros electrofisiológicos de cultivos neuronales de TG.

Se hicieron cultivos primarios de GT de ratones TRPM8^{BAC}-EYFP (de 3 y 24 meses) siguiendo un procedimiento ya descrito (Madrid et al., 2009). Las células disociadas del TG se sembraron en un cubreobjetos de vidrio con *poli-L-lisina* y se cultivaron en medio *Eagle´s minimal essential* (MEM) con *Earle´s BSS* y L-glutamina más suero fetal bovino inactivado por calor al 10%, solución vitamina al 1 % y penicilina/estreptomicina 100 µg/mL (todo ello de Invitrogen). Las células se usaron tras 12-36 horas en cultivo.

Se transfirieron los cubreobjetos a una cámara de registro de 0.15 mL (Warner Instrument Corporation, Hamden, CT) en la pletina de un microscopio invertido (Nikon Diaphot-TMD,

Nikon Instruments, Tokyo, Japón) y perfundida (1.5-3 $mL.min^{-1}$) a temperatura basal (32-34 ºC, mantenida con un dispositivo peltier controlado por ordenador, Embit, Modena, Italia) con solución fisiológica. Antes de cada registro, se tomaron imágenes de luz-transmitida y de fluorescencia de cada neurona (*filter cube* para GFP: 41017_Nikon; Watec camera), y se expresó la intensidad de fluoresciencia de cada neurona registrada como el porcentaje del valor máximo de fluorescencia medido en la población total, en condiciones no saturantes. Se registraron los potenciales de membrana usando la técnica de *patch-clamp* perforado. Las pipetas de borosilicato (Harvard Apparatus, UK, 2-4 MΩ) se rellenaron con una solución que contenía (en mM): 105 K gluconato, 50 KCl, 2 $CaCl_2$, 1 $MgCl_2$, 10 HEPES y 0.2 mg/mL nystatin (pH 7.3, ajustado con NaOH; concentración final de Na de ~10 mM). Las señales electrofisiológicas se registraron con un amplificador Axopatch 200B patch-clamp (Molecular Devices, CA). La liberación de estímulos, la adquisición de datos y el análisis se llevaron a cabo usando el software pClamp 9.2 (Molecular Devices). Se utilizaron rampas de frío hasta 20-22 ºC (de unos 50 segundos de duración) y L-mentol extracelular (100 μm) para el estudio de las características funcionales de las neuronas $TRPM8^{+}$.

5. Medidas de lágrima y osmolaridad.

Se midió la lágrima de ambos ojos en ratones de 3 y 24 meses $TRPM8^{BAC}$-EYFP y C57BL/6 anestesiados (n=110) usando tiras de rojo-fenol (Zone-Quick, Menicon Pharma S.A., Graffenstaden, Francia) colocadas con cuidado entre el párpado inferior y la conjuntiva bulbar en el ángulo nasal, durante 1 minuto (Parra et al., 2010). Como no se observaron diferencias entre las medidas de lágrima de los ratones $TRPM8^{BAC}$-EYFP y C57BL/6, los datos de ambos fueron analizados conjuntamente.

La osmolaridad de la lágrima se midió en ratones C57BL/6 de diferentes edades, usando el *Tearlab osmolarity System* (OcuSense Inc., San Diego, CA). El fluido lacrimal se recolectó de ratones inmovilizados y despiertos, colocando la sonda del instrumento en el menisco que se forma en el lado nasal del margen del párpado inferior. Las muestras se obtuvieron de ambos ojos.

6. Análisis Estadísticos.

Los datos se analizaron usando SPSS 15.0 (IBM, Armonk, New York), Instat3 (GraphPad Softwware, San Diego, CA) y SigmaStat v3.5 (Systat Software, Point Richmond, CA). Las diferencias significativas se determinaron usando t- test o ANOVA de un factor con corrección de comparaciones múltiples de Bonferroni o Dunn, para muestras paramétricas y pareadas; t- test para muestras no pareadas o test de Wilcoxon para muestras paramétricas y no pareadas; o test de Mann-Whitney para aquellas muestras no pareadas ni paramétricas. También se realizó el z test. *$p<0.05$; **$p<0.01$; ***$p<0.001$.

IV. RESULTADOS

1. Características funcionales y morfológicas de las terminaciones nerviosas sensoriales de la córnea de ratón joven.

Los experimentos se realizaron en 614 ojos, obtenidos de 307 ratones jóvenes y viejos (3 y 24 meses de edad) de ambos sexos.

Basándonos en la respuesta característica que presentaron a diferentes estímulos, las terminaciones nerviosas sensitivas corneales fueron clasificadas como: mecanorreceptores, nociceptores polimodales y termorreceptores de frío. La figura 1 muestra la proporción de registros en los que se detectó impulsos nerviosos originados en una terminación nerviosa (*NTIs, nerve terminal impulses* en inglés) del total de intentos, y la porción correspondiente a cada uno de los tipos de terminación mencionados. En más de la mitad de los intentos de registro (58.6 %), no se consiguió detectar actividad eléctrica alguna (Figura IV.1A); además, en otro 20 %, los impulsos detectados presentaban una amplitud demasiado pequeña, lo que impedía cualquier análisis y/o identificación fiable de las características de dichas terminaciones; Los termorreceptores de frío de alto y bajo umbral fueron las terminaciones más frecuentemente encontradas, seguidos de las nociceptores polimodales; las terminaciones mecano-nociceptoras fueron las más infrecuentemente localizadas (Figura IV.1B,C).

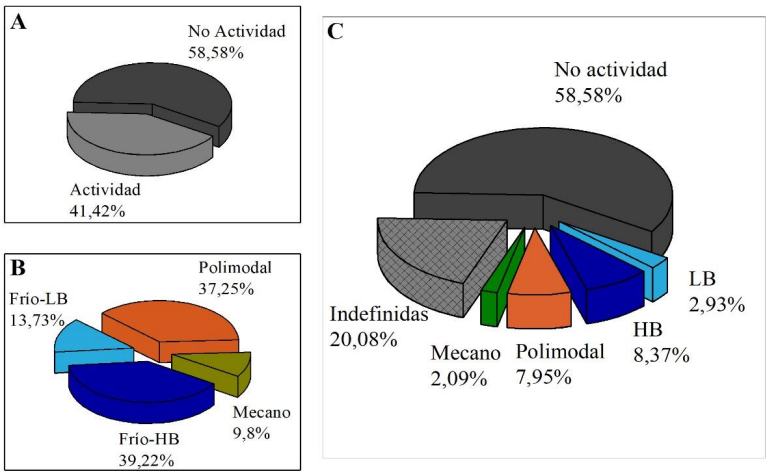

Figura IV.1. Porcentaje de éxito en el registro. Representación del porcentaje de éxito obtenido en el registro extracelular de la córnea de ratón. (A) representa el porcentaje total de actividad respecto del total de puestas realizadas (de todas las veces que se situó la pipeta sobre la superficie corneal, cuántas veces se encontró actividad frente a cuántas no). (B) representa ese mismo porcentaje de éxito desglosado entre los distintos tipos de terminaciones. (C) Es el porcentaje que representó cada tipo de terminación, teniendo en cuenta solo aquellas puestas en las que se encontró actividad y ésta se pudo clasificar.

1.1. Propiedades Funcionales.

1.1.1. Terminaciones mecano-nociceptoras.

Una fracción de las terminaciones nerviosas identificadas electrofisiológicamente en la superficie corneal (9.8 %) respondía únicamente a los estímulos mecánicos. La actividad espontánea, basal de estas terminaciones fue de 0.13 ± 0.04 imp.s^{-1} (n=18), no viéndose afectada por la estimulación mecánica repetida, excepto en una de ellas, en la que la actividad espontanea se incrementó ligeramente; la media después de realizar repetidos estímulos mecánicos fue de 0.19 ± 0.09 imp·s^{-1}, n=18.

Tabla IV.1. Características de los mecano-nociceptores y nociceptores polimodales

Edad			3 Meses		24 Meses	
Terminación			Mecano-nociceptores	Nociceptores-Polimodales	Mecano-nociceptores	Nociceptores-Polimodales
			(n=18)	(n=99)	(n=6)	(n=23)
Éxito		%	2.1	8	1.3	3.4
Frecuencia Basal		(Imp.s^{-1})	0.13 ± 0.04	0.3 ± 0.04	0.06 ± 0.02	0.3 ± 0.1
Respuesta a Frío	(Control)	(Imp.s^{-1})	7.6 ± 2.3	0.3 ± 0.03	1.7 ± 1.3	0.3 ± 0.1
	(Estímulo)	(Imp.s^{-1})	4.4 ± 1.5	0.14 ± 0.02 ***	1.8 ± 1.6	0.14 ± 0.04 *
	(Control)	(Imp.s^{-1})	0.5 ± 0.3	0.6 ± 0.1	0.2 ± 0.2	0.4 ± 0.2

	(Estímulo)	(Imp.s^{-1})	18.8 ± 2.8 ***	11.5 ± 1.2 ***	18.0 ± 6.7 **	12.1 ± 1.8 ***
	Duración	(Seg.)	1.2 ± 0.2	2.4 ± 0.3	2.2 ± 0.7	1.9 ± 0.3
	Respuesta	(%)	100	86.9	100	85.7
Respuesta a Calor	(Control)	(Imp.s^{-1})	5.4 ± 3.0	0.4 ± 0.08	0.3 ± 0.2	0.4 ± 0.1
	(Estímulo)	(Imp.s^{-1})	2.3 ± 0.7	2.3 ± 0.3 ***	0.7 ± 0.4	2.8 ± 0.7 ***
	(Umbral)	(ºC)	-	42.2 ± 0.4	-	41.5 ± 0.8

*Nota: *p<0.05; **p<0.01; ***p<0.001*

1.1.1.1. Estimulación mecánica.

Presionando la superficie corneal con la pipeta de registro (presión medida como desplazamiento del micromanipulador, 200 µm en este caso), y manteniendo dicha presión durante 5 segundos, se obtuvo una respuesta en ráfaga (*burst*) tan pronto se iniciaba la presión (Figura IV.2). La frecuencia de disparo durante el estímulo fue significativamente más alta que durante el registro control ($p < 0.001$, Tabla IV.1). La duración media de la respuesta fue de 1.2 ± 0.2 segundos (n=18), cesando bruscamente tras ese tiempo (Figura IV.2, Tabla IV .1), sin reaparecer aunque se mantuviera el estímulo mecánico incluso hasta 15 segundos (datos no mostrados). En alguna de las terminaciones mecanosensibles (n=7), se realizaron estímulos de 100 y 300 µm de desplazamiento, además de los habituales de 200 µm, para determinar el umbral de respuesta. A excepción de dos terminaciones en las que no se observó una respuesta con la aplicación del estímulo de 100 µm, todas ellas respondieron a los tres estímulos con una descarga significativamente más alta que la actividad control previa, si bien no se encontraron diferencias significativas en la magnitud de la respuesta obtenida con las diferentes intensidades (11.4 ± 3.2, 18.4 ± 2.8 y 23.8 ± 8.2 imp·s^{-1}, a 100, 200 y 300 µm, respectivamente). En cuanto a la duración de la respuesta, tampoco se han observado diferencias estadísticamente significativas entre las tres intensidades de estímulo (2.8 ± 1.4, 1.7 ± 0.6 y 2.9 ± 1.5 segundos, en 100, 200 y 300 µm de intensidad, respectivamente) (Figura IV .3).

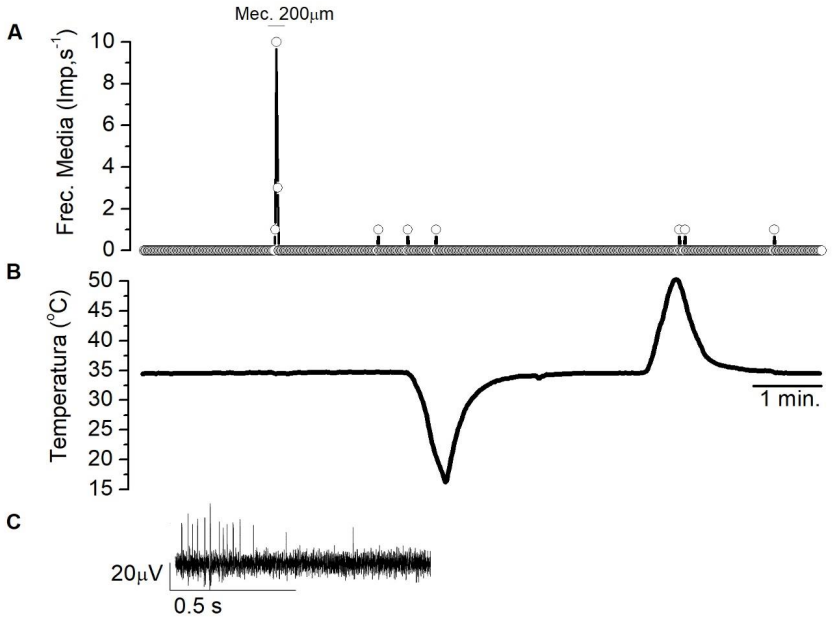

Figura IV.2. Ejemplo de la actividad de NTI en una terminación mecano-nociceptora. (A) Frecuencia media de disparo (medida en impulsos por segundo) de una terminación mecano-nociceptora expuesta a estímulos mecánico (con 200 μm de desplazamiento) y térmicos (tanto de frío como de calor). (B) Temperatura de la solución de perfusión registrada en el baño durante el mismo periodo de tiempo mostrado en A. (C) Muestra expandida del registro durante 1 s de la actividad de NTIs durante el estímulo mecánico representado en A.

1.1.1.2. Estimulación térmica.

La respuesta de las terminaciones mecano-receptoras a los estímulos térmicos, consistió en una reducción en el número de *NTIs* disparados durante una rampa de frío de14.0 ± 0.9 ºC, con una duración media de 51.3 ± 6.0 segundos n = 18, Tabla IV .1). Esta diferencia no resultó significativa estadísticamente hablando (p = 0.054); lo mismo sucedió cuando se aplicó una rampa de calor de 50.1 ± 0.5 ºC y 41.7 ± 4.0 segundos de duración (n=18; p = 0.279; Tabla IV .1) (Figura IV .3).

La Figura IV. 3 resume gráficamente los datos comentados arriba

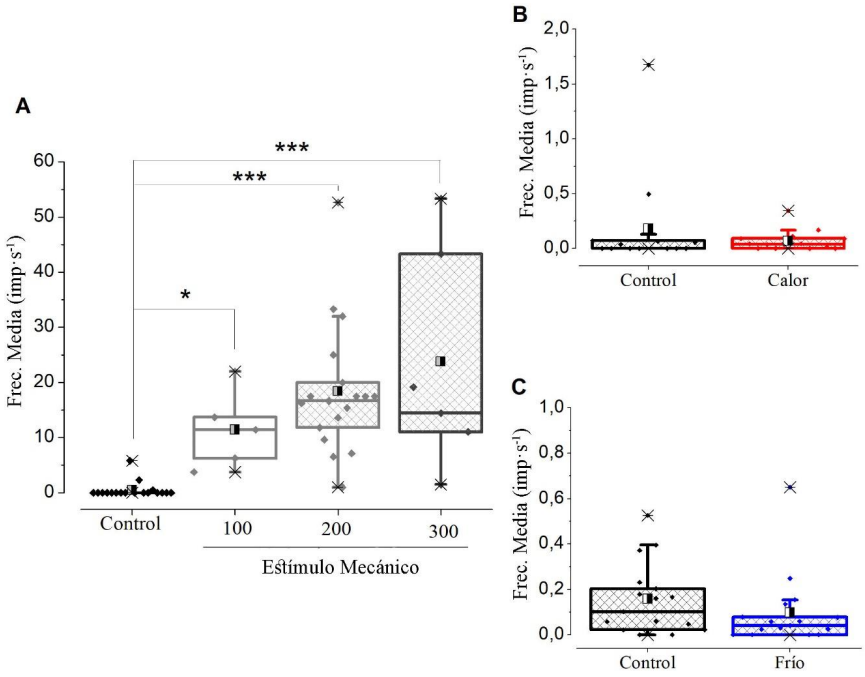

Figura IV.3. Respuesta media de las terminaciones mecano-nociceptoras a distintos estímulos mecánicos y térmicos. Frecuencia media de disparo (medida en impulsos por segundo) de las terminaciones mecano-nociceptoras (n=18) en control y durante los estímulos mecánicos (A) de 100, 200 y 300 µm de desplazamiento, en respuesta a una rampa de calor (B) y durante una rampa de frío (C). (p<0.05 y *** p<0.001).*

1.1.2. Terminaciones polimodales.

Aproximadamente un 40% de las terminaciones registradas (Figura IV.1) que presentaban durante el registro inicial una actividad espontánea claramente reconocible pero de baja frecuencia y en algunos casos nula, respondieron al calor; en su mayoría lo hicieron también a estímulo mecánico y en algún caso, a estímulo químico, siendo pues clasificadas como polimodales. En ausencia de estímulo, la actividad espontánea media de estas terminaciones nociceptoras polimodales fue de 0.3 ± 0.04 imp·s^{-1} (n=99) (Figura IV .4, Tabla IV .1).

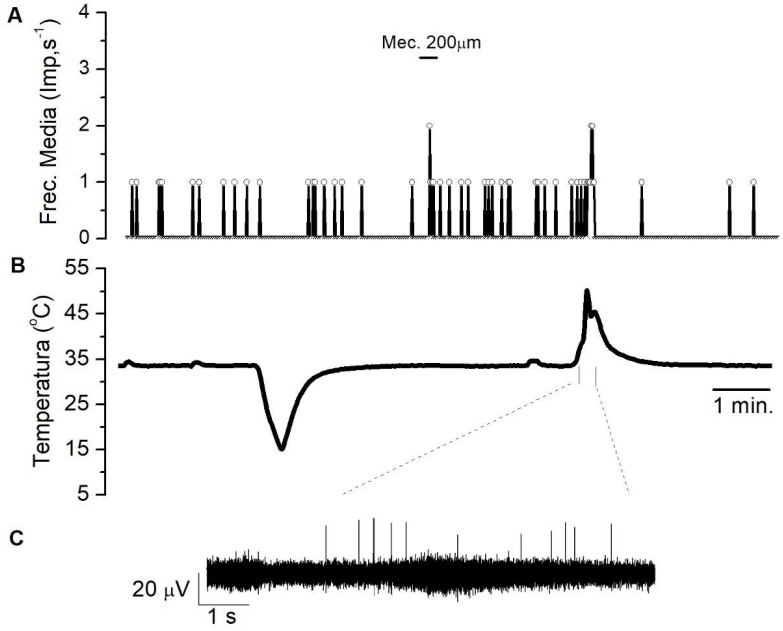

Figura IV.4. Ejemplo de la frecuencia de NTIs en una terminación nociceptora polimodal. Frecuencia media de disparo (mediad en impulsos por segundo) de una terminación nociceptora polimodal expuesta a estímulos mecánico (con 200 μm de desplazamiento) y térmicos (tanto de frío como de calor). (B) Temperatura de la solución de perfusión registrada en el baño durante el mismo periodo de tiempo mostrado en A. (C) Muestra de siete segundos del registro de la actividad de NTIs durante el estímulo de calentamiento mostrado en A.

1.1.2.1. Estimulación térmica.

1.1.2.1.1. Rampa de frío.

La aplicación de una rampa de frío (desde 34ºC a 13.6 ± 0.2 ºC) a las terminaciones nociceptoras polimodales generó una reducción en su actividad, de manera que el número

medio de *NTIs* disparados durante dicha rampa de enfriamiento fue significativamente menor que el observado durante un periodo de tiempo igual a la duración de la rampa de frío, medido inmediatamente anterior a la aplicación de ésta (la duración media de la rampa de frío fue de 43.7 ± 2.8 segundos). La actividad resultante fue de 0.29 ± 0.03 imp.s^{-1} en el periodo control, frente a 0.14 ± 0.02 imp·s^{-1} durante la estimulación con frío ($p<0.0001$, n=99; Tabla IV .1). (Figura IV .5).

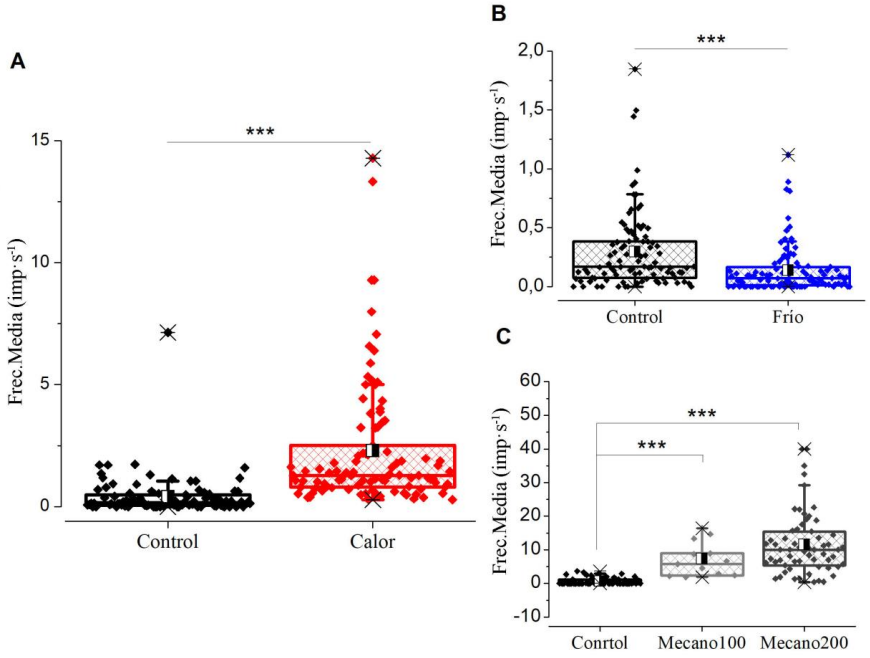

*Figura IV.5. Cambio en la frecuencia media de disparo en las terminaciones nociceptoras polimodales en respuesta a distintos estímulos mecánicos y térmicos. Frecuencia media de disparo (medida en impulsos por segundo) de las terminaciones nociceptoras polimodales en control y durante los estímulos de calor (A), de frío (B) y mecánicos de 100 y 200 µm de desplazamiento (C) (*** $p<0.001$).*

En contraste con el descenso de actividad durante el curso completo de la rampa de frío observado en la mayoría de las terminaciones nociceptoras-polimodales, en un pequeño

porcentaje de éstas (9.4 %, 5 de 53) se observó un incremento de actividad que apareció durante el tramo ascendente de dicha rampa desde los 13.6 ± 0.2 ºC de temperatura mínima alcanzada, hasta la temperatura control (34 ºC). Esta respuesta al calentamiento de vuelta al valor control se inició a una temperatura media de 26.1 ± 3.0 ºC, alcanzando una frecuencia media de 0.8 ± 0.2 imp·s^{-1}, estadísticamente superior a los 0.14 imp.s^{-1} de frecuencia media que presentaban estas terminaciones en condiciones basales (p=0.0489). La duración media de la respuesta fue de 17.8 ± 6.0 segundos (Tabla IV .2). Sin embargo, ninguna de estas cinco terminaciones presentó diferencias con el resto de terminaciones nociceptoras polimodales en sus respuestas a calor, frío o a estímulos mecánicos (Figura IV.6).

Tabla IV.2: Respuesta al Calentamiento-control		**Temperatura** (ºC)	**Actividad** (Imp.s^{-1})	**Duración** (Segundos)	**Respuesta** (%)
3 Meses	Nociceptores Polimodales	26.1 ± 3.0	0.8 ± 0.2 (n=5)	17.8 ± 6.0	9.4
	Termorreceptores de Frío HB	28.3 ± 0.3	10.7 ± 0.9 (n=46)	10.2 ± 1.7	35.1
24 Meses	Nociceptores Polimodales	27.1 ± 0.9	0.5 ± 0.1 (n=8)	29.7 ± 5.8	34.8
	Termorreceptores de Frío HB	29.3 ± 2.2	12.4 ± 2.1 (n=4)	9.5 ± 3.6	15.4

1.1.2.1.2. Rampa de calor.

La respuesta al calor se valoró aplicando una rampa de una duración aproximada de 30 segundos, que partió de aproximadamente 34 ºC y alcanzó alrededor de 50 ºC (n=99) y que evocó, en todos los casos, un marcado incremento en la frecuencia de disparo de las terminaciones nociceptoras polimodales (Figura IV .4). El umbral medio de la respuesta a calor fue de 42.2 ± 0.4 ºC, variando ampliamente de una terminación a otra, con un rango comprendido entre 35 y 50 ºC. Además, la frecuencia y duración de la descarga de *NTIs* durante la rampa de calor difirió marcadamente entre terminaciones nerviosas, con un valor de 2.3 ± 0.3 imp·s^{-1} de frecuencia media, significativamente superior respecto al registrado a

34 ºC durante los 30 segundos previos al inicio de la rampa (0.42 ± 0.08 imp·s^{-1}, $p<0.0001$; Tabla IV.1, Figura IV.5).

Todas las terminaciones nociceptoras polimodales se silenciaron durante el enfriamiento hasta la temperatura control que siguió a la rampa de calor. Alrededor del 14 % de las terminaciones no recuperó su actividad basal previa, dejando también de responder a estímulos posteriores a la rampa de calor, mientras que el resto recuperó, aproximadamente 2 minutos después de la rampa, una actividad basal similar a la observada en condiciones control (0.20 ± 0.02 imp·s^{-1} y 0.19 ± 0.04 imp·s^{-1}, respectivamente; $n = 73$, $p > 0.05$).

En 15 terminaciones se realizó una segunda rampa de calor 5-10 minutos después de la primera. En cuatro de ellas no se evocó descarga alguna de NTIs, indicando que las terminaciones habían sido inactivadas por la primera rampa; en otras 9 se observó una sensibilización, evidenciada tanto por caída del umbral térmico de aparición del primer NTI de la respuesta, hasta un valor 3.3 ± 0.4 ºC por debajo del obtenido con la primera rampa (n=3), como por el incremento en el número total de impulsos evocados por el pulso de calor sin cambio en el umbral (n = 3), o una combinación de ambos efectos, es decir, umbral de respuesta reducido y frecuencia de disparo aumentada (n = 3). En las dos terminaciones nociceptoras polimodales restantes ni la actividad ni el umbral variaron respecto a la primera rampa (Figura IV.6).

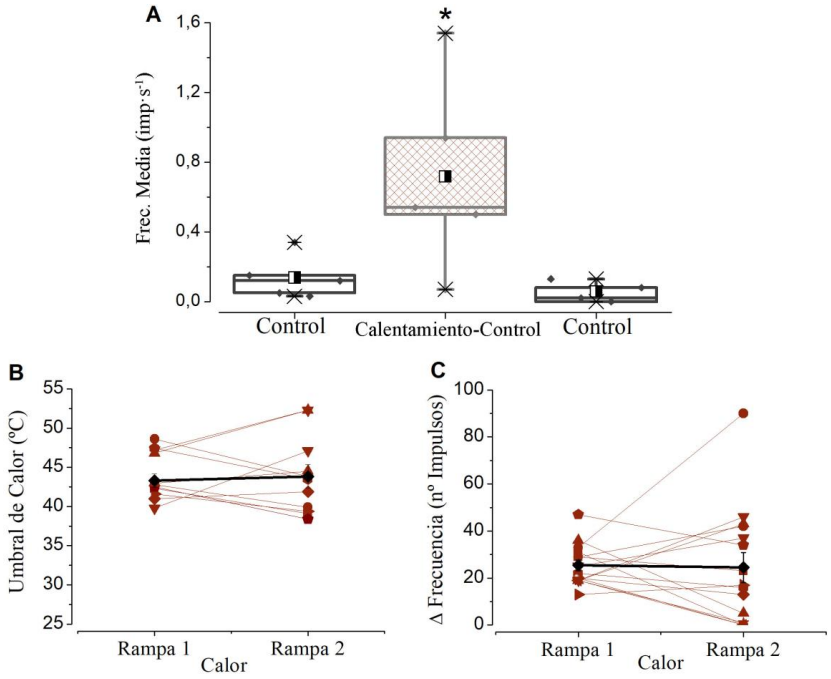

*<u>Figura IV.6. Calentamiento-control y segunda rampa de calor en nociceptores polimodales.</u> Representación de la respuestas al calentamiento-control que se observan en un pequeño número de terminaciones nociceptoras polimodales (5/51, 9.8%), así como su actividad antes y después de las misma (**A**); y variación del umbral (ºC) y de la actividad (número de NTIs en rampa) entre las dos rampas de calor realizadas en una misma terminación, con aproximadamente 10 minutos entre ellas. (**B** y **C**) (* $p<0.05$).*

1.1.2.2. Estimulación mecánica.

La estimulación mecánica con desplazamientos de 5s de duración y 200 µm de amplitud (n=84) activó a un total de 73 de las 84 terminaciones estudiadas (lo que supone un 86.9 %). Al igual que sucede en los las terminaciones mecano-nociceptoras, la respuesta a la estimulación mecánica consistió en una descarga fásica (*burst)* de NTIs al inicio del pulso mecánico, con una duración media de 2.4 ± 0.3 s, seguida de silenciamiento en la terminación durante el resto del estímulo. El número medio de NTIs evocados por el estímulo mecánico fue de 11.5 ± 1.2 imp·s^{-1}, un valor significativamente superior al de la actividad basal medida durante un periodo de tiempo similar justo antes del estímulo (0.6 ± 0.1 imp·s^{-1}, n = 73, $p < 0.001$; Tabla IV.1) (Figura IV.5).

En un total de 19 terminaciones nociceptoras polimodales, todas ellas sensibles al estímulo mecánico de 200 μm, se exploró también la sensibilidad a un estímulo mecánico de 5 segundos de duración con una intensidad de 100 μm. El porcentaje de terminaciones que respondía a esa menor indentación fue más bajo, del 63.2 % (12 de 19), aunque en las que ya respondían no se observaron diferencias significativas en la duración de la respuesta (2.5 ± 0.4 segundos) ni en la frecuencia media de NTIs disparados durante la misma (7.4 ± 1.5 $imp \cdot s^{-1}$) respecto a las estimulaciones con 200 μm y sí respecto al control ($p<0.001$) (Figura IV.5).

En siete de las terminaciones polimodales que habían disparado *NTIs* con la estimulación mecánica de 200 μm, el estímulo se repitió 2 minutos después, a la misma intensidad pero, en esta ocasión manteniendo la presión durante un período de 15 segundos. La respuesta de disparo observada fue de nuevo transitoria, estando compuesta por una fase inicial con disparo en *burst* de 1-2 s de duración y regreso al nivel de disparo basal durante el resto del estímulo. Hay que señalar que la actividad generada por este segundo estímulo mecánico (9.3 ± 2.1 $imp \cdot s^{-1}$, n = 7) no fue significativamente diferente de la evocada por el primero.

1.1.2.3. Estimulación química.

Con el objetivo de definir la quimio-sensibilidad de las terminaciones polimodales, se aplicaron estímulos químicos a terminaciones que habían respondido previamente a una rampa de calor y no a la rampa de frío.

El agonista del canal TRPV1 capsaicina (1 μM), activó a 25 de las 26 terminaciones en las que fue probado (0.2 ± 0.06 $imp \cdot s^{-1}$ antes y 2.0 ± 0.2 $imp \cdot s^{-1}$ en los 30 s de máxima actividad, durante los 3 minutos que duró la aplicación de capsaicina antes de su lavado, $p < 0.0001$) (Tabla IV.3; Figura IV.7).

Asimismo, el agonista del canal TRPA1, AITC (100 μM) probado en un total de 9 terminaciones, activó débilmente a cuatro de ellas (0.17 ± 0.06 antes y 0.78 ± 0.24 $imp \cdot s^{-1}$ durante los 30 s de máxima actividad durante los 3 minutos de perfusión del compuesto) (Tabla IV.3; Figura IV.7).

Tabla IV.3: Nociceptores-Polimodales: Estimulación Química		
Estímulo	Control (Imp.s^{-1})	Respuesta
Capsaicina (1 µM) ***	0.20 ± 0.06 (n=26)	2.0 ± 0.2
AITC (100 µM)	0.17 ± 0.06 (n=4)	0.78 ± 0.24
Hiperosmolar (850 mOms) *	0.20 ± 0.1 (n=5)	0.50 ± 0.1
Hiperosmolar (1000 mOms) *	0.50 ± 0.4 (n=6)	1.40 ± 0.7
Sopa Inflamatoria **	0.1 ± 0.04 (n=5)	0.28 ± 0.07

*NOTA: * p<0.05, ** p<0.01 y *** p<0.001*

En un total de 23 terminaciones identificadas como polimodales, se probó el efecto de la perfusión con soluciones hiperosmolares de distinta fuerza osmótica (Tabla IV.3; Figura IV.8). En todas ellas, la actividad basal se incrementó significativamente con soluciones a partir de 850 y 1000 mOsm.kg^{-1} durante al menos 3 minutos· pero no con osmolaridades inferiores (340, 360, 460 y 600 mOsm·kg^{-1}). Además del aumento de la frecuencia de disparo, la aplicación de las soluciones hiperosmolares de 850 y 1000 mOsm·kg^{-1} produjo una alteración en la forma de los NTIs, que pasaron a ser más anchos y de menor amplitud.

Para finalizar, la aplicación de sopa inflamatoria (ver métodos) a siete terminaciones polimodales, durante cinco minutos, evocó un incremento significativo en la tasa de disparo de *NTIs* en cinco de ellas (Tabla IV.3; Figura IV.7). El mentol (agonista del canal TRPM8, 20µM) fue probado en una de las terminaciones polimodales-nociceptoras, no apreciándose ningún cambio de actividad eléctrica, ni a 34 ºC ni durante la rampa de frío.

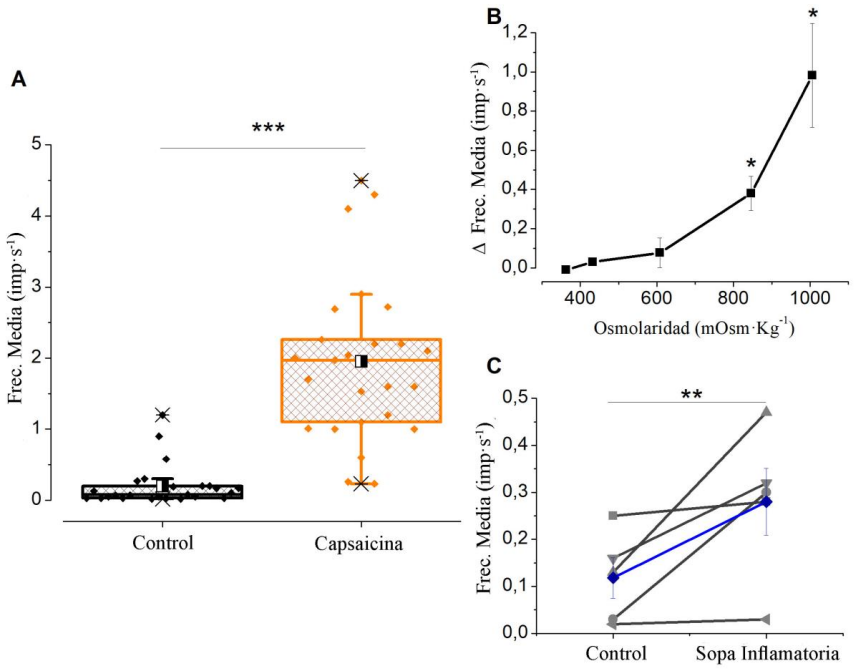

Figura IV.7.Frecuencia media de disparo de las terminaciones nociceptoras polimodales en respuesta a distintos estímulos químicos. Respuesta de los nociceptores polimodales a Capsaicina 1 μM (A), soluciones hiperosmolares (B) y sopa inflamatoria (C) (p<0.05, ** p<0.01 y *** p<0.001).*

1.1.3. Terminaciones termorreceptoras de frío.

Las terminaciones corneales que responden a frío representan, aproximadamente, un 50 % del total de las terminaciones registradas (Figura IV.1). Se caracterizan por el disparo tónico de NTIs a 34ºC de variable frecuencia y el incremento, también variable, de esa actividad cuando se aplica una rampa de frío.

Dentro de las terminaciones corneales de frío, hemos identificado dos grupos claramente diferenciados, tanto por su actividad basal como por su respuesta al frío. Si nos centramos en la frecuencia media de disparo que presentaron a 34 ºC y en ausencia de estímulo, podemos clasificarlas en terminaciones de frío con alta actividad basal (HB, del inglés *High Background activity*), cuya frecuencia media es de 5.8 ± 0.4 imp·s^{-1} (n=131), y terminaciones de frío con baja actividad basal (LB, del inglés *Low Background activity*), que presentaron

una frecuencia basal media significativamente inferior, de 0.4 ± 0.04 imp·s^{-1} (n=66, p<0.0001) (Tabla IV.4). En ratones jóvenes, la relación en número de estos dos tipos de terminaciones de frío es, aproximadamente, de 3:1 a favor de las HB (Figura IV.8, Tabla IV.4).

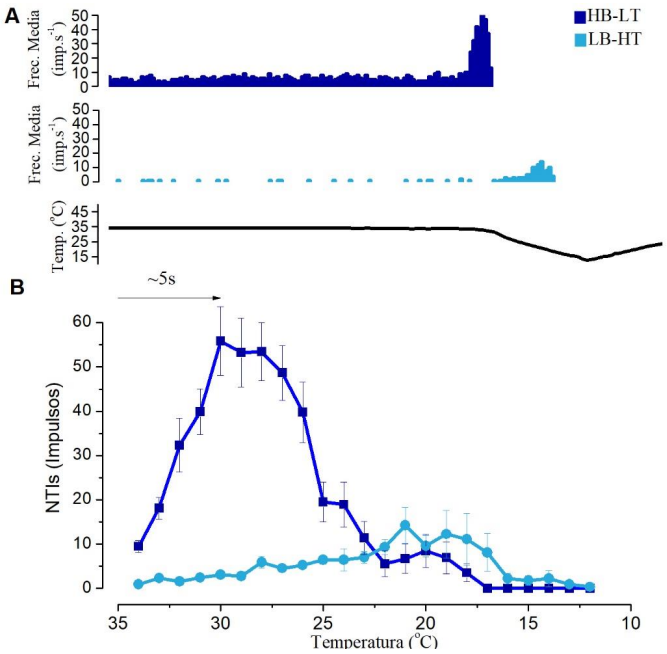

Figura IV.8. Poblaciones Termorreceptoras de Frío en ratones jóvenes. Ejemplos de la descarga de las terminaciones de frío HB y LB en respuesta a una rampa de frío desde 34 hasta 15 ºC (A) en ratones jóvenes. Y curva estímulo-respuesta de los termorreceptores HB y LB (B), en la que se representan los valores de la frecuencia media de disparo (imp·s^{-1}) frente a la temperatura durante una rampa de frío (desde 34 hasta 12 ºC) en aproximadamente 30 segundos de duración.

1.1.3.1. Rampas de frío.

La respuesta dinámica a las reducciones de temperatura se estudió aplicando rampas de frío (ver Métodos)

1.1.3.1.1. Termorreceptores HB.

Las terminaciones corneales de frío que presentaban una actividad basal elevada, apreciable inmediatamente después de aplicar la pipeta sobre la superficie corneal, respondían a la rampa de frío rápidamente, con un incremento robusto en su frecuencia de disparo. El patrón inicial de descarga a 34ºC, con NTIs aislados que aparecen regularmente, se transforma con el inicio de la rampa de frío en un disparo en ráfagas con un umbral medio de 32.5 ± 0.08 ºC que, tras alcanzar un pico de máxima respuesta (49.5 ± 1.8 imp·s^{-1}) a una temperatura media de 25.9 ± 0.4 ºC, los *NTIs* reducen su frecuencia y se silencian a una temperatura media de 23.9 ± 0.4 ºC, bastante antes de alcanzar la mínima temperatura de la rampa (14.5 ± 0.3 ºC). La frecuencia media de disparo de las terminaciones durante su respuesta a frío fue de 31.0 ± 1.1 imp·s^{-1}, que representa un incremento significativo de la frecuencia basal (5.8 ± 0.4 imp·s^{-1}, p<0.0001) (Figura IV.9 y IV.10, Tabla IV.4).

Tabla IV.4: Termorreceptores de Frío: Respuesta a Rampa de frío

Termorreceptor de frío		HB (n=131)	LB (n=66)
Actividad Basal	(Imp.s^{-1})	5.8 ± 0.4	0.4 ± 0.04***
Umbral de Enfriamiento	(ºC)	32.5 ± 0.08	27.3 ± 0.5***
Pico de máxima respuesta	(Imp.s^{-1})	49.5 ± 1.8	10.4 ± 1.2***
Respuesta a Frío	(Imp.s^{-1})	31.0 1.1	6.5 ± 0.8***
Tasa de Éxito	(%)	8.4	2.9

*NOTA: *** p<0.001.*

En muchas de estas terminaciones, la actividad de NTIs no reaparecía durante la recuperación de la temperatura basal hasta que se alcanzaban los 31 ºC; Sin embargo, en un 35 % de ellas (46 de 131 terminaciones), durante la fase de recalentamiento de vuelta a la temperatura basal de 34 ºC, se observaba una descarga transitoria de NTIs con una duración media de 10.2 ± 1.7 segundos y un número total de110.3 ± 18.7 NTIs, (correspondiendo a una frecuencia

media de 10.7 ± 0.9 imp.s^{-1}) y que aparece cuando se alcanzan los 28.3 ± 0.3 ºC (Tabla IV.3), seguida de un periodo de silencio hasta subir a 31.4± 0.3 ºC, momento en el que la descarga de NTIs se recupera gradualmente hasta llegar a una frecuencia media similar a la exhibida por la terminación antes de la rampa de frío.

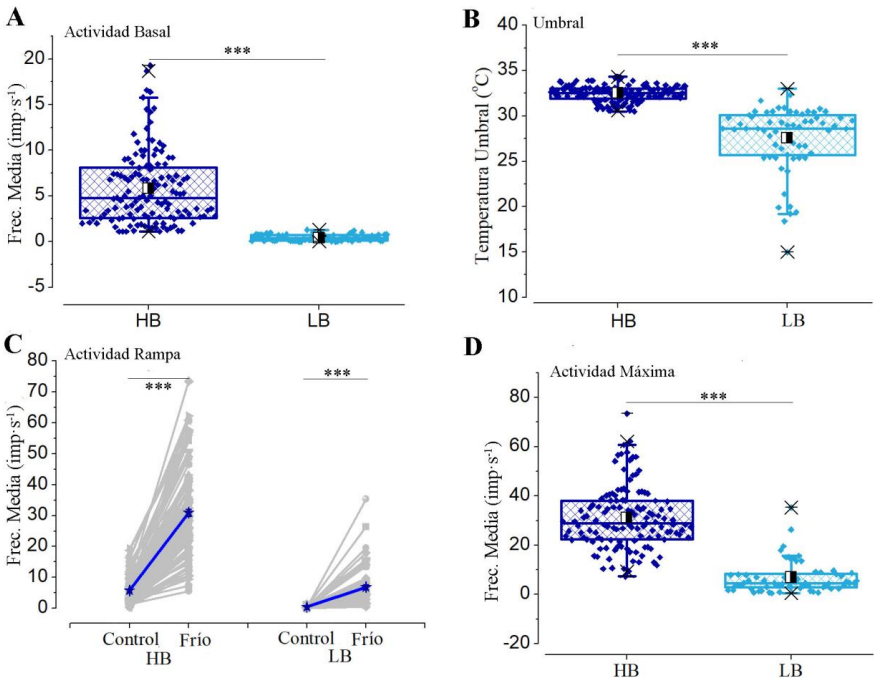

*Figura IV.9. Parámetros comparativos de la respuesta a frío en los termorreceptores HB y LB de ratones jóvenes. Comparativa de la frecuencia basal (**A**), umbral de respuesta a frío (**B**), incremento de la frecuencia de disparo en respuesta a frío (**C**) y el pico de máxima frecuencia durante dicha respuesta (**D**) entre los termorreceptores de frío HB (n=131) y LB (n=64) (*** p<0.001).*

1.1.3.1.2. Termorreceptores LB.

El segundo grupo de terminaciones corneales de frío disparaba a la temperatura basal de 34ºC con una frecuencia baja y respondía más débilmente a las rampas de frío (0.4 ± 0.04 imp.s^{-1} y 6.5 ± 0.8 imp.s^{-1} en actividad basal y en respuesta a frío, respectivamente, (n=64, p<0.0001;

Tabla IV.4). El umbral de temperatura al que se iniciaba la respuesta a frío cuando se aplicaba una rampa continua fue de 27.3± 0.5 ºC (n=69), significativamente más bajo que la temperatura umbral de las terminaciones HB ($p<0.0001$). Su pico de máxima respuesta (10.4 ± 1.2 $imp.s^{-1}$) y la temperatura a la que se alcanzaba este valor (21.4 ± 0.7 ºC) también resultaron ser significativamente inferiores en las terminaciones LB en comparación con los mismos parámetros en las HB ($p<0.0001$ en ambos parámetros), al igual que ocurrió con la frecuencia media de su respuesta a frío (6.5 ± 0.8 $imp.s^{-1}$, $p<0.0001$) (Figura IV.9 y IV.10, Tabla IV.4). Además, la temperatura media a la que silenciaron su descarga durante el enfriamiento fue de 18.0 ± 0.6 ºC; en ninguna de las terminaciones LB se detectó respuesta durante la fase de calentamiento, reapareciendo su actividad basal a los 30.6 ± 0.4 ºC (n = 69). Este tipo de termorreceptor de frío de baja actividad basal y alto umbral de respuesta al frío representa alrededor del 28 % del total de terminaciones sensibles al frío encontradas en la córnea.

Dentro del grupo de termorreceptores de frío clasificados como LB, se han encontrado también dos terminaciones cuyas características en respuesta a frío diferían de las del resto pues, a pesar de presentar una actividad basal de 0.12 $imp.s^{-1}$, daban una respuesta robusta a un umbral reducido (32.7 ± 0.4 ºC), asemejándose más a la observada en el grupo de termorreceptores HB. También eran más similares a éstos en su pico de máxima respuesta (27.5 ± 8.5 $imp.s^{-1}$) y el valor de su actividad media durante la respuesta (15.8 ± 2.2 $imp.s^{-1}$).

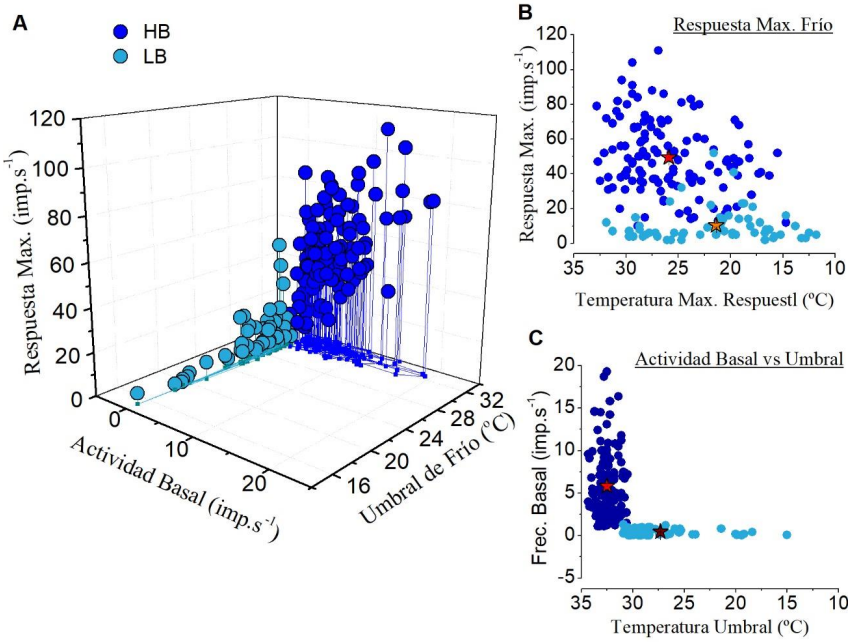

Figura IV.10. Representación individual en tres dimensiones de la distribución de los termorreceptores de frío HB y LB atendiendo a su actividad basal a 34 ºC, su pico de máxima respuesta al frío y su umbral de respuesta (A); Pico de respuesta máxima enfrentada a la temperatura a la que fue alcanzada (B). Frecuencia de disparo basal de cada termorreceptor de frío frente a su umbral de respuesta (C). En las tres representaciones se pueden apreciar los dos grupos de termorreceptores de frío corneales predominantes en ratones jóvenes (HB-LT y LB-HT).

1.1.3.2. Escalones de frío

Tras analizar la respuesta de las terminaciones de frío a los cambios dinámicos de temperatura (rampa de frío), se estudió en un grupo de ellas, tanto del tipo HB como del LB, las características de la descarga para valores estáticos de temperatura, alcanzados con escalones decrecientes y sostenidos (2 min) de frío a 34, 30, 25 y 20 ºC y midiendo las características de la descarga de NTIs durante los 30 segundos finales de cada escalón.

1.1.3.2.1. Termorreceptores HB.

En las terminaciones HB, el valor de la frecuencia basal a 34 ºC se incrementaba significativamente con cada escalón descendente de temperatura con respecto al anterior, a excepción del escalón de 20 ºC, en el que, posiblemente debido al bajo número de datos (n=5), tan solo se observan diferencias significativas con respecto al control (escalón de 34 ºC) (Figura IV.11, Tabla IV.5).

Tabla IV.5. Análisis de escalones de frío en termorreceptores HB y LB.

Terminación			HB		LB	
Frecuencia Media	34 ºC	(Imp.s^{-1})	6.7 ± 0.6		0.6 ± 0.2	
	30 ºC	(Imp.s^{-1})	12.6 ± 1.0***	(n=40)	1.3 ± 0.3**	(n=20)
	25 ºC	(Imp.s^{-1})	14.0 ± 0.8***		1.0 ± 0.2	
	20 ºC	(Imp.s^{-1})	15.4 ± 1.5**	(n=5)	0.7 ± 0.2	(n=9)
Ratio	30 ºC		2.3 ± 0.2***	(n=32)	4.8 ± 2**	(n=20)
	25 ºC		2.8 ± 0.4***		5.2 ± 1.6*	
	20 ºC		2.4 ± 0.4	(n=5)	2.5 ± 0.5	(n=9)
Parte dinámica	34-30 ºC	(Imp.s^{-1})	29.9 3.7	(n=40)	3.1 ± 0.4	(n=20)
	30-25 ºC	(Imp.s^{-1})	35.7 4.4		3.8 ± 0.5	
	25-20 ºC	(Imp.s^{-1})	38.5 8.1	(n=5)	3.1 ± 0.8	(n=9)

*Nota: ratio hace referencia al incremento de la actividad para cada escalón normalizada con el escalón control de 34 ºC. La estadística se ha realizado entre cada escalón y el escalón control. * p<0.05, ** p<0.01, *** p<0.001.*

En los termorreceptores HB, la frecuencia de descarga de NTIs por segundo durante los distintos escalones térmicos, normalizada respecto a la actividad del escalón control a 34ºC,

mostró en cada escalón un incremento significativo para 30ºC y 25 ºC ($p<0.0001$) (Figura IV.11).

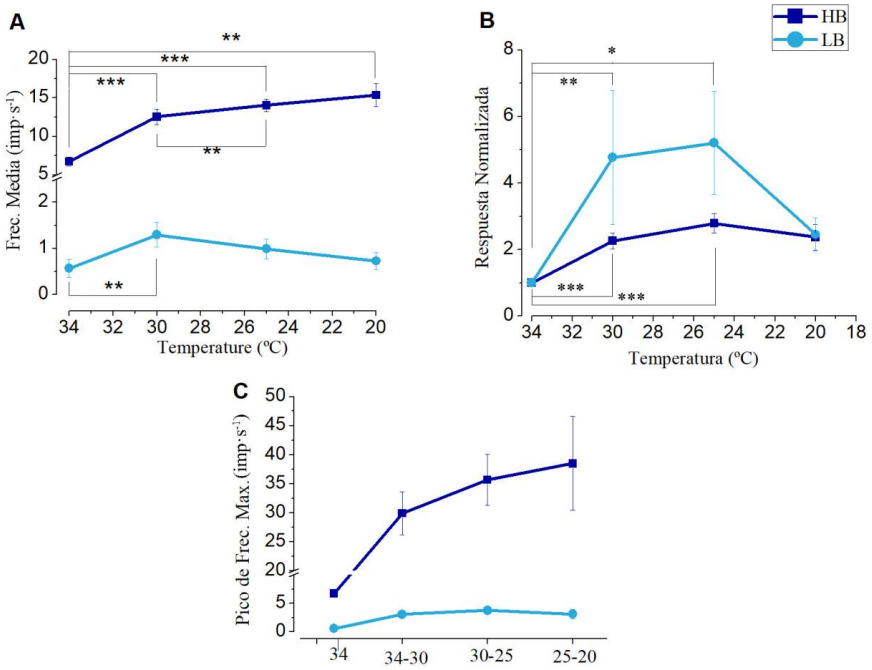

*Figura IV.11. Respuesta a frío evocada por escalones de temperatura. (A) Frecuencia de disparo media en respuesta a escalones de temperatura (34, 30, 25 y 20 ºC) de termorreceptores HB y LB. (B) Valores de respuesta a escalones de las mismas terminaciones representadas en A, normalizados respecto al escalón de 34 ºC. (C) Pico de frecuencia máxima de las mismas terminaciones de A y B durante la fase dinámica de cada escalón de temperatura estudiado (34-30, 30-25 y 25-20 ºC). * p<0.05, ** p<0.01, *** p<0.001.*

El incremento en la frecuencia de disparo de la terminación en cada escalón vino acompañado, en todos los casos, también de un cambio en el patrón de disparo, comenzando a ocurrir en *bursts* a partir del escalón de 30 ºC y acompañado de un aumento en el número de impulsos por *burst* en cada escalón (Figura IV.12).

Si analizamos ahora la parte inicial, dinámica, de los escalones, correspondiente al momento en el que la temperatura disminuye entre un escalón y el siguiente (a un ritmo medio de 0.8 ºC.s^{-1}), observamos que el pico máximo de respuesta se va incrementando con cada escalón (Tabla IV.5; Figura IV.11).

1.1.3.2.2. Termorreceptores LB.

En los termorreceptores de frío LB, el incremento en la frecuencia de disparo de NTIs en los diferentes escalones es mucho más moderado, y tan solo es significativa la diferencia entre el escalón de 30 ªC y el control (34 ºC) como se recoge en la Tabla IV.5Figura IV.11).

Sin embargo, la actividad normalizada de cada escalón respecto al escalón, refleja un incremento de actividad más pronunciado para los escalones de 30 y 25 en los termorreceptores de frío LB que el observado en los termorreceptores HB (Tabla IV.5; Figura IV.11).

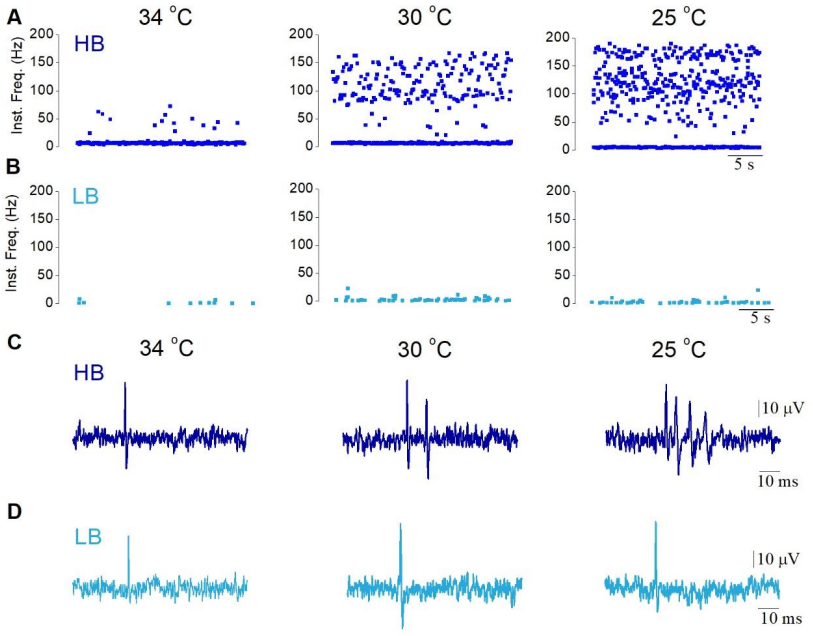

Figura IV.12. Ejemplo de Frecuencia Instantánea en tres escalones de temperaturas diferentes, para los termorreceptores HB (A) y LB (B). Nótese el disparo regular en burst de

las terminaciones de frío HB en los escalones de 30 y 25 ºC. Ejemplo de NTIs registrados en termorreceptores de frío HB (C) y LB (D) a los distintos escalones de temperatura.

Adicionalmente y al contrario de lo que sucedía con las terminaciones termorreceptoras de frío HB, en las terminaciones LB no se encontraron NTIs disparando en ráfagas (*bursts*) en ninguno de los escalones estudiados (Figura IV.12).

En lo que se refiere a la parte dinámica de los escalones, el pico máximo de respuesta en los termorreceptores de frío LB se mantuvo constante en cada escalón (Tabla IV.5; Figura IV.11), al contrario de lo que ocurría en los termorreceptores HB.

1.1.3.3. Rampas de calor.

Un 60.7 % de las terminaciones HB respondieron también a la rampa de calor con una descarga transitoria de NTIs ("respuesta paradójica") que comenzó a una temperatura media de 42.3 ± 1.0 ºC, alcanzando una frecuencia media en la descarga de NTIs evocados por calor de 34.3 ± 9.0 imp·s^{-1}, significativamente superior a los 8.1 ± 1.9 imp·s^{-1} medidos durante los 30 segundos previos al inicio de la rampa de calor (n=17, p=0.0045; Tabla IV.6).

Tabla IV.6. Respuestas a calor y a la estimulación mecánica de los termorreceptores de frío.

Terminación			HB		LB	
Respuesta Mecánica	(Control)	(Imp.s^{-1})	7.3 ± 1.3		0.9 ± 0.2	
	(Estímulo)	(Imp.s^{-1})	21.5 ± 2.5 ***	(n= 39)	12.3 ± 1.3***	(n=41)
	Duración	(Seg.)	4.3 ± 0.8		3.1 ± 0.3	
	Respuesta	(%)	83		77	
Respuesta a Calor	(Control)	(Imp.s^{-1})	8.1 ± 1.9	(n= 17)	0.8 ± 0.2	(n=24)
	(Estímulo)	(Imp.s^{-1})	34.3 ± 9.0 **		3.1 ± 0.5 ***	

	(Umbral)	(ºC)	42.3 ± 1.0		43.9 ± 0.7
	Respuesta	(%)	61		75

*NOTA: ** p<0.01; *** p<0.001.*

Se estudió también la posible correlación entre la respuesta evocada en algunas de estas terminaciones de frío HB cuando se asciende a la temperatura control de 34 ºC desde la rampa de frío (calentamiento-control) y la presencia y características de las respuestas a la rampa de calor. En 13 terminaciones HB que habían presentado una descarga durante la recuperación de la rampa de frío, se realizó además una estimulación con la rampa de calor. 9 de ellas (69.2 %) respondieron también a la rampa de calor, mientras que el resto no lo hizo. Las características de la respuesta a la rampa de calor no difieren entre el grupo que presentó respuesta al calentamiento-control frente al que no.

El 75% de las terminaciones LB respondió a la rampa de calor (24 de 32). En ellas, el umbral para la respuesta a calor no difirió del observado en las HB (43.9 ± 0.7 ºC), aunque la frecuencia media de disparo durante los 17.0 ± 2.2 segundos que duró la respuesta a calor, alcanzó tan solo los 3.1 ± 0.5 imp.s^{-1}, pero era significativamente diferente de la medida en condiciones control, 30 segundos antes de la rampa (0.8 ± 0.2 imp.s^{-1}; n=24, p<0.0001) (Tabla IV.6; Figura IV.13).

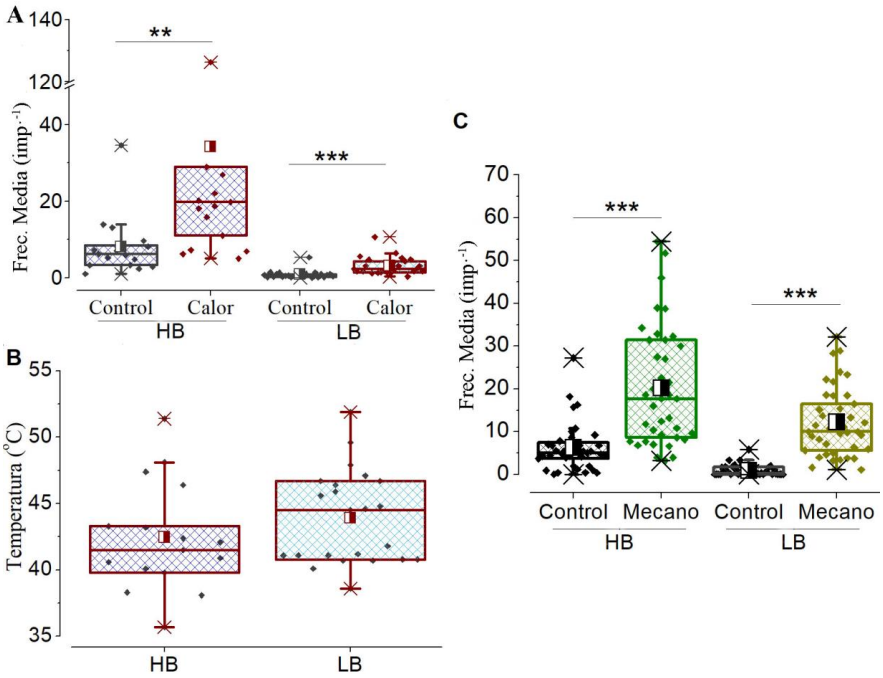

*Figura IV.13. Respuesta de los termorreceptores de frío HB y LB a estímulos mecánicos y de calor. Frecuencia media de disparo (medida en impulsos por segundo) de los termorreceptores HB y LB en control y durante el estímulo de calor (A), durante el estímulo mecánico de 200 µm de desplazamiento (C) y representación de los umbrales de calor registrados en ambas poblaciones (B) (** p<0.01 y *** p<0.001).*

1.1.3.4. Estimulación Mecánica.

La aplicación de fuerza mecánica mediante un desplazamiento de la pipeta de registro sobre la superficie corneal de 200 micras, mantenido durante 5 segundos (similar al realizado en las terminaciones nociceptoras mecano y polimodales), evocó una respuesta en modo de *burst* en un 83.0 % del total de terminaciones de frío HB exploradas (39 de 47). La amplitud de esta respuesta fue significativamente mayor que la frecuencia basal medida en los 10 segundos previos al estímulo (n=39, p<0.0001; Tabla IV.6).

En el caso de las terminaciones corneales de frío LB, 77.4 % (41 de 53) respondieron al estímulo mecánico, una proporción muy semejante a la observada con los HB. La respuesta

evocada duró 3.01 ± 0.3 segundos e incrementó la actividad basal desde 0.9 ± 0.2 imp.s^{-1} a 12.3 ± 1.3 imp.s^{-1} (n=41, p<0.0001) (Tabla IV.6; Figura IV.13).

La duración de la respuesta evocada por el estímulo mecánico de 200 micras fue significativamente más larga en las terminaciones HB (p=0.0022). Sin embargo, esto puede deberse a la diferencia en la actividad basal entre terminaciones HB y LB, ya que los NTIs de la descarga basal durante los 5 segundos de duración del estímulo se sumarían a los evocados por el estímulo mecánico, haciendo difícil definir de manera fiable el final de la respuesta a dicho estímulo.

1.1.3.5. Estimulación Química.

1.1.3.5.1. Agonistas del canal TRPM8.

Para comprobar la implicación del canal TRPM8 en las terminaciones termorreceptoras de frío, se llevó a cabo la perfusión de las córneas con uno de sus agonistas, mentol (20 μM), durante tres minutos.

Tabla IV.7. Respuesta a mentol de los termorreceptores de frío.

Terminal			HB				LB			
			Control	Mentol	Washing		Control	Mentol	Washing	
34 ºC	Frecuencia media a 34ºC	(Imp.s^{-1})	5.6 ± 1.4	18.6 ± 3.6**	7.4 ± 3.0	(n=11)	0.5 ± 0.2	2.0 ± 0.6*	0.7 ± 0.5	(n=6)
Rampa de frío	Frecuencia máxima	(Imp.s^{-1})	45.9±7.5	64.6 ± 8.0*	48.9±7.5		8.5 ± 1.4	16.2 ± 3.7	14.7±1.4	
	Frecuencia media	(Imp.s^{-1})	29.3±4.8	40.9 ± 4.9	31.8±3.8	(n=8)	4.4 ± 0.7	10.1 ± 2.2	7.2 ± 0.9	(n=5)
	Silenciamiento	(ºC)	24.9±0.8	28.1 ± 1.0*	26.1±0.8		18.5 ± 0.5	19.9 ± 1.7	15.8±0.8	
	Umbral de respuesta	(ºC)	32.7±0.3	32.6 ± 0.6	32.5±0.5		25.8 ± 2.0	28.3 ± 1.0	26.6±1.8	

*NOTA: *p<0.05; ** p<0.01; *** p<0.001.*

En los termorreceptores de frío HB, el mentol incrementó significativamente la frecuencia media de la terminación a 34 ºC (p=0.0017) regresando tras cinco minutos a valores control (Tabla IV.7). Además de esta clara respuesta a temperatura control, el mentol incrementó también el valor de la máxima respuesta alcanzada por la terminación durante una rampa de frío (p=0.0300 para control vs mentol). Lo hizo igualmente, aunque no de manera significativa, con la frecuencia media durante la respuesta en rampa de frío (p=0.0732 para control vs mentol). Además, las terminaciones perfundidas con mentol, se silenciaron durante la rampa de frío a temperaturas superiores respecto al control y tras lavado (p=0.0266 para control vs mentol) (Tabla IV.7).

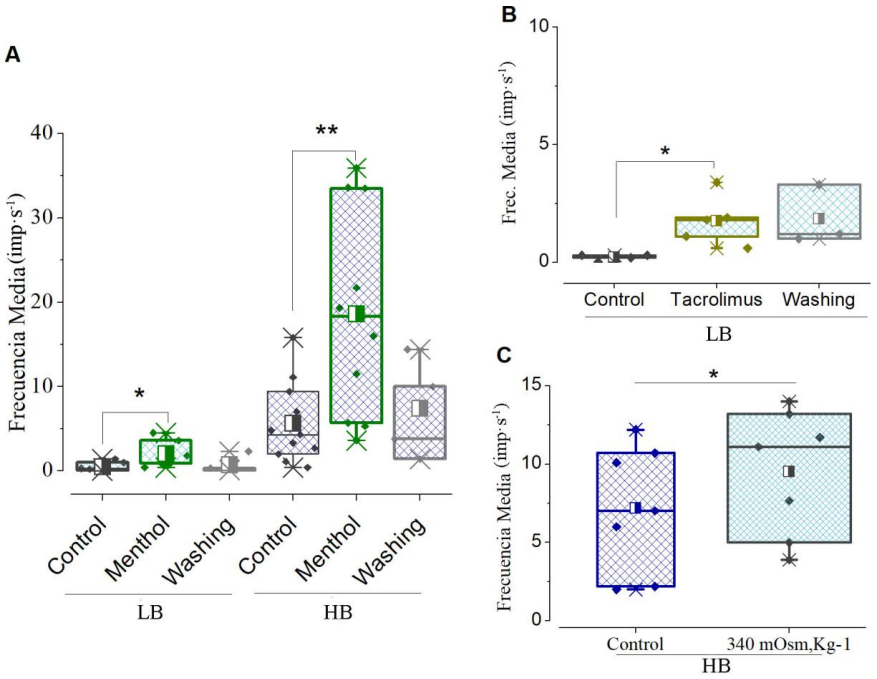

Figura IV.14. Respuestas de los termorreceptores corneales de frío HB y LB a distintos agonistas del canal TRPM8. Incremento de actividad observada en los termorreceptores de frío corneales HB y LB durante la perfusión a 34 ºC de Mentol (20 μM) (A), Tacrolimus (30 μM) (B) y solución hiperosmótica (340 mOsm.Kg^{-1}) (C) (p<0.05 y ** p<0.01).*

Sobre los termorreceptores de frío LB el mentol, perfundido a 34 ºC a la misma concentración que en los HB, generó efectos similares, aunque de menor envergadura. Así la frecuencia

media a temperatura control (34 ºC) se incrementó desde 0.5 ± 0.2 imp.s^{-1}, hasta 2.0 ± 0.6 imp.s^{-1} (n=6, p=0.0288); este incremento desapareció, regresando a los valores controles tras un periodo de lavado de 5 minutos (Tabla IV.7; Figura IV.14).

Sin embargo, tanto la máxima frecuencia de disparo durante la rampa como la actividad media durante la respuesta a frío) mostraban una tendencia a aumentar, pero sin alcanzar un nivel suficiente de significación (n=5 y p=0.1188, para el pico de máxima actividad; y n=5 y p=0.1932 para la actividad en respuesta) (Tabla IV.7).

En esta población de termorreceptores de frío corneales LB se ensayó también el agonista del TRPM8, Tacrolimus, cuya eficacia sobre los termorreceptores de frío HB ha sido demostrada recientemente [Arcas et al., 2018.] La perfusión con Tacrolimus 30 µM a 34 ºC, evocó un incremento en la frecuencia media basal en las terminaciones de frío LB (n=5; p=0.0291) (Tabla IV.8; Figura IV.14). Sin embargo, este fármaco no consiguió incrementar de manera significativa la máxima respuesta de la terminación durante la rampa de frío ni la frecuencia media de disparo durante dicha respuesta (Tabla IV.8).

Tabla IV.8. Efecto del Tacrolimus y 4-AP en los termorreceptores de frío LB				**LB**			
				Control	**Tratamiento**	**Lavado**	
Tacrolimus	**34 ºC**	**Frecuencia media**	(Imp.s^{-1})	0.2 ± 0.1	1.8 ± 0.5*	1.8 ± 0.8	
	Rampa de frío	**Frecuencia máxima**	(Imp.s^{-1})	6.4 ± 1.4	10.2 ± 2.7	9.0 ± 3.0	(n=5)
		Frecuencia media	(Imp.s^{-1})	4.4 ± 0.7	6.9 ± 2.0	5.6 ± 1.3	
4-AP	**34 ºC**	**Frecuencia media**	(Imp.s^{-1})	0.4 ± 0.1	7.5 ± 1.5	1.0 ± 0.2	(n=3)

*NOTA: * p<0.05.*

Finalmente, la perfusión de la córnea con una solución hiperosmolar de 340 mOsm.kg^{-1} generó un incremento de la frecuencia de disparo basal a 34ºC (n=7, p = 0.0141) en los termorreceptores de frío HB. En tres terminaciones LB, la perfusión con una solución hiperosmolar (397 mOsm.kg^{-1}) incrementó también la frecuencia basal de NTIs a 34 ºC (Tabla IV.9; Figura IV.14).

1.1.3.5.2. Agonistas del canal TRPV1

En un total de siete termorreceptores de frío HB la perfusión con el agonista del canal TRPV1, capsaicina (1 µM), generó un incremento significativo de la actividad a 34 ºC (p=0.0012) (Tabla IV.9; Figura IV.15). Cuatro de estas siete terminaciones respondían también a una rampa de calor (de 34 a 50 ºC) sin que su respuesta a capsaicina fuera distinta de las insensibles al calor (datos no mostrados).

En los termorreceptores corneales de frío LB la capsaicina (1 µM), evocó también un incremento significativo en la frecuencia media a 34 ºC (p=0.0159; Tabla IV.9).

Tabla IV.9. Respuestas a soluciones hiperosmóticas y a capsaicina de los termorreceptores de frío.

Terminación			HB		LB	
Solución hiperosmótica	(Control)	(Imp.s^{-1})	7.2 ± 1.2		0.2 ± 0.1	
	(Estímulo)	(Imp.s^{-1})	9.5 ± 1.5 *	(n= 7)	2.0 ± 1.7	(n=3)
	(Lavado)	(Imp.s^{-1})	-		0.4 ± 0.1	
Capsaicina	(Control)	(Imp.s^{-1})	2.3 ± 0.8		0.6 ± 0.2	
	(Estímulo)	(Imp.s^{-1})	14.8 ± 2.5**	(n= 7)	9.4 ± 2.4*	(n=6)

*Nota: la osmolaridad de la solución hiperosmótica usada sobre los termorreceptores HB fue de 340 mOsm.kg^{-1}, mientras que para lo termorreceptores LB fue de 397 mOsm.kg^{-1}. *p<0.05; ** p<0.01.*

Hay que señalar que el incremento de descarga generado por la perfusión con capsaicina normalizado con el valor de la descarga control, fue mayor en los termorreceptores de frío

LB que en los de HB (11.8 ± 4.3 y 40.3 ± 25.0, en HB y LB respectivamente), apoyando las especulaciones sobre el carácter nociceptor de los termorreceptores de frío LB.

1.1.3.5.3. Agonistas del canal TRPA1.

A pesar de la controversia respecto a la participación del canal TRPA1 como sensor de frío [Knowlton et al., 2010], en dos de las cuatro terminaciones de frío HB en las que se ensayó el efecto del agonista del canal TRPA1, AITC (30μM) se observó una duración más prolongada del disparo de NTIs durante la rampa de frío, que se mantuvo hasta alcanzar temperaturas inferiores a los 20 ºC (19.9 y 14.4 ºC en las dos terminaciones). Además, en esas dos terminaciones y en dos más (4 de 7) la perfusión con AITC (30 μM) incrementó la actividad basal de la terminación a 34 ºC, desde 1.5 ± 0.4 $imp.s^{-1}$ en control, frente a 4.0 ± 0.4 $imp.s^{-1}$ durante la perfusión con AITC (3 minutos) y 3.3 ± 0.4 $imp.s^{-1}$ tras 5 minutos de lavado.

En una terminación de frío LB en la que se ensayó, la perfusión con AITC no produjo cambio alguno sobre el disparo de NTIs a la temperatura control ni tampoco durante la rampa de frío.

1.1.3.5.4. Antagonistas del canal de potasio Kv1.

Por último, se testó el bloqueante de canales de potasio (Kv1) 4-AP (100 μM), sobre las dos poblaciones de termorreceptores corneales de frío.

En el grupo de HB, tan solo se testó el compuesto sobre una terminación, en la que la frecuencia media a temperatura control se vio incrementada (4.4, 11.9 y 6.3 $imp.s^{-1}$ en control, perfusión de 4-AP y lavado) (Tabla 4.8; Figura 4.15).

En el grupo de LB, fueron tres las terminaciones en las que se testó el compuesto. En todas ellas se incrementó ampliamente la actividad en 34 ºC (0.4 ± 0.1, 7.5 ± 1.5 y 1.0 ± 0.2 $imp.s^{-1}$ en control, perfusión de 4-AP y lavado) (Tabla 4.8; Figura 4.15). Sin embargo, ni el pico de respuesta máxima durante la rampa de frío ni su actividad en la respuesta a frío se vieron incrementados (29.5 ± 6.5, 23.0 ± 3.0 $imp \cdot s^{-1}$ de pico de máxima respuesta a frío, n=2; y 15.0

± 0.1 y 15.1 ± 1.5 imp·s^{-1} de frecuencia media en respuesta, n=2; ambos en control y 4-AP, respectivamente) (Figura IV.15).

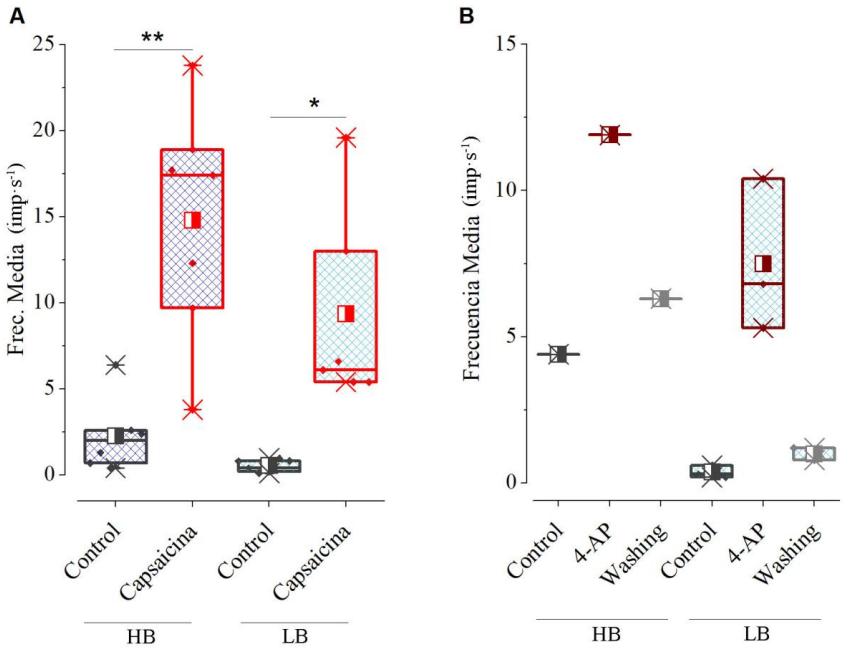

Figura IV.15. Respuestas de los termorreceptores corneales de frío HB y LB a otros químicos. Incremento de actividad observada en los termorreceptores de frío corneales HB y LB durante la perfusión a 34 ºC de Capsaicina (1 µM) (A) y 4-AP (100 µM) (B) (p<0.05 y ** p<0.01).*

1.2. Características Morfológicas de las Terminaciones Corneales TRPM8^{+}.

El estudio microscópico del soma y los axones de las neuronas corneales del ganglio trigémino (GT) de los ratones TRPM8BAC-EYFP (ratones EYFP+) evidenció claras diferencias en la intensidad de fluorescencia EYFP tanto en los somas como en los axones (Figura IV.16).

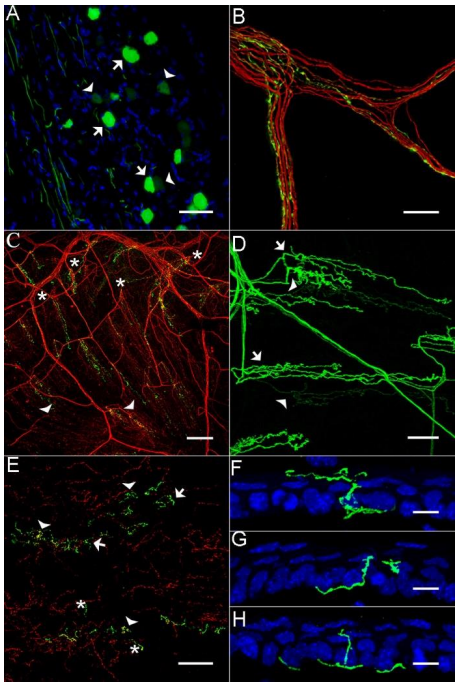

Figura IV.16. Inmunotinción de las neuronas del GT y de las ramas nerviosas corneales periféricas de ratones TRPM8^{BAC}-EYFP de tres meses de edad. (A) Fluorescencia en IF (flechas) y WF (puntas de flecha) en neuronas trigeminales. (B) Haces nerviosos estromales que contienen axones verdes EYFP^{+} mezclados con axones rojos no-EYFP^{+} (anti-β III tubulina). (C) Imagen de magnificación baja que muestra las penetraciones a través de la lámina basal de las ramas nerviosas ascendentes periféricas (asteriscos) y centrales (puntas de flecha). (D) Fibras nerviosas EYFP^{+} que muestran fluorescencia intensa (flechas) y débil (puntas de flecha). (E) Ramas nerviosas terminales intraepiteliales complejas (puntas de flecha) ramificadas (flechas) y simples (asteriscos). (F-H) Sección transversal de la córnea mostrando la trayectoria ascendente en las capas del epitelio corneal de, axones terminales complejos (F), ramificados (G) y simples (H). Los núcleos de las células epiteliales están teñidos con DAPI. Barras de escala: A y B 50 µm; C 150 µm; D y E 75 µm; F-H 10 µm.

1.2.1 Cuerpo Celular

De todas la neuronas contadas (2268.4 ± 266.5 neuronas por ganglio; n = 3) en secciones del trigémino de ratones jóvenes $EYFP^+$, un 17.8 ± 0.9 % presentaba fluorescencia EYFP (Figura 4.16a). En un 56.3 ± 1.3 % de ellas, la intensidad de la fluorescencia fue alta (> 90 unidades arbitrarias en una escala de grises de 256 canales) por lo que fueron denominadas neuronas Intensamente Fluorescentes (IF); la mayoría de ellas eran periferina-positivas y CGRP-negativas (Tabla 4.10). El resto de las neuronas $EYFP^+$ (43.7 ± 1.3%) mostraron una intensidad de fluorescencia débil (< 90 unidades arbitrarias en una escala de grises de 256 canales) y se llamaron, por tanto, neuronas de fluorescencia débil (WF, del inglés *Weak Fluorescense*; Figura 4.16); casi la mitad de ellas resultaron ser inmuno-reactivas a CGRP (tabla 4.10). Ambas, tanto IF como WF, fueron IB4 negativas (datos no mostrados). Además, las neuronas IF y WF, presentaron diferencias en su inmuno-reactividad frente a otros marcadores neuronales como neurofilamentos o TrkA (Tabla 4.10). En los cultivos de GT también se observaron claras diferencias entre las dos poblaciones de neuronas: IF y WF.

1.2.2. Axones Periféricos

Los axones corneales $EYFP^+$ podían ser reconocidos fácilmente, tanto por su fluorescencia como tras su tinción especifica con inmunoperoxidasa, en los troncos nerviosos estromales así como en sus extensas ramificaciones que ascienden hacia el epitelio en el que penetran a través de los orificios en la membrana basal (Figura IV.16B-E) (Figura IV.17) Los axones corneales EYFP del plexo sub-basal son morfológicamente heterogéneos. Aproximadamente la mitad de ellos eran IF, gruesos y presentaban dilataciones regulares que les daban un aspecto arrosariado a lo largo de toda su longitud. La otra mitad presentaban fluorescencia de menor intensidad (WF) y eran más más delgados y homogéneamente lisos (Figura IV.16 D y IV.17A).

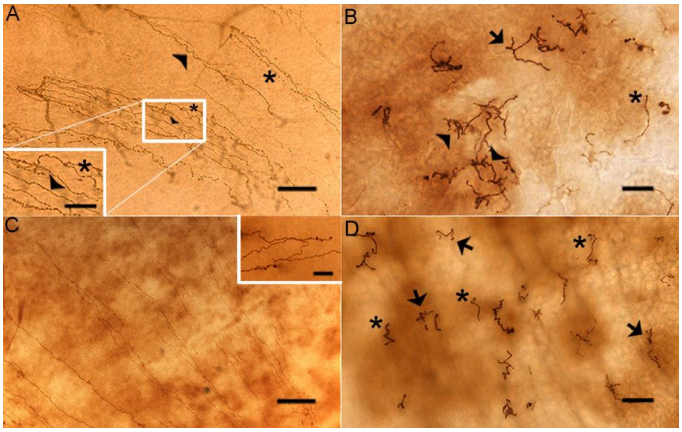

Figura IV.17. Inmunotinción anti-GFP de las fibras nerviosas corneales en la periferia de córneas" whole-mounted" *de ratones de 3 y 24 meses de edad. (A y B) Ratones de 3 meses. (A) Axones subbasales EYFP$^+$ largos, arrosariados (asteriscos) y lisos y cortos (flechas). Recuadro: mayor aumento del área señalada. (B) Ramas terminales intraepiteliales formando terminaciones complejas (punta de flecha), ramificada (flechas) y simples (asteriscos). (C y D) Ratones de 24 meses. Axones subbasales EYFP$^+$, algunos finalizando de manera abrupta (axones colapsados, recuadro). (D) Ramas terminales intraepiteliales formadas normalmente por terminaciones ramificadas (flechas) o simples (asteriscos). Barras de escala: A 100 µm; recuadro 50 µm; B y D 20 µm; C 100 µm; recuadro 20 µm.*

Las ramas terminales que ascienden desde los ramilletes subbasales (*leashes*) finalizan superficialmente como terminaciones intraepiteliales (Figura 4.16E-H y 4.17B). La densidad media de terminaciones intraepiteliales de los ratones jóvenes fue de 527.8 ± 23.2 terminaciones/mm^2 (n = 3); el 29.6 % de ellas fueron terminaciones EYFP$^+$ de complejidad morfológica variable [Ivanusic et al., 2013]. Una mayoría (51.1 ± 2.1 %) de las ramas ascendentes IF formaban terminaciones "complejas"; en una menor proporción (20.3 ± 2.8 %) produjeron terminaciones nerviosas "ramificadas" y el resto (28.6 ± 0.6 %) terminaron como terminaciones nerviosas "simples". Al contrario, los axones de WF se ramificaron menos en el plexo sub-basal y formaron terminaciones de tipo simple (57.9 ± 0.9 %) o ramificado (31.7 ± 1.8 %); tan solo el 10.4 ± 2.7 % de ellas produjeron terminaciones nerviosas complejos.

Tabla IV.10. Fenotipo molecular de las neuronas del GT TRPM8-EYFP+ en ratones jóvenes y viejos.

	% Neuronas IF-EYFP-TRPM8		% Neuronas WF-EYFP-TRPM8	
Edad	Ratones 3 meses	Ratones 24 meses	Ratones 3 meses	Ratones 24 meses
Periferina-IR	7.7 ± 0.5 (79.2 ± 4.1)	7.6 ± 1.0 (746 ± 4.9)	4.1 ± 0.6 (53.4 ± 4.9)	7.9 ± 0.4 ** (56.0 ± 5.0)
NF200-IR	1.3 ± 0.1 (12.1 ± 1.3)	2.8 ± 0.6 ** (22.5 ± 2.4)	1.6 ± 0.4 (20.2 ± 3.0)	2.7 ± 0.3 (17.1 ± 2.5)
TrkA-IR	1.3 ± 0.3 (13.8 ± 2.4)	1.6 ± 0.5 (16.4 ± 3.8)	3.9 ± 0.7 (48.7 ± 5.7)	5.2 ± 0.6 * (61.2 ± 2.4)
CGRP-IR	0 ± 0 (0 ± 0)	0 ± 0 (0 ± 0)	3.6 ± 1.2 (44.1 ± 11.4)	4.2 ± 0.4 * (43.9 ± 2.3)

*Nota. Los datos de las neuronas IF y WF se expresan como porcentaje del número total de neuronas contadas en el GT comparado en función de la edad, usando el z-test. *p<0.05; **p<0.01. Los datos en paréntesis son la proporción de neuronas IF y WF TRPM8-EYFP+, expresadas como porcentaje del número total de neuronas del GT TRPM8-EYFP+.*

1.3. Electrofisiología de las Neuronas Trigeminales EYFP$^+$.

Con el fin de evaluar la posible correlación entre la intensidad de fluorescencia en neuronas trigeminales EYFP$^+$ y el nivel de expresión de TRPM8, analizamos la relación entre fluorescencia del soma y respuesta electrofisiológica, al frío y al mentol en neuronas cultivadas del GT de ratones jóvenes, midiendo los cambios en el potencial de membrana (E_m) en respuesta a la aplicación de rampas de frío y a la aplicación de mentol (100 µM), en neuronas IF (fluorescencia media = 64.3 ± 5.6 % del máximo), neuronas WF (fluorescencia media = 6.3 ± 1.0 % del máximo), y neuronas no fluorescentes (NonF) como muestra la Figura 4.18 A y B.

Las neuronas IF eran despolarizadas tanto por el frío como por mentol (ΔEm = 10.0 ± 1.4 mV y 12.0 ± 1.7 mV, respectivamente, n = 15), produciendo una descarga de potenciales de acción. Además, las respuestas al enfriamiento eran potenciadas marcadamente por el mentol (ΔEm = 32.7 ± 2.0 mV). Por el contrario, el frío y el mentol, aplicados separadamente, apenas modificaban el E_m en las neuronas WF, pero todas ellas se despolarizaban cuando los estímulos se aplicaban de manera simultánea, generando en algunas un disparo de potenciales de acción (4/13, Figura 18 A). Por último, ninguna de las neuronas NonF (n = 12) mostró cambios en su E_m durante la aplicación del frío o mentol. La integridad de esas neuronas se confirmó por la potente despolarización con la que respondían a elevadas concentraciones de K^+ (ΔE_m = 25.7 ± 1.9 mV; n = 12). Las neuronas de los tres grupos estudiados no mostraban diferencias significativas en sus valores de E_m en reposo (IF = -57.3 ± 2.2 mV; WF = -56.0 ± 2.7 mV; NonF = -53.6 ± 2.5 mV: p = .571) o en la capacitancia de su membrana (IF = 11.8 ± 1.3 pF; WF = 14.4 ± 1.7 pF; y NonF = 14.7 ± 1.5 pF; p = .340). En contraposición al disparo espontaneo típico de la mayoría de las terminaciones nerviosas corneales periféricas, solo una neurona IF corneal, sensible al frío, mostró una descarga espontánea a 33 ºC.

Estos resultados indicaban (Figura IV.18B) que la intensidad de la fluorescencia en el soma de las neuronas TRPM8-EYFP$^+$ se correlaciona con su sensibilidad al frío, siendo las neuronas IF más sensibles a los agonistas de TRPM8 (frío y mentol) que las neuronas WF, lo que a su vez sugiere una mayor expresión del canal TRPM8 en las neuronas más fluorescentes. En la figura IV.18C se presentan los parámetros de electrofisiología de las neuronas fluorescentes de ratones jóvenes, que se utilizaron para su comparación con los de animales viejos, como discutiremos a continuación.

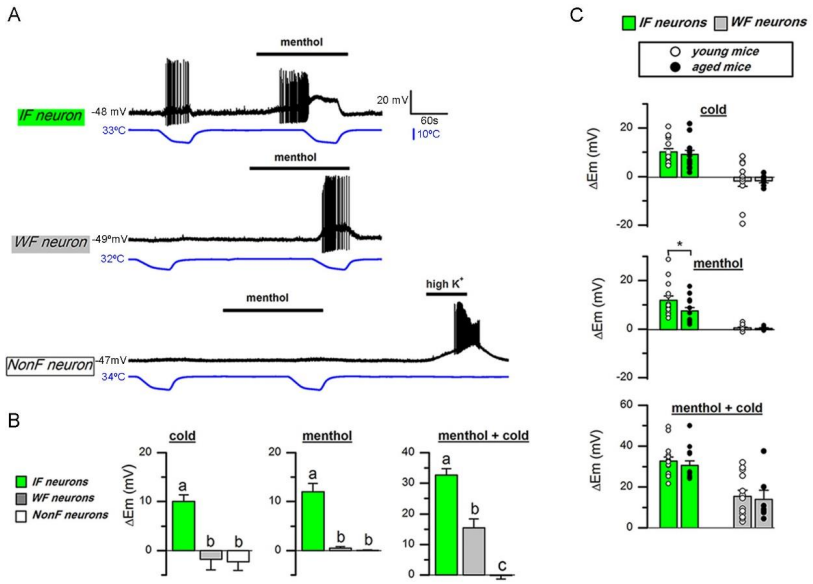

<u>Figura IV.18. Correlación entre intensidades de fluorescencia de neuronas del GT TRPM8-EYFP$^+$ cultivadas y su sensibilidad al frío y al mentol.</u> (A) Ejemplo de registros obtenidos de neuronas GT típicas de ratones de 3 meses, presentando neuronas IF, WF y NoF. El trazo del potencial de membrana (E_m) está representado en negro y el de la temperatura del baño en azul. Las barras negras horizontales indican la perfusión con mentol 100 μM y K^+ 37.5 mM, respectivamente. (B) Cambios promedio en E_m evocado por una rampa de frío, mentol y mentol más una rampa de frío en los tres tipos de neuronas. Los datos son la media ± SEM de neuronas IF (n=15), WF (n=13) y NoF (n=12).One-Way ANOVA ($p<0.001$ en todos los casos) con test post-hoc de Bonferroni o Dunn ($p<0.001$ para el estímulo de frío; $p<0.05$ para los estímulos de mentol y mentol más frío). (C) Cambios promedio (barras) e individuales (círculos) en E_m generados por las rampas de frío, mentol y mentol más frío en neuronas IF y WF de ratones de 3 () y 24 meses (). –p=0.05, t test.

2. Efectos del envejecimiento sobre las terminaciones sensoriales corneales.

2.1. Propiedades Funcionales.

En estos experimentos se utilizaron ratones de ambos sexos de 24 meses de edad, tanto C57 BL6 como TRPM8BAC-EYFP, en los que se registró la actividad eléctrica de las terminaciones nerviosas en la córnea, siguiendo los mismos procedimientos utilizados en ratones jóvenes.

Como muestra la figura 4.19, el porcentaje de puestas del electrodo en las que se encontró actividad se redujo significativamente del 41.4 % hallado en ratones jóvenes, al 22.9 % en ratones viejos ($p = 0.01732$,). De ellas, el 1.3 % correspondía a mecano-receptores (2.1 % en jóvenes, n.s.); el 3.4 % a nociceptores polimodales (8.0 % en jóvenes, $p= 0.00318$); el 4.2 % correspondió a termorreceptores de frío HB (8.37 % en jóvenes, $p= 0.047$) y el 5.2 % a termorreceptores de frío LB (2.9 % en jóvenes, n.s.). El 8.2 % correspondió a terminaciones con una amplitud de NTIs demasiado pequeña como para poder ser clasificadas funcionalmente de manera fiable.

También se calcularon, en ratones viejos, los porcentajes de terminaciones de cada tipo respecto al total de terminaciones identificadas funcionalmente y se compararon con los valores obtenidos en los ratones jóvenes. Así, no se apreciaron cambios significativos en la proporción de mecano-nociceptores (9.8 % en jóvenes y 8.6 % en viejos) ni en termorreceptores de frío HB (39.2 % en jóvenes y 33.3 % en viejos), o en los nociceptores polimodales (37.3 % frente a 22.9 %, $p= 0.05876$), pero sí se constataron diferencias entre ratones jóvenes y viejos, en los termorreceptores de frío LB (13.7 % frente a 35.2 %, respectivamente, $p=0.00512$) (Figura IV.19).

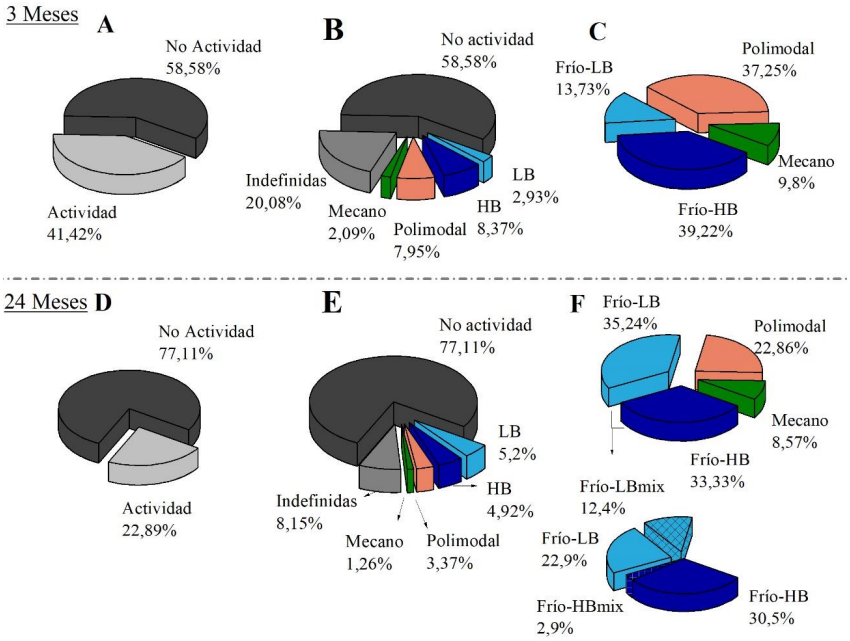

Figura IV.19. Comparativa del porcentaje de éxito en el registro en ratones jóvenes y viejos. Representación del porcentaje de éxito obtenido en el registro extracelular de la córnea de ratones jóvenes (A, B y C) y viejos (D, E y F). (A y D) Porcentaje total de actividad respecto al total de puestas realizadas (de todas las veces que se situó la pipeta sobre la superficie corneal, cuántas veces se encontró actividad frente a cuántas no). (B y E) Mismo porcentaje de éxito desglosado entre los distintos tipos de terminaciones. (C y F) Porcentaje que representó cada tipo de terminación, teniendo en cuenta solo aquellas puestas en las que se encontraron actividad y se pudo clasificar.

En conjunto, el porcentaje total de termorreceptores de frío respecto al total de terminaciones registradas se incrementa en los ratones viejos respecto a los jóvenes, aunque no significativamente (68.6 % en viejos frente a 53 % en jóvenes, p= 0.05744) a pesar de que el número total de terminaciones activas está claramente reducido.

Los cambios en las propiedades funcionales de las diferentes subpoblaciones de terminaciones sensoriales de la córnea de los ratones viejos en relación con las observadas en los animales jóvenes fueron los siguientes:

2.1.1. Mecano-nociceptores.

En los mecano-nociceptores de los ratones viejos, la actividad basal a 34 ºC (condiciones control) fue de 0.06 ± 0.02 imp·s^{-1}(n=6), un valor similar al presentado por los mecano-receptores de ratones jóvenes (Tabla IV.1). La frecuencia media de la descarga de NTIs evocada por el estímulo mecánico (200 µm de desplazamiento durante 5 s) fue de 18.0 ± 6.7 imp·s^{-1} frente a 0.2 ± 0.2 imp·s^{-1} antes del estímulo (P=0.0041) (Figura 4.20), con una duración media de la respuesta de 2.2 ± 0.7 s, valores todos ellos muy parecidos a los de los ratones jóvenes, correspondiendo como en éstos a una respuesta fásica, en ráfaga, que se inicia tan pronto se realiza la presión (Tabla IV.1), y desciende bruscamente al valor inicial de actividad basal aunque la presión se mantenga durante 15 s.

Al igual que sucedía en los mecano-receptores de los ratones jóvenes, en los viejos ninguna de estas terminaciones respondió a estímulos con rampas de frío o de calor (Tabla IV.1, Figura IV.20).

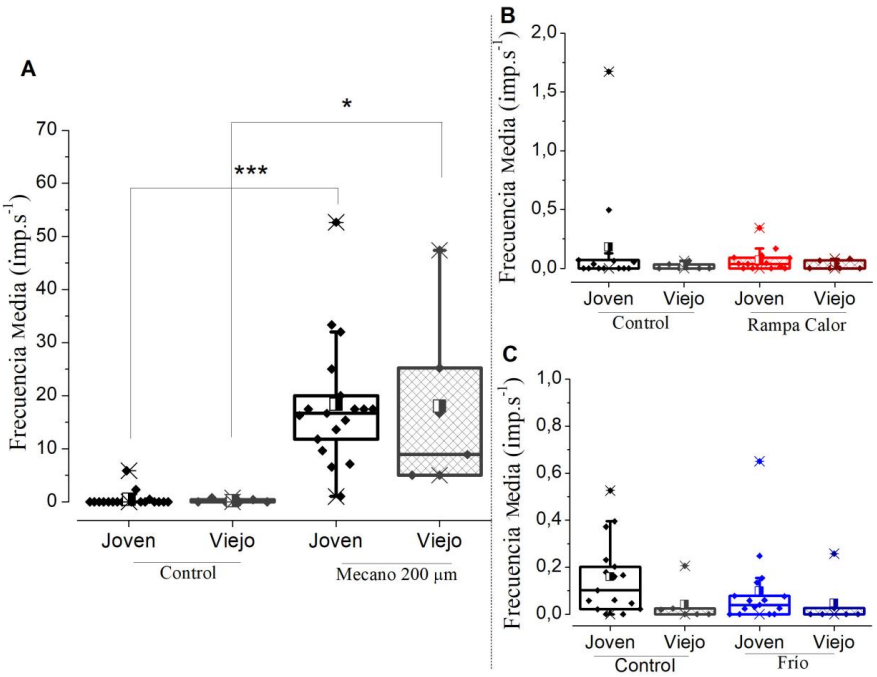

Figura IV.20. Frecuencia media de respuesta de las terminaciones mecano-nociceptoras a

distintos estímulos mecánicos y térmicos en ratones jóvenes y viejos. Frecuencia media de disparo (medida en impulsos por segundo) de las terminaciones mecano-nociceptoras de ratones jóvenes y viejos en control y durante el estímulo mecánico de 200 μm de desplazamiento (A), en respuesta a una rampa de calor (B) y durante una rampa de frío (C). (p<0.05 y *** p<0.001).*

2.1.2. Nociceptores Polimodales.

2.1.2.1. Estimulación Térmica.

La actividad basal media de las terminaciones polimodales en condiciones control fue de 0.3 ± 0.1 imp.s^{-1}, casi idéntica a la de los ratones jóvenes. Cuando se aplicó una rampa de frío, la terminación redujo significativamente su descarga espontánea de NTIs, durante los 40 segundos que duró el estímulo, p=0.0110), al igual que sucedía en los nociceptores polimodales de ratones jóvenes (Figura IV.21, Tabla IV.1).

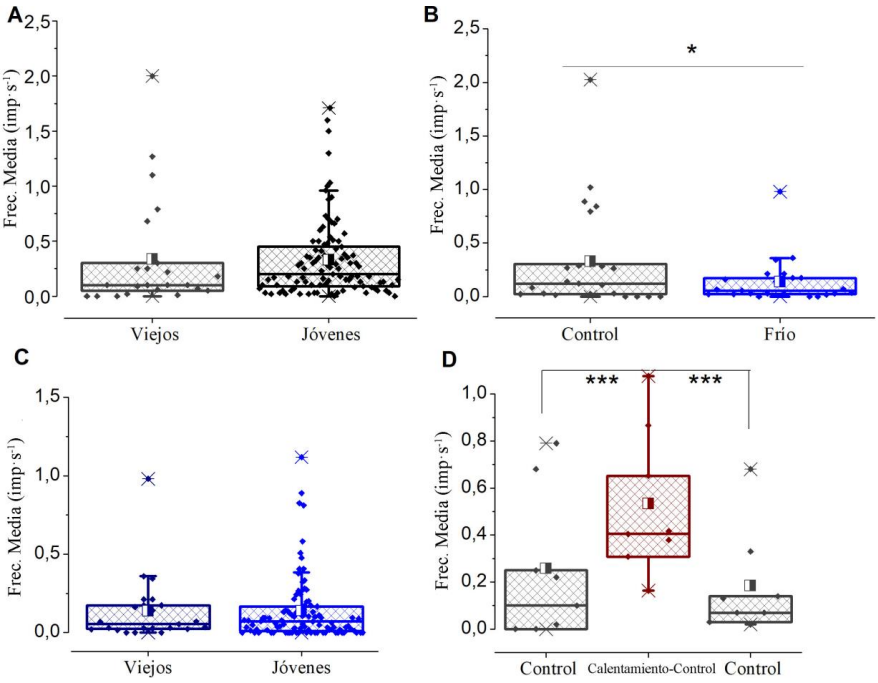

Figura IV.21. Comparativa de nociceptores polimodales de ratones jóvenes y viejos en su actividad basal (A) y su respuesta a una rampa de frío (C). Respuesta de los nociceptores polimodales de ratones viejos a una rampa de frío (B) y al calentamiento-control generado en el regreso desde la mínima temperatura de la rampa (~13 ºC) a la temperatura basal (34 ºC) (D). (p<0.05).*

Un 34.8% de estas terminaciones (8 de 23) mostraron un incremento en su actividad durante la fase de calentamiento-control, al regresar a la temperatura control tras la rampa de frío. Este porcentaje es más alto que el encontrado en los nociceptores polimodales de ratones jóvenes (9.4 %). Tal respuesta se inició a una temperatura media de 27.0 ± 0.9 ºC, incrementando significativamente su actividad, desde 0.3 ± 0.1 imp.s^{-1} a 0.5 ± 0.1 imp.s^{-1} durante los 30 segundos de media que duraba (n=8, p=0.0001) (Tabla IV.2, Figura IV.21).

Al igual que sucedía en los ratones jóvenes, este grupo de terminaciones no presentaba diferencia alguna con el resto de nociceptores polimodales registrados.

La respuesta de los nociceptores en los ratones viejos a la rampa de calor fue muy similar a la observada en los ratones jóvenes, (Figura IV.22). Así, en ellos el incremento de temperatura aumentó significativamente la frecuencia de disparo a 34 ºC, de 0.4 ± 0.1 hasta 2.9 ± 0.7 imp·s^{-1} durante la rampa de calor (n=22, p<0.0001, Tabla IV.1). La temperatura media a la que comenzaba dicha respuesta (umbral de calor) y su duración media no fueron diferentes de las obtenidas en ratones jóvenes (41.5 ± 0.8 ºC y 18.3 ± 2.9 s. frente a 42.2 ± 0.4 ºC y 18.9 ± 1.4 s; Tabla IV.1).

En los ratones viejos, un 18.2 % de las terminaciones nociceptoras (4 de 22) se silenció tras la aplicación de la rampa de calor (14 % en los ratones jóvenes). La actividad a 34ºC después de dicha rampa (0.13 ± 0.03 imp·s^{-1}), fue significativamente más baja que antes de la aplicación del estímulo (0.3 ± 0.1 imp·s^{-1}, n=18, p=0.0034).

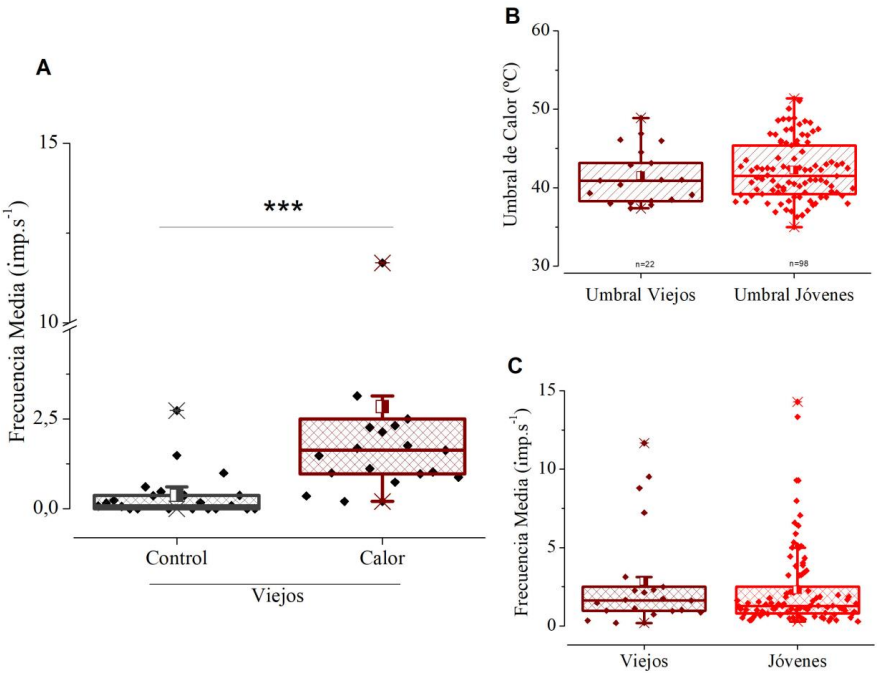

Figura IV.22. Respuesta a calor de nociceptores polimodales corneales de ratones viejos. (A) respuesta (medida en imp·s^{-1}) a la rampa de calor de las terminaciones nociceptoras polimodales de ratones viejos. (B) Umbral de respuesta a calor de nociceptores polimodales

*viejos y jóvenes. (C) Comparativa de la actividad (imp·s^{-1}) presentada durante las rampas de calor en los nociceptores polimodales de ratones viejos y jóvenes. (*** p<0.001).*

2.1.2.2. Estimulación Mecánica.

Un 85.7 % (18 de 21) de los nociceptores polimodales de los ratones viejos respondió al estímulo mecánico de 200 µm, un porcentaje casi igual al obtenido en ratones jóvenes (86.9 %) con una descarga transitoria de NTIs (duración media de 1.9 ± 0.3 s), que elevó la frecuencia basal de 0.4 ± 0.2 imp.s^{-1} a 12.1 ± 1.8 imp.s^{-1}, n=18 p<0.0001) (Tabla IV.7).

2.1.3. Termorreceptores de frío.

La probabilidad de encontrar termorreceptores de frío en las córneas de los de ratones viejos (10.1 %) fue casi la misma que en los jóvenes (11.3 %).

Tabla IV.12: Termorreceptores de Frío: Respuesta a Enfriamiento Dinámico

Tipo de termorreceptor de frío		Actividad Basal (Imp.s^{-1})	Umbral de Enfriamiento (ºC)	Máxima Respuesta (Imp.s^{-1})	Respuesta a Frío (Imp.s^{-1})	Tasa de Éxito (%)
3 Meses	HB (n=131)	5.8 ± 0.4	32.5 ± 0.08	49.5 ± 1.8	31.0 ± 1.1	8.4
	LB (n=66)	0.4 ± 0.04***	27.3 ± 0.5***	10.4 ± 1.2***	6.5 ± 0.8***	2.9
24 Meses	HB-LT (n=26)	4.7 ± 0.6	32.2 ± 0.2	37.9 ± 3.6	26.9 ± 2.8	4.6

	HB-HT (n=3)	5.3 ± 1.2	27.7 ± 0.8	43.0 ± 5.3	28.2 ± 1.0	0.6
	LB-HT (n=21)	0.6 ± 0.1	27.5 ± 0.5	9.6 ± 1.5	6.4 ± 1.0	4.0
	LB-LT (n=11)	0.3 ± 0.1	31.9 ± 0.3	16.8 ± 3.5	10.5 ± 1.8	1.8

*NOTA: ** $p<0.01$; *** $p<0.001$.*

Sin embargo, si consideramos el porcentaje de cada tipo de termorreceptor de frío frente al total de los mismos, para cada edad, la proporción de HB y LB varía significativamente de 74.1 % y 25.9 % en jóvenes frente a 48.6 % y 51.4 % en ratones viejos ($p = 0.0232$).

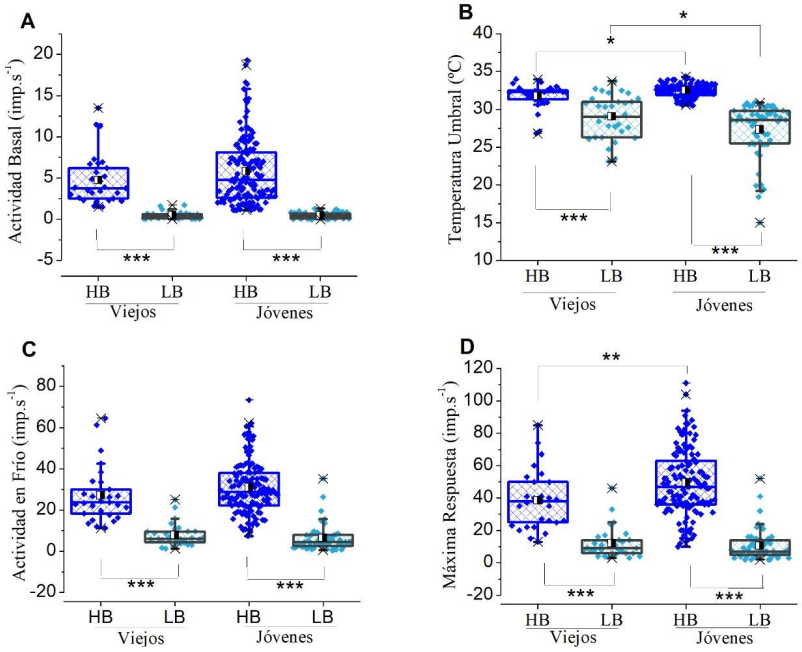

Figura IV.23. Parámetros comparativos de la respuesta a frío en los termorreceptores HB y LB de ratones jóvenes y viejos. Comparativa de la frecuencia basal (A), umbral de respuesta a frío (B), frecuencia media en respuesta a frío (C) y el pico de máxima respuesta durante dicha respuesta (D) entre los termorreceptores de frío HB y LB de ratones viejos y los valores para los mismos parámetros observados en los termorreceptores de frío HB y LB de ratones jóvenes ($p<0.05$ y ** $p<0.01$).*

2.1.3.1. Termorreceptores de frío HB.

En la córnea de los ratones viejos (24 meses), las terminaciones que mostraron una actividad basal elevada (>1.5 imp.s^{-1}, con 4.7 ± 0.6 imp-s^{-1} de media) a 34 ºC, clasificadas por ello como terminaciones de frío HB, presentaban un umbral de respuesta a frío ligeramente inferior al observado en los HB de ratones jóvenes (31.8 ± 0.3 ºC, frente a 32.5 ± 0.07 ºC, p=0.024), así como una frecuencia pico de respuesta a frío menor (38.5 ± 3.3 imp·s^{-1} frente a 49.6 ± 1.8 imp·s^{-1}, p=0.0079), si bien su frecuencia media durante dicha respuesta (27.1 ± 2.5 imp·s^{-1}) no difiere de la observada en ratones jóvenes (Figura IV.23).

Un 14 % (4 de 29) de estas terminaciones HB de ratones viejos también respondieron transitoriamente cuando la temperatura se recuperaba desde los 13 ºC alcanzados al final de la rampa de frío hasta la temperatura basal de 34 ºC. La frecuencia media de estas terminaciones durante tal respuesta transitoria, que se inició al alcanzarse 29.3 ± 2.2 ºC y duró 9.5 ± 3.6 s de media, fue de 12.4 ± 2.1 imp·s^{-1}, no siendo estadísticamente diferente de la obtenida en ratones jóvenes (Tabla IV.2). Los termorreceptores de frío HB de los ratones viejos también respondieron a mentol (20 μM) y a soluciones hiperosmolares de 397 mOsm·L^{-1} con un incremento de su frecuencia basal y de su máxima respuesta de disparo de NTIs en las rampas de frío, al igual que lo hacían los animales jóvenes.

2.1.3.2. Termorreceptores de frío LB.

Los termorreceptores de frío LB identificados en la córnea de los ratones viejos tenían una actividad basal baja (0.5 ± 0.08 imp·s^{-1}), así como una respuesta a frío débil (7.8 ± 1.0 imp·s^{-1}) similares a las de los ratones jóvenes (Figura IV.23). Sin embargo, en los viejos se observaron diferencias significativas en el umbral medio de temperatura al que se iniciaba la respuesta al frío, ya que éste fue de 29.0 ± 0.5 ºC mientras que en los ratones jóvenes el disparo de NTIs empezaba solo cuando se alcanzaban los 27.3 ± 0.5 ºC (p=0.0413) (Figura IV.23).

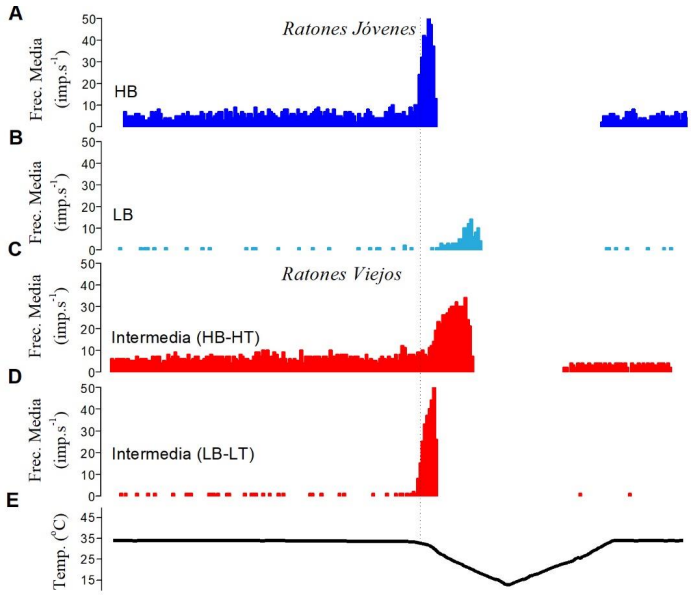

<u>Figura IV.24.</u> Ejemplos de la descarga de las terminaciones de frío HB y LB en respuesta a una rampa de frío desde 34 hasta 15 ºC (E) en ratones jóvenes (A y B) y las variaciones de estos dos grupos encontradas en ratones viejo (C y D).

2.1.3.3. Termorreceptores de frío mixtos.

El análisis individualizado de los datos de las dos clases de termorreceptores de frío anteriormente descritos, puso en evidencia la presencia de terminaciones termorreceptoras de frío atípicas, que compartían propiedades de los dos grupos HB y LB, que están nítidamente diferenciados en los ratones jóvenes.

Así, un pequeño porcentaje (en torno al 10 %, 3 de 29) de los termorreceptores HB presentaban un umbral de respuesta a frío bastante más alto que el observado en ratones jóvenes (27.7 ± 0.8 ºC) y por tanto más próximo al de los típicos termorreceptores LB (Figura IV.24 y IV.25; Tabla IV.12). Sin embargo, su frecuencia media durante la respuesta a la rampa de frío (28.2 ± 1.0 $imp \cdot s^{-1}$) resultaba ser más parecida a la de los típicos termorreceptores HB de los ratones jóvenes. A estos anómalos termorreceptores de frío les llamamos HB-HT (Tabla IV.12).

Por otro lado, entre los receptores LB de los ratones viejos se encontró una proporción no desdeñable de terminaciones (en torno al 31 %, 11 de 32, el 1.8 % del total de puestas realizadas en ratones viejos; 12.4 % del total, Figura IV.19) que aunque mostraban la típica baja frecuencia basal a 34 ºC, presentaban un umbral de respuesta a frío (31.9 ± 0.3 ºC) significativamente más bajo que el del resto de los termorreceptores LB, aunque disparaban durante la rampa de frío a una frecuencia media similar (Tabla IV.12; 10.5 ± 1.8 imp.s^{-1}). Además, dos de estas terminaciones presentaron respuesta al calentamiento durante el fin de la rampa de frío, una respuesta solo vista en los termorreceptores HB. A este segundo tipo de termorreceptores anómalos, con características mixtas entre las dos poblaciones de termorreceptores que se encuentran en los ratones jóvenes, los llamamos termorreceptores de frío LB-LT (Tabla IV.12 y Figuras IV.24 y IV.25).

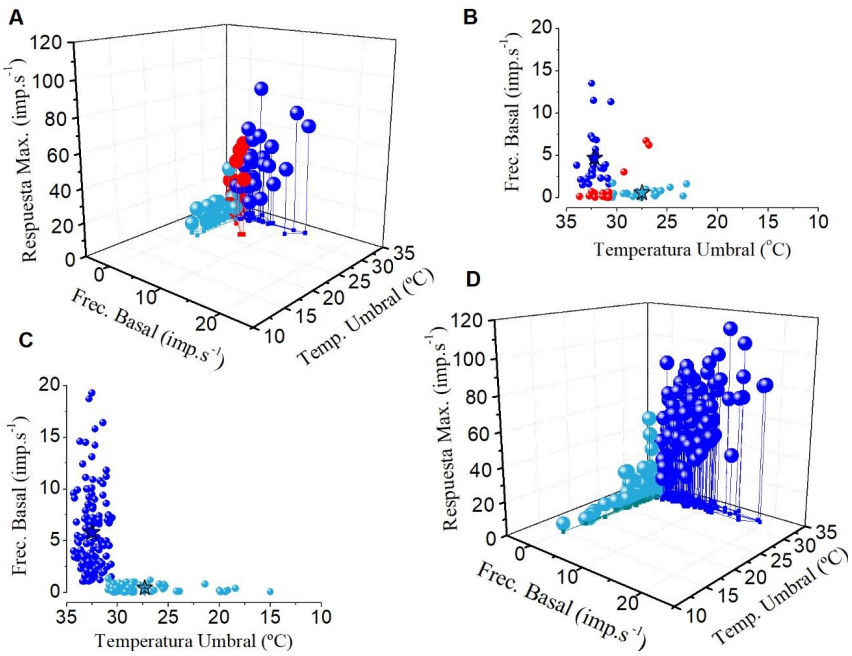

Figura IV.25. Representación individual en tres dimensiones de los termorreceptores de frío HB (círculo azul oscuro) y LB (círculos azul claro) atendiendo a su frecuencia basal a 34 ºC, a su pico de máxima respuesta a frío y a su umbral de respuesta (A y C); o en dos dimensiones enfrentando la frecuencia basal de cada termorreceptor de frío frente a su umbral de respuesta (B y D). En las cuatro representaciones se pueden apreciar los dos grupos de termorreceptores de frío corneales predominantes en ratones jóvenes, así como el

grupo de termorreceptores con características mixtas (círculos rojos) entre ellos. Los datos representados proceden de ratones de 24 meses de edad (A y B) y de 3 meses de edad (C y D).

2.2. Cambios morfológicos con la edad en las neuronasTRPM8$^+$

2.2.1. Cuerpo Celular

Un 21.6 ± 1.1 % de las neuronas exploradas en los GT de los ratones viejos (24M) (2723.0 ± 263.8 neuronas por ganglio, n=3) eran EYFP$^+$. Esta proporción es significativamente más alta que la obtenida en ratones jóvenes ($p= 0.0032$) y se corresponde con un mayor porcentaje de neuronas WF (10.7 ± 0.9 % en ratones de 24M frente a 7.8 ± 0.4% en los de 3M, $p < 0.001$), lo que concuerda con el mayor porcentaje de termorreceptores corneales de frío LB observada funcionalmente en ratones viejos respecto a los jóvenes. La proporción de neuronas WF que expresaron periferina, TrkA y CGRP también fue significativamente más alta con la edad (Tabla IV.10).

2.2.2. Fibras nerviosas corneales

En los ratones de 24M, la densidad y la arquitectura de los nervios sensoriales corneales, incluida la subpoblación de fibras EYFP$^+$, aparecían claramente modificadas en comparación con las de los animales jóvenes (Figura IV.17 y Tabla IV.11). En los ratones viejos, la densidad de puntos de penetración de troncos nerviosos a través de la lámina basal en los que se observaban axones EYFP$^+$ era significativamente más alta que en los animales jóvenes, con un incremento medio sobre estos del 49.6 %, ($p = .019$, Tabla IV.11), debido a la presencia en los ratones viejos de un mayor número de puntos de penetración en la periferia de la córnea (15.3 ± 1.5 penetraciones/mm^2 en los viejos contra 8.6 ± 0.6 penetraciones/mm^2 en los jóvenes; $p = 0.004$), mientras que en el centro de la córnea no se observaron diferencias significativas con la edad en cuanto a diferencias en densidad de puntos de penetración de axones EYFP$^+$.

En los ratones viejos, prácticamente todos (95.1 ± 2.9 %) los axones TRPM8-EYFP$^+$ eran lisos, débilmente fluorescentes, y más largos y finos que en los animales jóvenes (comparar A y C en Figura 4.16A) y alcanzaban normalmente el centro de la córnea (promedio de la longitud de los axones sub-basales en ratones viejos, 304.9 ± 14.0 µm frente a 227.6 ± 11.6 µm en los jóvenes, $p = 0.002$).

Tabla IV.11. Características morfológicas de los axones y terminaciones nerviosas epiteliales TRPM8-EYFP+ que inervan la córnea de ratones a distintas edades.

	Ratones 3 meses	Ratones 24 meses
Penetración de haces subepiteliales (número/mm²)	11.5 ± 0.5 (n=5)	17.2 ± 1.2 *** (n=5)
% de axones nerviosos subbasales arrosariados	50.1 ± 6.5 (n=3)	4.9 ± 2.9 *** (n=4)
% de axones subbasales lisos	49.9 ± 6.5 (n=3)	95.1 ± 2.9 *** (n=4)
Densidad de axones subbasales (número/mm2)	126.4 ± 5.9 (n=7)	91.6 ± 4.2 *** (n=10)
Número de axones por ramillete	5.2 ± 0.3 (n=3)	2.6 ± 0.2 *** (n=4)
Densidad de ramas terminales (número/mm2)	156.2 ± 8.0 (n=7)	111.2 ± 5.6 *** (n=10)

*Nota. Comparación de medidas realizada entre los ratones de 24 meses de edad contra las medidas obtenidas en los ratones de 3 meses. Se realizó el Mann-Whitney U test excepto en el caso del porcentaje de axones nerviosos subbasales arrosariados, en el que se empleó un z test. ***p<0.001. n = número de ratones.*

La densidad de axones sub-basales $EYFP^+$ en los ratones viejos fue significativamente inferior (27.7 %) a la medida en ratones jóvenes ($p < 0.001$; Tabla IV.11). Además, estaban distribuidos de manera diferente en los ramilletes, con un número mayor de éstos conteniendo axones $EYFP^+$ en ratones viejos, aunque con un número medio más bajo de axones fluorescentes por ramillete.

En conjunto, la densidad total de terminaciones $EYFP^+$ en el epitelio corneal de los ratones viejos fue un 35.6 % inferior a la de los ratones jóvenes ($p < 0.001$). Además, la proporción en los primeros, de los diferentes sub-tipos morfológicos de terminaciones intra-epiteliales $EYFP^+$ aparecía claramente alterada en los ratones viejos en comparación con los de 3M de edad Así, en los viejos un 59.7 ± 0.7 % de las terminaciones eran simples (43.4 ± 1.7 %, en los jóvenes, n.s.), 25.6 ± 1.2 % eran terminaciones ramificadas (26.0 ± 1.7% en los jóvenes, p = n.s.) y solo el 2.6 ± 0.7 % eran terminaciones complejas (30.6 ± 1.7 en los jóvenes, $p < 0.001$) (comparar con Figura IV.16B, D). Además, el 12.1 ± 2.6 % de los axones sub-basales $EYFP^+$ finalizan de manera abrupta en el plano sub-basal sin llegar a emitir ramas ascendentes que alcanzan la zona más superficial del epitelio y a las que hemos llamado "axones colapsados" (ver Figura IV.16C, *recuadro*), no existentes en los animales jóvenes ($p = 0.009$).

2.3. Características funcionales de las neuronas $EYFP^+$ en los ratones viejos.

Las neuronas trigeminales $EYFP^+$ de ratones viejos en cultivo se dividieron también en neuronas IF y WF. Aunque no se realizó su cuantificación, a simple vista se apreció que las neuronas WF eran claramente más abundantes en los cultivos de GT de animales viejos comparados con los de los jóvenes.

Los valores de fluorescencia media de las neuronas trigeminales de los ratones viejos fueron de 60.3 ± 5.1 % en las neuronas IF y 8.8 ± 2.5 % en las WF. El potencial de membrana en reposo a 33 ºC y la capacitancia de la membrana de las neuronas $EYFP^+$ de ratones viejos, eran similares a los observados en los mismos tipos neuronales en ratones jóvenes (E_m = -53.7 ± 2.7 y -56.7 ± 2.3 mV; C_m = 12.7 ± 1.4 y 17.9 ± 3.1 pF).

Al igual que en los ratones jóvenes, las neuronas IF resultaron más sensibles a los agonistas de TRPM8 que las WF (Figura IV.18c). En las neuronas de ratones viejos, el ΔE_m observado en las IF en comparación con las WF durante la exposición a frío fue 9.1 ± 1.6 frente a -1.7 ± 0.8 mV; el mentol produjo una despolarización en las IF de 7.5 ± 1.4 frente a 0.3 ± 0.3 mV en las WF y la aplicación de mentol + frío 30.6 ± 2.1 en las IF frente a 14.0 ± 4.3 mV en las WF. En conjunto, las amplitudes de la despolarización de la membrana inducidas por la exposición al frío, sola o en presencia de mentol fueron similares a las observadas en ratones jóvenes (ver Figura IV.18C) en ambos tipos neuronales, IF y WF. Solo en el grupo de las neuronas IF de ratones envejecidos, la amplitud de la despolarización evocada por mentol

resultó ligeramente inferior a la de las neuronas IF de ratones jóvenes (ΔE_m = 7.5 ± 1.4 mV contra 12.0 ± 1.7 mV; p = .05).

En conjunto, cabe afirmar que los somas de las neuronas EYFP$^+$ del GT de los ratones de 24 meses muestran propiedades de membrana activas y pasivas y respuestas al frío muy parecidas a los de los animales jóvenes, contrariamente con lo que ocurre con las terminaciones periféricas de estas neuronas en la córnea.

3. Tasa de lagrimación y osmolaridad de la lágrima.

Tanto el flujo lagrimal basal como la osmolaridad de la lágrima se ven alterados con el envejecimiento.

El flujo medio de lágrima basal en animales jóvenes, TRPM8^{BAC}-EYFP y C57BL/6, anestesiados fue de 2.4 ± 0.2 mm (n = 66). En los ratones viejos, la tasa de lagrimación era más variable y significativamente superior a la de los animales jóvenes (15.7 ± 1.6 mm, n = 44; p < 0.001) (Figura IV.26). Cabe resaltar que los valores del flujo de lagrimación basal experimentaron un aumento que ocurrió en paralelo con el incremento en la proporción de fibras WF, lo que sugiere una relación causal entre la lagrimación aumentada y el mayor número de fibras nerviosas del tipo WF, el decrecimiento paralelo de los axones IF y los trastornos en la actividad eléctrica de las terminaciones de frío observados en animales viejos (Figura 4.26). Por último, el valor medio de la osmolaridad en ratones viejos fue de 354.0 ± 2.8 mOsm.L^{-1} (n = 22), significativamente mayor que el obtenido en ratones adultos jóvenes (346.3 ± 2.4 mOsm·L^{-1}, n = 19, p = 0.008).

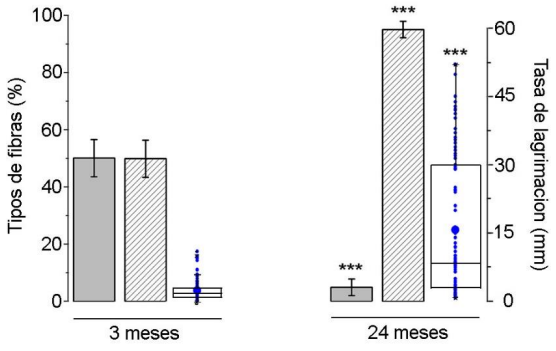

Figura IV.26. Cambio en la tasa de lagrimeo basal y en la densidad de las fibras nerviosas subbasales TROM8-EYFP+ con la edad. Las barras representan el porcentaje de fibras IF

*(gris) y WF (rayado) en ratones de 3 y 24 meses (p<0.001). En los mismos grupos de edad, valores individuales de lágrima basal medidos en mm de impregnación en tiras de rojo fenol (puntos azules pequeños) y su valor medio (punto azul grande). La media (línea horizontal), percentiles 25 y 75 (límites de la caja) y los percentiles 1 y 99 (X) también están representados (***p<0.001).*

V. Discusión

Esta Tesis confirma que la córnea de ratón está inervada por neuronas del ganglio trigémino que responden a las mismas modalidades de estímulo que las neuronas corneales en mamíferos de otras especies y como en éstas, se han caracterizado neuronas y terminaciones nerviosas corneales mecano-nociceptoras, nociceptoras polimodales y termorreceptoras (Belmonte *et al.*, 2017). Se han definido dos poblaciones distintas dentro de las terminaciones termorreceptoras de frío, identificadas como tales por vez primera en el gato (Gallar *et al.*, 1993) y posteriormente en el cobaya (Brock, McLachlan and Belmonte, 1998) y el ratón (Parra *et al.*, 2010). La existencia de esos dos subtipos funcionales de neuronas corneales termorreceptoras de frío parece tener una importante significación fisiológica para la detección de la sequedad ocular y la regulación refleja de la secreción lagrimal en condiciones normales, así como en las sensaciones de molestia que acompañan al ojo seco. Además de este hallazgo, nuestro estudio describe por vez primera los cambios que tienen lugar durante el envejecimiento en las diferentes poblaciones neuronales que inervan la córnea, que podrían explicar, al menos en parte, la aparición de disestesias, cambios en la secreción lagrimal y el parpadeo y desarrollo de alteraciones tróficas de la superficie ocular, en los seres humanos con la llegada de la vejez.

Categorización funcional de la inervación sensorial de la córnea

Los datos disponibles sobre la densidad y proporción de los diferentes tipos de terminaciones sensoriales en la córnea son muy variables, dependiendo de la especie animal analizada y la metodología empleada para su evaluación (Belmonte *et al.*, 1991; Gallar *et al.*, 1993; Brock, McLachlan and Belmonte, 1998; Fern *et al.*, 2016).

En el presente estudio llevado a cabo en la córnea de ratón, la identificación funcional de cada tipo funcional de terminación nerviosa se realizó aplicando un protocolo, con el que se seleccionaban de partida las terminaciones que presentaban actividad espontánea o que, en ausencia de ésta, respondían a un estímulo mecánico. Por tanto, quedaron excluidas aquellas terminaciones que no eran activadas por estímulos fisiológicos, incluso con intensidades de estímulo potencialmente dañinas para la integridad del tejido, como es el caso de los llamados

"nociceptores silentes" (Schaible and Schmidt, 1983; Michaelis, Häbler and Jäenig, 1996; Belmonte C, 2007), que parecen desarrollar un papel importante en la señalización del dolor en procesos inflamatorios en otros tejidos y cuya presencia en el ojo ha sido repetidamente sugerida (Belmonte *et al.*, 2017).

En la córnea del gato y del cobaya, los nociceptores polimodales son el tipo funcional de terminación sensorial más frecuentemente encontrado en estudios electrofisiológicos, representando un 65 % del total (Giraldez, Geijo and Belmonte, 1979; Belmonte and Giraldez, 1981; Belmonte *et al.*, 1991; Gallar *et al.*, 1993; Brock, McLachlan and Belmonte, 1998). En ratón la proporción de nociceptores polimodales respecto al total de terminaciones corneales fue comparativamente más baja, alrededor del 38 %. Lo mismo ocurre con las terminaciones mecano-nociceptoras, que en el ratón representan un 10 % mientras que en gato y cobaya varían entre el 15% y el 12 % (Belmonte *et al.*, 1991; Gallar *et al.*, 1993; Brock, McLachlan and Belmonte, 1998). En el lado opuesto, el porcentaje de termorreceptores de frío hallado en el ratón (casi el 45 %) es muy superior al del gato y el cobaya (17 y 21 %, respectivamente) (Belmonte *et al.*, 1991; Gallar *et al.*, 1993; Brock, McLachlan and Belmonte, 1998). Esta variabilidad podría ser atribuida a diferencias entre especies. Sin embargo, es también achacable a los distintos métodos de identificación de las fibras nerviosas sensoriales corneales, usados en cada caso. En los registros extracelulares de axones corneales en gato y cobaya, éstos se disecan en los nervios ciliares del ojo en la órbita de gatos anestesiados *in vivo* o en dichos nervios antes de penetrar en los ojos extraídos y perfundidos del cobaya (Giraldez, Geijo and Belmonte, 1979; Belmonte *et al.*, 1991). En ambos casos, la actividad eléctrica en las fibras nerviosas mecanosensibles Aδ ,ligeramente mielinizadas, se obtiene más fácilmente que en las fibras C, amielínicas, que corresponden mayoritariamente a nociceptores polimodales o fibras de frío (Gallar *et al.*, 1993; Acosta *et al.*, 2013; Fern *et al.*, 2016).

Por contra, la técnica utilizada para el registro de terminaciones nerviosas aisladas, in vitro, en ojos de ratón y cobaya, favorece la detección de los termorreceptores de frío, ya que presentan actividad espontánea, y en comparación con las terminaciones mecano-nociceptoras y polimodales, están localizadas más superficialmente, además de ramificarse extensamente, generando NTIs de mayor amplitud, lo que hace más fácil su detección

eléctrica (Gallar *et al.*, 1993; Carr, Pianova and Brock, 2002; Brock *et al.*, 2006; Carr *et al.*, 2009; Parra *et al.*, 2010; Acosta *et al.*, 2013; Ivanusic, Wood and Brock, 2013).

En la presente tesis hemos intentado compensar estas tendencias, realizando un muestreo sistemático de la presencia de NTIs, mediante la exploración de puntos de registro distribuidos regularmente sobre la superficie corneal, lo que, en teoría, facilita la localización de terminaciones nerviosas de cualquier tipo. Además, solo fueron tomadas en cuenta, para calcular la proporción relativa de cada tipo funcional de terminación respecto al total de éstas, aquellas que eran identificadas de manera inequívoca, distinguiéndose del ruido basal de modo claro y fiable. Por tanto, asumimos que, en conjunto, los datos obtenidos en la córnea de ratón ofrecen una imagen bastante aproximada de las proporciones relativas de los distintos tipos de terminaciones corneales en esta especie. Aun así, cabe señalar que dejamos de lado a un grupo de terminaciones no identificadas, que incluía las unidades de muy baja amplitud, en las que no fue posible evaluar la respuesta a los distintos estímulos y entre las que quizá podrían ocultarse los nociceptores silentes, o nociceptores polimodales generadores de NTIs de baja amplitud.

Tipos funcionales de terminaciones nerviosas en la córnea del ratón

Terminaciones mecanorreceptoras y polimodales

La respuesta al estímulo mecánico ha sido empleada anteriormente para segregar en la córnea del gato y el cobaya a las subpoblaciones de mecano-nociceptores y de nociceptores polimodales y así se ha hecho también en el presente estudio.

El método utilizado para aplicar estímulos mecánicos sobre la superficie corneal, un desplazamiento controlado hacia delante de la punta del electrodo, no permite medir con suficiente precisión y repetitividad el umbral de fuerza que activa las terminaciones mecano-nociceptoras puras y polimodales. En todo caso, la corta duración de la descarga de NTIs evocada por una presión sostenida, indica que ambas tipos de terminaciones pertenecen al grupo general de neuronas sensoriales primarias de respuesta fásica, compartiendo esta característica con sus equivalentes en la córnea de gato o cobaya (Belmonte *et al.*, 1991;

Gallar *et al.*, 1993; Brock, McLachlan and Belmonte, 1998; Acosta *et al.*, 2013, 2014). En los registros de la actividad extracelular de terminaciones nerviosas corneales en ratón no se encontraron diferencias de umbral mecánico entre terminaciones mecano-nociceptoras y nociceptoras polimodales. En la córnea de gato, el umbral mecánico medido con filamentos de von Frey es también muy similar en ambos tipos, por debajo de 1 mN (Belmonte and Giraldez, 1981; Belmonte *et al.*, 1991; Gallar *et al.*, 1993), como en nuestros experimentos empleando la fuerza generada por el desplazamiento de la pipeta, cuya fuerza exacta es difícilmente medible y comparable de un experimento a otro. En todo caso, los valores de umbral mecánico de los nociceptores mecánicos y polimodales de la córnea están en varios ordenes de magnitud por debajo de los de la piel de ratón (Reeh, 1986), lo cual es esperable, teniendo en cuenta la proximidad de las terminaciones nerviosas a la superficie, la ausencia de cornificación en el epitelio de la córnea y las diferentes propiedades viscoelásticas de ambos tejidos (Pubols, 1988).

Aunque el canal Piezo2 se consideró originalmente como la molécula transductora específica de los mecanorreceptores de bajo umbral (Ranade *et al.*, 2014; Woo *et al.*, 2015)se ha sugerido recientemente que este canal es también responsable de la mecano-sensibilidad nociceptora en la córnea y quizá otros tejidos (Murthy *et al.*, 2018; Fernández-Trillo *et al.*, 2020), como sugerían los estudios inmunocitoquímicos del grupo de Ivanusic (Bron *et al.*, 2014; Alamri *et al.*, 2015) en los que se mostraba la expresión de este canal en aproximadamente el 30 % de las neuronas trigeminales corneales, hipotéticamente en terminaciones ramificadas (Ivanusic, Wood and Brock, 2013). Un estudio muy reciente en la córnea de ratón ha demostrado que más del 80 % de las terminaciones nociceptoras polimodales son mecanosensibles y ha verificado la expresión del canal Piezo2 en las neuronas nociceptoras polimodales TRPV1, así como una drástica reducción de las respuestas mecánicas en las terminaciones nociceptoras polimodales y mecánicas puras en los ratones Piezo2 *ko* (Fernández-Trillo *et al.*, 2020). No se puede, sin embargo, descartar la presencia de otros canales implicados en mecanorrecepción, como el Nav 1.1 (Osteen *et al.*, 2016), expresado selectivamente en fibras mecano-sensoriales de alto umbral de la piel, el canal TRPA1 (Gallar *et al.*, 2017), o el papel de estructuras del epitelio corneal activadas por el desplazamiento causado por el estímulo mecánico en esta preparación.

Los nociceptores polimodales corneales de ratón respondieron de manera clara a estímulos mecánicos, calor nocivo, capsaicina y soluciones de osmolaridad alta (por encima de los 600 $mOsm \cdot Kg^{-1}$), y se sensibilizaron por aplicación de una 'sopa inflamatoria' que contenía una mezcla de mediadores de la inflamación (Kessler *et al.*, 1992), confirmando la similitud funcional de los nociceptores polimodales del ratón con los previamente descritos en gato o cobaya (Belmonte and Giraldez, 1981; Belmonte *et al.*, 1991; Gallar *et al.*, 1993). Los incrementos en frecuencia de disparo evocados por los diferentes estímulos en las terminaciones nociceptoras polimodales no son muy marcados. Es bien conocido, sin embargo, que en fibras nerviosas polimodales de otros tejidos en humanos, frecuencias de disparo por encima de 0.5 $imp \cdot s^{-1}$ son suficientes para evocar sensaciones dolorosas conscientes (Gybels, Handwerker and Van Hees, 1979; Yarnitsky *et al.*, 1992). Así pues, parece razonable concluir que la activación de las terminaciones nociceptoras polimodales, provocada por los diferentes estímulos empleados en nuestro estudio, presumiblemente evocan sensaciones dolorosas en ratones despiertos.

La sensibilidad al calor intenso, a la capsaicina y a la osmolaridad elevada, apoya la presencia de TRPV1 en estas terminaciones. El canal TRPV1 es considerado el principal transductor molecular del dolor (Julius and Basbaum, 2001). Su presencia en las terminaciones nociceptoras polimodales, que se activan por los estímulos nocivos, pero no por los inocuos de la misma modalidad, era previsible teniendo en cuenta la enérgica respuesta de lagrimeo y parpadeo provocada por la aplicación de capsaicina en la córnea de muchas especies animales, incluidos ratones y humanos (Gonzalez *et al.*, 1993; Vesaluoma *et al.*, 2000; Parra *et al.*, 2010). Es conocido que el AITC, agonista del canal TRPA1, un canal transductor identificado también en las terminaciones polimodales y que se abre por irritantes químicos exógenos, toxinas naturales, LPS bacterianos, agentes pruritogénicos, fuerzas mecánicas elevadas y temperaturas frías nocivas (Meseguer *et al.*, 2014) evoca lagrimeo y parpadeo irritativos, cuando se aplica en el ojo de ratón. Sin embargo, el bajo número de terminaciones nociceptoras polimodales que responden a la activación del canal TRPA1 en ratones(Parra *et al.*, 2010) y en cobayas (Acosta *et al.*, 2013) y que confirmamos en el presente estudio,

sugiere que los canales TRPA1 no están mayoritariamente expresados en los nociceptores polimodales corneales al menos en el ratón.

En general, cabe afirmar que nuestros datos confirman que los nociceptores polimodales que inervan la córnea del ratón son muy similares funcionalmente a los nociceptores polimodales que inervan la piel o la lengua del ratón (Zhang *et al.*, 2012; Meseguer *et al.*, 2014) y la córnea de otras especies de mamíferos.

En el epitelio corneal de cobaya se han descrito tres subpoblaciones de terminaciones nerviosas que expresan TRPV1, de acuerdo con su identidad molecular y su morfología: una de ellas presentando ramificaciones en la capa de células escamosas, que no expresan CGRP pero sí GFRα3, y las otras dos con terminaciones simples situadas en la capa de células aladas, una de las cuales expresa tanto CGRP como GFR α3, y la otra, presente además en el plexo sub-basal, que expresa CGRP pero no GFRα3 (Alamri *et al.*, 2015). Sin embargo, todavía no se ha podido establecer si existen diferencias funcionales entre ellas. Cabe señalar que un porcentaje muy pequeño de las terminaciones nociceptoras polimodales estudiadas aquí, presentaba una respuesta al calentamiento relativo causado por el regreso a la temperatura control desde la rampa de frío, sugiriendo que pudieran ser termorreceptores de calor, como los descritos en la piel de varias especies animales (Duclaux and Kenshalo DR, 1980; Hellon and Taylor, 1981; Spray, 1986). Sin embargo, estas terminaciones no diferían en su frecuencia basal o en la de respuesta a los diferentes estímulos, de las de los nociceptores polimodales canónicos, respondiendo además al calor nocivo, estímulos mecánicos y capsaicina. Además, no exhibían una relación entre la magnitud del cambio de temperatura y la frecuencia media de disparo, como es típico en los termorreceptores de calor (Sumino, Dubner and Starkman, 1973). Por ello, lo más plausible es considerarlos un subgrupo dentro de los nociceptores polimodales de la córnea también sensibles a calor inocuo (Sumino, Dubner and Starkman, 1973)s quizás debido a la expresión de canales termosensibles no identificados

.

Terminaciones termorreceptoras de frío

Las neuronas termorreceptoras de frío representan un 10-15 % de la población total de las neuronas sensitivas corneales (Belmonte *et al.*, 2004). Nuestro estudio confirma, funcionalmente, la abundante inervación de la córnea del ratón por axones periféricos de neuronas termorreceptoras de frío, también evidenciada en diversos estudios inmunohistoquímicos (Parra *et al.*, 2010; Ivanusic, Wood and Brock, 2013; Alcalde *et al.*, 2018).

Nuestro trabajo ha definido y caracterizado, por vez primera con criterios cuantitativos, dos tipos funcionalmente diferenciados de terminaciones de frío en la córnea, distinguibles por su actividad basal a 34ºC y su umbral térmico de respuesta al enfriamiento, que denominamos, por sus siglas en inglés, termorreceptores HB-y LB-. La variable sensibilidad térmica de las fibras nerviosas termorreceptoras de frío había sido ya detectada en registros de la actividad eléctrica en fibras nerviosas sensoriales de la piel, la lengua y también la córnea (Gallar *et al.*, 1993; Hirata and Oshinsky, 2012) Igualmente, los registros intracelulares de neuronas termorreceptoras de frío del GT o los ganglios raquídeos ponían en evidencia la existencia de dos poblaciones neuronales, diferenciables por el umbral de temperatura al que comienzan a disparar potenciales de acción en el soma cuando éste se enfría (Viana, De la Peña and Belmonte, 2002; Madrid *et al.*, 2006, 2009).

En esta tesis hemos descrito que la intensidad de fluorescencia somática en neuronas trigeminales de ratones adultos jóvenes TRPM8-EYFP correlaciona con la amplitud de la despolarización evocada por frío y mentol, lo que apoya la importancia de la densidad de canales TRPM8 en la sensibilidad al frío (De La Peña *et al.*, 2005; Xing *et al.*, 2006; Madrid *et al.*, 2009; Morenilla-Palao *et al.*, 2014). Otros factores que pueden influir en esta variable sensibilidad al frío de los termorreceptores de frío corneales, como las corrientes generadas por los canales de potasio IK_v, (Madrid *et al.*, 2006, 2009; Morenilla-Palao *et al.*, 2014) no han sido explorados en nuestro estudio. También hemos encontrado diferencias en la intensidad de fluorescencia EYFP entre los axones sensitivos periféricos $TRPM8^+$, lo que apoya la relevancia de este canal en las diferencias funcionales encontradas entre las dos poblaciones de termorreceptores de frío corneales.

Terminaciones termorreceptoras HB

El análisis sistemático de las poblaciones de fibras termorreceptoras de la córnea de ratón nos ha permitido caracterizar en ésta a terminaciones sensoriales con las características típicas de termorreceptores de frío canónicos descritos en otras especies y tejidos (Hensel, Iggo and Witt, 1960; Braun, Bade and Hensel, 1980; Belmonte *et al.*, 1991; Gallar *et al.*, 1993; Carr *et al.*, 2003). Estos, a los que denominamos HB, representan aproximadamente el 70 % del total de las terminaciones corneales de frío y presentan un bajo umbral térmico, es decir, responden marcadamente a pequeños descensos de temperatura, tanto estáticos como dinámicos por lo que de manera más precisa podrían ser denominados HB-LT. Este tipo de termorreceptores ya habían sido identificados previamente en la córnea (Gallar *et al.*, 1993; Carr *et al.*, 2003; Brock *et al.*, 2006; Parra *et al.*, 2010; Fern *et al.*, 2016). En los termorreceptores HB-LT la sensibilidad al frío depende críticamente de la expresión de TRPM8, un canal catiónico que se activa por enfriamiento, mentol y soluciones hiperosmolares (McKemy, Neuhausser and Julius, 2002; Peier *et al.*, 2002; De La Peña *et al.*, 2005; Parra *et al.*, 2010; Quallo *et al.*, 2015). Su eliminación por manipulación genética en ratones silencia totalmente a los termorreceptores de frío, mientras que su bloqueo con BCTC (N-(4-tertiarybutylphenyl)-4-(3-chloropyridin-2-yl) tetrahydropy-razine-1(2H)-carboxiamide), un antagonista del TRPM8, reduce significativamente la actividad basal en los termorreceptores de frío HB-LT e inhibe su respuesta al enfriamiento (Parra *et al.*, 2010).

Los termorreceptores corneales de frío HB-LT son también sensibles al mentol y a la hiperosmolaridad, tanto la obtenida con aumentos de concentración de NaCl en la película lagrimal, como con soluciones de manitol o sacarosa (Gallar *et al.*, 1993; Hirata and Meng, 2010; Hirata, Fried and Oshinsky, 2012; Hirata and Rosenblatt, 2014; Parra *et al.*, 2014; Hirata *et al.*, 2015; Quallo *et al.*, 2015). La sensibilidad osmótica parece estar mediada por una acción directa de los cambios de osmolaridad sobre la actividad del canal TRPM8 (Quallo *et al.*, 2015), si bien en el caso de la hiperosmolaridad por NaCl no puede excluirse un efecto adicional sobre la carga de superficie de la membrana neuronal por la alta concentración de iones sodio.

Las neuronas IF-EYFP TG de tamaño pequeño o medio, no peptidérgicas, son el origen más probable de los axones arrosariados que finalizan en el epitelio corneal como terminaciones

nerviosas complejas CGRP-negativas (Ivanusic, Wood and Brock, 2013; Alamri *et al.*, 2015). Cabe esperar que estas neuronas IF-EYFP posean una alta sensibilidad al frío, debido a la alta densidad de canales TRPM8 y a la baja expresión de canales Kv1 (Madrid *et al.*, 2009), además de la alta probabilidad de que este canal TRPM8 contribuya a la actividad basal que presentan los termorreceptores de frío corneales (Parra *et al.*, 2010). En conjunto, estos resultados sugieren una abundante expresión de canales TRPM8 en los axones arrosariados de elevada fluorescencia, cuyas terminaciones (mayoritariamente complejas en su morfología) son, posiblemente, una razón biofísica para sus características de disparo espontáneo, su bajo umbral y su intensa respuesta al enfriamiento; todas ellas características observadas en los termorreceptores de frío corneales HB (Carr *et al.*, 2009; Madrid *et al.*, 2009; Parra *et al.*, 2010; Teichert *et al.*, 2012; Olivares *et al.*, 2015; González-González *et al.*, 2017).

Terminaciones termorreceptoras LB

El presente estudio ha demostrado que, además de los termorreceptores HB, la córnea del ratón está inervada por otra subpoblación de terminaciones nerviosas sensibles al frío, que presentan una actividad muy baja a la temperatura basal de 34ºC y responden únicamente cuando el descenso de ésta es de 4 ºC o más, generando un incremento de frecuencia de impulsos nerviosos significativamente más débil que en el caso de los termorreceptores de frío HB, por lo que cabe denominarlos termorreceptores de frío LB-HT.

Este tipo de fibras termorreceptoras había sido detectado también en 1993 por Gallar et al. en la córnea del gato, denominándoles 'nociceptores de frío'. Muy posiblemente se corresponden también con las neuronas corneales "dry sensitive" descritas por Hirata et al (Hirata, Fried and Oshinsky, 2012) en el GT de la rata, que eran excitadas por niveles de sequedad corneal elevados y también por soluciones hiperosmolares y mentol, mostrando igualmente sensibilidad al enfriamiento de la superficie corneal (Hirata, Fried and Oshinsky, 2012; Hirata and Rosenblatt, 2014). El estudio detallado de la subpoblación de termorreceptores LB-HT prueba que éstos responden a soluciones hiperosmolares y a agonistas del canal TRPM8 como el mentol o el tacrolimus (González-González *et al.*, 2017; Arcas *et al.*, 2019), lo que confirma la dependencia de su sensibilidad térmica del canal

TRPM8, como ocurre en los termorreceptores HB-LT. Sin embargo, las diferencias con éstos en actividad basal, umbral de frío y magnitud de su respuesta al enfriamiento, a soluciones hiperosmóticas y a otros compuestos químicos, sugieren diferencias entre ambas subpoblaciones en densidad de expresión de TRPM8 y otros canales y posiblemente también en el papel que juega la información que transmiten al cerebro en la elaboración de las diferentes respuestas cognitivas y autónomas que evocan los estímulos corneales.

El origen de las terminaciones termorreceptoras LB son de acuerdo con nuestro trabajo, las neuronas WF que representan una segunda población de neuronas del GT que expresa TRPM8. Sus axones corneales, caracterizados por una fluorescencia débil, superficie lisa y diámetro pequeño, finalizan como terminaciones simples o ramificadas, funcionalmente caracterizadas por su baja actividad espontánea, alto umbral de respuesta a frío y débil respuesta al enfriamiento (González-González *et al.*, 2017). Las neuronas WF-TRPM8^{+} son TrkA y CGRP positivas, un fenotipo observado en nociceptores polimodales peptidérgicos de otros tejidos (Abe *et al.*, 2005; Takashima *et al.*, 2007; Knowlton *et al.*, 2013) por lo que es legítimo sugerir su pertenencia en términos de la modalidad sensorial que transmiten, a los nociceptores, encargados de la transducción de estímulos potencialmente dañinos y primer escalón en la génesis del dolor periférico, del que la sequedad molesta puede ser considerada una variedad perceptual más. Cabe resaltar, además, que la supresión genética de los canales TRPM8 así como la ablación condicionada de las neuronas que expresan TRPM8, reducen claramente las respuestas comportamentales no solo al frío inocuo sino también al nocivo, lo que apoya la observación de que las neuronas WF TRPM8 están conectadas con las vías del dolor (Palkar, Lippoldt and McKemy, 2015).

Mecanismos de transducción y codificación

En su conjunto, el análisis de las respuestas evocadas por los cambios de temperatura y osmolaridad en los dos tipos de terminaciones corneales termorreceptoras de frío HB-LT y LB-HT identificados en la córnea, y los efectos sobre su actividad de fármacos agonistas y antagonistas de canales iónicos, nos lleva a la conclusión de que la específica, aunque cuantitativamente diferente, sensibilidad al frío que exhiben ambos tipos de terminaciones termorreceptoras, depende fundamentalmente de la expresión de canales TRPM8, cuya

apertura por el descenso de temperatura genera la corriente despolarizante I_{cold} (Viana, De la Peña and Belmonte, 2002). No obstante, la expresión variable en cada uno de estos tipos neuronales de TRPM8 y de otros canales iónicos, es la que finalmente determina las diferencias entre ellos en el umbral, la magnitud de su descarga de impulsos nerviosos en respuesta al frío y su sensibilidad a otras modalidades de estímulo. Tales diferencias acaban definiendo el diferente contenido final del mensaje sensorial que envía cada una de ellas a sus neuronas diana en el SNC.

El registro electrofisiológico de las neuronas termorreceptoras de frío de los ganglios sensoriales ha precisado que la heterogeneidad observada en sus umbrales de frío viene determinada principalmente por la densidad de expresión de canales TRPM8 y también por la expresión de canales de potasio Kv1.1-1.2, responsables de la corriente $I_{KD,}$ que en las neuronas sensoriales primarias actúa como un freno a su despolarización inespecífica por los descensos de temperatura (Viana, De la Peña and Belmonte, 2002). En cultivos de neuronas trigeminales termorreceptoras de frío, se ha demostrado que aquellas de bajo umbral carecen de la corriente I_{KD}, mientras que en las que respondían solo a enfriamientos más intensos esta corriente I_{KD} era prominente (Madrid *et al.*, 2009), demostrando que en las neuronas termorreceptoras de frío tanto el umbral como su frecuencia de impulsos evocados por un enfriamiento dependen del balance entre los niveles de expresión de los canales TRPM8 y Kv1. Por tanto, es razonable asumir que las terminaciones termorreceptoras de frío HB de bajo umbral del ratón correspondan a los axones de neuronas del GT con alta expresión de canales TRPM8 y baja, o incluso nula, expresión de canales Kv1. Por otro lado, las terminaciones de frío LB de alto umbral provendrían de neuronas con una más baja expresión de TRPM8 y mayor de canales Kv1. En favor de esta interpretación está la mayor excitación provocada por el agonista de TRPM8 mentol en las terminaciones termorreceptores de frío HB-LT respecto de los LB-HT y la observación de que la perfusión con 4-AP, un bloqueante de los canales Kv1 que por tanto neutraliza la corriente I_{KD}, estimula los termorreceptores de frío LB-HT más enérgicamente que el mentol, reforzando la mayor importancia de la corriente I_{KD} en relación con la I_{cold} en esta subpoblación de termorreceptores de frío.

Las alta incidencia en las dos subpoblaciones de termorreceptores de frío corneales identificadas en el ratón, de respuestas evocadas por otras modalidades de estímulo tales como calor, estímulos mecánicos o diferentes agentes químicos irritantes, confirma la

expresión adicional en las neuronas termorreceptoras de frío de la córnea, de otros canales iónicos involucrados en la transducción sensorial (Belmonte and Viana, 2008). La expresión de canales TRPV1 ha sido sugerida repetidamente tras la observación de una acción excitante de la capsaicina en muchas terminaciones termorreceptoras de frío y se ha propuesto que este canal contribuye a la respuesta paradójica al calor (Hirata, Fried and Oshinsky, 2012). Contrariamente, no se ha obtenido evidencia funcional de que las neuronas termorreceptoras de frío expresen Piezo2 ni TRPA1 en magnitud suficiente como para explicar la sensibilidad mecánica de casi la mitad de los termorreceptoras de frío del ratón. Es posible que su sensibilidad mecánica esté mediada por un canal mecanosensible todavía no identificado o, lo que parece más probable, por algún canal de potasio, sodio o calcio no particularmente selectivo para la detección de fuerza mecánica pero que se abre cuando la membrana se distiende por ésta. Finalmente, la expresión prominente en los termorreceptores HB-LT de canales que regulan la excitabilidad neuronal como los HCN (*hyperpolarization-activated cyclic-nucleotide-modulated channels*), modulan la corriente despolarizante y contribuyen al disparo regular característico de ese tipo de termorreceptores de frío (P. Orio *et al.*, 2012).
En resumen nuestros datos sugieren que la expresión de diferentes canales de transducción con capacidad para responder a estímulos de modalidad diferente (Belmonte and Viana, 2008) es una característica prominente en los termorreceptores de frío corneales, que permite a la superficie ocular disponer de un set de receptores sensoriales particularmente equipados para la detección de los principales parámetros físicos asociados con los cambios en la humedad de la superficie corneal (temperatura, osmolaridad, deformación de la membrana celular) (Belmonte *et al.*, 2015).

Proyección central de la información sensorial de la cornea

Una de las dos ramas en las que se dividen los axones de las neuronas corneales situadas en el GT se dirige centralmente hacia el eje neural. La información de las neuronas corneales mecano-nociceptoras, que responden preferentemente a estímulos mecánicos y las nociceptoras polimodales, activadas por una amplia variabilidad de estímulos químicos, mecánicos y térmicos nocivos, constituye el sustrato nervioso periférico de las sensaciones de dolor ocular, tanto agudo como crónico (Belmonte *et al.*, 2004; Belmonte, Tervo and Gallar, 2011). Las neuronas de segundo orden con las que conectan directamente las neuronas

corneales periféricas de estas dos modalidades están localizadas principalmente en los niveles caudales del núcleo espinal trigeminal, en la región de transición entre el subnucleus caudalis espino-trigeminal y la médula espinal cervical (Vc/C1) (Meng *et al.*, 1997; Bereiter *et al.*, 2005).

En contraste, la evidencia experimental apunta a que la mayoría de los termorreceptores corneales HB–LT proyectan en neuronas de segundo orden localizadas más arriba, en la zona de transición entre los nucleus caudalis e interpolaris (Vi/Vc) en el complejo nuclear trigeminal, un área que parece ser el centro de procesamiento neuronal de la lagrimación y el parpadeo vía el núcleo salivar superior (SSN) y el núcleo motor del facial (Hirata, 2004; Kurose and Meng, 2013a). Estas dos áreas también reciben información de las neuronas Vc/C1 conectadas periféricamente con nociceptores corneales, a través de proyecciones a Vi/Vc, encargadas del reflejo palpebral motor y la lagrimación aguda evocados por los estímulos dañinos (Bereiter *et al.*, 2005; Katagiri *et al.*, 2015).

En condiciones ambientales normales, se ha sugerido que los pequeños cambios en la temperatura de la superficie ocular y en la osmolaridad resultante de la evaporación del fluido de la película lagrimal que cubre la superficie del ojo, son codificados por los termorreceptores de frío HB (Belmonte *et al.*, 1991, 2015; Gallar *et al.*, 1993; Carr *et al.*, 2003; Hirata and Meng, 2010; Parra *et al.*, 2010, 2014; Belmonte and Gallar, 2011) y transmitidos a las neuronas de segundo orden Vi/Vc (Hirata, 2004; Kurose and Meng, 2013b). Esto permite modular la secreción lagrimal y el ritmo basal de parpadeo, ajustando reflejamente el grado de humidificación de la superficie del ojo a la sequedad ambiental, sin evocar sensaciones conscientes. Cuando se produce un exceso de evaporación, una secreción lagrimal patológicamente reducida y/o una hiperosmolaridad de la película lacrimal, los termorreceptores de frío LB-HT serían también reclutados. Las fibras nerviosas mecano-nociceptoras y polimodales se activarían igualmente como resultado de la deformación celular y la inflamación local generadas por la sequedad. En conjunto, el mensaje sensorial multi-receptor evoca un aumento en la lagrimación y en el parpadeo, a la vez que genera sensaciones desagradables e irritantes. Éstas se asocian con la enfermedad del ojo seco crónico y otra serie de patologías de la superficie ocular (Belmonte *et al.*, 2015; Fern *et al.*, 2016).

La proyección de los termorreceptores de frío LB no está definida del todo. Algunos autores han señalado que solo con un enfriamiento elevado se consigue la activación de un grupo de neuronas de segundo orden de la región Vi/Vc (Kurose and Meng, 2013a), que se activaban, además, por estimulación ácida de la córnea, lo que sugiere que exista un input directo de los termorreceptores LB-HT y los nociceptores polimodales a esta zona. Además, en la sequedad ocular crónica en la que los termorreceptores de frío de alto umbral LB-HT están sensibilizados selectivamente (Fern *et al.*, 2016) hay un incremento en la actividad de las neuronas oculares de 2º orden tanto en Vi/Vc como Vc/C1 (Kurose and Meng, 2013a; Hirata and Rosenblatt, 2014; Rahman *et al.*, 2015). Ello sugiere que las neuronas LB de alto umbral contribuyen de manera relevante a las sensaciones de malestar que acompañan a la sequedad de la superficie ocular crónica (Belmonte *et al.*, 2015; Fern *et al.*, 2016). Así pues, cabe especular con que esta subpoblación de termorreceptores de frío proyecta de manera primaria en las neuronas de la vía nociceptora de la región Vc/C1, evocando malestar y también, junto con las conectadas con nociceptores polimodales de ese mismo área, con la región Vi/Vc involucrada en la regulación con fines de protección de la lagrimación y el parpadeo tras el daño tisular.

De acuerdo con esta interpretación, las neuronas TRPM8^{+} del GT son el origen de las vías centrales sensitivas tanto para la detección del enfriamiento inocuo de la superficie ocular, principalmente implicado en la regulación de la lagrima basal (los termorreceptores de frío HB), como para la detección de la sequedad potencialmente lesiva, evocando respuestas desagradables, de lagrimación refleja y de parpadeo (los termorreceptores de frío LB) (Parra *et al.*, 2010; Belmonte *et al.*, 2015, 2017; Quallo *et al.*, 2015; Fern *et al.*, 2016).

A pesar de que la especificidad funcional de varias clases de poblaciones de neuronas sensitivas primarias para un tipo particular de estímulo está bien definida, esta promiscuidad molecular determina su activación potencial por estímulos de otras modalidades, particularmente bajo condiciones anormales. Es concebible que la heterogeneidad molecular de neuronas pertenecientes a un tipo funcional general pueda estar detrás, al menos en parte, de la llamativa variabilidad de mensajes sensitivos periféricos generados por los tejidos de la superficie ocular en condiciones patológicas, tales como la inflamación o la lesión.

Esta tesis ha sido realizada en córneas de ratón, un modelo experimental particularmente útil para el estudio de las bases moleculares de las sensaciones de la superficie ocular. Se han definido las características electrofisiológicas de las diferentes clases de terminaciones nerviosas sensitivas que inervan la córnea de esta especie, proporcionando nuevos datos que pueden, bajo nuestro punto de vista, ser útiles para una aproximación multidisciplinar que estudie estas sensaciones en condiciones normales y patológicas. Una de estas condiciones es el envejecimiento, y los datos electrofisiológicos aportados en los dos primeros apartados de la Tesis han servido como base comparativa para dilucidar posibles cambios ocurridos con la edad

Efectos morfo-funcionales del envejecimiento sobre la inervación corneal.

A pesar de las diferencias cuantitativas en la duración de la vida en humanos y ratones, las curvas de supervivencia entre ambas especies son muy parecidas (ComfortA., 1964). De hecho, el ratón ha sido un modelo experimental ampliamente usado para estudiar los efectos biológicos del envejecimiento (Wang and Albers, 2009). De ahí la elección de ratones transgénicos TRPM8^{BAC}-EYFP para analizar combinadamente los cambios morfológicos y funcionales inducidos por la edad avanzada en la inervación de la superficie corneal por una población, la de los termorreceptores de frío, con una función importante en la homeostasis corneal.

Los estudios morfológicos previos sobre las variaciones en la inervación corneal con el envejecimiento han arrojado resultados conflictivos. En humanos se ha descrito que la densidad nerviosa medida tanto *in vivo* (Parissi *et al.*, 2013) como en córneas teñidas (He, Bazan and Bazan, 2010) disminuye con la edad. Por el contrario, en ratas, la densidad de las fibras nerviosas subbasales pareció aumentar con el envejecimiento pero con un descenso simultaneo y progresivo de las terminaciones nerviosas epiteliales (Dvorscak and Marfurt, 2008). En el ratón, en el que la densidad de los nervios corneales subbasales varía ampliamente dependiendo de la tinción empleada, se ha reportado una reducción general de los mismos en los animales viejos (Reichard *et al.*, 2016).

Nuestro estudio muestra que el número de neuronas del GT en los ratones jóvenes y viejos no difería significativamente, lo que sugiere que el envejecimiento tiene un efecto más pronunciado sobre la densidad y arquitectura de los axones periféricos que sobre los cuerpos celulares de las neuronas sensoriales primarias. Sin embargo, éstas experimentaron cambios sutiles asociados a su fenotipo, como evidencia el mayor porcentaje de neuronas TRPM8^{+} en los animales viejos, un incremento observado principalmente en la subpoblación de neuronas WF-EYFP que expresaban periferina, TrkA y CGRP, una inmunoreactividad típica de los nociceptores polimodales, mientras que la población de neuronas IF-EYFP, termorreceptoras de frío HB-LT con axones corneales arrosariados y de fluorescencia más intensa, permaneció relativamente estable.

La conservación en los animales viejos de una correspondencia entre la despolarización inducida por frío y la intensidad en la fluorescencia del soma observada en ratones jóvenes, y unas respuestas al enfriamiento y al mentol muy similares, confirma la mayor resistencia de los cuerpos neuronales a los efectos de la edad, con la única diferencia de una respuesta algo menor de las neuronas IF al mentol en los ratones viejos., en paralelo o combinado con una mayor vulnerabilidad de las neuronas IF-TRPM8^{+} al envejecimiento.

Los escasos cambios causados por la edad en los cuerpos neuronales de las neuronas termorreceptoras de frío, contrastan con las marcadas alteraciones morfológicas y funcionales desarrolladas por los axones periféricos y las terminaciones corneales en ratones viejos.

En conjunto, la densidad total de axones corneales subbasales TPM8-EYFP fue significativamente menor, a expensas de una amplia reducción de los axones más intensamente fluorescentes y arrosariados, compensada en parte por el incremento en la densidad de los axones lisos y finos. La reducción en la inervación se reflejó también en una disminución de las terminaciones nerviosas electrofisiológicamente activas.

Los termorreceptores de frío corneales HB siguen presentes en los ratones viejos, si bien exhibiendo menor actividad basal y más débil respuesta al enfriamiento. Este cambio podría explicarse por la marcada disminución en los animales viejos de las ramificaciones complejas, características de los termorreceptores canónicos de frío (Ivanusic, Wood and Brock, 2013) lo que representa una reducción del área total de membrana en la que se genera el potencial generador, de cuya amplitud total depende la frecuencia final de disparo de

potenciales de acción en el axón principal (Brock, Pianova and Belmonte, 2001; Carr *et al.*, 2009; Olivares *et al.*, 2015)t. El mismo mecanismo explica también las diferencias en las características de disparo en los ratones jóvenes de los termorreceptores de frío LB-HT, que disponen de una menor densidad de canales TRPM8 en comparación con los termorreceptores HB-LT. La presencia de un mayor porcentaje de neuronas y terminaciones termorreceptoras de frío LB-HT en los animales viejos explica adicionalmente la presencia en éstos de una actividad eléctrica alterada.

El número de nociceptores polimodales también está afectado en los ratones viejos. Aunque los cambios funcionales de los nociceptores polimodales resultantes de su lesión periférica tras cirugía o sequedad del ojo experimental son menores que los observados en los termorreceptores durante reducciones prolongadas de la humedad de la superficie ocular (Fern *et al.*, 2016; Bech *et al.*, 2018), no puede descartarse la posibilidad de que, en los animales viejos, una proporción de los mismos se haya sensibilizado (Belmonte, Garcia-Hirschfeld and Gallar, 1997) y adquirido un fenotipo que les haga sensibles a los estímulos de frío intenso, frecuente en los nociceptores polimodales de otros tejidos (Darian-Smith, Johnson and Dykes, 1973; Johnson, Darian-Smith and LaMotte, 1973; Belmonte, Brock and Viana, 2009). La alta correlación morfológica y molecular entre las terminaciones polimodales y los termorreceptores de frío LB-HT, así como la probabilidad de que compartan vías nociceptivas, sugiere que parte de los efectos cognitivos (disestesias, sensaciones de sequedad) y reflejos (lagrimación y parpadeo alterados) presentes en los ancianos sean debidos a la actividad alterada de ambos tipos terminaciones nerviosas en la superficie ocular.

En conjunto, nuestros datos indican que el envejecimiento determina la aparición progresiva de cambios morfológicos y funcionales que aparecen antes en las ramificaciones periféricas de las neuronas de frío y varían dependiendo del subtipo neuronal, mientras el cuerpo celular resulta menos afectado. Los efectos diferenciales de la senescencia sobre las distintas modalidades de neuronas sensoriales han sido también señalados en otros tejidos somatosensoriales y viscerales en roedores y humanos (Namer *et al.*, 2009; Nolano *et al.*, 2013).

Las modificaciones morfológicas y funcionales de la inervación sensorial inducidas por la edad son parte de los procesos de senescencia generales, asociadas con daño del ADN y el estrés oxidativo ((Long *et al.*, 2014) para revisión). Cabe pensar que las alteraciones morfométricas, ultraestructurales y funcionales de los axones periféricos de los nervios corneales periféricos pueden aparecer más precozmente con el envejecimiento, debido a la celeridad de los procesos de regeneración y remodelación que tienen lugar normalmente en las terminaciones nerviosas corneales de los sujetos jóvenes, debido a la rápida y continua renovación de las capas más superficiales del epitelio corneal (Harris and Purves, 1989).

Alteraciones de la lagrimación con el envejecimiento

Hay una evidencia experimental y clínica cada vez más abundante, apoyando la propuesta de que la activación de las fibras de frío TRPM8^{+} por los pequeños cambios de temperatura y osmolaridad resultantes de la evaporación normal de la película lagrimal constituye la rama aferente de un sistema de regulación neural de la lagrimación basal (Belmonte *et al.*, 2015, 2017; Belmonte, 2019). El incremento en la tasa de lagrimación basal y la osmolaridad de la lágrima observado en los ratones viejos aparece en paralelo con una reducción en la densidad de los axones subbasales arrosariados IF, cuya actividad basal (HB) se considera la responsable del mantenimiento de la lagrimación basal en animales jóvenes (Parra *et al.*, 2010), pero va acompañado de un aumento significativo de los axones y terminaciones WF, cuya posible asociación con los nociceptores polimodales y sus neuronas de proyección comentamos anteriormente. La anómala actividad y respuesta al frío en los animales viejos de esta subpoblación de terminaciones corneales podrían explicar el acusado aumento del flujo lagrimal irritativo, pese a la disminución del mecanismo de secreción basal más dependiente de los termorreceptores de frío HB.

En persona ancianas diagnosticadas del SOS (síndrome de ojo seco), a menudo se observa también un incremento de la lagrimación (epifora) acompañada de irritación y malestar. En seres humanos, se han evocado experimentalmente sensaciones similares de malestar, acompañadas de lagrimación aumentada, mediante la estimulación de la córnea con frío intenso y mentol (Acosta *et al.*, 2004; Fern *et al.*, 2016). Aunque la epifora en personas ancianas se atribuye principalmente a la oclusión parcial o completa de las vías de drenaje (Sousa *et al.*, 1993), es posible que en los pacientes con este padecimiento, al igual que en

los ratones viejos, la actividad anómala de las neuronas sensibles al frío contribuya adicionalmente al exceso de lagrimación, y que la actividad aumentada en las fibras sensibles al frío LB-HT conectadas a las vías nociceptivas, genere las paradójicas sensaciones desagradables de "ojo seco" reportadas por los pacientes con epifora. No puede, sin embargo, descartarse que la inflamación paralela de la superficie ocular sensibilice a los nociceptores polimodales, que se sumarían al desarrollo de las disestesias y la lagrimación (Belmonte, 2019).

Podemos, pues, concluir que nuestro estudio experimental en ratones viejos demuestra que el envejecimiento reduce el número y la actividad funcional de las neuronas receptoras de frío de la superficie ocular que contribuyen al mantenimiento tónico de la lagrimación basal (los termorreceptores de frío HB), pero provoca, al tiempo, un cambio fenotípico y la alteración de la actividad de las neuronas de frío LB de alto umbral, haciendo que algunas de ellas pasen a ser sensibles al enfriamiento moderado y favoreciendo, por tanto, la aparición, en condiciones externas normales, de sensaciones de sequedad desagradables y lagrimación irritativa. El equilibrio alterado entre las terminaciones que expresan TRPM8 jugaría, en definitiva, un papel importante en los cambios de la calidad y cantidad de lágrima y la aparición de sensaciones desagradables, frecuentemente observados en pacientes ancianos que padecen SOS.

VI. Conclusiones

1. Se han caracterizado y diferenciado en la córnea del ratón, tres tipos funcionales de terminaciones sensoriales: mecano-nociceptores, nociceptores polimodales y termorreceptores de frío.

2. Dentro de los termorreceptores de frío, se han caracterizado dos subpoblaciones: termorreceptores de frío HB-LT, con actividad basal alta, bajo umbral y alta frecuencia de respuesta al enfriamiento que parecen ser responsables de la lagrimación y el parpadeo basales, no irritativos; y termorreceptores de frío LB-HT, con baja actividad basal, de alto umbral de frío y baja frecuencia de respuesta al enfriamiento, que parecen asociados las sensaciones nociceptivas y la lagrimación irritativa.

3. El envejecimiento en ratones genera cambios en las características funcionales y morfológicas en las dos poblaciones de termorreceptores de frío corneales.

4. Estos cambios serían los principales responsables de la aparición de lagrimación irritativa y de las sensaciones desagradables de sequedad asociadas con el envejecimiento.

VII. Bibliografía

Abe, J. *et al.* (2005) 'TRPM8 protein localization in trigeminal ganglion and taste papillae', *Molecular Brain Research*, 136(1–2), pp. 91–98. doi: 10.1016/j.molbrainres.2005.01.013.

Acosta, M. C. *et al.* (2004) 'Tear Secretion Induced by Selective Stimulation of Corneal and Conjunctival Sensory Nerve Fibers', *Investigative Opthalmology & Visual Science*, 45(7), p. 2333. doi: 10.1167/iovs.03-1366.

Acosta, M. C. *et al.* (2013) 'Changes in sensory activity of ocular surface sensory nerves during allergic keratoconjunctivitis.', *Pain*. Netherlands, 154(11), pp. 2353–2362. doi: 10.1016/j.pain.2013.07.012.

Acosta, M. C. *et al.* (2014) 'Corneal Sensory Nerve Activity in an Experimental Model of UV Keratitis', *Investigative Opthalmology & Visual Science*, 55(6), p. 3403. doi: 10.1167/iovs.13-13774.

Acosta, M. C., Belmonte, C. and Gallar, J. (2001) 'Sensory experiences in humans and single-unit activity in cats evoked by polymodal stimulation of the cornea', *The Journal of Physiology*, 534(2), pp. 511–525. doi: 10.1111/j.1469-7793.2001.t01-1-00511.x.

Adrian, E. D. (1926) 'The impulses produced by sensory nerve endings', *The Journal of Physiology*, 61(1), pp. 49–72. doi: 10.1113/jphysiol.1926.sp002273.

Alamri, A. *et al.* (2015) 'Transient receptor potential cation channel subfamily V member 1 expressing corneal sensory neurons can be subdivided into at least three subpopulations', *Frontiers in Neuroanatomy*, 9(June), p. 71. doi: 10.3389/fnana.2015.00071.

Alamri, A. S. *et al.* (2018) 'The neurochemistry and morphology of functionally identified corneal polymodal nociceptors and cold thermoreceptors', *PLOS ONE*. Edited by D. D. McKemy, 13(3), p. e0195108. doi: 10.1371/journal.pone.0195108.

Alcalde, I. *et al.* (2018) 'Morphological and functional changes in TRPM8-expressing corneal cold thermoreceptor neurons during aging and their impact on tearing in mice.', *The Journal of comparative neurology*, 526(11), pp. 1859–1874. doi: 10.1002/cne.24454.

Alghamdi, Y. A. *et al.* (2016) 'Epidemiology of Meibomian Gland Dysfunction in an Elderly Population', *Cornea*, 35(6), pp. 731–735. doi: 10.1097/ICO.0000000000000815.

Arcas, J. M. *et al.* (2019) 'The Immunosuppressant Macrolide Tacrolimus Activates Cold-Sensing TRPM8 Channels.', *The Journal of neuroscience : the official journal of the Society for Neuroscience*. Society for Neuroscience, 39(6), pp. 949–969. doi: 10.1523/JNEUROSCI.1726-18.2018.

Baljet, B. and VanderWerf, F. (2005) 'Connections between the lacrimal gland and sensory trigeminal neurons: a WGA/HRP study in the cynomolgous monkey', *Journal of Anatomy*, 206(3), pp. 257–263. doi: 10.1111/j.1469-7580.2005.00374.x.

Bech, F. *et al.* (2018) 'Functional and Morphologic Alterations in Mechanical, Polymodal, and Cold Sensory Nerve Fibers of the Cornea Following Photorefractive Keratectomy.',

Investigative ophthalmology & visual science, 59(6), pp. 2281–2292. doi: 10.1167/iovs.18-24007.

Begley, C. *et al.* (2013) 'Quantitative Analysis of Tear Film Fluorescence and Discomfort During Tear Film Instability and Thinning', *Investigative Opthalmology & Visual Science*, 54(4), p. 2645. doi: 10.1167/iovs.12-11299.

Belmonte, C. *et al.* (1991) 'Excitation by irritant chemical substances of sensory afferent units in the cat's cornea.', *The Journal of Physiology*, 437(1), pp. 709–725. doi: 10.1113/jphysiol.1991.sp018621.

Belmonte, C. (1996) 'Signal transduction in nociceptors: general principles', in Belmonte, C. and Cervero, F. (eds) *Neurobiology of Nociceptors*. Oxford University Press, pp. 243–257. doi: 10.1093/acprof:oso/9780198523345.003.0010.

Belmonte, C. *et al.* (2004) 'Nerves and Sensations from the Eye Surface', *The Ocular Surface*. Elsevier, 2(4), pp. 248–253. doi: 10.1016/S1542-0124(12)70112-X.

Belmonte, C. *et al.* (2015) 'What Causes Eye Pain?', *Current Ophthalmology Reports*. Springer US, 3(2), pp. 111–121. doi: 10.1007/s40135-015-0073-9.

Belmonte, C. *et al.* (2017) 'TFOS DEWS II pain and sensation report.', *The ocular surface*, 15(3), pp. 404–437. doi: 10.1016/j.jtos.2017.05.002.

Belmonte, C. (2019) 'Pain, dryness, and itch sensations in eye surface disorders are defined by a balance between inflammation and sensory nerve injury', *Cornea. In Press.*

Belmonte, C., Brock, J. A. and Viana, F. (2009) 'Converting cold into pain', *Experimental Brain Research*. Germany, 196(1), pp. 13–30. doi: 10.1007/s00221-009-1797-2.

Belmonte, C. and Gallar, J. (2011) 'Cold Thermoreceptors, Unexpected Players in Tear Production and Ocular Dryness Sensations', *Investigative Opthalmology & Visual Science*, 52(6), p. 3888. doi: 10.1167/iovs.09-5119.

Belmonte, C., Garcia-Hirschfeld, J. and Gallar, J. (1997) 'Neurobiology of ocular pain', *Progress in Retinal and Eye Research*, 16(1), pp. 117–156. doi: 10.1016/S1350-9462(96)00027-4.

Belmonte, C. and Giraldez, F. (1981) 'Responses of cat corneal sensory receptors to mechanical and thermal stimulation.', *The Journal of Physiology*. Wiley-Blackwell, 321(1), pp. 355–368. doi: 10.1113/jphysiol.1981.sp013989.

Belmonte, C., Tervo, T. and Gallar, J. (2011) 'Sensory innervation of the eye', in *Alder's: physiology of the eye*, pp. 363–383.

Belmonte, C. and Viana, F. (2008) 'Molecular and Cellular Limits to Somatosensory Specificity', *Molecular Pain*, 4(1), pp. 1744-8069-4–14. doi: 10.1186/1744-8069-4-14.

Belmonte C, V. F. (2007) 'Transduction and encoding of noxious stimuli', *Encyclopedia of Pain. R.F. Schmidt & W. Willis, Eds. Springer-Verlag. Berlin.*

Bereiter, D. A. *et al.* (2005) 'Endotoxin-Induced Uveitis Causes Long-Term Changes in Trigeminal Subnucleus Caudalis Neurons', *Journal of Neurophysiology*, 94(6), pp. 3815–3825. doi: 10.1152/jn.00616.2005.

Bereiter, D. A., Hirata, H. and Hu, J. W. (2000) 'Trigeminal subnucleus caudalis: beyond homologies with the spinal dorsal horn.', *Pain*, 88(3), pp. 221–4. Available at: http://www.ncbi.nlm.nih.gov/pubmed/11068108 (Accessed: 6 June 2019).

Bois, P. *et al.* (1996) 'Mode of action of bradycardic agent, S 16257, on ionic currents of rabbit sinoatrial node cells', *British Journal of Pharmacology*, 118(4), pp. 1051–1057. doi: 10.1111/j.1476-5381.1996.tb15505.x.

Braun, H. A., Bade, H. and Hensel, H. (1980) 'Static and dynamic discharge patterns of bursting cold fibers related to hypothetical receptor mechanisms.', *Pflugers Archiv : European journal of physiology*. GERMANY, WEST, 386(1), pp. 1–9.

Brierley, S. M. *et al.* (2009) 'The Ion Channel TRPA1 Is Required for Normal Mechanosensation and Is Modulated by Algesic Stimuli', *Gastroenterology*, 137(6), pp. 2084-2095.e3. doi: 10.1053/j.gastro.2009.07.048.

Brock, J. *et al.* (2006) 'Barium ions inhibit the dynamic response of guinea-pig corneal cold receptors to heating but not to cooling', *The Journal of Physiology*, 575(2), pp. 573–581. doi: 10.1113/jphysiol.2006.110130.

Brock, J. A., McLachlan, E. M. and Belmonte, C. (1998) 'Tetrodotoxin-resistant impulses in single nociceptor nerve terminals in guinea-pig cornea', *The Journal of Physiology*, 512(1), pp. 211–217. doi: 10.1111/j.1469-7793.1998.211bf.x.

Brock, J. A., Pianova, S. and Belmonte, C. (2001) 'Differences between nerve terminal impulses of polymodal nociceptors and cold sensory receptors of the guinea-pig cornea', *The Journal of Physiology*, 533(2), pp. 493–501. doi: 10.1111/j.1469-7793.2001.0493a.x.

Bron, A. J. *et al.* (2004) 'Functional aspects of the tear film lipid layer.', *Experimental eye research*, 78(3), pp. 347–60. Available at: http://www.ncbi.nlm.nih.gov/pubmed/15106912 (Accessed: 11 June 2019).

Bron, R. *et al.* (2014) 'Piezo2 expression in corneal afferent neurons', *Journal of Comparative Neurology*, 522(13), pp. 2967–2979. doi: 10.1002/cne.23560.

Cabanes, C., Viana, F. and Belmonte, C. (2006) 'Differential Thermosensitivity of Sensory Neurons in the Guinea Pig Trigeminal Ganglion', *Journal of Neurophysiology*, 90(4), pp. 2219–2231. doi: 10.1152/jn.00299.2003.

Callejo, G. *et al.* (2015) 'Acid-sensing ion channels detect moderate acidifications to induce ocular pain', *Pain*, 156(3), pp. 483–495. doi: 10.1097/01.j.pain.0000460335.49525.17.

Carr, R. W. *et al.* (2003) 'Effects of heating and cooling on nerve terminal impulses recorded from cold-sensitive receptors in the guinea-pig cornea.', *The Journal of general physiology*, 121(5), pp. 427–439. doi: 10.1085/jgp.200308814.

Carr, R. W. *et al.* (2009) ‘Action potential initiation in the peripheral terminals of cold-sensitive neurones innervating the guinea-pig cornea.’, *The Journal of physiology*, 587(Pt 6), pp. 1249–64. doi: 10.1113/jphysiol.2008.167023.

Carr, R. W., Pianova, S. and Brock, J. A. (2002) ‘The Effects of Polarizing Current on Nerve Terminal Impulses Recorded from Polymodal and Cold Receptors in the Guinea-pig Cornea’, *The Journal of General Physiology*, 120(3), pp. 395–405. doi: 10.1085/jgp.20028628.

Carstens, E., Kuenzler, N. and Handwerker, H. O. (1998) ‘Activation of Neurons in Rat Trigeminal Subnucleus Caudalis by Different Irritant Chemicals Applied to Oral or Ocular Mucosa’, *Journal of Neurophysiology*, 80(2), pp. 465–492. doi: 10.1152/jn.1998.80.2.465.

Caterina, M. J. *et al.* (1997) ‘The capsaicin receptor: a heat-activated ion channel in the pain pathway.’, *Nature*. ENGLAND, 389(6653), pp. 816–824. doi: 10.1038/39807.

Chao, C. *et al.* (2015) ‘Structural and functional changes in corneal innervation after laser in situ keratomileusis and their relationship with dry eye’, *Graefe’s Archive for Clinical and Experimental Ophthalmology*, 253(11), pp. 2029–2039. doi: 10.1007/s00417-015-3120-1.

Chen, W.-H. *et al.* (2012) ‘Salt-and-pepper eye pain and brainstem stroke’, *Clinical Neurology and Neurosurgery*, 114(7), pp. 972–975. doi: 10.1016/j.clineuro.2012.02.023.

Chen, X. *et al.* (1995) ‘CO2 stimulation of the cornea: a comparison between human sensation and nerve activity in polymodal nociceptive afferents of the cat.’, *The European journal of neuroscience*, 7(6), pp. 1154–63. Available at: http://www.ncbi.nlm.nih.gov/pubmed/7582088 (Accessed: 6 June 2019).

Chen, X., Belmonte, C. and Rang, H. P. (1997) ‘Capsaicin and carbon dioxide act by distinct mechanisms on sensory nerve terminals in the cat cornea.’, *Pain*. NETHERLANDS, 70(1), pp. 23–29.

Chiang, C. Y. *et al.* (2002) ‘Central Sensitization of Nociceptive Neurons in Trigeminal Subnucleus Oralis Depends on Integrity of Subnucleus Caudalis’, *Journal of Neurophysiology*, 88(1), pp. 256–264. doi: 10.1152/jn.00944.2001.

Clapham, C. *et al.* (2000) ‘Vanilloid receptor-1 is essential for inflammatory thermal hyperalgesia’, *Nature*, 405(6783), pp. 183–7. doi: 10.1038/35012076.

ComfortA. (1964) *Ageing. The biology of senescence.* London: Routledge & Kegan Paul Ltd. Eev. ed.

Corcoran, P. *et al.* (2017) ‘Dynamic Sensitivity of Corneal TRPM8 Receptors to Menthol Instillation in Dry Eye Versus Normal Subjects’, *Journal of Ocular Pharmacology and Therapeutics*, 33(9), pp. 686–692. doi: 10.1089/jop.2017.0050.

Corfield, A. P. *et al.* (1997) ‘Ocular mucins: Purification, metabolism and functions’, *Progress in Retinal and Eye Research*, 16(4), pp. 627–656. doi: 10.1016/S1350-9462(96)00039-0.

Coste, B. *et al.* (2010) 'Piezo1 and Piezo2 Are Essential Components of Distinct Mechanically Activated Cation Channels', *Science*, 330(6000), pp. 55–60. doi: 10.1126/science.1193270.

Craig, J. P. *et al.* (2017) 'TFOS DEWS II Definition and Classification Report', *The Ocular Surface*, 15(3), pp. 276–283. doi: 10.1016/j.jtos.2017.05.008.

Danjo, Y. *et al.* (1998) 'Alteration of mucin in human conjunctival epithelia in dry eye.', *Investigative ophthalmology & visual science*, 39(13), pp. 2602–9. Available at: http://www.ncbi.nlm.nih.gov/pubmed/9856770 (Accessed: 11 June 2019).

Darian-Smith, I., Johnson, K. O. and Dykes, R. (1973) '"Cold" fiber population innervating palmar and digital skin of the monkey: responses to cooling pulses.', *Journal of Neurophysiology*, 36(2), pp. 325–346. doi: 10.1152/jn.1973.36.2.325.

Dartt, D. A. (2009) 'Neural regulation of lacrimal gland secretory processes: Relevance in dry eye diseases', *Progress in Retinal and Eye Research*, 28(3), pp. 155–177. doi: 10.1016/j.preteyeres.2009.04.003.

Dartt, D. A. (2011) 'Formation and function of the tear film', in *Alder's: physiology of the eye*, pp. 350–362.

Davis, K. D. and Dostrovsky, J. O. (1988) 'Responses of feline trigeminal spinal tract nucleus neurons to stimulation of the middle meningeal artery and sagittal sinus', *Journal of Neurophysiology*, 59(2), pp. 648–666. doi: 10.1152/jn.1988.59.2.648.

Davis, K. D. and Pope, G. E. (2002) 'Noxious cold evokes multiple sensations with distinct time courses.', *Pain*, 98(1–2), pp. 179–85. Available at: http://www.ncbi.nlm.nih.gov/pubmed/12098630 (Accessed: 6 June 2019).

Dawson, D., Ubels, J. and Edelhauser, H. (2011) 'Cornea and Sclera', in *Alder's: physiology of the eye*, pp. 71–131.

DeMaria, S. and Ngai, J. (2010) 'The cell biology of smell', *The Journal of Cell Biology*. The Rockefeller University Press, 191(3), pp. 443–452. doi: 10.1083/jcb.201008163.

Dhaka, A. *et al.* (2007) 'TRPM8 Is Required for Cold Sensation in Mice', *Neuron*, 54(3), pp. 371–378. doi: 10.1016/j.neuron.2007.02.024.

Duclaux, R. and Kenshalo DR, S. (1980) 'Response characteristics of cutaneous warm receptors in the monkey', *Journal of Neurophysiology*, 43(1), pp. 1–15. doi: 10.1152/jn.1980.43.1.1.

Dupuy, B., Thompson, H. and Beuerman, R. (1988) 'No Title', *Investigative Ophthalmology & Visual Science*, 29.

Dvorscak, L. and Marfurt, C. F. (2008) 'Age-Related Changes in Rat Corneal Epithelial Nerve Density', *Investigative Opthalmology & Visual Science*. The Association for Research in Vision and Ophthalmology, 49(3), p. 910. doi: 10.1167/iovs.07-1324.

Ebersberger, A. *et al.* (1997) ‘Recordings From Brain Stem Neurons Responding to Chemical Stimulation of the Subarachnoid Space’, *Journal of Neurophysiology*, 77(6), pp. 3122–3133. doi: 10.1152/jn.1997.77.6.3122.

El-Fadaly, A. B. *et al.* (2014) ‘Age-related alterations in the lacrimal gland of adult albino rat: A light and electron microscopic study’, *Annals of Anatomy - Anatomischer Anzeiger*, 196(5), pp. 336–351. doi: 10.1016/j.aanat.2014.06.005.

Felipe *et al.* (1999) ‘Quantification and immunocytochemical characteristics of trigeminal ganglion neurons projecting to the cornea: effect of corneal wounding.’, *European journal of pain (London, England)*, 3(1), pp. 31–39. doi: 10.1053/eujp.1998.0100.

Fern, L. *et al.* (2016) ‘Abnormal activity of corneal cold thermoreceptors underlies the unpleasant sensations in dry eye disease’, *PAIN*, 157(2), pp. 399–417. doi: 10.1097/j.pain.0000000000000455.

Fernández-Trillo, J. *et al.* (2020) ‘Pain evoked by activation of mechanoreceptors in the cornea is mediated by Piezo2 channels’, *In press*.

Gallar, J. *et al.* (1990) ‘Effects of capsaicin on corneal wound healing.’, *Investigative ophthalmology & visual science*, 31(10), pp. 1968–74. Available at: http://www.ncbi.nlm.nih.gov/pubmed/1698737.

Gallar, J. *et al.* (1993) ‘Response of Sensory Units With Unmyelinated Fibres’, *Journal of Physiology*, 468, pp. 609–622.

Gallar, J. *et al.* (2017) ‘Interference of TRPA1 function affects background activity of corneal cold thermoreceptors in ageing mice’, *Acta Ophthalmologica*, 95. doi: 10.1111/j.1755-3768.2017.0S013.

Garcia-Hirschfeld, J., Lopez-Briones, L. G. and Belmonte, C. (1994) ‘Neurotrophic influences on corneal epithelial cells’, *Experimental Eye Research*, pp. 597–605. doi: 10.1006/exer.1994.1145.

Gasparini, S. and DiFrancesco, D. (1997) ‘Action of the hyperpolarization-activated current (Ih) blocker ZD 7288 in hippocampal CA1 neurons.’, *Pflugers Archiv : European journal of physiology*, 435(1), pp. 99–106. Available at: http://www.ncbi.nlm.nih.gov/pubmed/9359908 (Accessed: 6 June 2019).

Gipson, I. K. and Argüeso, P. (2003) ‘Role of mucins in the function of the corneal and conjunctival epithelia.’, *International review of cytology*, 231, pp. 1–49. Available at: http://www.ncbi.nlm.nih.gov/pubmed/14713002 (Accessed: 11 June 2019).

Giraldez, F., Geijo, E. and Belmonte, C. (1979) ‘Response characteristics of corneal sensory fibers to mechanical and thermal stimulation.’, *Brain research*. NETHERLANDS, 177(3), pp. 571–6. doi: 10.1016/0006-8993(79)90475-x.

Gong, S., Zhou, Q. and LeDoux, M. S. (2003) ‘Blink-related sensorimotor anatomy in the rat’, *Anatomy and Embryology*, 207(3), pp. 193–208. doi: 10.1007/s00429-003-0341-6.

González-González, O. *et al.* (2017) 'Functional Properties of Sensory Nerve Terminals of the Mouse Cornea', *Investigative Opthalmology & Visual Science*. The Association for Research in Vision and Ophthalmology, 58(1), p. 404. doi: 10.1167/iovs.16-20033.

Gonzalez, G. G. *et al.* (1993) 'Reduction of capsaicin-induced ocular pain and neurogenic inflammation by calcium antagonists', *Investigative Ophthalmology and Visual Science*, 34(12), pp. 3329–3335.

Gover, T. D., Kao, J. P. Y. and Weinreich, D. (2003) 'Calcium signaling in single peripheral sensory nerve terminals.', *The Journal of neuroscience : the official journal of the Society for Neuroscience*, 23(12), pp. 4793–7. Available at: http://www.ncbi.nlm.nih.gov/pubmed/12832498.

GRAY, J. A. B. and SATO, M. (1953) 'Properties of the receptor potential in Pacinian corpuscles.', *The Journal of physiology*. Wiley-Blackwell, 122(3), pp. 610–36. doi: 10.1113/jphysiol.1953.sp005025.

Green, B. G. (2004) 'Temperature perception and nociception', *Journal of Neurobiology*, 61(1), pp. 13–29. doi: 10.1002/neu.20081.

Greenwood, L. F. and Sessle, B. J. (1976) 'Inputs to trigeminal brain stem neurones from facial, oral, tooth pulp and pharyngolaryngeal tissues: II. Role of trigeminal nucleus caudalis in modulating responses to innocuous and noxious stimuli.', *Brain research*, 117(2), pp. 227–38. Available at: http://www.ncbi.nlm.nih.gov/pubmed/186152 (Accessed: 11 June 2019).

Guo, A. *et al.* (1999) 'Immunocytochemical localization of the vanilloid receptor 1 (VR1): relationship to neuropeptides, the P2X3 purinoceptor and IB4 binding sites.', *The European journal of neuroscience*, 11(3), pp. 946–58. Available at: http://www.ncbi.nlm.nih.gov/pubmed/10103088 (Accessed: 11 June 2019).

Gybels, J., Handwerker, H. O. and Van Hees, J. (1979) 'A comparison between the discharges of human nociceptive nerve fibres and the subject's ratings of his sensations.', *The Journal of Physiology*, 292(1), pp. 193–206. doi: 10.1113/jphysiol.1979.sp012846.

Harris, L. W. and Purves, D. (1989) 'Rapid remodeling of sensory endings in the corneas of living mice.', *The Journal of neuroscience : the official journal of the Society for Neuroscience*, 9(6), pp. 2210–4. Available at: http://www.ncbi.nlm.nih.gov/pubmed/2723770.

He, J., Bazan, N. G. and Bazan, H. E. P. (2010) 'Mapping the entire human corneal nerve architecture.', *Experimental eye research*. NIH Public Access, 91(4), pp. 513–23. doi: 10.1016/j.exer.2010.07.007.

Hellon, B. Y. R. F. and Taylor, D. C. M. (1981) 'AN ANALYSIS OF A THERMAL AFFERENT PATHWAY IN THE RAT', 326, pp. 319–328.

Henriquez, V. M. and Evinger, C. (2007) 'The three-neuron corneal reflex circuit and modulation of second-order corneal responsive neurons', *Experimental Brain Research*, 179(4), pp. 691–702. doi: 10.1007/s00221-006-0826-7.

Hensel, H. (1981) ‘Thermoreception and temperature regulation.’, *Monographs of the Physiological Society*, 38, pp. 1–321. Available at: http://www.ncbi.nlm.nih.gov/pubmed/6820811.

Hensel, H., Iggo, A. and Witt, I. (1960) ‘A quantitative study of sensitive cutaneous thermoreceptors with C afferent fibres’, *The Journal of Physiology*. Wiley-Blackwell, 153(1), pp. 113–126. doi: 10.1113/jphysiol.1960.sp006522.

Hirata, H. *et al.* (2000) ‘Cornea-Responsive Medullary Dorsal Horn Neurons: Modulation by Local Opioids and Projections to Thalamus and Brain Stem’, *Journal of Neurophysiology*, 84(2), pp. 1050–1061. doi: 10.1152/jn.2000.84.2.1050.

Hirata, H. (2004) ‘A Novel Class of Neurons at the Trigeminal Subnucleus Interpolaris/Caudalis Transition Region Monitors Ocular Surface Fluid Status and Modulates Tear Production’, *Journal of Neuroscience*, 24(17), pp. 4224–4232. doi: 10.1523/JNEUROSCI.0381-04.2004.

Hirata, H. *et al.* (2015) ‘Hyperosmolar Tears Induce Functional and Structural Alterations of Corneal Nerves: Electrophysiological and Anatomical Evidence Toward Neurotoxicity’, *Investigative Opthalmology & Visual Science*, 56(13), p. 8125. doi: 10.1167/iovs.15-18383.

Hirata, H., Fried, N. and Oshinsky, M. L. (2012) ‘Quantitative characterization reveals three types of dry-sensitive corneal afferents: pattern of discharge, receptive field, and thermal and chemical sensitivity’, *Journal of Neurophysiology*. United States, 108(9), pp. 2481–2493. doi: 10.1152/jn.00523.2012.

Hirata, H., Hu, J. W. and Bereiter, D. a (1999) ‘Responses of medullary dorsal horn neurons to corneal stimulation by CO(2) pulses in the rat.’, *Journal of neurophysiology*, 82(5), pp. 2092–107. doi: 10.1152/jn.1999.82.5.2092.

Hirata, H. and Meng, I. D. (2010) ‘Cold-Sensitive Corneal Afferents Respond to a Variety of Ocular Stimuli Central to Tear Production: Implications for Dry Eye Disease’, *Investigative Opthalmology & Visual Science*, 51(8), p. 3969. doi: 10.1167/iovs.09-4744.

Hirata, H. and Oshinsky, M. L. (2012) ‘Ocular dryness excites two classes of corneal afferent neurons implicated in basal tearing in rats: involvement of transient receptor potential channels’, *Journal of Neurophysiology*. United States, 107(4), pp. 1199–1209. doi: 10.1152/jn.00657.2011.

Hirata, H. and Rosenblatt, M. I. (2014) ‘Hyperosmolar Tears Enhance Cooling Sensitivity of the Corneal Nerves in Rats: Possible Neural Basis for Cold-Induced Dry Eye Pain’, *Investigative Opthalmology & Visual Science*, 55(9), p. 5821. doi: 10.1167/iovs.14-14642.

Holly, F. J. and Lemp, M. A. (1977) ‘Tear physiology and dry eyes.’, *Survey of ophthalmology*, 22(2), pp. 69–87. Available at: http://www.ncbi.nlm.nih.gov/pubmed/335548 (Accessed: 11 June 2019).

Huang, C.-C. *et al.* (2018) ‘Anatomical and functional dichotomy of ocular itch and pain’, *Nature Medicine*, 24(8), pp. 1268–1276. doi: 10.1038/s41591-018-0083-x.

Hykin, P. G. and Bron, A. J. (1992) 'Age-related morphological changes in lid margin and meibomian gland anatomy.', *Cornea*, 11(4), pp. 334–42. Available at: http://www.ncbi.nlm.nih.gov/pubmed/1424655 (Accessed: 12 June 2019).

Imbert, Y. *et al.* (2006) 'MUC1 splice variants in human ocular surface tissues: Possible differences between dry eye patients and normal controls', *Experimental Eye Research*, 83(3), pp. 493–501. doi: 10.1016/j.exer.2006.01.031.

Imbert, Y. *et al.* (2009) 'MUC1 and estrogen receptor α gene polymorphisms in dry eye patients', *Experimental Eye Research*, 88(3), pp. 334–338. doi: 10.1016/j.exer.2008.05.019.

Immke, D. C. and Gavva, N. R. (2006) 'The TRPV1 receptor and nociception', *Seminars in Cell and Developmental Biology*, 17(5), pp. 582–591. doi: 10.1016/j.semcdb.2006.09.004.

Ivanusic, J. J., Wood, R. J. and Brock, J. A. (2013) 'Sensory and sympathetic innervation of the mouse and guinea pig corneal epithelium', *Journal of Comparative Neurology*. United States, 521(4), pp. 877–893. doi: 10.1002/cne.23207.

Johnson, K. O., Darian-Smith, I. and LaMotte, C. (1973) 'Peripheral neural determinants of temperature discrimination in man: a correlative study of responses to cooling skin.', *Journal of Neurophysiology*, 36(2), pp. 347–370. doi: 10.1152/jn.1973.36.2.347.

Johnson, M. E. and Murphy, P. J. (2004) 'Changes in the tear film and ocular surface from dry eye syndrome', *Progress in Retinal and Eye Research*, 23(4), pp. 449–474. doi: 10.1016/j.preteyeres.2004.04.003.

Julius, D. and Basbaum, A. I. (2001) 'Molecular mechanisms of nociception', *Nature*, 413(6852), pp. 203–210. doi: 10.1038/35093019.

Kang, D., Choe, C. and Kim, D. (2005) 'Thermosensitivity of the two-pore domain K+ channels TREK-2 and TRAAK', *Journal of Physiology*, 564(1), pp. 103–116. doi: 10.1113/jphysiol.2004.081059.

Katagiri, A. *et al.* (2015) 'Evidence for TRPA1 involvement in central neural mechanisms in a rat model of dry eye HHS Public Access', *Neuroscience*, 290, pp. 204–213. doi: 10.1016/j.neuroscience.2015.01.046.

Kessler, W. *et al.* (1992) 'Excitation of cutaneous afferent nerve endings in vitro by a combination of inflammatory mediators and conditioning effect of substance P', *Experimental Brain Research*, 91(3). doi: 10.1007/BF00227842.

Kimball, S. H., King-Smith, P. E. and Nichols, J. J. (2010) 'Evidence for the Major Contribution of Evaporation to Tear Film Thinning between Blinks', *Investigative Opthalmology & Visual Science*, 51(12), p. 6294. doi: 10.1167/iovs.09-4772.

Kirch, W., Horneber, M. and Tamm, E. R. (1996) 'Characterization of Meibomian gland innervation in the cynomolgus monkey (Macaca fascicularis).', *Anatomy and embryology*, 193(4), pp. 365–75. Available at: http://www.ncbi.nlm.nih.gov/pubmed/8694272 (Accessed: 6 June 2019).

Knowlton, W. M. *et al.* (2013) 'A Sensory-Labeled Line for Cold: TRPM8-Expressing Sensory Neurons Define the Cellular Basis for Cold, Cold Pain, and Cooling-Mediated Analgesia', *Journal of Neuroscience*, 33(7), pp. 2837–2848. doi: 10.1523/JNEUROSCI.1943-12.2013.

Kurose, M. and Meng, I. D. (2013a) 'Corneal dry-responsive neurons in the spinal trigeminal nucleus respond to innocuous cooling in the rat', *Journal of Neurophysiology*. United States, 109(10), pp. 2517–2522. doi: 10.1152/jn.00889.2012.

Kurose, M. and Meng, I. D. (2013b) 'Dry eye modifies the thermal and menthol responses in rat corneal primary afferent cool cells', *Journal of Neurophysiology*. United States, 110(2), pp. 495–504. doi: 10.1152/jn.00222.2013.

De La Peña, E. *et al.* (2005) 'The contribution of TRPM8 channels to cold sensing in mammalian neurones', *The Journal of Physiology*. Wiley-Blackwell, 567(2), pp. 415–426. doi: 10.1113/jphysiol.2005.086546.

Lamb, T. D. (2009) 'Evolution of vertebrate retinal photoreception', *Philosophical Transactions of the Royal Society B: Biological Sciences*. The Royal Society, 364(1531), pp. 2911–2924. doi: 10.1098/rstb.2009.0102.

Li, W. *et al.* (2015) 'Ocular Surface Cooling Corresponds to Tear Film Thinning and Breakup', *Optometry and Vision Science*, 92(9), pp. e248–e256. doi: 10.1097/OPX.0000000000000672.

Liu, H. *et al.* (2009) 'A Link between Tear Instability and Hyperosmolarity in Dry Eye', *Investigative Opthalmology & Visual Science*, 50(8), p. 3671. doi: 10.1167/iovs.08-2689.

Long, Y. C. *et al.* (2014) 'The biochemistry and cell biology of aging: metabolic regulation through mitochondrial signaling', *American Journal of Physiology-Endocrinology and Metabolism*, 306(6), pp. E581–E591. doi: 10.1152/ajpendo.00665.2013.

MacIver, M. B. and Tanelian, D. L. (1993) 'Structural and functional specialization of A delta and C fiber free nerve endings innervating rabbit corneal epithelium.', *The Journal of neuroscience : the official journal of the Society for Neuroscience*, 13(10), pp. 4511–24. Available at: http://www.ncbi.nlm.nih.gov/pubmed/8410200 (Accessed: 6 June 2019).

Madrid, R. *et al.* (2006) 'Contribution of TRPM8 Channels to Cold Transduction in Primary Sensory Neurons and Peripheral Nerve Terminals', *Journal of Neuroscience*, 26(48), pp. 12512–12525. doi: 10.1523/JNEUROSCI.3752-06.2006.

Madrid, R. *et al.* (2009) 'Variable Threshold of Trigeminal Cold-Thermosensitive Neurons Is Determined by a Balance between TRPM8 and Kv1 Potassium Channels', *Journal of Neuroscience*, 29(10), pp. 3120–3131. doi: 10.1523/JNEUROSCI.4778-08.2009.

Maingret, F. *et al.* (1999) 'TRAAK is a mammalian neuronal mechano-gated K+ channel', *Journal of Biological Chemistry*, 274(3), pp. 1381–1387. doi: 10.1074/jbc.274.3.1381.

Maingret, F. *et al.* (2000) 'TREK-1 is a heat-activated background K(+) channel.', *The EMBO journal*, 19(11), pp. 2483–91. doi: 10.1093/emboj/19.11.2483.

Malick, A., Strassman, R. M. and Burstein, R. (2000) 'Trigeminohypothalamic and Reticulohypothalamic Tract Neurons in the Upper Cervical Spinal Cord and Caudal Medulla of the Rat', *Journal of Neurophysiology*, 84(4), pp. 2078–2112. doi: 10.1152/jn.2000.84.4.2078.

Mantelli, F. *et al.* (2010) 'Neurogenic inflammation of the ocular surface', *Current Opinion in Allergy and Clinical Immunology*, 10(5), pp. 498–504. doi: 10.1097/ACI.0b013e32833e16cc.

Marfurt, C. F. (1981) 'The central projections of trigeminal primary afferent neurons in the cat as determined by the tranganglionic transport of horseradish peroxidase', *Journal of Comparative Neurology*, 203(4), pp. 785–798. doi: 10.1002/cne.902030414.

Marfurt, C. F. (2000) 'Nervous control of the cornea', in *Nervous control of the eye*, pp. 40–92.

Marfurt, C. F. *et al.* (2010) 'Anatomy of the human corneal innervation', *Experimental Eye Research*. Academic Press, 90(4), pp. 478–492. doi: 10.1016/J.EXER.2009.12.010.

Marfurt, C. F. (2010) 'Corneal Nerves: Anatomy', in *Encyclopedia of the Eye*. Elsevier, pp. 485–492. doi: 10.1016/B978-0-12-374203-2.00068-3.

Marfurt, C. F. and Echtenkamp, S. F. (1988) 'Central projections and trigeminal ganglion location of corneal afferent neurons in the monkey, Macaca fascicularis', *Journal of Comparative Neurology*, 272(3), pp. 370–382. doi: 10.1002/cne.902720307.

Marfurt, C. F., Kingsley, R. E. and Echtenkamp, S. E. (1989) 'Sensory and sympathetic innervation of the mammalian cornea. A retrograde tracing study', *Investigative Ophthalmology and Visual Science*, 30(3), pp. 461–472.

Marfurt, C. F. and Del Toro, D. R. (1987) 'Corneal sensory pathway in the rat: a horseradish peroxidase tracing study.', *The Journal of comparative neurology*, 261(3), pp. 450–9. doi: 10.1002/cne.902610309.

May, C. A. (1997) 'Description and function of the ciliary nerves - Some historical remarks on choroidal innervation', *Experimental Eye Research*, 65(1), pp. 1–5. doi: 10.1006/exer.1997.0312.

May, P. J. and Porter, J. D. (1998) 'The distribution of primary afferent terminals from the eyelids of macaque monkeys.', *Experimental brain research*, 123(4), pp. 368–81. Available at: http://www.ncbi.nlm.nih.gov/pubmed/9870597 (Accessed: 6 June 2019).

McKemy, D. D., Neuhausser, W. M. and Julius, D. (2002) 'Identification of a cold receptor reveals a general role for TRP channels in thermosensation', *Nature*. England, 416(6876), pp. 52–58. doi: 10.1038/nature719.

McNabb, P. C. and Tomasi, T. B. (1981) 'Host Defense Mechanisms at Mucosal Surfaces', *Annual Review of Microbiology*, 35(1), pp. 477–496. doi: 10.1146/annurev.mi.35.100181.002401.

Meng, I. D. *et al.* (1997) 'Encoding of Corneal Input in Two Distinct Regions of the Spinal Trigeminal Nucleus in the Rat: Cutaneous Receptive Field Properties, Responses to Thermal and Chemical Stimulation, Modulation by Diffuse Noxious Inhibitory Controls, and Projections to the P', *Journal of Neurophysiology*, 77(1), pp. 43–56. doi: 10.1152/jn.1997.77.1.43.

Meng, I. D., Hu, J. W. and Bereiter, D. A. (1998) 'Differential Effects of Morphine on Corneal-Responsive Neurons in Rostral Versus Caudal Regions of Spinal Trigeminal Nucleus in the Rat', *Journal of Neurophysiology*, 79(5), pp. 2593–2602. doi: 10.1152/jn.1998.79.5.2593.

Meseguer, V. *et al.* (2014) 'TRPA1 channels mediate acute neurogenic inflammation and pain produced by bacterial endotoxins', *Nature Communications*, 5(1), p. 3125. doi: 10.1038/ncomms4125.

Michaelis, M., Häbler, H. J. and Jäenig, W. (1996) 'Silent afferents: a separate class of primary afferents?', *Clinical and experimental pharmacology & physiology*, 23(2), pp. 99–105. Available at: http://www.ncbi.nlm.nih.gov/pubmed/8819636 (Accessed: 6 June 2019).

Momin, A. *et al.* (2008) 'Role of the hyperpolarization-activated current I h in somatosensory neurons', *Journal of Physiology*, 586(24), pp. 5911–5929. doi: 10.1113/jphysiol.2008.163154.

Morenilla-Palao, C. *et al.* (2014) 'Ion Channel Profile of TRPM8 Cold Receptors Reveals a Role of TASK-3 Potassium Channels in Thermosensation', *Cell Reports*. NIH Public Access, 8(5), pp. 1571–1582. doi: 10.1016/j.celrep.2014.08.003.

Morin, C. and Bushnell, M. C. (1998) 'Temporal and qualitative properties of cold pain and heat pain: A psychophysical study', *Pain*, 74(1), pp. 67–73. doi: 10.1016/S0304-3959(97)00152-8.

Mountcastle, V. (1968) 'Chapter 61 Physiology of Sensory receptors: introduction to sensory processes', in The CV Mosby Company (ed.) *Medical Physiology*. 2nd edn, pp. 1345–1381.

Müller, L. J. *et al.* (2003) 'Corneal nerves: structure, contents and function.', *Experimental eye research*, 76(5), pp. 521–42. doi: 10.1016/S0014-4835(03)00050-2.

Müller, L. J., Pels, L. and Vrensen, G. F. J. M. (1996) 'Ultrastructural organization of human corneal nerves', *Investigative Ophthalmology and Visual Science*, 37(4), pp. 476–488.

Murata, Y. and Masuko, S. (2006) 'Peripheral and central distribution of TRPV1, substance P and CGRP of rat corneal neurons', *Brain Research*, 1085(1), pp. 87–94. doi: 10.1016/j.brainres.2006.02.035.

Murthy, S. E. *et al.* (2018) 'The mechanosensitive ion channel Piezo2 mediates sensitivity to mechanical pain in mice', *Science Translational Medicine*, 10(462), p. eaat9897. doi: 10.1126/scitranslmed.aat9897.

Namer, B. *et al.* (2009) 'Microneurographic assessment of C-fibre function in aged healthy subjects', *The Journal of Physiology*. Wiley-Blackwell, 587(2), pp. 419–428. doi: 10.1113/jphysiol.2008.162941.

Nichols, B., Dawson, C. R. and Togni, B. (1983) 'Surface features of the conjunctiva and cornea', *Investigative Ophthalmology and Visual Science*, 24(5), pp. 570–576.

Nishida, T. (2008) '[The cornea: stasis and dynamics].', *Nippon Ganka Gakkai zasshi*, 112(3), pp. 179–212; discussion 213. Available at: http://www.ncbi.nlm.nih.gov/pubmed/18411711 (Accessed: 10 June 2019).

Nolano, M. *et al.* (2013) 'Cutaneous innervation of the human face as assessed by skin biopsy.', *Journal of anatomy*. Wiley-Blackwell, 222(2), pp. 161–9. doi: 10.1111/joa.12001.

Okamoto, K. *et al.* (2010) 'Bright light activates a trigeminal nociceptive pathway', *Pain*, 149(2), pp. 235–242. doi: 10.1016/j.pain.2010.02.004.

Okamoto, K. *et al.* (2012) 'Trigeminal interpolaris/caudalis transition neurons mediate reflex lacrimation evoked by bright light in the rat', *European Journal of Neuroscience*, 36(11), pp. 3492–3499. doi: 10.1111/j.1460-9568.2012.08272.x.

Olivares, E. *et al.* (2015) 'TRPM8-Dependent Dynamic Response in a Mathematical Model of Cold Thermoreceptor', *PLOS ONE*. Edited by D. D. McKemy, 10(10), p. e0139314. doi: 10.1371/journal.pone.0139314.

Orio, Patricio *et al.* (2012) 'ROLE OF Ih IN THE FIRING PATTERN OF MAMMALIAN COLD THERMORECEPTOR ENDINGS', *Journal of Neurophysiology*, 108(11), pp. 3009–3023. doi: 10.1152/jn.01033.2011.

Orio, P. *et al.* (2012) 'ROLE OF Ih IN THE FIRING PATTERN OF MAMMALIAN COLD THERMORECEPTOR ENDINGS', *Journal of Neurophysiology*. doi: 10.1152/jn.01033.2011.

Osteen, J. D. *et al.* (2016) 'Selective spider toxins reveal a role for the Nav1.1 channel in mechanical pain', *Nature*. Nature Publishing Group, 534(7608), pp. 494–499. doi: 10.1038/nature17976.

de Paiva, C. S. (2017) 'Effects of Aging in Dry Eye', *International Ophthalmology Clinics*, 57(2), pp. 47–64. doi: 10.1097/IIO.0000000000000170.

Palkar, R., Lippoldt, E. K. and McKemy, D. D. (2015) 'The molecular and cellular basis of thermosensation in mammals', *Current Opinion in Neurobiology*. NIH Public Access, 34, pp. 14–19. doi: 10.1016/j.conb.2015.01.010.

Panneton, W. M. and Burton, H. (1981) 'Corneal and periocular representation within the trigeminal sensory complex in the cat studied with transganglionic transport of horseradish peroxidase', *Journal of Comparative Neurology*, 199(3), pp. 327–344. doi: 10.1002/cne.901990303.

Panneton, W. M., Hsu, H. and Gan, Q. (2010) 'Distinct central representations for sensory

fibers innervating either the conjunctiva or cornea of the rat', *Experimental Eye Research*, 90(3), pp. 388–396. doi: 10.1016/j.exer.2009.11.018.

Parissi, M. *et al.* (2013) 'Standardized baseline human corneal subbasal nerve density for clinical investigations with laser-scanning in vivo confocal microscopy.', *Investigative ophthalmology & visual science*, 54(10), pp. 7091–102. doi: 10.1167/iovs.13-12999.

Parra, A. *et al.* (2014) 'Tear fluid hyperosmolality increases nerve impulse activity of cold thermoreceptor endings of the cornea', *Pain*. Netherlands: Elsevier, 155(8), pp. 1481–1491. doi: 10.1016/j.pain.2014.04.025.

Parra, A. A. *et al.* (2010) 'Ocular surface wetness is regulated by TRPM8-dependent cold thermoreceptors of the cornea.', *Nature medicine*. United States, 16(12), pp. 1396–1399. doi: 10.1038/nm.2264.

Patapoutian, A. *et al.* (2003) 'ThermoTRP channels and beyond: mechanisms of temperature sensation', *Nature Reviews Neuroscience*, 4(7), pp. 529–539. doi: 10.1038/nrn1141.

Pattmöller, J. *et al.* (2015) 'Correlation of corneal thickness, endothelial cell density and anterior chamber depth with ocular surface temperature in normal subjects', *Zeitschrift für Medizinische Physik*, 25(3), pp. 243–250. doi: 10.1016/j.zemedi.2014.09.008.

Patton, H. D. (1965) 'Receptor mechanism', in Philadelphia: W. B. Saunders and Company (ed.) *Physiology and biophysics*, pp. 95–112.

Payrau, P. *et al.* (1967) '[Corneal transparence].', *Bulletins et memoires de la Societe francaise d'ophtalmologie*, 80, pp. 1–35. Available at: http://www.ncbi.nlm.nih.gov/pubmed/4936696 (Accessed: 6 June 2019).

Peier, A. M. *et al.* (2002) 'A TRP channel that senses cold stimuli and menthol.', *Cell*, 108(5), pp. 705–15. Available at: http://www.ncbi.nlm.nih.gov/pubmed/11893340.

Pellegrini, J. J., Horn, A. K. and Evinger, C. (1995) 'The trigeminally evoked blink reflex. I. Neuronal circuits.', *Experimental brain research*, 107(2), pp. 166–80. Available at: http://www.ncbi.nlm.nih.gov/pubmed/8773237 (Accessed: 11 June 2019).

Pflugfelder, S. C. (2008) 'Prevalence, burden, and pharmacoeconomics of dry eye disease.', *The American journal of managed care*, 14(3 Suppl), pp. S102-6. Available at: http://www.ncbi.nlm.nih.gov/pubmed/18452369 (Accessed: 12 June 2019).

Pozo, M. A. and Cervero, F. (1993) 'Neurons in the rat spinal trigeminal complex driven by corneal nociceptors: receptive-field properties and effects of noxious stimulation of the cornea', *Journal of Neurophysiology*, 70(6), pp. 2370–2378. doi: 10.1152/jn.1993.70.6.2370.

Pubols, B. H. (1988) 'Spread of skin deformation and mechanoreceptor discharge.', *Progress in brain research*, 74, pp. 263–70. Available at: http://www.ncbi.nlm.nih.gov/pubmed/3055048.

PURSLOW, C. and WOLFFSOHN, J. (2007) 'The Relation between Physical Properties of the Anterior Eye and Ocular Surface Temperature', *Optometry and Vision Science*, 84(3), pp. 197–201. doi: 10.1097/OPX.0b013e3180339f6e.

Quallo, T. *et al.* (2015) 'TRPM8 is a neuronal osmosensor that regulates eye blinking in mice', *Nature Communications*. Nature Publishing Group, 6(1), p. 7150. doi: 10.1038/ncomms8150.

Rahman, M. *et al.* (2014) 'Trigeminal pathways for hypertonic saline- and light-evoked corneal reflexes', *Neuroscience*, 277, pp. 716–723. doi: 10.1016/j.neuroscience.2014.07.052.

Rahman, M. *et al.* (2015) 'Sensitization of trigeminal brainstem pathways in a model for tear deficient dry eye', *PAIN*, 156(5), pp. 942–950. doi: 10.1097/j.pain.0000000000000135.

Ranade, S. S. *et al.* (2014) 'Piezo2 is the major transducer of mechanical forces for touch sensation in mice.', *Nature*. NIH Public Access, 516(7529), pp. 121–5. doi: 10.1038/nature13980.

Reeh, P. W. (1986) 'Sensory receptors in mammalian skin in an in vitro preparation.', *Neuroscience letters*. NETHERLANDS, 66(2), pp. 141–146. Available at: http://www.ncbi.nlm.nih.gov/pubmed/3725179 (Accessed: 6 June 2019).

Reichard, M. *et al.* (2016) 'Age-Related Changes in Murine Corneal Nerves', *Current Eye Research*, 41(8), pp. 1021–1028. doi: 10.3109/02713683.2015.1088952.

Reid, G. (2005) 'ThermoTRP channels and cold sensing: what are they really up to?', *Pflügers Archiv - European Journal of Physiology*, 451(1), pp. 250–263. doi: 10.1007/s00424-005-1437-z.

Reid, T. W. *et al.* (1993) 'Stimulation of epithelial cell growth by the neuropeptide substance P', *Journal of Cellular Biochemistry*, 52(4), pp. 476–485. doi: 10.1002/jcb.240520411.

Robbins, A. *et al.* (2012) 'Menthol activation of corneal cool cells induces TRPM8-mediated lacrimation but not nociceptive responses in rodents', *Investigative Ophthalmology and Visual Science*, 53(11), pp. 7034–7042. doi: 10.1167/iovs.12-10025.

Rocha, E. M. *et al.* (2008) 'The aging lacrimal gland: changes in structure and function.', *The ocular surface*, 6(4), pp. 162–74. Available at: https://www.ncbi.nlm.nih.gov/pmc/articles/PMC4205956/pdf/nihms634174.pdf (Accessed: 12 June 2019).

Saraux, H. *et al.* (1985) 'La córnea', in *Anatomía e histología del ojo*. Masson, pp. 91–105.

Saude, T. (1993) *Ocular anatomy and physiology*. Blackwell Scientific Publications INC., Boston.

Schaible, H. G. and Schmidt, R. F. (1983) 'Responses of fine medial articular nerve afferents to passive movements of knee joints', *Journal of Neurophysiology*, 49(5), pp.

1118–1126. doi: 10.1152/jn.1983.49.5.1118.

Schepelmann, K. *et al.* (1999) 'Response properties of trigeminal brain stem neurons with input from dura mater encephali in the rat.', *Neuroscience*, 90(2), pp. 543–54. Available at: http://www.ncbi.nlm.nih.gov/pubmed/10215158 (Accessed: 11 June 2019).

Simons, E. and Smith, P. G. (1994) 'Sensory and autonomic innervation of the rat eyelid: Neuronal origins and peptide phenotypes', *Journal of Chemical Neuroanatomy*, 7(1–2), pp. 35–47. doi: 10.1016/0891-0618(94)90006-X.

Simsek, C. *et al.* (2018) 'Alterations of Murine Subbasal Corneal Nerves After Environmental Dry Eye Stress', *Investigative Opthalmology & Visual Science*, 59(5), p. 1986. doi: 10.1167/iovs.17-23743.

Sousa, P. C. *et al.* (1993) 'Morphological and/or functional imagiology diagnosis of epiphora.', *Documenta ophthalmologica. Advances in ophthalmology*, 83(4), pp. 337–48. Available at: http://www.ncbi.nlm.nih.gov/pubmed/8223104 (Accessed: 13 June 2019).

Spray, D. (1986) 'Cutaneous Temperature Receptors', *Annual Review of Physiology*, 48(1), pp. 625–382. doi: 10.1146/annurev.physiol.48.1.625.

Stern, M. E. *et al.* (1998) 'The pathology of dry eye: the interaction between the ocular surface and lacrimal glands.', *Cornea*, 17(6), pp. 584–9. Available at: http://www.ncbi.nlm.nih.gov/pubmed/9820935 (Accessed: 6 June 2019).

Stern, M. E. *et al.* (2004) 'The role of the lacrimal functional unit in the pathophysiology of dry eye.', *Experimental eye research*, 78(3), pp. 409–16. doi: 10.1016/j.exer.2003.09.003.

Stern, M. E. (2005) 'Dry eye--is this a disease or a natural consequence of aging?', *Archivos de la Sociedad Espanola de Oftalmologia*, 80(3), pp. 125–31. Available at: http://www.ncbi.nlm.nih.gov/pubmed/15803420 (Accessed: 12 June 2019).

Straub, R. H. (2014) 'TRPV1, TRPA1, and TRPM8 channels in inflammation, energy redirection, and water retention: Role in chronic inflammatory diseases with an evolutionary perspective', *Journal of Molecular Medicine*, 92(9), pp. 925–937. doi: 10.1007/s00109-014-1175-9.

Sumino, R., Dubner, R. and Starkman, S. (1973) 'Responses of small myelinated "warm" fibers to noxious heat stimuli applied to the monkey's face', *Brain Research*, 62(1), pp. 260–263. doi: 10.1016/0006-8993(73)90638-0.

Takashima, Y. *et al.* (2007) 'Diversity in the Neural Circuitry of Cold Sensing Revealed by Genetic Axonal Labeling of Transient Receptor Potential Melastatin 8 Neurons', *Journal of Neuroscience*. NIH Public Access, 27(51), pp. 14147–14157. doi: 10.1523/JNEUROSCI.4578-07.2007.

Tanelian, D. L. and Beuerman, R. W. (1984) 'Responses of rabbit corneal nociceptors to mechanical and thermal stimulation', *Experimental Neurology*, 84(1), pp. 165–178. doi: 10.1016/0014-4886(84)90013-X.

Teichert, R. W. *et al.* (2012) 'Characterization of two neuronal subclasses through constellation pharmacology', *Proceedings of the National Academy of Sciences*, 109(31), pp. 12758–12763. doi: 10.1073/pnas.1209759109.

Tepelus, T. C. *et al.* (2017) 'Correlation between corneal innervation and inflammation evaluated with confocal microscopy and symptomatology in patients with dry eye syndromes: a preliminary study', *Graefe's Archive for Clinical and Experimental Ophthalmology*, 255(9), pp. 1771–1778. doi: 10.1007/s00417-017-3680-3.

Tominaga M. *et al.* (1998) 'The cloned capsaicin receptor integrates multiple pain-producing stimuli', *Neuron*, 21(3), pp. 531–543. doi: 10.1016/S0896-6273(00)80564-4.

Toshida, H. *et al.* (2007) 'Evaluation of Novel Dry Eye Model: Preganglionic Parasympathetic Denervation in Rabbit', *Investigative Opthalmology & Visual Science*, 48(10), p. 4468. doi: 10.1167/iovs.06-1486.

Tran, M. T. *et al.* (2000) 'Calcitonin Gene-Related Peptide Induces IL-8 Synthesis in Human Corneal Epithelial Cells', *The Journal of Immunology*, 164(8), pp. 4307–4312. doi: 10.4049/jimmunol.164.8.4307.

Versura, P. *et al.* (2015) 'Subjective Discomfort Symptoms Are Related to Low Corneal Temperature in Patients With Evaporative Dry Eye', *Cornea*, 34(9), pp. 1079–1085. doi: 10.1097/ICO.0000000000000512.

Vesaluoma, M. *et al.* (2000) 'Effects of oleoresin capsicum pepper spray on human corneal morphology and sensitivity.', *Investigative ophthalmology & visual science*, 41(8), pp. 2138–47. Available at: http://www.ncbi.nlm.nih.gov/pubmed/10892855.

Viana, F., De la Peña, E. and Belmonte, C. (2002) 'Specificity of cold thermotransduction is determined by differential ionic channel expression', *Nature Neuroscience*. United States, 5(3), pp. 254–260. doi: 10.1038/nn809.

Walcott, B. (1998) 'The Lacrimal Gland and Its Veil of Tears.', *News in physiological sciences : an international journal of physiology produced jointly by the International Union of Physiological Sciences and the American Physiological Society*, 13, pp. 97–103. Available at: http://www.ncbi.nlm.nih.gov/pubmed/11390770 (Accessed: 6 June 2019).

Wang, C. *et al.* (2012) 'Changes in mouse corneal epithelial innervation with age', *Investigative Opthalmology & Visual Science*, 53(8), pp. 5077–5084. doi: 10.1167/iovs.12-9704.

Wang, S. and Albers, K. M. (2009) 'Behavioral and Cellular Level Changes in the Aging Somatosensory System', *Annals of the New York Academy of Sciences*. NIH Public Access, 1170, p. 745. doi: 10.1111/J.1749-6632.2009.04011.X.

Warren, S. and May, P. J. (2013) 'Morphology and connections of intratrigeminal cells and axons in the macaque monkey', *Frontiers in Neuroanatomy*, 7, p. 11. doi: 10.3389/fnana.2013.00011.

WHITEAR, M. (1960) 'An electron microscope study of the cornea in mice, with special

reference to the innervation.', *Journal of anatomy*, 94, pp. 387–409. Available at: http://www.ncbi.nlm.nih.gov/pubmed/13844416%0Ahttp://www.pubmedcentral.nih.gov/articlerender.fcgi?artid=PMC1244376.

Widmaier, E., Raff, H. and Strang, K. (2006) *Vander's human physiology: the mechanisms of body function.* Boston: McGraw-Hill.

Woo, S.-H. *et al.* (2015) 'Piezo2 is the principal mechanotransduction channel for proprioception.', *Nature neuroscience*. NIH Public Access, 18(12), pp. 1756–62. doi: 10.1038/nn.4162.

Xing, H. *et al.* (2006) 'Chemical and Cold Sensitivity of Two Distinct Populations of TRPM8-Expressing Somatosensory Neurons', *Journal of Neurophysiology*. American Physiological Society, 95(2), pp. 1221–1230. doi: 10.1152/jn.01035.2005.

Yamaguchi, T. (2018) 'Inflammatory Response in Dry Eye', *Investigative Opthalmology & Visual Science*, 59(14), p. DES192. doi: 10.1167/iovs.17-23651.

Yarnitsky, D. *et al.* (1992) 'Single C nociceptor responses and psychophysical parameters of evoked pain: effect of rate of rise of heat stimuli in humans.', *The Journal of Physiology*, 450(1), pp. 581–592. doi: 10.1113/jphysiol.1992.sp019144.

ZANDER, E. and WEDDELL, G. (1951) 'Observations on the innervation of the cornea.', *Journal of anatomy*, 85(1), pp. 68–99. Available at: http://www.ncbi.nlm.nih.gov/pubmed/14814019%0Ahttp://www.pubmedcentral.nih.gov/articlerender.fcgi?artid=PMC1273614.

Zhang, X. *et al.* (2012) 'Direct inhibition of the cold-activated TRPM8 ion channel by Gαq', *Nature Cell Biology*, 14(8), pp. 851–858. doi: 10.1038/ncb2529.

Zollman, T. M., Bragg, R. M. and Harrison, D. A. (2000) 'Clinical effects of oleoresin capsicum (pepper spray) on the human cornea and conjunctiva', *Ophthalmology*, 107(12), pp. 2186–2189. doi: 10.1016/S0161-6420(00)00463-2.

VIII. Anexos

Functional Properties of Sensory Nerve Terminals of the Mouse Cornea

Omar González-González,[1] Federico Bech,[1] Juana Gallar,[2] Jesús Merayo-Lloves,[1] and Carlos Belmonte[1,2]

[1]Instituto Universitario Fernández-Vega, Universidad de Oviedo & Fundación de Investigación Oftalmológica, Oviedo, Spain
[2]Instituto de Neurociencias, Universidad Miguel Hernández-Consejo Superior de Investigaciones Cientificas, San Juan de Alicante, Spain

Correspondence: Carlos Belmonte, Instituto Universitario Fernández-Vega, Avda. Dres. Fernández-Vega, 34, 33012 Oviedo, Spain; carlos.belmonte@umh.es.

Submitted: May 31, 2016
Accepted: November 13, 2016

Citation: González-González O, Bech F, Gallar J, Merayo-Lloves J, Belmonte C. Functional properties of sensory nerve terminals of the mouse cornea. *Invest Ophthalmol Vis Sci.* 2017;58:404–415. DOI:10.1167/iovs.16-20033

Purpose. To define the firing properties of sensory nerve terminals innervating the adult mouse cornea in response to external stimuli of differing modality.

Methods. Extracellular electrical activity of single corneal sensory nerve terminals was recorded in excised eyes of C57BL/6J mice. Eyes were placed in a recording chamber and were continuously superfused with warm saline solution. Nerve terminal impulse (NTI) activity was recorded by means of a glass pipette (tip ~ 50 μm), applied on the corneal surface. Nerve terminal impulse discharges were stored in a computer for offline analysis.

Results. Three functionally distinct populations of nerve terminals were identified in the mouse cornea. Pure mechanonociceptor terminals (9.5%) responded phasically and only to mechanical stimuli. Polymodal nociceptor terminals (41.1%) were tonically activated by heat and hyperosmolal solutions (850 mOsm·kg^{-1}), mechanical force, and/or TRPV1 and TRPA1 agonists (capsaicin and allyl isothiocyanate [AITC], respectively). Cold-sensitive terminals (49.4%) responded to cooling. Approximately two-thirds of them fired continuously at 34°C and responded vigorously to small temperature reductions, being classified as high-background activity, low-threshold (HB-LT) cold thermoreceptor terminals. The remaining one-third exhibited very low ongoing activity at 34°C and responded weakly to intense cooling, being named low-background activity, high-threshold (LB-HT) cold thermoreceptor terminals.

Conclusions. The mouse cornea is innervated by trigeminal ganglion (TG) neurons that respond to the same stimulus modalities as corneal receptors of other mammalian species. Mechano- and polymodal endings underlie detection of mechanical and chemical noxious stimuli while HB-LT and LB-HT cold thermoreceptors appear to be responsible for basal and irritation-evoked tearing and blinking, respectively.

Keywords: corneal sensory nerves, thermoreceptors, corneal innervation, polymodal nociceptors, mechanonociceptors

The use of mice in biomedical studies is receiving growing attention due to the ample possibilities of genetic manipulation offered by this species. Such interest extends also to the eye, and in recent years, many publications have used mice to analyze normal and pathologic ocular processes, including those affecting the sensory innervation of the corneal surface.[1–3]

As a result of these studies, the distribution and architecture of mouse corneal sensory innervation is reasonably well known, confirming that it follows the morphologic pattern of corneal nerve branching described in other mammalian species,[4,5] although remarkable differences exist in nerve density between mice strains.[4] Additionally, the corneal innervation of mice has been used to explore the origin and trophic dependence of peripheral sensory nerves during prenatal development[6] and postinjury nerve regeneration in adults,[3,7,8] as well as age-dependent changes in the architecture and function of corneal nerves.[2,9] Moreover, mice have been extensively employed to define the morphologic alterations of corneal nerves caused by a number of pathologic conditions such as diabetes,[10] surgical injury,[1,11,12] herpes virus infections,[13,14] and dry eye disease.[15,16]

In contrast to the ample knowledge of the anatomy of the corneal innervation in mice, its functional characteristics are still poorly defined. Impulse activity of mouse corneal sensory axons and nerve terminals has been recorded in a few studies, and these were mainly centered on the population of low-threshold cold thermoreceptors, whose electrical activity is easiest to record and characterize.[9,17–19]

Electrophysiological experiments in other species (cat, rabbit, guinea pig, rat) firmly established that the cornea is functionally innervated by the peripheral axons of three distinct classes of peripheral sensory receptor neurons: mechanosensory, responding only to mechanical forces; polymodal nociceptor, activated by mechanical stimuli as well as heat and a variety of endogenous and exogenous chemicals; and cold thermoreceptor neurons, primarily excited by moderate cooling and hyperosmolar solutions.[20–36] In the present work, we performed a systematic analysis of the firing properties of the various functional classes of sensory nerve terminals innervating the adult mouse cornea and defined their functional properties and firing pattern in response to stimuli of differing modality.

Investigative Ophthalmology & Visual Science

Methods

All experiments were conducted in accordance with the ethical guidelines of the ARVO Statement for the Use of Animals in Ophthalmic and Vision Research and the European and Spanish regulations on the protection of animals used for research, and followed a protocol approved by the Ethics Committee of the University of Oviedo. Animals were euthanized with an overdose of sodium pentobarbital (Dolethal; Vetoquinol, Lure, France) injected intraperitoneally.

Recordings of single corneal nerve terminals in vitro were performed as described in previous studies.[17,35] The posterior pole of the eyeball and optic nerve was introduced into a silicone tube located at the bottom of a recording chamber filled with saline and secured in place by continuous suction. The eye was continuously superfused with a physiological saline solution of the following composition (in mM): NaCl (128), KCl (5), NaH_2PO_4 (1), $NaHCO_3$ (26), $CaCl_2$ (2.4), $MgCl_2$ (1.3), and glucose (10). The solution was bubbled with a gas mixture (5% CO_2 and 95% O_2) and maintained at the desired temperature (~34°C) with a home-made Peltier device. A borosilicate glass micropipette electrode with a tip diameter of approximately 50 μm filled with saline solution was gently placed in contact with the corneal surface, using a micromanipulator. Light suction was then applied through the pipette to produce a high-resistance seal with the corneal surface, to allow recording of nerve impulses generated at single nerve terminals located beneath the electrode tip. An Ag-AgCl electrode in the recording chamber served as the indifferent electrode. Nerve terminal impulses (NTIs) were amplified with an AC amplifier (Neurolog NL104; Digitimer, Welwyn, UK) and stored at 10 kHz in a computer, using a CED micro 1401 interface and Spike 2 software (both from Cambridge Electronic Design, Cambridge, UK). Only recordings containing NTIs originating from a single nerve terminal were analyzed. At these sites the NTIs were clearly distinguished from noise (~10 μV peak to peak) and had similar amplitudes and waveforms indicating that they originated from the same sensory nerve ending. To minimize deterioration of the preparation with time, the total duration of the experiment was limited to a maximum of 5 hours.

Solutions

Menthol (Sigma-Aldrich Corp., St. Louis, MO, USA) was prepared as a 20 mM stock solution in ethanol and diluted to a final concentration of 20 μM with saline solution. Capsaicin (Sigma-Aldrich Corp.) was prepared as a 1 mM stock solution in ethanol and diluted to a final concentration of 1 μM with saline solution. Allyl isothiocyanate (Sigma-Aldrich Corp.) was prepared as a 100 mM stock solution in dimethyl sulfoxide (DMSO) and diluted with the saline solution to a final concentration of 100 μM. Hyperosmolal solutions were prepared by adding NaCl (3 M) to the physiological saline solution (310 ± 1.5 mOsm·kg^{-1}) until reaching the desired osmolality values (340, 400, and 850 mOsm·kg^{-1}), measured with a freezing point osmometer (OSMOSTAT OM-6020; Kyoto Daiichi, Kyoto, Japan). The "inflammatory soup"[18] contained the following substances dissolved in saline solution: bradykinin (5 μM), histamine (100 μM), PGE_2 (10 μM), 5-HT (100 μM), and ATP (100 μM), all from Sigma-Aldrich Corp.

Experimental Protocol

In order to obtain an estimation of the relative density of the different functional types of corneal terminals, the recording pipette was placed at sequential points on the corneal surface separated by an approximate distance of 0.2 mm, and aligned at the intersections of a 6 by 3 grid formed by evenly spaced straight lines going between opposite sides of the limbal border (Figs. 1A, 1B). First, one half of the cornea was explored for nerve activity, and the eye was then rotated and the opposite half of the cornea was explored. After application of the pipette to the corneal surface, responses to cold or mechanical stimuli were assessed. The appearance of spontaneous or stimulus-evoked NTI activity at the recording site was used to ascertain success in detecting an active sensory nerve terminal. If no spontaneous or cold- or mechanically evoked activity was obtained, the electrode was moved to the next recording point. Responsiveness to mechanical stimulation was assessed with a gentle forward displacement (10 μm) of the recording electrode with the micromanipulator. Thereafter, thermal and chemical stimuli were sequentially applied. The same general protocol was applied to sensory terminals of all modalities.

Cold stimulation was first performed by decreasing the background temperature of the perfusion solution from 34°C down to ~14°C. This generated a cooling ramp lasting ~35 seconds at mean cooling rate of ~0.6°C·s^{-1}. When the peak temperature fall was attained, warming was applied to return to the basal temperature at a similar speed. After a resting period of 120 seconds, a mechanical stimulation was made, applying pressure with the pipette with a 10-μm forward displacement of the tip of the electrode for 2 or 15 seconds. The number of NTIs evoked during the stimulation period was counted.

After another 120 seconds, a heating ramp from 34°C to ~52°C at 0.5°C·s^{-1} (~30-second duration) was applied, and when the peak value was reached, temperature was returned to 34°C at a similar rate.

Chemical stimulation was initiated after a resting period of at least 300 seconds, by switching the perfusion with control saline solution at 34°C to a saline solution containing the drug at 34°C. Menthol (20 μM) was always tested first. Two minutes after the onset of the perfusion with menthol, a cooling ramp down to ~14°C was applied to explore the presence of menthol-induced sensitization of the cold response. After warming back to 34°C, the cornea was washed with the control saline solution for a period of at least 5 minutes. Afterward, stimulation with one or several other test solutions (AITC, "inflammatory soup," hyperosmolal solutions) was sequentially performed using the same protocol: Namely, after a control recording period of 2 minutes, perfusion with the test solution for 2 to 3 minutes was initiated, including a cooling ramp, followed by a washing time of at least 5 minutes. Capsaicin (1 μM) was applied whenever possible for 2 to 3 minutes at 34°C, always at the end of experiment due to the strong inactivating effect of this drug.

Analysis of NTI Activity

The following parameters of the NTI activity were analyzed. Background activity, defined as the mean basal ongoing frequency in impulses per second (imp·s^{-1}) at the basal temperature (33.9 ± 0.07°C), was measured during the 30-second period that preceded the onset of a stimulus. Cooling threshold was the temperature (°C) value during a cooling ramp at which NTI frequency in imp·s^{-1} increased to a value greater than the value of the mean basal NTI frequency during the 10-second period preceding the onset of a cooling ramp, plus three times its standard deviation. Cooling response was mean NTI frequency during cooling. Maximum response to cold was the highest-frequency value measured during a cooling ramp (imp·s^{-1}). Silencing temperature was temperature (°C) needed to silence NTI firing during a cooling ramp. Response to heat was the total number of NTIs during 30

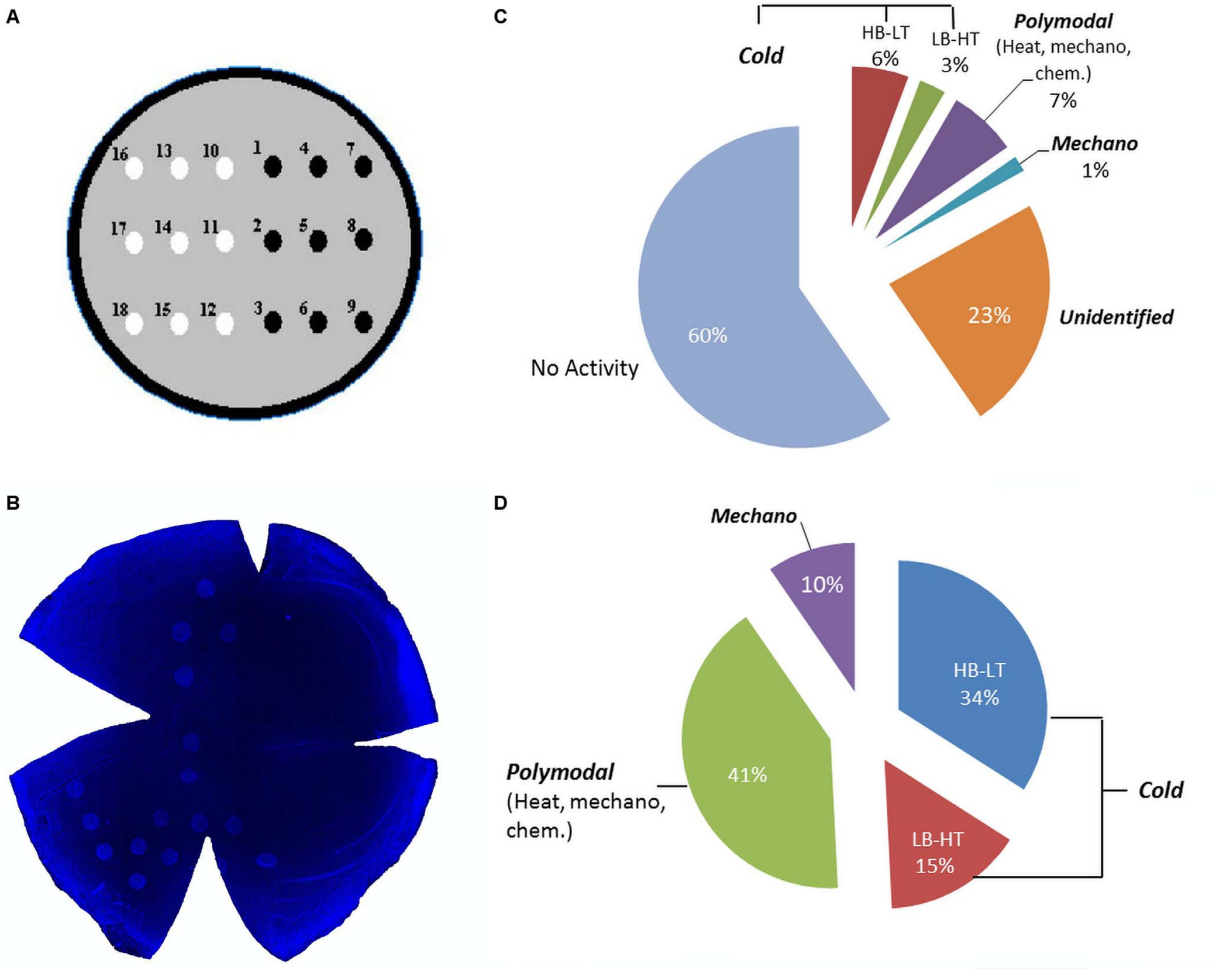

FIGURE 1. (**A**) Schematic representation of the cornea to show the location and sequence of points at which the recording electrode was placed during the experiment. (**B**) Picture of an excised cornea, showing the marks left by the recording electrode tip on the epithelial surface. (**C**) Probability of finding NTI activity associated with the different modalities of stimuli. (**D**) Percent of terminals belonging to the different functional classes of corneal receptor terminals identified in all experiments.

seconds following the onset of the heating ramp. Comparison was made with the number of NTIs during the 30-second period immediately preceding the heating ramp. Heating threshold was temperature (°C) value during a heating ramp at which NTI frequency in imp·s^{-1} increased to a value greater than the value of the mean basal NTI frequency during the 30-second period preceding the onset of a heating ramp, plus three times its standard deviation. Mechanical response was the total number of NTIs during 10 seconds following the onset of mechanical stimulation. As a control, the total number of NTIs fired during the 10-second period immediately prior to mechanical stimulation was used. Chemical response, the mean firing frequency (in imp·s^{-1}) during the last 30 seconds of perfusion with the test substance (AITC, capsaicin, inflammatory soup, menthol, hyperosmolal solutions), was measured and compared with the NTI firing frequency during the 30-second period preceding chemical stimulation.

Statistical Analysis

Data from NTI recordings were exported from Spike 2 (CED) to Origin 8 software for analysis. Statistical comparisons were performed using Microsoft Excel 2010 (Microsoft Corporation, Redmond, WA, USA), Origin 8 (OriginLab Corporation, Northampton, MA, USA), and InStat 3 (GraphPad Software, Inc., La Jolla, CA, USA). Paired Student's *t*-test was used unless the characteristics of the data distribution required the use of the nonparametric Wilcoxon signed-rank test, as indicated in the text. Values are expressed as mean ± standard error (SE) of the mean, with n denoting the number of terminals.

RESULTS

Experiments were performed in 124 eyes obtained from 62 young adult mice of both sexes (3–6 months of age). A mean of 15 points per cornea were explored.

Based on the response characteristics to different stimuli, corneal sensory terminals were classified as high-threshold mechanoreceptor, polymodal nociceptor, and cold thermoreceptor terminals. Figures 1C and 1D show the proportion of successful attempts, that is, those in which NTIs were detected, as well as the percentage of each functional class of terminal. In more than half of the recording points, no NTI

Table 1. Functional Characteristics of Mechanonociceptor and Polymodal Nociceptor Terminals

	Terminal Type	
NTI Activity Parameter	**Mechanonociceptor**	**Polymodal Nociceptor**
Success, %	1.6	6.9
Cooling response, No. NTI/30 s		
Before	7.7 ± 4.7	8.4 ± 1.4
	$n = 3$	$n = 50$
During	7.7 ± 6.7	3.9 ± 0.7
	$n = 3$	$n = 50$
Mechanical stimulation, No. NTI/10 s		
Before	2.5 ± 1.7	1.9 ± 0.5
	$n = 4$	$n = 38$
During	22.3 ± 4.5	14.3 ± 1.4
	$n = 4$	$n = 38$
Heating response, No. NTI/30 s		
Before	10 ± 8.5	6 ± 0.9
	$n = 3$	$n = 48$
During	5 ± 2.1	30.2 ± 2.4
	$n = 3$	$n = 48$
Chemical stimulation, Δ imp·s^{-1}		
100 μM AITC	nd	0.3 ± 0.1
		$n = 4$
1 μM capsaicin	nd	1.6 ± 0.2
		$n = 23$
Hyperosmolal 850 mOsm	nd	0.38 ± 0.09
		$n = 5$

Success % indicates the percentage of successful attempts of recording a terminal from each group with regard to the total number of attempts. The cooling, heating, and mechanical response are expressed as the total number of NTIs during the 30 seconds immediately before and the 30 seconds during the cooling and the heating ramp, and 10 seconds immediately before and during the first 10 seconds of the mechanical pulse, respectively. Chemical stimulation is expressed as the difference increment of activity in the 30 seconds of maximum activity during the 2 to 3 minutes of chemical perfusion with regard to the 30 seconds immediately before (see Methods). nd, no response or quantitative data available.

activity was observed; in an additional 23% of trials, the impulses had small amplitude, preventing reliable identification and quantitative analysis of the nerve terminal characteristics.

Mechanoreceptor Terminals

Some terminals (9.5%) responding exclusively to mechanical stimulation were found (Table 1). Two of them had very low frequency of ongoing activity (0.1 and 0.5 imp·s^{-1}, one of them increased its basal activity after the different experimental maneuvers) while the rest remained silent during the 30-second background activity measuring period prior to stimulation. Pushing the recording pipette against the corneal surface for 2 seconds evoked a burst of NTIs that stopped immediately with the removal of the pipette's pressure (Figs. 2A, 2C). A similar, transient NTI firing response was obtained when pressure was maintained for 15 seconds (Fig. 2C). The mean number of NTIs fired during this stimulus was 22.3 ± 4.5 ($n = 4$).

Polymodal Nociceptor Terminals

Of the nerve terminals exhibiting a very low or no activity during the initial recording period, 41.1% responded to heat and generally also to mechanical pressure as well as to one or more of the chemical stimuli (Table 1). In the absence of an applied stimulus, the mean spontaneous activity of these polymodal nociceptor terminals was 0.3 ± 0.04 ($n = 50$; range, 0.02–1.5 imp·s^{-1}).

Thermal Stimulation. Application of a 30-second cooling ramp (from 34°C to 13.7 ± 0.3°C) to polymodal terminals reduced their ongoing activity, so that the mean number of NTIs fired during the cooling ramp was significantly lower than during the 30-second period before applying the cold stimulus (8.4 ± 1.4 NTIs before versus 3.9 ± 0.7 NTIs during the cooling ramp, $n = 50$, $P < 0.001$; Table 1; Fig. 3).

In contrast, in response to a 30-second heating ramp (from 33.7 ± 0.1°C to 52.0 ± 0.2°C, $n = 48$), polymodal terminals showed a marked increase in their firing frequency (Table 1), sometimes adopting a bursting pattern (Fig. 3). The heating threshold was 41.5 ± 0.5°C ($n = 48$). However, such threshold temperature value for the heating response varied widely among individual terminals, ranging between 36.3°C and 51.4°C. Also, the frequency and duration of the NTI discharge differed between the nerve terminals, although, in all cases, NTI activity silenced completely at the onset of cooling at the termination of the heating ramp. The magnitude of the response to heating, measured as the total number of impulses fired during the complete duration of the heating ramp, was 30.2 ± 2.4 NTIs, a value significantly higher than during the 30-second period at 34°C that preceded the heat ramp (6.0 ± 0.9 NTI $n = 48$, $P < 0.001$, Table 1). Around 14% of the polymodal terminals became silent and irresponsive after the first heating stimulus, whereas the rest resumed activity approximately 2 minutes after the end of the heat-evoked NTI discharge, with their activity before and after heating being similar (0.2 ± 0.02 imp·s^{-1} and 0.15 ± 0.03 imp·s^{-1}, respectively, $n = 43$, $P > 0.05$). In 11 of 18 tested terminals, a second heat ramp was applied 5 to 10 minutes later. In four of them no firing response was evoked; that is, they had been inactivated by the first heating ramp. In the remaining seven terminals, sensitization developed. This appeared either as a drop in heating threshold to −3.3 ± 0.4°C below the value determined during the first heat ramp ($n = 3$), as an increase in the total number of impulses during the heating pulse without change in threshold ($n = 3$), or as a threshold reduction combined with an increase in firing ($n = 1$).

Mechanical Stimulation. Mechanical stimulation for 2 seconds activated 38 of 44 polymodal terminals, classified as such by their activation by heat and/or chemical stimuli. The mechanically activated polymodal receptor terminals generated a short burst of NTIs at the onset of the maneuver (Fig. 3). On average, 14.3 ± 1.4 NTIs ($n = 38$) were counted during the 10-second period following the onset of the stimulus, a value that was significantly higher than that counted during the 10 seconds prior to the application of the stimulus (1.9 ± 0.5 NTIs, $n = 38$, $P < 0.001$, Wilcoxon matched-pairs test). In seven of the polymodal terminals responding to mechanical stimulation, the stimulus was repeated 2 minutes later but on this occasion was maintained for 15 seconds. The firing response was again transient, being composed of an initial burst of NTIs lasting for 1 to 2 seconds that returned to the basal firing level for the remainder of the stimulus; the total number NTIs during the first 10 seconds of the mechanical stimulus (9.3 ± 2.1, $n = 7$) was not significantly different from that measured in response to the 2-second stimulus (see above).

Chemical Stimulation. To define chemosensitivity of polymodal terminals, various chemical agents were applied to terminals that previously responded to a heat ramp (Fig. 3). Table 1 summarizes the response of polymodal terminals to the different chemical stimuli tested. Hyperosmolal solutions were tried in a total of 23 terminals (Table 1). The ongoing activity

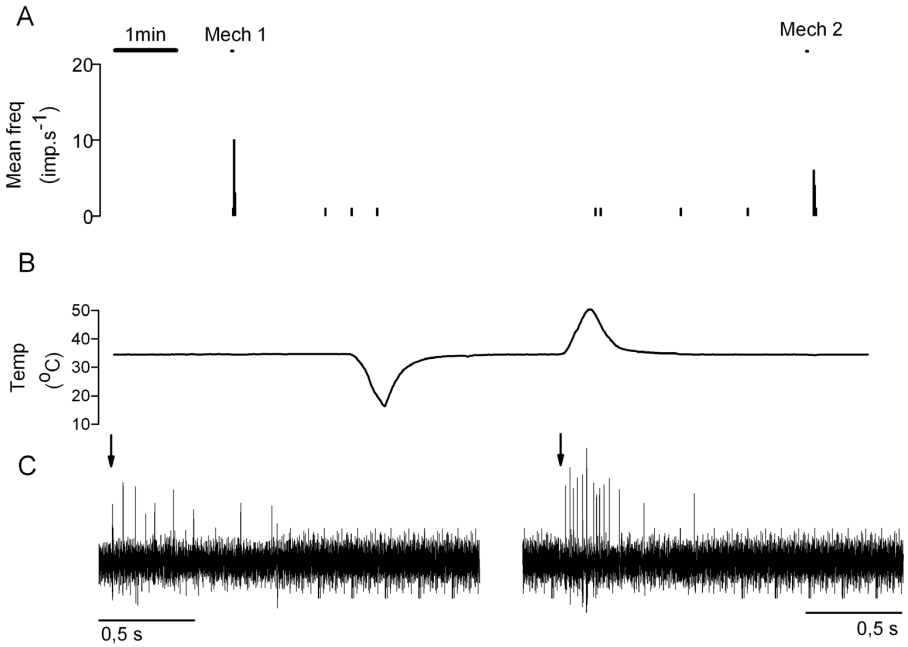

Figure 2. Example of NTI activity in a mechanonociceptor terminal. (**A**) Time histogram of the NTI discharge evoked by a 2-second (Mech 1) or a 15-second (Mech 2) forward displacement (10 μm) of the recording electrode. (**B**) Temperature record of the perfusing solution during the same time period shown in (**A**). (**C**) Samples of the recordings of NTI impulse activity evoked in the same mechanonociceptor terminal by a displacement of the electrode during a 2-second (*left*) and a 15-second (*right*) mechanical stimulation. *Arrows* indicate the onset of the stimulus.

increased during perfusion with 850 mOsm·kg^{-1} solution from 0.2 ± 0.1 to a mean value of 0.5 ± 0.1 imp·s^{-1} ($n = 5$, $P < 0.05$). Also, when this high-osmolality solution was applied, the NTI irregular firing pattern changed to a bursting pattern and the shape of NTIs was altered, becoming wider and of smaller amplitude (data not shown; see also Ref. 35). The TRPA1 agonist AITC (100 μM) was tested in 9 terminals and weakly activated 4 of them, while the TRPV1 agonist capsaicin (1 μM)

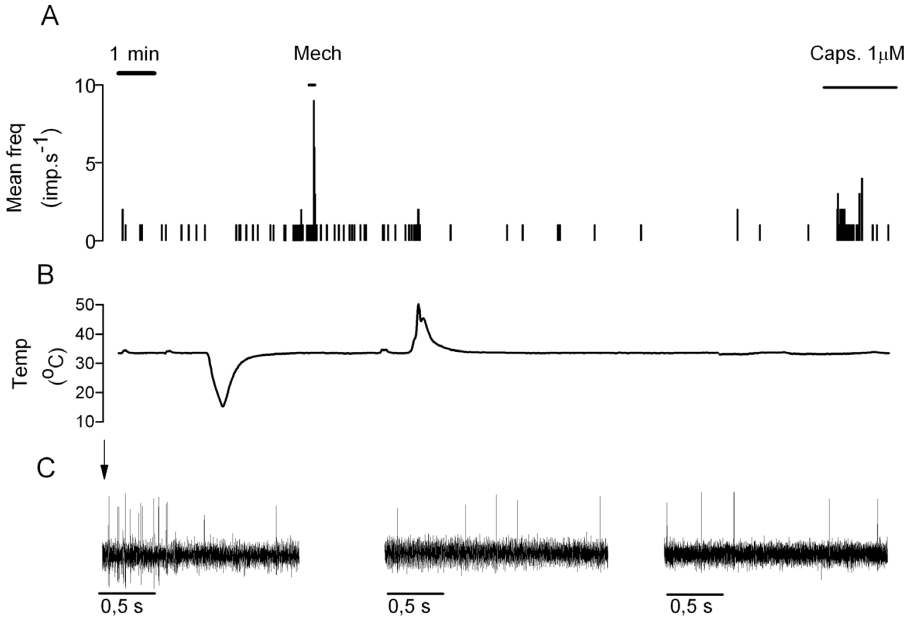

Figure 3. Example of the NTI response of a polymodal nociceptor terminal. (**A**) Time histogram of the NTI discharge of a polymodal nociceptor terminal evoked by a 10-μm forward displacement of the recording electrode for 2 seconds (Mech), changes in bath temperature (see record of temperature of perfusion solution in [**B**]), and perfusion with 1-μM capsaicin. (**C**) Sample records of the NTI impulse activity during a 2-second mechanical stimulation (*left trace*), at the beginning of the response in heating ramp (*center trace*), and during the perfusion with capsaicin (*right trace*), in the same polymodal nociceptor. *Arrow* indicates the onset of the mechanical stimulus.

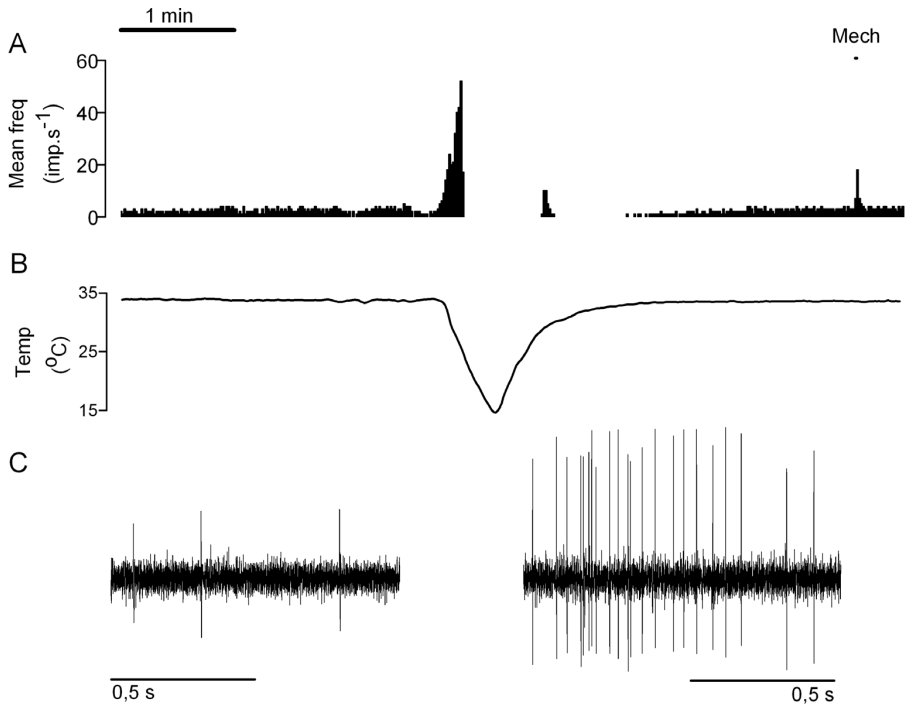

FIGURE 4. Example of the NTI response of a HB-LT cold thermoreceptor terminal to a cooling ramp. (**A**) Time histogram of the NTI discharge. Notice the transient firing observed during temperature recovery (see text). Mech, mechanical stimulation (10-μm forward displacement of the electrode for 2 seconds). (**B**) Bath temperature trace during the same time period shown in (**A**). (**C**) Sample records of the NTI impulse activity during control recording at 34°C (*left*) and during the mechanical stimulation (*right*) in the same HB-LT terminal.

activated 23 of the 24 terminals tested (0.1 ± 0.04 imp·s^{-1} before and 1.4 ± 0.2 imp·s^{-1} during capsaicin application, $P <$ 0.001). Application of inflammatory soup (see Methods) to seven polymodal terminals for 5 minutes evoked a significant increase in the ongoing NTI firing rate (from 0.1 ± 0.02 to 0.2 ± 0.04 imp·s^{-1}, $P < 0.003$).

Cold Thermoreceptor Terminals

Corneal terminals responding to cooling represented a 49.4% of the total.

High-Background/Low-Threshold (HB-LT) Cold-Sensitive Terminals. All nerve terminals exhibiting a repetitive background activity immediately after application of the pipette also responded readily to a cooling ramp with a robust increase in firing frequency. We classified these nerve terminals as high-background activity, low-threshold (HB-LT) cold thermoreceptor terminals; they represented 72% of the total population of cold-sensitive nerve endings found in the cornea. Mechanical pressure evoked a few NTIs in six HB-LT terminals where it was tested (Fig. 4). Table 2 summarizes the firing characteristics of the HB-LT cold thermoreceptor terminals. Their background activity at 34°C was usually composed of regularly appearing individual or paired NTIs, firing at a mean frequency ranging between 1.3 and 19.3 imp·s^{-1} (mean 6.6 ± 1.0 imp·s^{-1}, $n = 26$). During the initial portion of the cooling ramp, firing pattern often changed from regular beating to bursting and, after reaching a peak frequency value of 57.8 ± 3.9 imp·s^{-1} at 26 ± 0.7°C, NTIs usually silenced at around 23°C, well before reaching the lowest temperature point (14–15°C). During the 30-second heating period back to the control temperature, a transient NTI discharge (mean number 102.1 ± 40 NTIs), appearing at a mean temperature of 27.5 ± 0.5°C and lasting on the average 7.5 ± 1.8 seconds, was observed in 14 out of 26 HB-LT terminals (Fig. 4), followed again by a silence until a temperature of 31.4 ± 0.3°C was attained, at which point the NTI activity gradually recovered to the frequency that it had prior to the cooling ramp. The application of 20 μM menthol increased significantly ongoing activity of HB-LT terminals (Table 2). Also, perfusion with 340 mOsm·kg^{-1} hyperosmolal solution increased the ongoing firing frequency (from 8.0 ± 1.5 to 10.3 ± 1.6 imp·s^{-1}, $P < 0.05$). Sixty-seven percent of the HB-LT terminals responded to a heating ramp with a transient NTI discharge ("paradoxical response") starting at 41.9 ± 2°C (mean number of NTIs, 355.5 ± 111.4; mean duration of the firing period, 9.4 ± 2.1 seconds). Four HB-LT terminals with a paradoxical response were tested with 1 μM capsaicin; in all of them, capsaicin increased the mean firing rate at 34°C ($\Delta = 13.0 \pm 3.5$ imp·s^{-1}, $n = 4$) and reduced the cooling threshold to temperature values 3°C to 4°C lower than the pretreatment value. Intriguingly, in two out of four terminals tested, the TRPA1 agonist AITC prolonged the duration of NTI firing during the cooling ramp to a temperature below 20°C (19.9°C and 14.4°C in the two responsive terminals).

Low-Background/High-Threshold (LB-HT) Cold-Sensitive Terminals. Among corneal terminals exhibiting a very low initial background activity at 34°C, a proportion were characterized by the firing of a sustained NTI discharge when the temperature decreased by around 6°C, and silencing upon rewarming to 34°C (Figs. 1, 5). These low-background activity, high-threshold (LB-HT) cold thermoreceptor terminals represented 28% of the total number of cold-sensitive terminals. Table 2 summarizes the firing characteristics for these LB-HT cold terminals. Peak frequency and temperature at which cold-evoked firing appeared were significantly lower than in HB-LT

Table 2. Values of the Different Parameters of the NTI Response Measured in HB-LT and LB-HT Cold Terminals

	Cold Terminal Type	
NTI Activity Parameter	**HB-LT**	**LB-HT**
Success, %	6	3
Background activity*, imp·s^{-1}	6.6 ± 1.0	0.5 ± 0.1
	$n = 26$	$n = 9$
Cooling threshold*, °C	32.1 ± 0.2	28.2 ± 0.5
	$n = 26$	$n = 9$
Cooling response*, imp·s^{-1}	34.4 ± 2.3	6.3 ± 1.2
	$n = 26$	$n = 9$
Silencing temperature, °C	23.1 ± 0.9	17.1 ± 1.1
	$n = 26$	$n = 9$
Mechanical stimulation, No. NTI/10 s		
Before	39.0 ± 15.9	6.3 ± 1.8
	$n = 6$	$n = 3$
During	74.1 ± 17.0	25.3 ± 6.0
	$n = 6$	$n = 3$
Heating response, No. NTI/30 s		
Before	56.8 ± 16.3	7.8 ± 2.7
	$n = 6$	$n = 4$
During	355.5 ± 111.4	32.3 ± 11.0
	$n = 6$	$n = 4$
Menthol response, Δ imp·s^{-1}	9.5 ± 6.9	5.5 ± 3.1
	$n = 2$	$n = 3$

Success % indicates the percentage of successful attempts of recording a terminal from each group with regard to the total number of attempts. Background activity, cooling threshold, cooling response, and silencing temperature (see Methods) are measured during a cooling ramp. Mechanical and heating response are expressed as the total number of NTIs immediately before and during the mechanical pulse and heating ramp (in 10 and 30 seconds, respectively). Menthol response is expressed as the increment of activity during menthol perfusion with regard to the 30 seconds immediately before starting menthol perfusion. The statistical analyses were made comparing the values of HB-LT with LB-HT using a Student's *t*-test.

* $P < 0.01$.

cold thermoreceptor terminals (cf. Figs. 5, 6). In five LB-HT terminals where a 30-second heating ramp was applied, a discharge of impulses (mean 32.3 ± 11.1 NTIs, $n = 4$) was evoked (Fig. 5) with a mean duration of 13.9 ± 5.6 seconds. Also, three out of the five LB-HT terminals tested fired NTIs in response to mechanical stimulation (Table 2).

Three out of four LB-HT tested for sensitivity to a 3-minute application of menthol (20 μM) at 34°C had a marked increase of ongoing activity from 0.7 ± 0.2 to 6.1 ± 3.1 imp·s^{-1} ($n = 3$). Moreover, in all four units treated with menthol, this agent decreased cold threshold to a cooling ramp from 28.1 ± 0.2°C to 30.4 ± 0.8°C, $n = 4$. In two LB-HT terminals explored for sensitivity to a 397 mOsm·kg^{-1} hyperosmolal solution at 34°C, NTI frequency approximately doubled compared to the pretreatment activity (data not shown).

Discussion

In this study, we confirmed that the mouse cornea is innervated by trigeminal ganglion (TG) neurons, which respond to the same stimulus modalities as those of other mammalian species, and characterized them as mechanonociceptor, polymodal nociceptor, and cold thermoreceptor sensory nerve terminals. We also defined electrophysiologically two distinct classes of cold thermoreceptor endings whose activity may underlie, respectively, basal and irritation-evoked tearing and blinking.

Functional categorization of corneal receptor terminals was performed, selecting the population of terminals that exhibited spontaneous activity or responded positively to mechanical pressure before the electrode was moved to the next recording point. Mechanosensitive terminals were subsequently tested for responsiveness to thermal and chemical stimuli in order to define their polymodality. Hence, this recording strategy does not recruit "silent nociceptors," that is, sensory neurons that are not excited by physiological stimuli, even at potentially tissue-damaging intensities, but develop nerve impulse activity when inflammation develops,[37] and whose existence in the eye has been suggested.[38]

Corneal polymodal nociceptor neurons are the most frequently encountered functional type of sensory nerve terminal in the cat and guinea pig cornea, where they represent around 65% of the total number of corneal nerve fibers.[21–25] Comparatively, polymodal nociceptors appear to be less abundant (approximately 40%) in the mouse. Mechanonociceptors comprise 15% and 12% of all corneal sensory fibers in the cat and guinea pig, respectively,[23–25] and only 9.5% in mice, while the percentage of cold thermoreceptors identified in the mouse is almost double that found in the cat (17%) and the guinea pig (21%).[23–25]

Such variability in the proportion of modality-specific sensory fibers can be attributed to species differences; however, it may also reflect the bias introduced by the use of different identification methods to sample the sensory modality of corneal sensory nerve fibers. The percentage of axons of a given modality has been generally calculated based on their presence in extracellular recordings of single nerve fibers dissected from the ciliary nerves at the back of the eye, in anesthetized cats or in excised and superfused guinea pig eyes.[22,33] In both cases, thinly myelinated A-delta mechanosensory fibers tend to be picked up more easily than the unmyelinated (C) fibers that are in most cases polymodal nociceptor and cold fibers.[24,33,36] In contrast, the technique used to record from single corneal nerve terminals in vitro in guinea pig or mouse eyes favors the detection of thin cold thermoreceptor terminals, which display spontaneous activity, are more superficially located, and branch more extensively than polymodal and mechanoreceptor endings, thus producing larger-amplitude NTIs.[17,24,26–28,33,34,39,40] In the present work, we tried to confront this caveat through a systematic sampling of impulse activity at regularly distributed points on the corneal surface, thus reaching theoretically all types of nerve terminals. Only terminals that were unambiguously identified were counted. Hence, the data obtained in mice corneas probably provide a reasonably accurate picture of the relative proportion of terminals of different modality in this species. Still, the group of unidentified terminals, containing units of very low amplitude or not responding clearly to any of the stimuli, may include an unknown proportion of "silent nociceptors."

The method used for application of mechanical force to the corneal surface precluded an accurate measurement of force threshold of purely mechanoreceptor endings, which has been reported to be higher than in polymodal nociceptor endings.[21,24] Still, the short-lasting discharge of NTIs evoked by a sustained pressure in these terminals suggests that they belong to the general class of high-threshold, phasic mechanonociceptive primary sensory neurons also identified in the cornea of the cat and guinea pig.[23–25,33,34] The transducing channels conferring mechanosensitivity to these endings have not been identified yet, although expression of the mechanosensory channel Piezo2[41] has been reported in approximately 30% of corneal TG neurons. This Piezo2-positive subpopulation of neurons possesses an immunocytochemical profile very different from canonical cold or

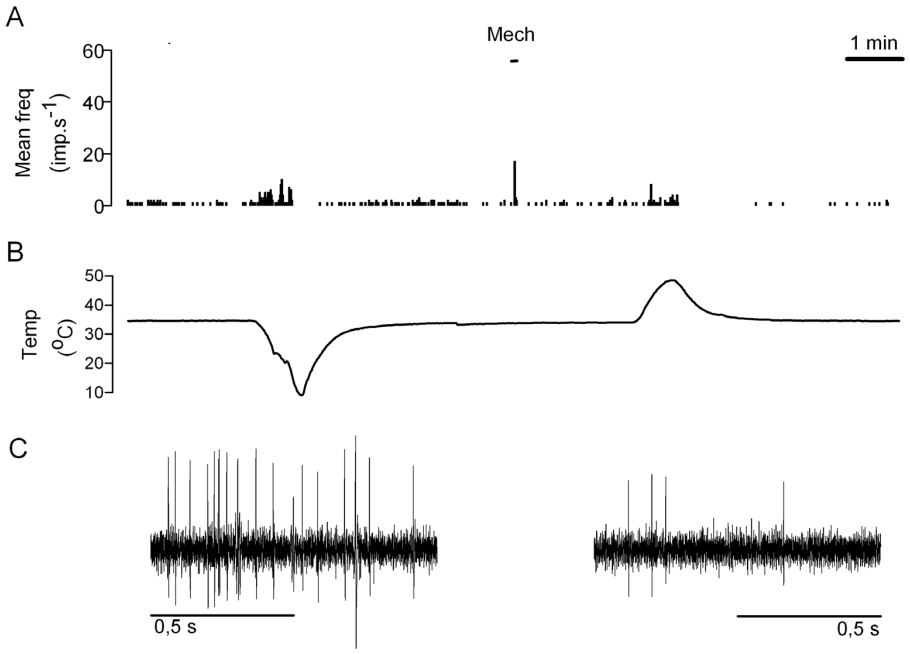

FIGURE 5. Example of the NTI response of a LB-HT cold thermoreceptor terminal. (**A**) Time histogram of the NTI discharge. Mech, mechanical stimulation (10-µm forward displacement of the electrode for 2 seconds). (**B**) Bath temperature trace during the time period shown in (**A**). (**C**) Sample records of the NTI impulse activity during the cooling ramp (*left*) and the heating ramp (*right*) in the same LB-HT terminal.

polymodal nociceptor neurons, thus suggesting that they may correspond functionally to pure mechanonociceptive neurons.[42] It could be further speculated that the morphologically distinct group of corneal nerve terminals named "ramified endings"[39] are given by this group of corneal mechanonociceptor neurons. The recent finding of a selective expression of Nav1.1 channels in high-threshold mechanosensitive fibers of the skin opens new venues for a more

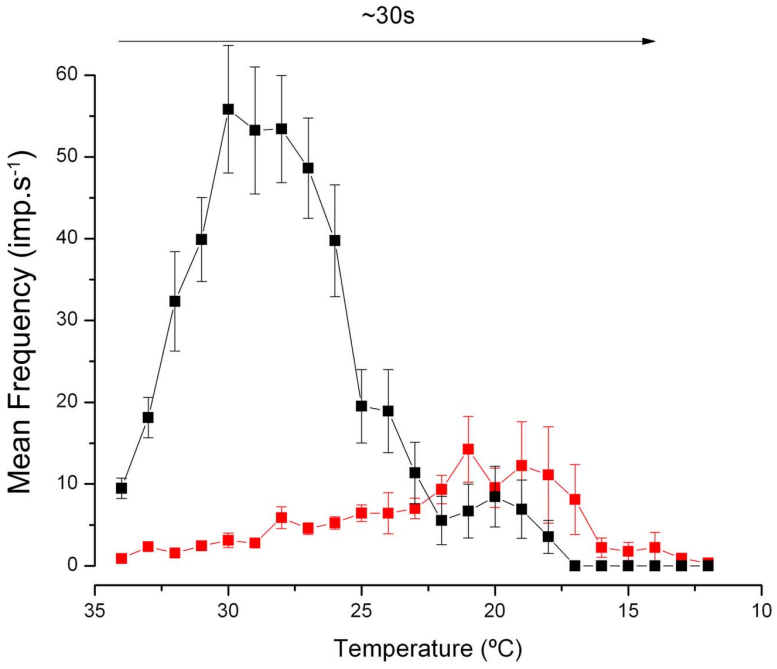

FIGURE 6. Stimulus–response curves of HB-LT and LB-HT cold-sensitive terminals. Mean NTI firing frequency values (imp·s^{-1}) are represented versus temperature during a cooling ramp from 34°C to 12°C in ~30 seconds, as indicated by the *horizontal arrow*. *Black squares*, HB-LT terminals ($n = 26$). *Red squares*, LB-HT terminals ($n = 9$).

precise identification of the transducing mechanisms in corneal pure mechanosensory terminals.[43]

Corneal polymodal nociceptors of the mouse responded unambiguously with a NTI discharge to mechanical stimuli, noxious heating, and capsaicin and were sensitized by a mixture of inflammatory agents. Their frequency rises with osmolality increases to discrete values; however, it is well established that firing frequency values over 0.5 imp·s^{-1} in polymodal human nerve fibers already evoke conscious pain sensations.[44,45] Thus, it seems reasonable to assume that activation of corneal polymodal terminals produced by the different stimuli used in our study would also evoke pain sensation in the awake mouse.

The sensitivity to heating and capsaicin supports the presence of TRPV1 channels, the molecular integrator of noxious heat, and a large variety of algesic substances[46–48] in this class of nerve terminals. The presence of TRPV1 channels in corneal polymodal nociceptors contributing to ocular surface pain is to be expected from the strong tearing and blinking response evoked by application of capsaicin to the eye in many species including mice.[17,49] A smaller proportion of polymodal terminals was also activated by the TRPA1 channel agonist AITC, which also evokes irritative tearing and blinking when applied to mouse eyes.[17] Nonetheless, the low number of polymodal terminals responding to TRPA1 activation in mice, as also seen in guinea pigs,[33] suggests that TRPA1 channels are not highly expressed in corneal polymodal nociceptor endings.

Altogether, mouse polymodal nociceptors innervating the cornea are functionally very similar to polymodal fibers of the mouse skin or tongue[18,50,51] and of the cornea of other species.[22,23,25] They encode approximately the intensity of mechanical stimuli, develop inactivation/sensitization upon repeated noxious stimulation, and respond to a large variety of endogenous and exogenous chemicals.[38,52]

Our study confirms with functional data the dense innervation of the mouse cornea by cold thermoreceptor axon terminals, evidenced by recent immunocytochemical studies.[17,39,48] Canonical low-threshold cold thermoreceptors of various species and tissues are easily recognized by their regular background impulse activity at the normal temperature of the tissue, whose frequency of discharge changes with temperature oscillations of 1°C or less.[23,24,28,53,54] We distinguished in the mouse cornea a high number of HB-LT cold terminals that typically responded to static and dynamic changes in temperature and were activated by menthol and hyperosmotic stimuli, as reported for canonical cold thermoreceptors of the cornea and of various other tissues in many species.[19,32,54–57] In the eye, it has been postulated that these low-threshold corneal thermoreceptors detect small temperature changes linked to interblink tear film evaporation, thereby providing a tonic sensory input to the brain encoding wetness of the eye surface.[17,29,58,59]

The additional presence in the cornea of a subpopulation of unmyelinated cold thermoreceptor axons responding only to strong cooling and osmolality was originally reported in the cat in 1993 by Gallar et al.,[24] who named them "cold" nociceptors. More recently, corneal "dry-sensitive" neurons responding to weak or strong levels of ocular surface desiccation, hyperosmolarity, and menthol and exhibiting parallel high or low sensitivity to corneal cooling were reported in the TG of the rat.[30,32,60] Here, we unambiguously identified and characterized these two subclasses of cold-thermosensitive neurons in the mouse cornea and propose their inclusion within the general class of cold thermoreceptor primary sensory neurons.

The sensitivity of cold thermoreceptor neurons to low temperatures is primarily determined by the expression of TRPM8, a nonselective cationic channel gated by moderate cold and also by menthol and hyperosmolar solutions.[19,61,62] TRPM8 channel opening contributes to an excitatory, depolarizing current in sensory neurons named I_{cold} that triggers propagated impulse responses to cooling (for review see Refs. 63, 64). It has been shown that the cell bodies of cold-thermosensitive neurons in dorsal root and trigeminal sensory ganglia display a wide range of thresholds for cold stimuli.[65–69] This heterogeneity of cooling thresholds is determined to large extent by variability in the density of TRPM8 channels, but is also attributed to the absence or limited expression of the potassium channels Kv1.1-1.2.[70,71] These K^+ channels sustain an outward current termed I_{KD} in most primary sensory neurons that opposes the inward current generated by cold activation of TRPM8, thereby acting as an excitability break that prevents unspecific cold-induced depolarization.[65] In TG cold-sensitive neurons in culture, it has been convincingly demonstrated that low-threshold cold thermoreceptor neurons virtually lack I_{KD}, while in high-threshold cold thermoreceptor neurons, which respond only to stronger cooling, this current is prominent.[71] Accordingly, cold threshold and cooling-evoked firing rate in cold thermoreceptor sensory neurons depend on a balance between the expression levels of TRPM8 and Kv1 channels.[65,71,72] Therefore, it is conceivable that HB-LT cold thermoreceptor terminals of the mouse cornea belong to TG cold-sensitive neurons presenting a high expression of TRPM8 channels and low or no expression of Kv1 channels, whereas LB-HT terminals originate from TG cold-sensitive neurons with lower levels of TRPM8 channels and a significant presence of Kv1 channels.[70,71]

It is worth noting that the two subtypes of corneal cold thermoreceptor terminals found in the mouse cornea also responded to stimuli such as heat, osmolality changes, mechanical forces, menthol, and a variety of other irritant agents. A variable sensitivity of canonical cold thermoreceptors to these stimuli has been reported earlier.[17–19,24,29,30,32,35,55] This is not exceptional. Other classes of peripheral somatosensory receptors equipped with specific transducing channels that confer preferential sensitivity for a particular form of stimulating energy, also express transduction channels for other stimulus qualities.[73] Our data suggest that this is a prominent characteristic of corneal cold thermoreceptors, where the expression of multiple transduction channels equips the ocular surface with a set of sensory receptors particularly tuned for the detection of the main physical parameters associated with changes in corneal surface wetness (temperature, osmolality, cell shrinking).[59]

It is generally accepted that corneal mechanonociceptor axons, preferentially tuned to fire phasically in response to mechanical stimulation, and polymodal nociceptors tonically activated by a large variety of noxious chemical, mechanical, and thermal stimuli, are the peripheral substrate of acute and chronic eye pain.[52,74] Second-order neurons of this pathway are mainly located at the caudal levels of the spinal trigeminal nucleus, in the transition area between nucleus caudalis and cervical spinal cord (Vc/C1).[75–77] In contrast, there is considerable evidence that a majority of corneal HB-LT cold thermoreceptors project to second-order neurons located at the transition zone between the spinal trigeminal subnucleus caudalis and subnucleus interpolaris (Vi/Vc), an area proposed as the processing center for neural regulation of lacrimation and blinking via the superior salivatory nucleus (SSN) and the facial motor nucleus.[20,32,78] The SSN and facial motor nucleus also receive an input from Vc/C1 neurons connected to corneal nociceptors for reflex motor and autonomic ocular responses evoked by injurious stimuli.[77,79] The location in the brainstem of the second-order neurons connecting with LB-HT cold thermoreceptors is not certain. Kurose and Meng[20]

reported the activation of a subset of second-order neurons of the Vi/Vc region only by strong cooling. These neurons were also activated by acidic stimulation of the cornea, suggesting that they may receive inputs from both LB-HT and polymodal nociceptor corneal fibers. In conditions such as experimental chronic eye dryness where the LB-HT cold thermoreceptors become selectively sensitized,[20,31,36,80] there is enhanced neural activity in ocular responsive neurons in both the Vi/Vc and Vc/C1 regions.[80] It has been suggested that LB-HT neurons contribute importantly to discomfort sensations accompanying chronic eye surface dryness.[36,59] Hence it is tempting to speculate that this subclass of cold thermoreceptor primarily projects into nociceptor-driven second-order neurons of the Vc/C1 region evoking discomfort and, also together with the polymodal nociceptors reaching that area, on the neurons of the Vi/Vc involved in the regulation of tearing and blinking.

Under normal environmental conditions, it has been postulated that small changes in ocular surface temperature and osmolality resulting from tear fluid evaporation at the exposed eye surface are encoded by HB-LT cold thermoreceptors[17,23,24,28,29,35,58,59] and transmitted to second-order Vi/Vc neurons.[20,78] When there is excessive evaporation and/or hyperosmolarity of tear film, the LB-HT cold thermoreceptors may also be recruited, and evoke a sense of irritation through the same pain-labeled pathways as corneal mechano- and polymodal nociceptor nerve fibers. These three sensory receptors types may also be activated by cell shrinkage and local inflammation caused by dryness. Together, this multireceptor sensory message evokes augmented tearing and blinking as well as the irritative, unpleasant dryness sensations associated with chronic dry eye.[36,59] A similar, variable involvement of the different functional classes of peripheral sensory receptors is expected to occur after injury or pathologic processes affecting the ocular surface.

Electrophysiological classification of somatosensory receptor types, based both on the form of energy to which they preferentially respond and on the stimulus intensity required for their activation, has been a useful approach to correlate stimulus modalities and activation of specific sets of peripheral sensory neurons leading to qualitatively distinct sensations, but has a number of technical limitations. Repeated application of different stimuli may cause tissue damage, favoring the apparition of inactivation, fatigue, or sensitization.[81] This is particularly true for polymodal nociceptors, whose stimulus threshold is by definition close to injurious intensities. The discovery in sensory receptor neurons of specific membrane transducing molecules for different forms of energy[82–84] served as an essential tool to refine the identification of peripheral receptor classes. Still, there is considerable variability in transducing molecule expression within neurons of the same functional receptor category; moreover, neurons with peripheral terminals responding preferentially to a specific stimulus often express also transducing molecules for other stimulus modality.[70,85] Although the functional specificity of the various populations of primary sensory neuron for a particular class of stimulus is well defined, this molecular promiscuity determines their potential excitation by other modalities of stimuli, particularly under abnormal conditions. It is conceivable that the molecular heterogeneity of neurons belonging to a general functional type may be, at least in part, behind the striking variability of the peripheral sensory messages generated at ocular surface tissues under pathological conditions, including inflammation and injury.

The present work has been performed in mice, an experimental model particularly suitable to study the molecular basis of eye surface sensations. It defines in this species the electrophysiological characteristics of the different classes of sensory nerve endings innervating the cornea, providing new data that can in our view be used for a multidisciplinary approach to the study of normal and pathological eye sensations.

Acknowledgments

The authors thank Rodolfo Madrid for the contribution to the preparation of corneal nerve terminal recording in the mouse. For critical reading of the manuscript, they also thank James A. Brock. In addition they thank Enol Artime and Paola Braga for their technical assistance.

Supported by Grants FC-15-GRUPIN14-141 from the Consejería de Economía y Empleo del Gobierno del Principado de Asturias, Spain, cosponsored with FEDER funds from the European Union and the Fundación Ramón Areces, Caja Rural de Asturias, and Ministerio de Economía y Competitividad of Spain and FEDER (SAF2014-54518-C3-1-R and SAF2014-54518-C3-2-R). C.B. acknowledges financial support from the Spanish State Research Agency, through the "Severo Ochoa" Programme for Centres of Excellence in R&D (SEV-2013-0317).

Disclosure: **O. González-González**, None; **F. Bech**, None; **J. Gallar**, None; **J. Merayo-Lloves**, None; **C. Belmonte**, None

References

1. Namavari A, Chaudhary S, Sarkar J, et al. In vivo serial imaging of regenerating corneal nerves after surgical transection in transgenic thy1-YFP mice. *Invest Ophthalmol Vis Sci*. 2011; 52:8025–8032.
2. Wang C, Fu T, Xia C, Li Z. Changes in mouse corneal epithelial innervation with age. *Invest Ophthalmol Vis Sci*. 2012;53: 5077–5084.
3. Reichard M, Weiss H, Poletti E, et al. Age-related changes in murine corneal nerves. *Curr Eye Res*. 2015;1–8.
4. Marfurt CF, Murphy CJ, Florczak JL. Morphology and neurochemistry of canine corneal innervation. *Invest Ophthalmol Vis Sci*. 2001;42:2242–2251.
5. Muller LJ, Marfurt CF, Kruse F, Tervo TMT. Corneal nerves: structure, contents and function. *Exp Eye Res*. 2003;76:521–542.
6. de Castro F, Silos-Santiago I, Lopez de Armentia M, Barbacid M, Belmonte C. Corneal innervation and sensitivity to noxious stimuli in trkA knockout mice. *Eur J Neurosci*. 1998;10:146–152.
7. Guaiquil VH, Pan Z, Karagianni N, Fukuoka S, Alegre G, Rosenblatt MI. VEGF-B selectively regenerates injured peripheral neurons and restores sensory and trophic functions. *Proc Natl Acad Sci U S A*. 2014;111:17272–17277.
8. Shevalye H, Yorek MS, Coppey LJ, et al. Effect of enriching the diet with menhaden oil or daily treatment with resolvin D1 on neuropathy in a mouse model of type 2 diabetes. *J Neurophysiol*. 2015;114:199–208.
9. Íñigo-Portugués A, Alcalde I, Gonzalez-Gonzalez O, Gallar J, Belmonte C, Merayo-Lloves J. Decreased basal tear in aged mice is linked to morphological and functional changed in corneal sensory nerve fibers. *Acta Ophthalmol*. 2014:92.
10. Cai D, Zhu M, Petroll WM, Koppaka V, Robertson DM. The impact of type 1 diabetes mellitus on corneal epithelial nerve morphology and the corneal epithelium. *Am J Pathol*. 2014; 184:2662–2670.
11. Pal-Ghosh S, Pajoohesh-Ganji A, Tadvalkar G, et al. Topical Mitomycin-C enhances subbasal nerve regeneration and reduces erosion frequency in the debridement wounded mouse cornea. *Exp Eye Res*. 2015;146:361–39.
12. Pajoohesh-Ganji A, Pal-Ghosh S, Tadvalkar G, Kyne BM, Saban DR, Stepp MA. Partial denervation of sub-basal axons persists

following debridement wounds to the mouse cornea. *Lab Invest*. 2015;95:1305–1318.

13. Hu K, Harris DL, Yamaguchi T, Von Andrian UH, Hamrah P. A dual role for corneal dendritic cells in herpes simplex keratitis: local suppression of corneal damage and promotion of systemic viral dissemination. *PLoS One*. 2015;10:1–23.
14. Chucair-Elliott AJ, Zheng M, Carr DJJ. Degeneration and regeneration of corneal nerves in response to HSV-1 infection. *Invest Ophthalmol Vis Sci*. 2015;56:1097–1107.
15. Esquenazi S, He J, Li N, Bazan NG, Esquenazi I, Bazan HEP. Comparative in vivo high-resolution confocal microscopy of corneal epithelium, sub-basal nerves and stromal cells in mice with and without dry eye after photorefractive keratectomy. *Clin Experiment Ophthalmol*. 2007;35:545–549.
16. Bian F, Pelegrino FSA, Pflugfelder SC, Volpe EA, Li D-Q, de Paiva CS. Desiccating stress-induced MMP production and activity worsens wound healing in alkali-burned corneas. *Invest Ophthalmol Vis Sci*. 2015;56:4908–4918.
17. Parra A, Madrid R, Echevarria D, et al. Ocular surface wetness is regulated by TRPM8-dependent cold thermoreceptors of the cornea. *Nat Med*. 2010;16:1396–1399.
18. Zhang X, Mak S, Li L, et al. Direct inhibition of the cold-activated TRPM8 ion channel by Gαq. *Nat Cell Biol*. 2012;14:851–858.
19. Quallo T, Vastani N, Horridge E, et al. TRPM8 is a neuronal osmosensor that regulates eye blinking in mice. *Nat Commun*. 2015;6:7150.
20. Kurose M, Meng ID. Corneal dry-responsive neurons in the spinal trigeminal nucleus respond to innocuous cooling in the rat. *J Neurophysiol*. 2013;109:2517–2522.
21. Belmonte C, Giraldez F. Responses of cat corneal sensory receptors to mechanical and thermal stimulation. *J Physiol*. 1981;321:355–368.
22. Giraldez F, Geijo E, Belmonte C. Response characteristics of corneal sensory fibers to mechanical and thermal stimulation. *Brain Res*. 1979;177:571–576.
23. Belmonte C, Gallar J, Pozo MA, Rebollo I. Excitation by irritant chemical substances of sensory afferent units in the cat's cornea. *J Physiol*. 1991;437:709–725.
24. Gallar J, Pozo MA, Tuckett RP, Belmonte C. Response of sensory units with unmyelinated fibres to mechanical, thermal and chemical stimulation of the cat's cornea. *J Physiol*. 1993;468:609–622.
25. Brock JA, McLachlan EM, Belmonte C. Tetrodotoxin-resistant impulses in single nociceptor nerve terminals in guinea-pig cornea. *J Physiol*. 1998;512:211–217.
26. Brock JA, Pianova S, Belmonte C. Differences between nerve terminal impulses of polymodal nociceptors and cold sensory receptors of the guinea-pig cornea. *J Physiol*. 2001;533:493–501.
27. Carr RW. The effects of polarizing current on nerve terminal impulses recorded from polymodal and cold receptors in the guinea-pig cornea. *J Gen Physiol*. 2002;120:395–405.
28. Carr RW. Effects of heating and cooling on nerve terminal impulses recorded from cold-sensitive receptors in the guinea-pig cornea. *J Gen Physiol*. 2003;121:427–439.
29. Hirata H, Meng ID. Cold-sensitive corneal afferents respond to a variety of ocular stimuli central to tear production: implications for dry eye disease. *Invest Ophthalmol Vis Sci*. 2010;51:3969–3976.
30. Hirata H, Oshinsky ML. Ocular dryness excites two classes of corneal afferent neurons implicated in basal tearing in rats: involvement of transient receptor potential channels. *J Neurophysiol*. 2012;107:1199–1209.
31. Hirata H, Rosenblatt MI. Hyperosmolar tears enhance cooling sensitivity of the corneal nerves in rats: possible neural basis for cold-induced dry eye pain. *Invest Ophthalmol and Vis Sci*. 2014;55:5821–5833.
32. Kurose M, Meng ID. Dry eye modifies the thermal and menthol responses in rat corneal primary afferent cool cells. *J Neurophysiol*. 2013;110:495–504.
33. Acosta MC, Luna C, Quirce S, Belmonte C, Gallar J. Changes in sensory activity of ocular surface sensory nerves during allergic keratoconjunctivitis. *Pain*. 2013;154:2353–2362.
34. Acosta MC, Luna C, Quirce S, Belmonte C, Gallar J. Corneal sensory nerve activity in an experimental model of UV keratitis. *Invest Ophthalmol Vis Sci*. 2014;55:3403–3412.
35. Parra A, Gonzalez-Gonzalez O, Gallar J, Belmonte C. Tear fluid hyperosmolality increases nerve impulse activity of cold thermoreceptor endings of the cornea. *Pain*. 2014;155:1481–1491.
36. Kovacs I, Luna C, Quirce S, et al. Abnormal activity of corneal cold thermoreceptors underlies the unpleasant sensations in dry eye disease. *Pain*. 2016;157:399–417.
37. Michaelis M, Habler HJ, Jaenig W. Silent afferents: a separate class of primary afferents? *Clin Exp Pharmacol Physiol*. 1996;23:99–105.
38. Belmonte C, Viana F. Transduction and encoding of noxious stimuli. In: Schmidt RF, Willis W, eds. Encyclopedia of Pain. Vol. 2513. Berlin: Springer-Verlag; 2007:2515–2528.
39. Ivanusic JJ, Wood RJ, Brock JA. Sensory and sympathetic innervation of the mouse and guinea pig corneal epithelium. *J Comp Neurol*. 2013;521:877–893.
40. Carr RW, Pianova S, McKemy DD, Brock JA. Action potential initiation in the peripheral terminals of cold-sensitive neurones innervating the guinea-pig cornea. *J Physiol*. 2009;587:1249–1264.
41. Ranade SS, Woo SH, Dubin AE, et al. Piezo2 is the major transducer of mechanical forces for touch sensation in mice. *Nature*. 2014;516:121–125.
42. Bron R, Wood RJ, Brock JA, Ivanusic JJ. Piezo2 expression in corneal afferent neurons. *J Comp Neurol*. 2014;522:2967–2979.
43. Osteen JD, Herzig V, Gilchrist J, et al. Selective spider toxins reveal a role for the Nav1.1 channel in mechanical pain. *Nature*. 2016;534:494–499.
44. Gybels J, Handwerker HO, Van Hees J. A comparison between the discharges of human nociceptive nerve fibres and the subject's ratings of his sensations. *J Physiol*. 1979;292:193–206.
45. Yarnitsky D, Simone DA, Dotson RM, Cline MA, Ochoa JL. Single C nociceptor responses and psychophysical parameters of evoked pain: effect of rate of rise of heat stimuli in humans. *J Physiol*. 1992;450:581–592.
46. Caterina MJ, Schumacher MA, Tominaga M, Rosen TA, Levine JD, Julius D. The capsaicin receptor: a heat-activated ion channel in the pain pathway. *Nature*. 1997;389:816–824.
47. Julius D. TRP channels and pain. *Annu Rev Cell Dev Biol*. 2013;29:355–384.
48. Alamri A, Bron R, Brock JA, Ivanusic JJ. Transient receptor potential cation channel subfamily V member 1 expressing corneal sensory neurons can be subdivided into at least three subpopulations. *Front Neuroanat*. 2015;9:71.
49. Gonzalez GG, De la Rubia PG, Gallar J, Belmonte C. Reduction of capsaicin-induced ocular pain and neurogenic inflammation by calcium antagonists. *Invest Ophthalmol Vis Sci*. 1993;34:3329–3335.
50. Reeh PW. Sensory receptors in mammalian skin in an in vitro preparation. *Neurosci Lett*. 1986;66:141–146.
51. Meseguer V, Alpizar YA, Luis E, et al. TRPA1 channels mediate acute neurogenic inflammation and pain produced by bacterial endotoxins. *Nat Commun*. 2014;5:3125.

Investigative Ophthalmology & Visual Science

52. Belmonte C, Tervo T, Gallar J. Sensory innervation of the eye. In: Levin LA, Nilsson SFE, Ver Hoeve J, Wu S, Kaufman PL, Aim A, eds. *Adler's Physiology of the Eye*. Amsterdam: Elsevier; 2011:363–384.
53. Hensel H. Neural processes in thermoregulation. *Physiol Rev*. 1973;53:948–1017.
54. Braun HA, Bade H, Hensel H. Static and dynamic discharge patterns of bursting cold fibers related to hypothetical receptor mechanisms. *Pflugers Arch*. 1980;386:1–9.
55. Hensel H, Zotterman Y. The effect of menthol on the thermoreceptors. *Acta Physiol Scand*. 1951;24:27–34.
56. Orio P, Parra A, Madrid R, González O, Belmonte C, Viana F. Role of Ih in the firing pattern of mammalian cold thermoreceptor endings. *J Neurophysiol*. 2012;108:3009–3023.
57. Olivares E, Salgado S, Maidana JP, et al. TRPM8-dependent dynamic response in a mathematical model of cold thermoreceptor. *PLoS One*. 2015;10:e0139314.
58. Belmonte C, Gallar J. Cold thermoreceptors, unexpected players in tear production and ocular dryness sensations. *Invest Ophthalmol Vis Sci*. 2011;52:3888–3892.
59. Belmonte C, Acosta MC, Merayo-Lloves J, Gallar J. What causes eye pain? *Curr Ophthalmol Rep*. 2015;3:111–121.
60. Hirata H, Fried N, Oshinsky ML. Quantitative characterization reveals three types of dry-sensitive corneal afferents: pattern of discharge, receptive field, and thermal and chemical sensitivity. *J Neurophysiol*. 2012;108:2481–2493.
61. McKemy DD, Neuhausser WM, Julius D. Identification of a cold receptor reveals a general role for TRP channels in thermosensation. *Nature*. 2002;416:52–58.
62. Dhaka A, Murray AN, Mathur J, Earley TJ, Petrus MJ, Patapoutian A. TRPM8 is required for cold sensation in mice. *Neuron*. 2007;54:371–378.
63. Latorre R, Brauchi S, Madrid R, Orio P. A cool channel in cold transduction. *Physiology*. 2011;26:273–285.
64. Almaraz L, Manenschijn J-A, de la Pena E, Viana F. TRPM8. *Handb Exp Pharmacol*. 2014;222:547–579.
65. Viana F, de la Pena E, Belmonte C. Specificity of cold thermotransduction is determined by differential ionic channel expression. *Nat Neurosci*. 2002;5:254–260.
66. Nealen ML, Gold MS, Thut PD, Caterina MJ. TRPM8 mRNA is expressed in a subset of cold-responsive trigeminal neurons from rat. *J Neurophysiol*. 2003;90:515–520.
67. Thut PD, Wrigley D, Gold MS. Cold transduction in rat trigeminal ganglia neurons in vitro. *Neuroscience*. 2003;119:1071–1083.
68. Babes A, Zorzon D, Reid G. Two populations of cold-sensitive neurons in rat dorsal root ganglia and their modulation by nerve growth factor. *Eur J Neurosci*. 2004;20:2276–2282.
69. Teichert RW, Raghuraman S, Memon T, et al. Characterization of two neuronal subclasses through constellation pharmacology. *Proc Natl Acad Sci U S A*. 2012;109:12758–12763.
70. Madrid R, Donovan-Rodríguez T, Meseguer V, Acosta MC, Belmonte C, Viana F. Contribution of TRPM8 channels to cold transduction in primary sensory neurons and peripheral nerve terminals. *J Neurosci*. 2006;26:12512–12525.
71. Madrid R, de la Peña E, Donovan-Rodriguez T, Belmonte C, Viana F. Variable threshold of trigeminal cold-thermosensitive neurons is determined by a balance between TRPM8 and Kv1 potassium channels. *J Neurosci*. 2009;29:3120–3131.
72. Viana F. Chemosensory properties of the trigeminal system. *ACS Chem Neurosci*. 2011;2:38–50.
73. Belmonte C, Viana F. Molecular and cellular limits to somatosensory specificity. *Mol Pain*. 2008;4:14.
74. Belmonte C, Aracil A, Acosta MC, Luna C, Gallar J. Nerves and sensations from the eye surface. *Ocul Surf*. 2004;2:248–253.
75. Meng ID, Hu JW, Benetti AP, Bereiter DA. Encoding of corneal input in two distinct regions of the spinal trigeminal nucleus in the rat: cutaneous receptive field properties, responses to thermal and chemical stimulation, modulation by diffuse noxious inhibitory controls, and projections to the parabrachial area. *J Neurophysiol*. 1997;77:43–56.
76. Hirata H, Hu JW, Bereiter DA. Responses of medullary dorsal horn neurons to corneal stimulation by CO(2) pulses in the rat. *J Neurophysiol*. 1999;82:2092–2107.
77. Bereiter DA, Okamoto K, Tashiro A, Hirata H. Endotoxin-induced uveitis causes long-term changes in trigeminal subnucleus caudalis neurons. *J Neurophysiol*. 2005;94:3815–3825.
78. Hirata H, Okamoto K, Tashiro A, Bereiter DA. A novel class of neurons at the trigeminal subnucleus interpolaris/caudalis transition region monitors ocular surface fluid status and modulates tear production. *J Neurosci*. 2004;24:4224–4232.
79. Katagiri A, Thompson R, Rahman M, Okamoto K, Bereiter DA. Evidence for TRPA1 involvement in central neural mechanisms in a rat model of dry eye. *Neuroscience*. 2015;290:204–213.
80. Rahman M, Okamoto K, Thompson R, Katagiri A, Bereiter DA. Sensitization of trigeminal brainstem pathways in a model for tear deficient dry eye. *Pain*. 2015;156:942–950.
81. Mountcastle VB. Physiology of sensory receptors: introduction to sensory processes. In: Mountcastle VB. *Medical Physiology*. 12th ed, Vol. II. St. Louis: Mosby; 1968:1341–1375.
82. Gees M, Owsianik G, Nilius B, Voets T. TRP channels. *Compr Physiol*. 2012;2:563–608.
83. Zhang X. Molecular sensors and modulators of thermoreception. *Channels (Austin)*. 2015;9:73–81.
84. Hao J, Bonnet C, Amsalem M, Ruel J, Delmas P. Transduction and encoding sensory information by skin mechanoreceptors. *Pflugers Arch*. 2015;467:109–119.
85. Belmonte C, Brock JA, Viana F. Converting cold into pain. *Exp Brain Res*. 2009;196:13–30.

Investigative Ophthalmology & Visual Science

Received: 1 February 2018 | Revised: 15 March 2018 | Accepted: 16 March 2018

DOI: 10.1002/cne.24454

RESEARCH ARTICLE

WILEY JCN RESEARCH IN SYSTEMS NEUROSCIENCE THE JOURNAL OF COMPARATIVE NEUROLOGY

Morphological and functional changes in TRPM8-expressing corneal cold thermoreceptor neurons during aging and their impact on tearing in mice

Ignacio Alcalde[1] | Almudena Íñigo-Portugués[1,2] | Omar González-González[1] | Laura Almaraz[2] | Enol Artime[1] | Cruz Morenilla-Palao[2] | Juana Gallar[2] | Félix Viana[2] | Jesús Merayo-Lloves[1] | Carlos Belmonte[1,2]

[1]Instituto Universitario Fernández-Vega, Universidad de Oviedo & Fundación de Investigación Oftalmológica, Oviedo, Spain

[2]Instituto de Neurociencias, Universidad Miguel Hernández-CSIC, San Juan de Alicante, Spain

Correspondence
Carlos Belmonte, Instituto de Neurociencias, UMH-CSIC, Avenida Santiago Ramon y Cajal, 2, 03550 San Juan de Alicante.
Email: carlos.belmonte@umh.es

Funding information
Ministerio de Economía, Industria y Competitividad, Grant/Award Number: SAF2014-54518-C3-1-R, SAF2014-54518-C3-2-R, SAF2016-77233-R, SAF2017-83674-C2-1-R, SAF2017-83674-C2-2-R, SEV-2013-0317; Consejería de Economía y Empleo, Grant/Award Number: FC-15-GRUPIN14-141

Abstract

Morphological and functional alterations of peripheral somatosensory neurons during the aging process lead to a decline of somatosensory perception. Here, we analyze the changes occurring with aging in trigeminal ganglion (TG), TRPM8-expressing cold thermoreceptor neurons innervating the mouse cornea, which participate in the regulation of basal tearing and blinking and have been implicated in the pathogenesis of dry eye disease (DED). TG cell bodies and axonal branches were examined in a mouse line (TRPM8^{BAC}-EYFP) expressing a fluorescent reporter. In 3 months old animals, about 50% of TG cold thermoreceptor neurons were intensely fluorescent, likely providing strongly fluorescent axons and complex corneal nerve terminals with ongoing activity at 34°C and low-threshold, robust responses to cooling. The remaining TRPM8^{+} corneal axons were weakly fluorescent with nonbeaded axons, sparsely ramified nerve terminals, and exhibited a low-firing rate at 34°C, responding moderately to cooling pulses as do weakly fluorescent TG neurons. In aged (24 months) mice, the number of weakly fluorescent TG neurons was strikingly high while the morphology of TRPM8^{+} corneal axons changed drastically; 89% were weakly fluorescent, unbranched, and often ending in the basal epithelium. Functionally, 72.5% of aged cold terminals responded as those of young animals, but 27.5% exhibited very low-background activity and abnormal responsiveness to cooling pulses. These morpho-functional changes develop in parallel with an enhancement of tear's basal flow and osmolarity, suggesting that the aberrant sensory inflow to the brain from impaired peripheral cold thermoreceptors contributes to age-induced abnormal tearing and to the high incidence of DED in elderly people.

KEYWORDS

aging, cold thermoreceptors, dry eye, pain, tearing, trigeminal ganglion, RRID: AB_221569, RRID: AB_300798, RRID: AB_291637, RRID: AB_477272, RRID: AB_90725, RRID: AB_310180, RRID: AB_725807, RRID: AB_2313606, RRID: AB_2534095, RRID: AB_2576217, RRID: AB_142924, RRID: AB_142540, RRID: AB_2313921

1 | INTRODUCTION

Wetness of the ocular surface is maintained by the tear film, a complex entity that is composed of a muco-aqueous fluid layer, isolated from air

Ignacio Alcalde, Almudena Íñigo-Portugués, and Omar González-González contributed equally to this study.

by a superficial lipid layer (Stern et al., 2004). Aqueous tear fluid is continuously produced by the lacrimal glands at a mean basal rate of ~2 $\mu L \cdot min^{-1}$ in humans (basal tearing) (Furukawa & Polse, 1978). Basal, continuous tear production is tonically modulated by peripheral sensory input from the eye surface (Lamberts et al., 1979; Robbins et al., 2012). Recent evidence suggests a prominent role for ocular cold thermoreceptors in the regulation of basal tear production. When activity of cold thermoreceptors is silenced in mice by genetic deletion of TRPM8, the ion channel conferring them cold sensitivity (McKemy et al., 2002; Peier et al., 2002), basal tear flow is markedly reduced (Parra et al., 2010). Likewise, warming the ocular surface in humans, which decreases cold thermoreceptor sensory input, reduces basal tearing while cooling increases tear secretion (Acosta et al., 2004; Parra et al., 2010). The majority of cold thermoreceptors innervating the ocular surface display a continuous ongoing firing at normal eye surface temperatures of 33–34°C, that is augmented or reduced by cooling or heating, respectively (Brock et al., 2001; Gallar et al., 1993; González-González et al., 2017). Together, these observations support the hypothesis that sensory inflow from cold thermoreceptors, which is increased by evaporation-induced cooling, modulates tear flow, and possibly also contributes to conscious dryness sensations of the eye surface (Belmonte & Gallar, 2011; Belmonte et al., 2015, 2017; González-González et al., 2017; Hirata & Oshinsky, 2012; Kovács et al., 2016).

Dry eye disease (DED) is a multifactorial disease defined by an inability to produce a tear film of volume and/or quality adequate to allow proper lubrication and protection of the corneal surface. It is accompanied by discomfort or pain, increased tear osmolarity, disturbed visual acuity, inflammation, and an elevated susceptibility to infection. DED is the most common ocular disease, affecting >5% of the world's population (Craig et al., 2017). Noteworthy, DED incidence increases sharply with age, reaching prevalence values of 25–30% in individuals over sixty (Craig et al., 2017).

At the eye surface, aging causes a variety of morphological and functional changes (Gipson, 2013), including a reduced mechanical sensitivity and a decrease in the number of subbasal axons and nerve terminals in the corneal epithelium (Acosta et al., 2006; Dvorscak & Marfurt, 2008). Accordingly, a relationship between age-dependent reduction of eye innervation and disturbed tear production has been repeatedly suggested (Acosta et al., 2006; Belmonte et al., 2015; Hirata & Meng, 2010; Hirata & Oshinsky, 2012; Meng & Kurose, 2013). Aging affects the structure and performance of peripheral sensory nerves in all tissues (Bergman & Ulfhake, 1998; Wang & Albers, 2009). Corneal nerves represent an ideal experimental model to study the aging process in sensory nerves due to their accessibility, ordered distribution, and well-established function. Furthermore, the noted dependence of basal tearing rate on cold thermoreceptor input in mice (Parra et al., 2010) opens the possibility that age-induced disturbances in this subpopulation of sensory fibers are linked to the sensory and tearing alterations observed in patients with DED.

In the present work, we used transgenic TRPM8^{BAC}-EYFP mice (Morenilla-Palao et al., 2014; Parra et al., 2010) in which TRPM8-expressing cold thermoreceptor neurons are intrinsically fluorescent, to investigate the effects of aging on the morphology and function of the cell bodies and sensory nerve terminals of this population of somatosensory neurons. We also determined whether the changes detected for cold thermoreceptor neurons are related with the changes in basal tearing flow that occur with aging.

2 | METHODS

2.1 | Experimental animals

Experiments were conducted in accordance with the ARVO Statement for the Use of Animals in Ophthalmic and Vision Research, the European Union Directive (2010/63/EU) and the Spanish regulations on the protection of animals used for research (RD 53/2013), and followed a protocol approved and supervised by the Ethics Committee of the Universities of Oviedo and Miguel Hernandez.

A total of 60 TRPM8^{BAC}-EYFP and 105 C57BL/6 mice of 3 months (3M) and 24 months (24M) of both sexes were used. Animals were housed conventionally in temperature- and humidity-controlled facilities with food and water available ad libitum.

2.2 | Immunohistochemistry

TRPM8^{BAC}-EYFP mice were anesthetized with a mixture of ketamine (80 mg/kg; Imalgène 500®, Merial; Toulouse, France) and xylazine (5 mg/kg; Rompun®, Bayer, Munich, Germany) and euthanized with an overdose of intraperitoneal sodium pentobarbital (Dolethal®, Vetoquinol, Lure, France). Eyes and trigeminal ganglia (TG) were carefully removed and processed, as detailed below.

2.2.1 | Whole-mounted corneas

ABC-peroxidase method

Eyeballs were fixed for 1 hr at room temperature (RT) in 4% paraformaldehyde and 0.2% picric acid in 0.1 M phosphate buffer saline (PBS, pH 7.4). Corneas were dissected and washed in PBS. To increase their permeability, corneas were incubated overnight at 37°C in 0.01% hyaluronidase type IV-S (Sigma-Aldrich, St. Louis, MO) and 0.1% ethylenediaminetetraacetic acid (EDTA; Sigma-Aldrich) (Marfurt et al., 2010) in 0.1 M acetate buffer (pH 6.0). Afterward, the corneas were rinsed in PBS containing 0.1% Triton X-100 (PBS-TX) and incubated for 2 hr in blocking solution containing 1% bovine serum albumin (BSA; Vector Laboratories, Burlingame, CA) and 10% normal goat serum (Vector Laboratories) in PBS-TX at RT. Corneas were then incubated overnight at 4°C with a rabbit polyclonal antibody against GFP (1:500; Molecular Probes, Eugene, OR). After rinsing with PBS-TX, corneas were incubated for 2 hr at RT with a goat anti-rabbit IgG biotinylated secondary antibody (1:200; Vector Laboratories). After again rinsing with PBS-TX, the corneas were incubated for 2 hr at RT in avidin-biotin-horseradish peroxidase complex (ABC reagent; Vector Laboratories). Corneas were washed with PBS-TX and incubated for 2 min at RT in 0.1% diaminobenzidine (Sigma-Aldrich) and 0.03% H_2O_2. After rinsing with PBS, the corneas were dehydrated in graded ethanol, cleared with xylol and mounted on slides with Entellan mounting medium (Merck Millipore, Darmstadt, Germany).

Immunofluorescence

Corneas were fixed for 2 hr at RT in methanol and DMSO (4:1), rehydrated, and washed in PBS. They were incubated for 1 hr in blocking solution containing 1% BSA (Vector Laboratories) and 10% normal goat serum (Vector Laboratories) in PBS-TX at RT. After rinsing with PBS-TX, corneas were incubated for 48 hr at 4°C with the primary antibodies diluted in PBS-TX. Rabbit anti-neuronal class III β-tubulin (1:500; Covance Research Products, Berkeley, CA) and chicken anti-GFP (1:500; Abcam, Cambridge, MA) were used. After rinsing with PBS-TX, corneas were incubated for 2 hr at RT with Alexa Fluor 594 goat anti-rabbit IgG and Alexa Fluor 488 goat anti-chicken IgG, respectively (1:500; Molecular Probes) in PBS, followed by incubation for 10 min at RT with 4′, 6-diamidino-2-phenylindole (DAPI; 2 μg/mL; Molecular Probes).

2.2.2 | Trigeminal ganglia

Deeply anesthetized mice, in which eyeballs were removed to use their corneas for whole mount immunostaining as described above, were perfused immediately afterward with physiological saline through the ascending aorta, followed by 15 min perfusion with 4% paraformaldehyde and 0.2% picric acid in PBS. TG were then removed and postfixed for 1 hr at RT in the same fixative, cryoprotected overnight at 4°C in 30% sucrose in PBS, embedded in OCT medium (Sakura Finetek, Torrance, CA) and rapidly frozen in liquid nitrogen. Blocks were stored at −80°C until used. TG were cut on a cryostat microtome in serial 7-μm thick sections and mounted on Superfrost Plus slides. Tissue sections were washed in PBS containing 0.03% Triton X-100 for 10 min and blocked for 1 hr in PBS containing 10% goat serum or donkey serum (depending on secondary antibodies used) at RT and incubated overnight at 4°C with primary antibodies diluted in blocking solution. The following rabbit polyclonal antibodies were used: anti-NF200 (1:1000, Sigma-Aldrich), anti-Peripherin (1:500, Millipore) and anti-TrkA (1:500, Millipore). In addition, goat polyclonal anti-CGRP (1:500, Abcam) was used. Sections were then washed with PBS and incubated for 2 hr at RT with goat anti-rabbit IgG or donkey anti-goat IgG secondary antibodies conjugated to Alexa Fluor 594 (1:500, Molecular Probes) in PBS. To detect IB4 staining, sections were incubated overnight with *Griffonia Simplicifolia* isolectin, (GS-IB_4 Alexa Fluor 594 conjugate, 1:500; Molecular Probes) in PBS at 4°C. Thereafter, sections were washed in PBS and incubated with DAPI for 10 min at RT. Finally, slides were coverslipped with fluorescence mounting medium (Dako, Glostrup, Denmark).

2.2.3 | Antibody characterization

Details of antibodies and dilutions are provided in Table 1. The anti-GFP (Molecular Probes, A11122, RRID: AB_221569) is a polyclonal antibody raised in rabbit against GFP isolated directly from the jellyfish *Aequorea Victoria* and is an IgG fraction purified by ion-exchange chromatography. The anti-GFP (Abcam, ab13970, RRID: AB_300798) is a polyclonal antibody raised in chicken using as munogen a recombinant full-length protein corresponding to GFP from *A. victoria* (UniProt number P42212). The anti-tubulin β III (Covance, PRB-435P, RRID: AB_291637) is a polyclonal rabbit IgG (clone Poly 18020) generated against the same epitope as recognized by TUJ1 using microtubules derived from rat brain as immunogen. The epitope is located within the last 15 *C*-terminal residues. It was subsequently purified on a peptide affinity column. This antibody is well characterized and highly reactive to neuron specific class III β-tubulin (βIII) but does not identify β-tubulin found in glial cells. Anti-NF200 (Sigma-Aldrich, N4142, RRID: AB 477272) is a polyclonal antibody produced in rabbit using as immunogen purified neurofilament 200 from bovine spinal cord. Whole antiserum is purified to provide an IgG fraction of antiserum. Anti-peripherin (Millipore, AB1530, RRID: AB_90725) is a polyclonal antibody produced in rabbit as purified serum using as immunogen electrophoretically pure trp-E-peripherin fusion protein, containing all but the 4 *N* terminal amino acids of rat peripherin. The antibody recognizes Peripherin (UniProt number P41219) and stains a ∼57 kDa band cleanly and specifically and does not stain vimentin, GFAP, alpha-internexin or any of the neurofilament subunits. Strong staining on rat, mouse, human, pig, and cow peripherin. Does not stain chicken, quail, or other more distantly related species which appear to lack peripherin. The anti-TrkA (Millipore, 06–574, RRID: AB_310180) is a purified polyclonal antibody (IGg) raised in rabbit immunized with bacterially expressed purified protein corresponding to the entire extracellular domain of rat TrkA receptor. Recognizes TrkA, Mr 140 kDa (UniProt number P04629). Does not cross-react with TrkB or TrkC. The anti-CGRP (Abcam, ab36001, RRID: AB_725807) is a polyclonal antibody produced in goat immunized with a synthetic peptide corresponding to rat CGRP (*C* terminal, VKDNFVPTNVGSEAF). The antibody reacts with whole molecule (1–37) and 23–37 fragment (*C* terminal).

The secondary antibody used for immunoperoxidase technique (Vector Laboratories, BA-1000, RRID: AB_2313606) is an affinity purified (chromatography), polyclonal biotynilated anti-rabbit IgG, made in goat following proprietary immunization schedules from the manufacturer. The antibody recognizes both heavy and light chains of rabbit IgG. The incubation solution contained secondary antibody to a 1:200 dilution. The following polyclonal secondary antibodies were all purchased from Molecular Probes and were used to a final dilution of 1:500. AF594-anti-rabbit (A11037, RRID: AB_2534095) is a secondary antibody raised in goat against heavy and light chains of rabbit Gamma immunoglobulins IgG and conjugated with the Alexa Fluor® 594 fluorescent dye (6 fluorophore molecules per IgG molecule with ideal excitation at 594 nm). AF488-anti-rabbit IgG (A11034, RRID: AB_2576217) is a secondary antibody raised in goat against heavy and light chains of chicken Gamma immunoglobulins IgG and conjugated with the Alexa Fluor® 488 fluorescent dye (6 fluorophore molecules per IgG molecule with ideal excitation at 488 nm). According to manufacturer's description, to minimize the cross-reactivity of goat anti-rabbit IgGs whole antibodies have been cross-adsorbed against bovine, goat, mouse, rat and human IgG. AF488-anti-Chicken IgY (A11039, RRID: AB_142924) is a secondary antibody raised in goat against heavy and light chains of chicken Gamma immunoglobulins IgY and conjugated with the Alexa Fluor® 488 fluorescent dye (7 fluorophore molecules per IgY molecule with ideal excitation at 488 nm). This goat anti-chicken IgY whole antibody has been purified by cross-adsorption through a column matrix containing immobilized serum proteins from potentially cross-reactive species.

TABLE 1 Antibodies and lectins used in this study

Name	Immunogen	Manufacturer; catalog number; RRID; host species; mono/polyclonal	Dilution
Primary antibodies			
Anti-GFP	The GFP was isolated directly from the jellyfish *A. victoria*	Molecular Probes; A11122; AB_221569; rabbit; polyclonal	1:500
Anti-GFP	Recombinant full-length protein corresponding to GFP from *A. victoria*	Abcam; ab13970; AB_300798; chicken; polyclonal	1:500
Anti-tubulin β III	Neuronal class III beta tubulin	Covance Research Products; PRB-435P; AB_291637; rabbit; polyclonal	1:500
Anti-NF200	Neurofilament 200 from bovine spinal cord	Sigma Aldrich; N4142; AB_477272; rabbit; polyclonal	1:1000
Anti-peripherin	Trp-E-peripherin fusion protein containing all but the 4 *N*-terminal amino acids of rat peripherin	Millipore; AB1530; AB_90725; rabbit; polyclonal	1:500
Anti-TrkA	Purified protein corresponding to the entire extracellular domain of rat TrkA receptor	Millipore; 06–574; AB_310180; rabbit; polyclonal	1:500
Anti-CGRP	Synthetic peptide corresponding to rat CGRP (*C*-terminal)	Abcam; ab36001; AB_725807; goat; polyclonal	1:500
Secondary antibodies			
Biotinylated anti-rabbit IgG	Gamma immunoglobulins heavy and light chains; IgG	Vector Laboratories; BA-1000; AB_2313606; goat; polyclonal	1:200
AF594-anti-rabbit	Gamma Immunoglobulins heavy and light chains; IgG	Molecular Probes; A11037; AB_2534095; goat; polyclonal	1:500
AF488-anti-rabbit	Gamma immunoglobulins heavy and light chains; IgG	Molecular Probes; A11034; AB_2576217; goat; polyclonal	1:500
AF488-anti-chicken	Gamma immunoglobulins heavy and light chains; IgY	Molecular probes; A11039; AB_142924; goat; polyclonal	1:500
AF594-anti-goat	Gamma immunoglobulins heavy and light chains; IgG	Molecular Probes; A11058; AB_142540; donkey; polyclonal	1:500
Lectin stain			
GS-IB_4	The GS-IB_4 was isolated from the seeds of the *G. simplicifolia*	Molecular Probes; I21413: AB_2313921	1:500

AF594-anti-goat (A11058, RRID: AB_142540) is a secondary antibody raised in donkey against heavy and light chains of goat gamma immunoglobulins IgG and conjugated with the Alexa Fluor® 594 fluorescent dye (4 fluorophore molecules per IgG molecule with ideal excitation at 594 nm).

Additionally, isolectin GS-IB_4 (Molecular Probes, I21413, RRID: AB_2313921) was isolated from the seeds of the *G. simplicifolia* legume conjugated with the Alexa Fluor® 594 fluorescent dye (6 fluorophore molecules per IgG molecule with ideal excitation at 594 nm). Subunit A binds preferentially to *N*-acetyl-*D*-galactosamine end groups while the B subunit is selective for terminal α-*D*-galactosyl residues. It was used at a final concentration of 1:500.

The antibody specificity was assured by performing a battery of control experiments consisting in: (a) incubation of the sections without secondary antibodies to check for unspecific background or autofluorescence from the tissue; (b) elimination of the primary antibodies to check for unspecific cross-reactivity of the antibodies with other immunoglobins in the tissue; (c) incubation with the peroxidase reveal system (ABC) only to assure the specificity of the DAB deposits; (d) immunostaining of positive control tissue sections (brain sections from C57BL/6n young mice and dorsal root ganglion sections from TRPM8-EYFP mice).

2.2.4 | Image acquisition

Bright field and fluorescence images were collected using a Leica DM 6000B microscope, equipped with a Leica CTR 6000 fluorescence filter set and a Leica DFC310 FX camera (Leica Microsystems, Germany) and with a Laser Scanning Spectral Confocal Microscope Olympus Fluoview FV1200 (Olympus Corp, Tokyo, Japan).

2.3 | Electrophysiological recording of cultured TG neurons

Primary cultures of TG obtained from $TRPM8^{BAC}$-EYFP mice (3M or 24M) were prepared following the procedure described elsewhere (Madrid et al., 2009). In brief, TG dissociated cells were plated on poly-

L-lysine-coated glass coverslips and cultured in Eagle's minimal essential medium (MEM) with Earle's BSS and *L*-glutamine plus 10% heat-inactivated fetal bovine serum, 1% vitamin solution and 100 μg/mL penicillin/streptomycin (all from Invitrogen). Cells were used after 12–36 hr in culture.

Coverslips were transferred to a 0.15 mL recording chamber (Warner Instrument Corporation, Hamden, CT) on the stage of an inverted microscope (Nikon Diaphot-TMD, Nikon Instruments, Tokyo, Japan) and superfused (1.5–3 $mL{\cdot}min^{-1}$) at basal temperature (32–34°C, maintained with a computer-controlled Peltier device, Embit, Modena, Italy) with physiological solution. Before each recording, light-transmitted and fluorescent images of each neuron were taken (filter cube for GFP: 41017_Nikon; Watec camera), and the fluorescence intensity of each recorded neuron was expressed as percent of the maximum value of fluorescence measured in the whole population, in non-saturating conditions. Cell membrane potentials were recorded using the perforated patch clamp technique. Pipettes of borosilicate glass (Harvard Apparatus, UK, 2–4 MΩ) were filled with a solution containing (in mM): 105 K gluconate, 50 KCl, 2 $CaCl_2$, 1 $MgCl_2$, 10 HEPES, and 0.2 mg/mL nystatin (pH 7.3 adjusted with NaOH; final Na^+ concentration ≈ 10 mM). Electrophysiological signals were recorded with an Axopatch 200B patch-clamp amplifier (Molecular Devices, CA). Stimulus delivery, data acquisition and analysis were performed using pClamp 9.2 software (Molecular Devices). Cooling ramps to 20–22°C (50 s duration) and extracellular *L*-menthol (100 μM) were used to study the functional characteristics of $TRPM8^+$ neurons.

2.4 | Extracellular recording of corneal nerve terminals

C57BL/6 mice aged 3M or 24M were killed by cervical dislocation and their corneas used for electrophysiological recordings of cold nerve terminals.

Extracellular recordings of single corneal nerve terminals in vitro were performed as described in previous studies (González-González et al., 2017; Parra et al., 2010). The eye ball and the attached optic nerve were dissected and fixed with a suction tube to the bottom of a recording chamber and were continuously perfused with a solution (~310 $mOsm{\cdot}L^{-1}$) of the following composition (in mM): 128 NaCl, 5 KCl, 1 NaH_2PO_4, 26 $NaHCO_3$, 2.4 $CaCl_2$, 1.3 $MgCl_2$, and 10 d-glucose. The solution was bubbled with carbogen gas (5% CO_2 and 95% O_2) and maintained at the desired temperature with a Peltier device. A borosilicate glass microelectrode (tip diameter ~50 μm) with an Ag/AgCl wire inside and filled with the extracellular solution was placed in contact with the cornea surface using a micromanipulator. Gentle suction was then applied to record nerve terminal impulse (NTI) activity. NTIs were amplified with an AC amplifier (Neurolog NL104, Digitimer, Welwyn, UK) and digitized at 10 KHz and stored in a computer using a CED micro 1401 interface and Spike 2 software (both from Cambridge Electronic Design, Cambridge, UK). Only recording sites where the NTI activity arose from a single nerve terminal were used for further analysis. At these sites, the NTIs were clearly distinguished from noise (~10 μV peak to peak) and identifiable by their similar waveform shape and firing pattern as arising from a single nerve terminal (Brock et al., 1998). To minimize the effects introduced by the deterioration of the preparation with time, the total duration of the experiment was restricted to a maximum of 5 h.

2.4.1 | Experimental protocol

The corneal surface was systematically explored with the microelectrode, from the center to the periphery, keeping the microelectrode in place at each location for 2 min to detect the possible occurrence during this time of at least one spontaneous NTI. The appearance of activity after application of the pipette onto the cornea was used to ascertain the successful location of a responsive sensory nerve terminal (González-González et al., 2017).

Cold thermoreceptor terminals were recognized either by the immediate detection of ongoing NTI activity at the control temperature of the bath (~34°C), which increased markedly in response to cooling, or by a NTI discharge in response to cooling, in terminals that had fired at least one NTI during the 2 min waiting period following application of the pipette to the cornea (González-González et al., 2017; see "Results" section). For cold stimulation, a cooling ramp was applied from the mean basal temperature of 34°C down to 12–13°C at a mean rate of $0.7 \pm 0.03°C{\cdot}s^{-1}$. Temperature was returned to basal values at the end of cold thermal stimuli at a similar rate.

Mechanical stimulation was performed by gentle (20 μm) forward displacement of the recording electrode against the ocular surface for 2 s. Chemical stimulation with *L*-menthol (20 μM) was carried out by shifting the perfusion from saline solution to saline solution plus the drug. A cooling ramp from 34°C was applied 2 min after the onset of perfusion with menthol, followed by a washing period of at least 5 min before testing other stimuli. Stimulation with a hyperosmolar solution was carried out by shifting the perfusion from the control solution to a 397 $mOsm.L^{-1}$ solution for 2 min followed by a 5 min washing period.

2.4.2 | Solutions

L-Menthol (Sigma-Aldrich) was prepared as a 20 mM stock solution in ethanol and diluted to a final concentration of 20 μM with saline solution. Hyperosmolar solutions were prepared by adding NaCl (3 M) to the physiological saline solution (310 ± 1.5 $mOsm{\cdot}L^{-1}$) until reaching the desired osmolarity value of 397 $mOsm{\cdot}L^{-1}$, measured with a freezing point osmometer (OSMOSTAT OM-6020, Kyoto Daiichi Kagaku, Kyoto, Japan).

2.5 | Tear flow and tear osmolarity measurements

Basal tear flow was measured in both eyes in 3M and 24M anesthetized $TRPM8^{BAC}$-EYFP and C57BL/6 mice ($n = 110$) using phenol red threads (Zone-Quick, Menicon Pharma S.A., Graffenstaden, France) gently placed between the lower lid and the bulbar conjunctiva at the nasal angle during 1 min (Parra et al., 2010). No differences in the tear flow measurements were observed between $TRPM8^{BAC}$-EYFP and C57BL/6 mice. Therefore, data from both strains were analyzed together.

Osmolarity of the tear fluid was measured in C57BL/6 mice of different ages, using the TearLab Osmolarity System (OcuSense Inc., San

Diego, CA). Tear fluid (50 nL) was collected from restrained, awake mice by gently placing the probe of the instrument into the meniscus formed at the nasal side of the inferior lid margin. Samples were obtained from both eyes in each mouse.

2.6 | Data analysis

2.6.1 | Morphological data

Whole-mounted corneas were divided into four quadrants. Epithelial innervation densities were determined in one central and two peripheral zones of each quadrant. The peripheral zones were defined as two 0.25 mm^2 square regions (a 500 × 500 μm box) whose peripheral borders were ~200 μm away from the limbus internal border. The two peripheral zones were separated 500 μm from each other. The central zone was defined as a 0.25 mm^2 region, 500 μm away from the peripheral boxes, that is, located at a distance of 1.2 mm from the limbus. Corneal nerve densities in the 0.25 mm^2 boxes were determined from microphotographs captured with a Leica DM6000B light microscope. Two independent images were obtained from each 0.25 mm^2 zone: one image was taken at the level of subbasal fibers, and the other at the level of the corneal epithelium layers, including the intraepithelial nerve terminals that derive from subbasal axons. Images were analyzed using the image analysis software FIJI (ImageJ 1.4, NIH, Bethesda, MD). Nerve density was calculated as the number of subbasal nerves or nerve terminals per mm^2. Subbasal nerves were quantified as the number of them intersecting a line drawn inside the square area. The total number of the intraepithelial nerve terminals was counted inside each square area, defining the type of nerve terminal (simple, ramified, or complex) (Ivanusic et al., 2013). No differences in the number of subbasal nerves and nerve terminals per mm^2 were observed between peripheral and central zones both in 3M and 24M mice. Therefore, values from both areas were averaged. Penetration sites of subepithelial bundles through the basal lamina were counted throughout the total area of the cornea and expressed as penetrations per mm^2.

Counts of TG neurons were performed on reconstructions of the ganglion made by tiling each image of the serial TG sections under the fluorescence microscope using a 20× objective magnification, a motorized slide holder, and the Tile Scan module of the Leica AF6000 software, so that the entire extension of the ganglion was scanned and imaged. For the quantitation of the number of $TRPM8^{BAC}$-EYFP neurons in the TG, the FIJI software was used. Only neurons with a visible nucleus were counted. Neurons exhibiting a fluorescence intensity between cero and 90 arbitrary units on a 256-channel gray scale were considered weak fluorescent neurons. To avoid overestimation of the number of TG neurons, images of one in every nine microtome sections (that is, one image in every 63 microns) were analyzed. A minimum of three TG of each group were used.

2.6.2 | Analysis of NTI activity

In computer-stored recordings of NTI activity of corneal nerve terminals, the following parameters were analyzed off-line:

- Background activity: Mean basal ongoing frequency in impulses per second (imp·s^{-1}) at 34°C, measured during the 30 s preceding the onset of a cooling ramp.
- Cooling threshold: Temperature (°C) during a cooling ramp at which NTI frequency increased to a value that was the mean NTI frequency measured during the 10-s period preceding the onset of a cooling ramp plus 3 times its standard deviation.
- Cooling response: The increase in firing rate (imp·s^{-1}), measured between the cooling threshold and the peak frequency value reached during a cooling ramp.

2.7 | Statistical analysis

Data were analyzed using SigmaStat v3.5 (Systat Software, Point Richmond, CA). Statistical significance was determined by Mann–Whitney *U* test or *Z* test for morphological and tearing studies; *t*-test or one-way ANOVA followed by Bonferroni or Dunn's post hoc test for analysis of data of electrophysiological recording of cultured TG neurons; *t* test or Mann–Whitney test for analysis of data of extracellular electrophysiological recordings. $^{*}p < .05$, $^{**}p < .01$, $^{***}p < .001$.

3 | RESULTS

3.1 | $TRPM8\text{-}EYFP^{+}$ TG neurons exhibit different fluorescence levels

Microscopic inspection of EYFP fluorescence in TG cell bodies and corneal nerve fibers of $TRPM8^{BAC}$-EYFP mice ($EYFP^{+}$ mice) evidenced clear differences in fluorescence intensity both between individual somas and peripheral axons (Figure 1).

3.1.1 | Cell body

17.8 ± 0.9% of the neurons counted (2268.4 ± 266.5 neurons per ganglion, $n = 3$) in TG tissue sections of 3M $EYFP^{+}$ mice displayed fluorescence (Figure 1a). In 56.3 ± 1.3% of them, fluorescence intensity was high (>90 arbitrary units on a 256-channel gray scale) being thus called intensely fluorescent (IF) neurons. The majority of these neurons were peripherin positive and CGRP negative (Table 2). The remaining $EYFP^{+}$ neurons (43.7 ± 1.3%) showed a weaker fluorescence intensity (≤90 arbitrary units on the 256-channel gray scale) and were named weakly fluorescent (WF) neurons (Figure 1a); almost half of them were immunoreactive to CGRP (Table 2). Both IF and WF neurons were IB4 negative (data not shown). Immunoreactivity to other neuronal markers (neurofilaments, TrkA) differed between IF and WF neurons (Table 2). In TG cultures, the two populations of IF and WF neurons were also clearly differentiated (see below).

3.1.2 | Peripheral axons

Corneal $EYFP^{+}$ axons were easily recognized within stromal nerve trunks and their extensively ramified, ascending intraepithelial branches, by their YFP immunofluorescence (Figure 1b–e), and specific immunoperoxidase staining (Figure 2).

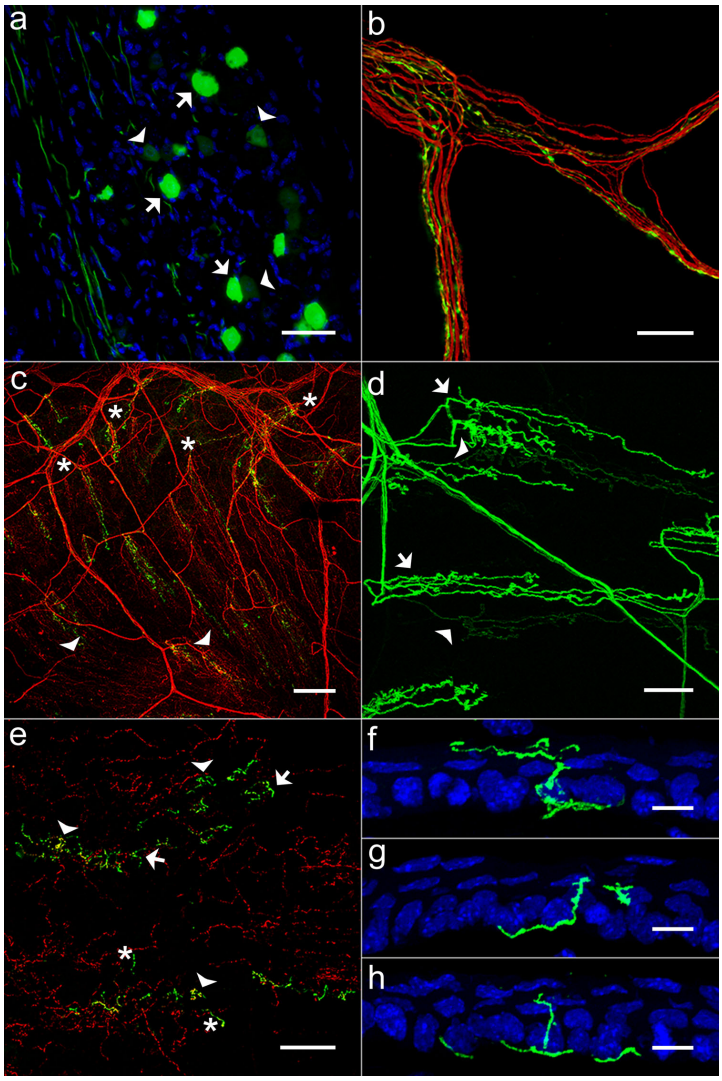

FIGURE 1 Immunostaining of TG neurons and peripheral corneal nerve branches of 3M TRPM8^{BAC}-EYFP mice. (a) Fluorescence in IF (arrows) and WF (arrowheads) TG neurons. (b) Stromal nerve bundle containing EYFP$^+$ green axons mixed with non-EYFP$^+$ anti-β III tubulin red axons. (c) Low-magnification image showing penetrations through the basal lamina of ascending peripheral (asterisks) and central (arrowheads) nerve branches. (d) EYFP$^+$ nerve fibers displaying intense (arrows) and weak (arrowheads) fluorescense. (e) TRPM8$^+$ intraepithelial, complex (arrowheads), ramifying (arrows), and simple (asterisk) terminal branches. (f–h) Corneal cross sections showing the ascending trajectory within the corneal epithelium layers of presumed complex (f), ramified (g) and simple (h) immunofluorescent terminal axons. Epithelium cell nuclei are counterstained with DAPI. Scale bars: a and b, 50 μm; c, 150 μm; d and e, 75 μm; f–h, 10 μm

Corneal EYFP$^+$ axons of the subbasal plexus were morphologically heterogeneous. About half of them were IF, thick axons and showed beads along their length. The other half appeared as less intense fluorescent (WF), thinner, smooth axons (Figures 1d and 2a). Overall mean density of subbasal EYFP$^+$ fibers was 22.4% of the total number of corneal sensory fibers running in

TABLE 2 Molecular phenotype of TRPM8-EYFP+ TG neurons in young and aged mice

	% IF-EYFP-TRPM8 neurons		% WF-EYFP-TRPM8 neurons	
	3-month-old mice	24-month-old mice	3-month-old mice	24-month-old mice
Peripherin-IR	7.7 ± 0.5 (79.2 ± 4.1)	7.6 ± 1.0 (74.6 ± 4.9)	4.1 ± 0.6 (53.4 ± 4.9)	7.9 ± 0.4** (56.0 ± 5.0)
NF200-IR	1.3 ± 0.1 (12.1 ± 1.3)	2.8 ± 0.6** (22.5 ± 2.4)	1.6 ± 0.4 (20.2 ± 3.0)	2.7 ± 0.3 (17.1 ± 2.5)
TrkA-IR	1.3 ± 0.3 (13.8 ± 2.4)	1.6 ± 0.5 (16.4 ± 3.8)	3.9 ± 0.7 (48.7 ± 5.7)	5.2 ± 0.6* (61.2 ± 2.4)
CGRP-IR	0 ± 0 (0 ± 0)	0 ± 0 (0 ± 0)	3.6 ± 1.2 (44.1 ± 11.4)	4.2 ± 0.4* (43.9 ± 2.3)

Note. Data of IF and WF neurons are expressed as percentage of total number of neurons counted in the TG and compared as a function of age using the *z* test. $^{*}p < .05$; $^{**}p < .01$. The data in parenthesis give the proportion of IF and WF TRPM8-EYFP^{+} neurons, expressed as percentage of the total number of TRPM8-EYFP^{+} TG neurons.

the leashes (Figure 1c). The ascending terminal branches from the leashes end superficially as intraepithelial endings (Figures 1e–h and 2b). Mean density of intraepithelial endings of 3M mice was 527.8 ± 23.2 endings/mm^2 ($n = 3$); 29.6% of this total were EYFP^{+} endings of variable morphological complexity (Ivanusic et al., 2013). A majority (51.1 ± 2.1%) of the IF ascending branches formed "complex" endings; a smaller proportion (20.3 ± 2.8%) produced "ramifying" nerve endings or terminate as "simple" nerve endings (28.6 ± 0.6%). In contrast, WF axons branched less in the subbasal plexus and formed simple (57.9 ± 0.9%) or ramifying (31.7 ± 1.8%) ending types; only 10.4 ± 2.7% of them produced complex nerve endings.

3.2 | Fluorescence intensity in TRPM8-EYFP^{+} neurons correlates with their cold sensitivity

3.2.1 | Cell body

To evaluate the possible correlation between fluorescent intensity in EYFP^{+} TG neurons and their TRPM8 expression levels, we analyzed the relationship between somatic fluorescence intensity and electrophysiological responses to cold and menthol in TG cultured neurons of 3M mice. We recorded changes in membrane potential (E_m) to cooling ramps and during application of menthol (100 μM) in the two groups of EYFP^{+} neurons (Figure 3a,b): IF neurons (mean fluorescence = 64.3 ± 5.6% of maximum), WF neurons (mean fluorescence = 6.3 ± 1.0% of maximum), and in NonF neurons (no fluorescence).

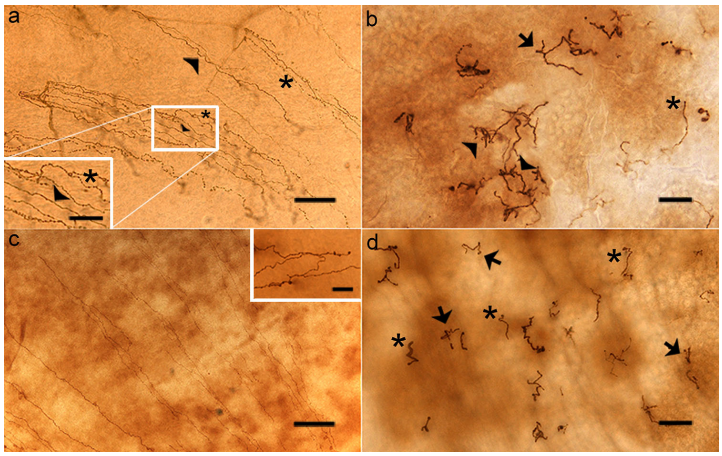

FIGURE 2 Anti-GFP immunostaining of corneal nerve fibers in the periphery of whole-mounted corneas of 3M and 24M old mice. (a and b) 3M mouse. (a) Subbasal EYFP^{+} longer, beaded (asterisks) and smooth, shorter (arrowheads) axons. Inset: Higher magnification the dashed area. (b) Intraepithelial, terminal branches forming complex (arrowhead), ramifying (arrows) and simple (asterisks) endings. (c and d) 24M mouse. (c) EYFP^{+} subbasal axons, some ending abruptly forming "collapsed axons" (inset). (d) Intraepithelial terminal branches generally form ramifying (arrows) or simple endings (asterisks). Scale bars: a, 100 μm, inset, 50 μm; b and d, 20 μm; c, 100 μm, inset 20 μm

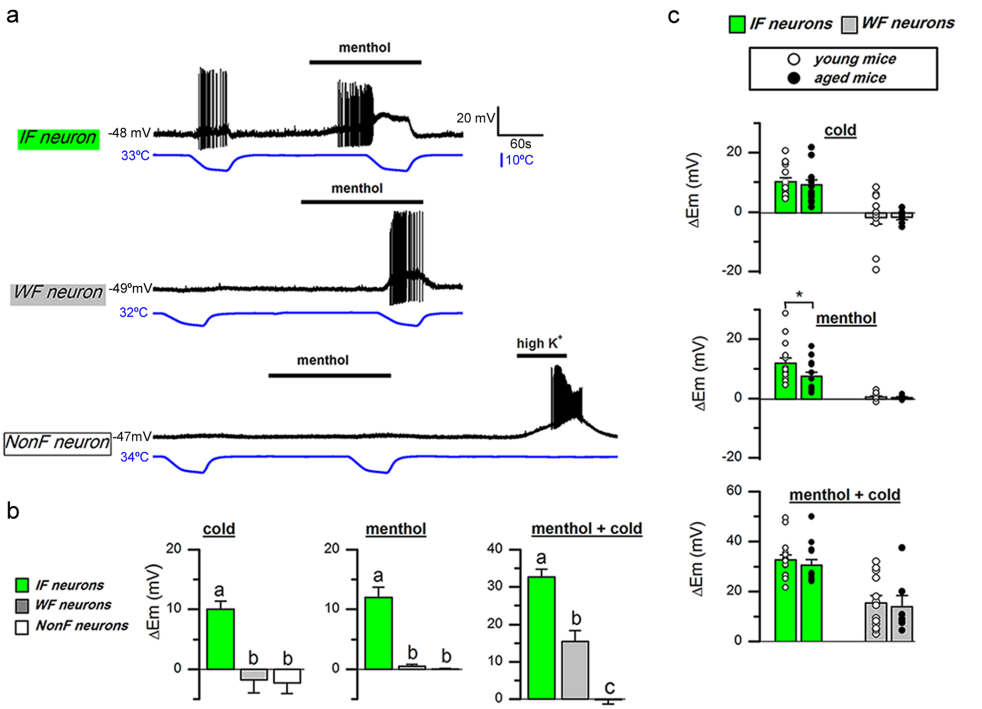

FIGURE 3 Correlation between fluorescence intensity of cultured TRPM8-EYFP$^+$ TG neurons and cold and menthol sensitivity. (a) Sample recordings obtained from typical TG neurons of 3M mice presenting IF, WF and NonF neurons. Membrane potential (E_m) trace is represented in black and bath temperature in blue. Horizontal black bars mark perfusion with 100 μM menthol and 37.5 mM K^+, respectively. (b) Average changes in E_m elicited by a cold ramp, menthol, and menthol plus a cold ramp in the three classes of neurons. Data are mean ± *SEM* of IF ($n = 15$), WF ($n = 13$) and NonF ($n = 12$) neurons. One-way ANOVA ($p < .001$ in all cases) with Bonferroni or Dunn's post hoc test ($p < .001$ for cold stimulus; $p < .05$ for menthol and menthol + cold stimuli). (c) Average (bars) and individual (circles) changes in E_m elicited by cold ramps, menthol and menthol plus cold in IF and WF neurons from 3M (○), and 24M (●) mice. *$p = .05$ by *t* test

IF neurons were depolarized by cold and menthol ($\Delta E_m = 10.0 \pm 1.4$ mV and 12.0 ± 1.7 mV, respectively, $n = 15$). In addition, their responses to cooling were strongly potentiated by menthol ($\Delta E_m = 32.7 \pm 2.0$ mV). In WF neurons ($n = 13$), the effects of cold or menthol on E_m, when applied separately, were weak or negligible, although all neurons were depolarized by simultaneous application of both stimuli, leading to action potential firing in a few of them (4/13, Figure 3a). Finally, none of the NonF neurons ($n = 12$) showed E_m changes during application of cold or menthol; their functional integrity was proved by the strong depolarization evoked by high K^+ exposure ($\Delta E_m = 25.7 \pm 1.9$ mV; $n = 12$). There were no significant differences between the three classes of neurons recorded regarding values of resting E_m (IF = −57.3 ± 2.2 mV; WF = −56.0 ± 2.7 mV; NonF = −53.6 ± 2.5 mV; $p = .571$, one-way ANOVA), or membrane capacitance (IF = 11.8 ± 1.3 pF; WF = 14.4 ± 1.7 pF; NonF = 14.7 ± 1.5 pF; $p = .340$, one-way ANOVA). In sharp contrast with the typical ongoing firing of most peripheral corneal cold nerve terminals, only one of the IF cold-sensitive neurons exhibited spontaneous discharge at 33°C. Altogether, these results indicate (Figure 3b) that IF neurons are more sensitive to TRPM8 agonists (cold and menthol) than WF neurons, suggesting their differential TRPM8 expression levels. Figure 3c presents the electrophysiological parameters of fluorescent neurons in young mice, to allow their comparison with those of old animals, as discussed below.

3.2.2 | Peripheral terminals

The presence of two-functional subpopulations of cold thermoreceptors with different sensitivity to cooling (González-González et al., 2017) was confirmed in 18 corneas of 3M C57BL/6 mice. In 5.7 ± 1.6% of all recording attempts, terminals exhibiting a robust ongoing repetitive activity (more than 2 imp·s^{-1}) at the holding temperature of 34°C were identified. These endings also gave a vigorous response to cooling ramps, firing readily during temperature decreases (Figure 4a). Menthol (20 μM) and hyperosmolar solutions (397 mOsm·L^{-1})

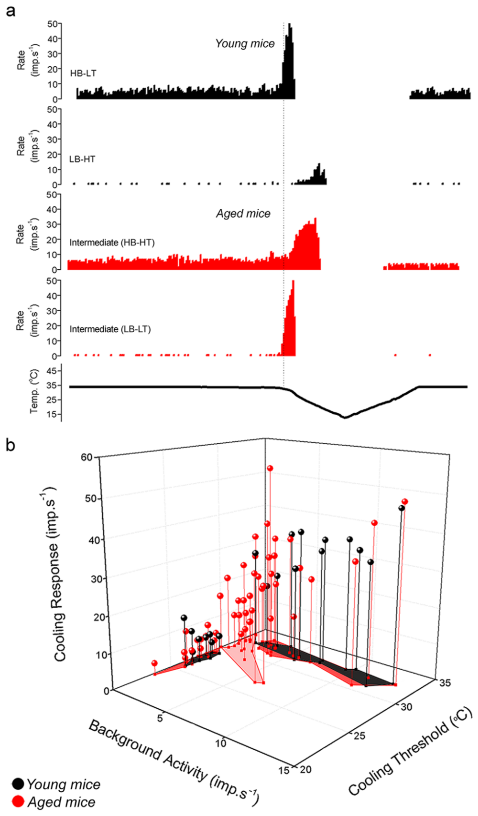

FIGURE 4 Aging effects on NTI activity of corneal cold-sensitive terminals. (a) Examples of the NTI discharge and the response to a cooling ramp from 34 to 15°C (lowest trace) recorded in the different classes of cold-sensitive terminals. Traces of high background, low threshold (HB-LT) and low background, high threshold (LB-HT) NTI activity were obtained from 3M mice. Those from terminals exhibiting intermediate properties (high background, high threshold, HB-HT and low background, low threshold, LB-LT; in red) were obtained from 24M mice. (b) Plot of individual cold-sensitive endings attending to background activity at 34°C, firing response to cooling and cooling threshold in °C. Data from 3M mice (black) and from 24M mice (red) are projected onto the horizontal plane as black or red-filled areas, separating the intermediate fibers of the last group (light red) to highlight their differences with HB-LT and LB-HT terminals

increased significantly their spontaneous activity and peak firing response to cooling ramps. Accordingly, these endings were classified as high-background, low-threshold (HB-LT) cold thermoreceptors.

In 2.6 ± 1.2% of the recording attempts, low-background, high-threshold (LB-HT) cold thermoreceptor terminals were also identified. These endings exhibited a very low mean firing frequency at 34°C and responded to cooling ramps with a relatively modest increase in firing frequency, starting at a mean threshold temperature 4–5°C below the value seen in HB-LT cold receptor terminals (Figure 4a). Menthol (20 μM) and perfusion with 397 mOsm·L^{-1} solution augmented their spontaneous activity and reduced their threshold, also increasing the maximum firing response to cooling ramps. Table 4 summarizes the firing characteristics of HB-LT and LB-HT cold thermoreceptor endings in young mice.

3.3 | The number and molecular phenotype of TRPM8-EYFP$^+$ TG neurons and the architecture and density of corneal axonal branches change with age

3.3.1 | Cell body

In aged, 24M mice, 21.6 ± 1.1% of the TG neurons (2723.0 ± 263.8 neurons per ganglion, $n = 3$) were EYFP$^+$, a proportion significantly larger than in young animals ($p = .002$, z test). This increase was accompanied by a higher percentage of WF neurons (10.7 ± 0.9% in 24M mice vs. 7.8 ± 0.4 in 3M mice, $p < .001$, z test). The proportion of WF neurons expressing peripherin, TrkA, and CGRP also increased significantly with age (Table 2).

3.3.2 | Peripheral axons

In 24M mice, the number and architecture of corneal sensory nerves including the subpopulation of EYFP$^+$ fibers appeared strikingly modified in comparison with younger animals (Figure 2 and Table 3). In this age group, the density of penetration points into the lamina basal containing EYFP axons was significantly higher than in young animals (49.6% increase, $p = .019$, Table 3). This was due to a higher number of penetration points at the periphery in old mice (15.3 ± 1.5 penetrations/mm^2 vs. 8.6 ± 0.6 penetrations/mm^2, in 24M and 3M mice, respectively, $p = .004$), while in the center of the cornea differences in penetration points density with age were not significant.

Notably, in 24M mice, nearly all (95.1 ± 2.9%) TRPM8-EYFP$^+$ axons were nonbeaded (smooth), faintly fluorescent, and remarkably long and thin (compare Figure 2a,c), often reaching the center of the cornea, in sharp contrast with young animals (average length of the subbasal axons: 304.9 ± 14.0 μm vs. 227.6 ± 11.6 μm, $p = .002$, t test). On the other hand, the density of EYFP$^+$ subbasal axons of 24M mice was significantly lower (27.7%) than in 3M mice ($p < .001$; Table 3). Also, they were distributed differently within the leashes, with more leashes containing EYFP$^+$ axons in aged mice albeit with a lower mean number of fluorescent axons per leash.

The total density of EYFP$^+$ terminals in 24M mice was 35.6% lower than in 3M mice ($p < .001$). In addition, the proportion of the different morphological subtypes of EYFP$^+$ intraepithelial nerve endings was markedly altered for complex endings in aged mice; there, 59.7 ± 0.7% of terminals had simple endings (3M: 43.4 ± 1.7, p = n.s., Mann–Whitney U test), 25.6 ± 1.2% had ramifying endings (3M: 26.0 ± 1.7%, p = n.s., z test), and only 2.6 ± 0.7% had complex endings (3M: 30.6 ± 1.7, $p < .001$, z test) (compare Figure 2b,d). Moreover, 12.1 ± 2.6% of the subbasal EYFP$^+$ axons ended abruptly within the subbasal plane without emitting any branches that ascend to terminate more

TABLE 3 Morphological characteristics of TRPM8-EYFP$^+$ axons and epithelial nerve endings innervating the cornea of mice at different ages

Morphometric parameter	3-month-old mice	24-month-old mice
Penetration of subepithelial bundles (number/mm^2)	11.5 ± 0.5 *n* = 5	17.2 ± 1.2*** *n* = 5
% beaded subbasal nerve axons	50.1 ± 6.5 *n* = 3	4.9 ± 2.9*** *n* = 4
% smooth subbasal nerve axons	49.9 ± 6.5 *n* = 3	95.1 ± 2.9*** *n* = 4
Density of subbasal axons (number/mm^2)	126.4 ± 5.9 *n* = 7	91.6 ± 4.2*** *n* = 10
Number of axons per leash	5.2 ± 0.3 *n* = 3	2.6 ± 0.2*** *n* = 4
Density of terminal branches (number/mm^2)	156.2 ± 8.0 *n* = 7	111.2 ± 5.6*** *n* = 10

Note. Comparisons of measures performed in 24-month-old mice were made against the values obtained in 3-month-old mice. Mann–Whitney *U* test was used except for the data of percentage of beaded and smooth subbasal axons, which were analyzed using a *z* test. ***$p < .001$, *n* = number of mice.

superficially in the epithelium. We called such terminations, "collapsed axons" (see Figure 2c, inset) and were not found in young animals ($p = .009$, *z* test).

3.4 | Aging modifies the electrophysiological responses of peripheral cold-sensitive endings but not of TG TRPM8-EYFP$^+$ neurons

Next, we analyzed the functional changes developed with aging by TG EYFP$^+$ neurons and their cold-sensitive nerve terminals.

3.4.1 | Cell body

Cultured TG EYFP$^+$ neurons of 24M mice were also divided into IF and WF neurons. Even though they were not counted, WF neurons were clearly more abundant in these cultures compared with those from young animals. As in young mice, IF neurons were more sensitive to TRPM8 agonists than WF neurons (Figure 3c). ΔE_m observed in IF versus WF neurons during exposure to cold, menthol, and menthol plus cold were 9.1 ± 1.6 versus −1.7 ± 0.8 mV; 7.5 ± 1.4 versus 0.3 ± 0.3 mV; and 30.6 ± 2.1 versus 14.0 ± 4.3 mV, respectively. Moreover, the amplitudes of membrane depolarizations induced by cold exposure alone or in the presence of menthol were similar to those of young mice (see Figure 3c) for both neuronal types, IF and WF. Only in the group of the IF neurons of aged mice, the amplitude of the menthol-evoked depolarization was slightly lower than in IF neurons of young animals ($\Delta E_m = 7.5 \pm 1.4$ mV vs. 12.0 ± 1.7 mV; $p = .05$, *t* test). Resting membrane potential at 33°C, membrane capacitance and fluorescence intensity of the recorded IF and WF neurons in aged animals did not differ from those reported in the same neuronal types of young mice. ($E_m = -53.7 \pm 2.7$ and −56.7 ± 2.3 mV; $C_m = 12.7 \pm 1.4$ and 17.9 ± 3.1 pF, and mean fluorescence = 60.3 ± 5.1% and 8.8 ± 2.5% for IF and WF neurons, respectively).

3.4.2 | Peripheral terminals

In 24M mice corneas, terminals displaying an ongoing activity >2 imp·s^{-1} at 34°C, characteristic of HB-LT cold terminals of young

TABLE 4 Functional characteristics of corneal cold-sensitive nerve endings

Cold terminal type		Background activity (imp·s^{-1})	Cooling threshold (°C)	Cooling response (imp·s^{-1})	Successrate (%)
3-month-old mice	HB-LT	6.8 ± 1.1 (*n* = 12)	32.5 ± 0.2 (*n* = 12)	33 ± 2.2 (*n* = 12)	5.7
	LB-HT	0.5 ± 0.1 (*n* = 8)	28.1 ± 0.5 (*n* = 8)	6.6 ± 1.3 (*n* = 8)	2.6
24-month-old mice	HB-LT	4.7 ± 0.8 (*n* = 20)	32 ± 0.2 (*n* = 20)	24.6 ± 2.3 (*n* = 20)	4.6
	HB-HT	5.3 ± 1.2 (*n* = 3)	27.7 ± 0.8 (*n* = 3)	28.2 ± 1.0 (*n* = 3)	0.6
	LB-HT	0.6 ± 0.1 (*n* = 17)	27.1 ± 0.5 (*n* = 17)	6.3 ± 1.2 (*n* = 17)	4.0
	LB-LT	0.5 ± 0.1 (*n* = 11)	32.1 ± 0.3 (*n* = 11)	13 ± 2.6 (*n* = 11)	1.8

Note. Success rate percentage indicates the percentage of successful attempts of recording a terminal from each group referred to the total number of attempts. HB, high-background activity; HT, high threshold; LB, low-background activity; LT, low-threshold; *n* = number of endings.

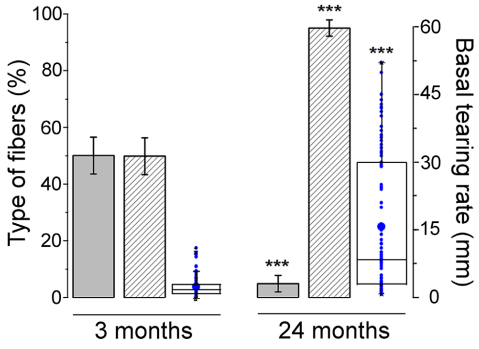

FIGURE 5 Change of basal tearing rate and TRPM8-EYFP^{+} subbasal nerve fiber density with aging. Bars represent the percentage of IF fibers (gray) and WF (stripped) in 3M and 24M mice (***$p < .001$, *t* test). In the same age groups, individual values of basal tearing measured in mm of wet phenol red thread (small blue dots) and their mean value (large blue dot), median (horizontal line), 25th and 75th percentiles (white box limits), and 1st and 99th percentiles (×) are also represented (***$p < .001$, Mann–Whitney *U* test)

animals were found in 5.1 ± 1.1% of the total recording attempts. As shown in Table 4, most of these terminals had a cooling threshold similar to HB-LT terminals of young animals, although they showed on the average lower mean values of background NTI frequency and weaker firing responses to cooling pulses. They also responded to 20 μM menthol and to 397 mOsm·L^{-1} solutions with a rise in background frequency and an enhancement of the maximum NTI firing response to cooling ramps. In aged mice, we also frequently encountered (5.8% of recording sites) corneal cold terminals with very low-background activity and a weak response to cold that resembled the LB-HT units found in young animals (Table 4). Noteworthy, in 24M mice, we detected a small fraction of the spontaneously firing cold-sensitive terminals had distinctly higher thresholds for activation during cooling (HB-HT terminals in Figure 4 and Table 4). Moreover, in 24M mice, a large proportion of the terminals with very low-basal activity at 34°C exhibited a remarkable sensitivity to cold, showing cold threshold values within the range observed in the canonical HB-LT cold thermoreceptor endings, although their impulse response to cooling ramps was significantly weaker (LB-LT cold terminals of Figure 4 and Table 4). Another notable observation made in aged mice was that the probability of detecting cold-sensitive terminals either with high or low background activity at 34°C was overall higher in comparison with young mice (Table 4).

In Figure 4b, we plotted all units recorded in young and old mice according to the values of the three parameters used for their functional characterization. This representation highlights the appearance in old mice of new, functionally distinct endings (drawn in light red in the horizontal plane) exhibiting a mixture of the firing characteristics of the two classes of cold-sensitive fibers typical of younger animals.

3.5 | Aging alters tear's basal flow and osmolarity

Mean basal tearing flow in anesthetized 3M TRPM8^{BAC}-EYFP and C57BL/6 mice was 2.4 ± 0.2 mm ($n = 66$). In 24M mice, tearing rate values were more variable and significantly higher than in young animals (15.7 ± 1.6 mm, $n = 44$; $p < .001$, *t* test) (Figure 5). Notably, the values of basal tearing flow augmented in parallel with the higher proportion of WF fibers, suggesting that basal tearing rate increased in parallel with the increase of WF and the decrease of IF corneal nerve fibers observed with aging (Figure 5). Finally, we measured mean tear osmolarity in 24M, awake mice obtaining a mean value of 354.0 ± 2.8 mOsm·L^{-1}, $n = 22$). This value was significantly higher than in young adult awake mice (346.3 ± 2.4 mOsm·L^{-1}, $n = 19$, $p = .008$, Mann–Whitney *U* test).

4 | DISCUSSION

We quantified EYFP-labeled, TRPM8-expressing TG neurons and axons in the mouse cornea, in combination with electrophysiological recordings and measures of tearing to follow their alterations with age. To our knowledge, this is the first description of aging related alterations in the morphology and function of cold thermoreceptor endings of any species.

4.1 | Cold-sensitive neurons and corneal nerve endings are morphologically and functionally heterogeneous

TRPM8 channels are the main molecular transducers for cold temperature sensing in mammalian thermoreceptors (Knowlton et al., 2013; McKemy et al., 2002; Peier et al., 2002). Previous studies reported marked differences in menthol sensitivity and cold threshold of individual TG and DRG neurons (Babes et al., 2004; Viana et al., 2002), which were directly associated to the amplitude of their cold-evoked TRPM8 currents (Madrid et al., 2009).

Here, we found that somatic fluorescence intensity in TRPM8-EYFP TG neurons of young adult mice correlated with the amplitude of cold- and menthol-evoked depolarizations, strongly suggesting that TRPM8 channel density is one determinant of cold sensitivity (de la Peña et al., 2005; Madrid et al., 2009; Morenilla-Palao et al., 2014; Xing et al., 2006). Other factors influencing cold sensitivity, including the variable expression of different potassium channels, were not explored in the present study (Madrid et al., 2006, 2009; Morenilla-Palao et al., 2014; Viana et al., 2002). We also found differences in EYFP fluorescence intensity and cold sensitivity among TRPM8^{+} peripheral sensory axons of the cornea, suggesting that their functional differences are linked to TRPM8 expression as well. Small and medium-size, nonpeptidergic IF-EYFP TG neurons are the likely origin of the strongly fluorescent, beaded axons which terminate in the corneal epithelium predominantly as CGRP-negative, complex nerve endings (Alamri et al., 2015; Ivanusic et al., 2013). The remarkable high-thermal sensitivity to cold of IF-EYFP neurons are expected considering their high density of TRPM8 channels and low-Kv1 expression (Madrid

et al., 2009). Furthermore, TRPM8 likely contributes to the ongoing activity of corneal cold thermoreceptors (Parra et al., 2010). Together, these findings suggest a high expression of TRPM8 in the strongly fluorescent, beaded axons; their predominately complex endings are possibly a biophysical reason for their characteristic spontaneous firing, low threshold and vigorous response to cooling typical of HB-LT cold thermoreceptors (Carr et al., 2009; González-González et al., 2017; Madrid et al., 2009; Olivares et al., 2015; Parra et al., 2010; Teichert et al., 2012).

WF neurons represent a second population of TRPM8-expressing TG neurons and are presumably the origin of corneal TRPM8-EYFP axons characterized by fainter fluorescence, smooth surface and thin diameter, terminating as simple or ramifying endings. In all likelihood, they correspond to the LB-HT corneal cold thermoreceptors (González-González et al., 2017). WF-TRPM8^{+} neurons are TrkA and CGRP positive, a phenotype observed in peptidergic polymodal nociceptors of other tissues (Abe et al., 2005; Knowlton et al., 2013; Takashima et al., 2007). It is worth noting that genetic deletion of TRPM8 channels or conditioned ablation of TRPM8-expressing neurons reduces markedly behavioral responses to innocuous but also to noxious cold, supporting the view that a part of the peripheral neurons expressing TRPM8 are connected to pain-labeled lines (Palkar et al., 2015). According to this interpretation, TRPM8^{+} TG neurons are the origin of labeled sensory lines both for sensing innocuous ocular surface cooling chiefly involved in basal tearing regulation (HB-LT cold thermoreceptors) and for sensing of potentially injuring dryness, evoking discomfort, reflex tearing and blink responses (LB-HT cold thermoreceptors) (Belmonte et al., 2015, 2017; Kovács et al., 2016; Parra et al., 2010; Quallo et al., 2015).

4.2 | Morphological and functional changes in TRPM8-expressing neurons and corneal endings with age

In spite of the quantitative differences in human life span, survival curves in mice resemble notably those seen in humans (Comfort, 1964). Indeed, mice have been used extensively to study the biological effects of aging (Wang & Albers, 2009). This justifies the use of TRPM8^{BAC}-EYFP transgenic mice to analyze the morphological and functional changes in the ocular surface innervation produced by aging.

Earlier morphological studies on age-induced variations in corneal innervation yielded conflicting results. In humans, nerve density measured in vivo (Parissi et al., 2013) or in stained corneas (He et al., 2010) decreases with age. Notably, in rats, density of subbasal corneal nerve fibers apparently rises with aging but is accompanied by a simultaneous, progressive decline of epithelial nerve endings (Dvorscak & Marfurt, 2008). In mice, where subbasal corneal nerve density varies hugely among different strains, an overall reduction was reported in old animals (Reichard et al., 2016).

In our study, the number of TG neurons in old mice was not significantly different from younger animals suggesting that aging has a more pronounced effect on the architecture and density of peripheral sensory nerve terminal axons than on cell bodies. Nonetheless, the percentage of TRPM8^{+} neurons was larger, an increment that occurred mainly in the subpopulation of WF-EYFP TG neurons expressing peripherin, TrkA, and CGRP, a polymodal nociceptor immunoreactive phenotype, whereas the population of canonical low-threshold cold thermoreceptor neurons, represented by low-threshold, IF-EYFP neurons, with strongly fluorescent beaded corneal axons, remained relatively stable. Electrophysiologically, cell bodies of both IF- and WF-TRPM8^{+} neurons of 24-month-old mice maintained the correspondence between amplitude of cold-induced depolarization and somatic fluorescence intensity seen in young animals. Moreover, they exhibit responses to cooling and menthol very similar to those shown by the corresponding neuron types of young mice, with the sole difference of a weaker response of old IF neurons to menthol. The change in the proportion of neurons with different fluorescence intensity may reflect a phenotypic change in the expression of TRPM8 by TG neurons, in parallel or combined with a higher vulnerability of IF TRPM8^{+} neurons to aging.

In contrast with the relatively discrete changes observed in cell bodies, the morphological and functional characteristics of corneal TRPM8-EYFP axons and terminals appeared markedly altered in aged mice. The total density of subbasal corneal TRPM8-EYFP axons was significantly lower, primarily at the expenses of a very large reduction of TRPM8-EYFP beaded axons, which was partially compensated by an increased density of TRPM8-EYFP axons with smooth, thin axons. HB-LT cold-sensitive endings were still present in aged animals but generally exhibited a lower background activity and weaker responses to cooling. We interpret these changes as caused by the sharp reduction with aging of the characteristic complex branching associated to cold thermoreceptors (Ivanusic et al., 2013) leading to a smaller membrane area available for the generation of cold-induced depolarization at the terminals branches where TRPM8 channels are located (Brock et al., 2001; Carr et al., 2009; Olivares et al., 2015). In young adult mice, we attribute the distinct firing characteristics of LB-HT cold terminals to a comparatively low-TRPM8 channel density. The presence in old animals of a larger number of this type of neurons and terminals supports the tenet that they correspond to functionally impaired axons that give rise to sparser terminal branching.

Altogether, our data indicate that the morphological and functional consequences of aging appear earlier in the peripheral branches than in the soma of cold sensory neurons and vary depending on the functional subtype of neuron. Such differential effects of senescence on the distinct subclasses of sensory neurons are not entirely surprising. In other somatosensory and visceral tissues of rodents and humans, age-induced cellular and molecular changes are not reflected in simultaneous and general disturbances of all modalities of sensory innervation (Fundin et al., 1997; Namer et al., 2009; Nolano et al., 2013).

The morphological and functional modifications of corneal cold-sensitive innervation with age are part of the general, senescence-induced degenerative processes affecting primary sensory neurons, associated with DNA damage and oxidative stress (for review see Long et al., 2014). These changes are likely reflected in morphometric, ultrastructural, and functional alterations of peripheral axons that, in the case of peripheral corneal nerves, may be accelerated by the slowdown

in regeneration and remodeling of the nerve terminals that are needed to maintain the innervation of the rapidly turning over surface layers of the corneal epithelium.

4.3 | Role of TRPM8-expressing endings in the altered basal tearing of aged mice

There is growing evidence that modulation of basal tearing involves TRPM8$^+$ cold fibers activated by evaporation-induced temperature and osmolality changes of the tear film (Belmonte et al., 2015, 2017). Notably, an enhancement of tearing rate developed in mice when aging progressed; tear osmolarity was also slightly higher, in spite of the augmented aqueous tear flow. Paradoxically, this effect appears in parallel with a reduction in density of beaded, IF subbasal axons, whose tonic activity is expected to maintain the basal tearing of young animals (Parra et al., 2010). However, such decline in density is accompanied by an increase of WF axons and endings phenotypically associated with polymodal nociceptors, whose abnormal ongoing and cold-evoked activity could explain an irritative, augmented tear flow.

In old people diagnosed with DED, an increased tearing (epiphora) accompanying irritation and discomfort is often observed. Discomfort sensations and augmented tearing are experimentally evoked in humans by selective, strong cold receptor stimulation (Acosta et al., 2004; Kovács et al., 2016). Although epiphora in elderly people has been primarily attributed to partial or complete occlusion of the tear drainage pathways (Sousa et al., 1993), it is possible that in these patients, as in aged mice, abnormal activity of functionally impaired cold-sensitive neurons contribute to the overflow of tears. In these subjects, it is also possible that sensory signaling by cold-sensitive fibers connected to nociceptive pathways produce the unpleasant "dry eye" sensations paradoxically reported by epiphora patients.

Taken together, our study shows that aging causes a reduction of the number and functional activity of canonical low-threshold cold receptor neurons of the eye surface which contribute to maintenance tonic basal tearing and also provokes a disturbed responsiveness of high-threshold cold thermoreceptor neurons, making some of them sensitive to moderate cooling, thereby favoring the appearance of unpleasant ocular dryness sensations and irritative tearing. The disturbed equilibrium between TRPM8-expressing endings ultimately determine the changes in the quality and amount of tears observed in aged DED patients and the development of accompanying unpleasant dryness sensations.

ACKNOWLEDGMENTS

This work was supported by grants FC-15-GRUPIN14–141 (Consejería de Economía y Empleo, Asturias, Spain), Fundación Ramón Areces, Caja Rural de Asturias, SAF2014–54518-C3-2-R, SAF2014–54518-C3-1-R, SAF2017–83674-C2-2-R, SAF2017–83674-C2-1-R, and SAF2016–77233-R (Ministerio de Economía, Industria y Competitividad, Spain and European Regional Development Funds, European Union), and "Severo Ochoa" Program for Centers of Excellence in R&D (SEV-2013-0317). Authors thank Dr. James Brock for critical reading of the manuscript and Paola Braga for technical assistance.

CONFLICT OF INTEREST

The authors have no conflicts of interest.

ORCID

Ignacio Alcalde http://orcid.org/0000-0001-6051-9240
Almudena Íñigo-Portugués https://orcid.org/0000-0003-4368-5495
Juana Gallar https://orcid.org/0000-0002-3559-3649
Félix Viana https://orcid.org/0000-0003-1439-949X
Jesús Merayo-Lloves https://orcid.org/0000-0001-8168-478X
Carlos Belmonte http://orcid.org/0000-0001-6891-5942

REFERENCES

Abe, J., Hosokawa, H., Okazawa, M., Kandachi, M., Sawada, Y., Yamanaka, K., … Kobayashi, S. (2005). TRPM8 protein localization in trigeminal ganglion and taste papillae. *Molecular Brain Research*, *136*(1–2), 91–98.

Acosta, M. C., Alfaro, M. L., Borras, F., Belmonte, C., & Gallar, J. (2006). Influence of age, gender and iris color on mechanical and chemical sensitivity of the cornea and conjunctiva. *Experimental Eye Research*, *83*(4), 932–938.

Acosta, M. C., Peral, A., Luna, C., Pintor, J., Belmonte, C., & Gallar, J. (2004). Tear secretion induced by selective stimulation of corneal and conjunctival sensory nerve fibers. *Investigative Ophthalmology & Visual Science*, *45*(7), 2333–2336.

Alamri, A., Bron, R., Brock, J. A., & Ivanusic, J. J. (2015). Transient receptor potential cation channel subfamily V member 1 expressing corneal sensory neurons can be subdivided into at least three subpopulations. *Frontiers in Neuroanatomy*, *9*, 71.

Babes, A., Zorzon, D., & Reid, G. (2004). Two populations of cold-sensitive neurons in rat dorsal root ganglia and their modulation by nerve growth factor. *European Journal of Neuroscience*, *20*(9), 2276–2282.

Belmonte, C., Acosta, M. C., Merayo-Lloves, J., & Gallar, J. (2015). What causes eye pain? *Current Ophthalmology Reports*, *3*(2), 111–121.

Belmonte, C., & Gallar, J. (2011). Cold thermoreceptors, unexpected players in tear production and ocular dryness sensations. *Investigative Ophthalmology & Visual Science* , *52*(6), 3888–3892.

Belmonte, C., Nichols, J. J., Cox, S. M., Brock, J. A., Begley, C. G., Bereiter, D. A., … Wolffsohn, J. S. (2017). TFOS DEWS II pain and sensation report. *Ocular Surface*, *15*(3), 404–437.

Bergman, E., & Ulfhake, B. (1998). Loss of primary sensory neurons in the very old rat: Neuron number estimates using the disector method and confocal optical sectioning. *Journal of Comparative Neurology*, *396*(2), 211–222.

Brock, J. A., McLachlan, E. M., & Belmonte, C. (1998). Tetrodotoxin-resistant impulses in single nociceptor nerve terminals in guinea-pig cornea. *Journal of Physiology*, *512*(Pt 1), 211–217.

Brock, J. A., Pianova, S., & Belmonte, C. (2001). Differences between nerve ending impulses of polymodal nociceptors and cold sensory receptors of the guinea-pig cornea. *Journal of Physiology*, *533*(Pt 2), 493–501.

Carr, R. W., Pianova, S., McKemy, D. D., & Brock, J. A. (2009). Action potential initiation in the peripheral endings of cold-sensitive

neurones innervating the guinea-pig cornea. *Journal of Physiology*, *587*(Pt 6), 1249–1264.

Comfort, A. (1964). *Aging: The biology of senescence*. New York, NY: Holt, Rinehart and Winston.

Craig, J. P., Nelson, J. D., Azar, D. T., Belmonte, C., Bron, A. J., Chauhan, S. K., … Sullivan, D. A. (2017). TFOS DEWS II report executive summary. *Ocular Surface*, *15*(4), 802–812.

de la Peña, E., Malkia, A., Cabedo, H., Belmonte, C., & Viana, F. (2005). The contribution of TRPM8 channels to cold sensing in mammalian neurones. *Journal of Physiology*, *567*(Pt 2), 415–426.

Dvorscak, L., & Marfurt, C. F. (2008). Age-related changes in rat corneal epithelial nerve density. *Investigative Ophthalmology & Visual Science*, *49*(3), 910–916.

Fundin, B. T., Bergman, E., & Ulfhake, B. (1997). Alterations in mystacial pad innervation in the aged rat. *Experimental Brain Research*, *117*(2), 324–340.

Furukawa, R. E., & Polse, K. A. (1978). Changes in tear flow accompanying aging. *American Journal of Optometry and Physiological Optics*, *55*(2), 69–74.

Gallar, J., Pozo, M. A., Tuckett, R. P., & Belmonte, C. (1993). Response of sensory units with unmyelinated fibres to mechanical, thermal and chemical stimulation of the cat's cornea. *Journal of Physiology*, *468*, 609–622.

Gipson, I. K. (2013). Age-related changes and diseases of the ocular surface and cornea. *Investigative Opthalmology & Visual Science*, *54*(14), ORSF48–ORSF53.

González-González, O., Bech, F., Gallar, J., Merayo-Lloves, J., & Belmonte, C. (2017). Functional properties of sensory nerve terminals of the mouse cornea. *Investigative Opthalmology & Visual Science*, *58*(1), 404–415.

He, J., Bazan, N. G., & Bazan, H. E. (2010). Mapping the entire human corneal nerve architecture. *Experimental Eye Research*, *91*(4), 513–523.

Hirata, H., & Meng, I. D. (2010). Cold-sensitive corneal afferents respond to a variety of ocular stimuli central to tear production: Implications for dry eye disease. *Investigative Ophthalmology & Visual Science*, *51*(8), 3969–3976.

Hirata, H., & Oshinsky, M. L. (2012). Ocular dryness excites two classes of corneal afferent neurons implicated in basal tearing in rats: Involvement of transient receptor potential channels. *Journal of Neurophysiology*, *107*(4), 1199–1209.

Ivanusic, J. J., Wood, R. J., & Brock, J. A. (2013). Sensory and sympathetic innervation of the mouse and guinea pig corneal epithelium. *Journal of Comparative Neurology*, *521*(4), 877–893.

Knowlton, W. M., Palkar, R., Lippoldt, E. K., McCoy, D. D., Baluch, F., Chen, J., & McKemy, D. D. (2013). A sensory-labeled line for cold: TRPM8-expressing sensory neurons define the cellular basis for cold, cold pain, and cooling-mediated analgesia. *Journal of Neuroscience: Official Journal of the Society for Neuroscience*, *33*(7), 2837–2848.

Kovács, I., Luna, C., Quirce, S., Mizerska, K., Callejo, G., Riestra, A., … Gallar, J. (2016). Abnormal activity of corneal cold thermoreceptors underlies the unpleasant sensations in dry eye disease. *Pain*, *157*(2), 399–417.

Lamberts, D. W., Foster, C. S., & Perry, H. D. (1979). Schirmer test after topical anesthesia and the tear meniscus height in normal eyes. *Archives of Ophthalmology*, *97*(6), 1082–1085.

Long, Y. C., Tan, T. M., Takao, I., & Tang, B. L. (2014). The biochemistry and cell biology of aging: Metabolic regulation through mitochondrial signaling. *American Journal of Physiology Endocrinology and Metabolism*, *306*(6), E581–E591.

Madrid, R., de la Peña, E., Donovan-Rodriguez, T., Belmonte, C., & Viana, F. (2009). Variable threshold of trigeminal cold-thermosensitive neurons is determined by a balance between TRPM8 and Kv1 potassium channels. *Journal of Neuroscience*, *29*(10), 3120–3131.

Madrid, R., Donovan-Rodríguez, T., Meseguer, V., Acosta, M. C., Belmonte, C., & Viana, F. (2006). Contribution of TRPM8 channels to cold transduction in primary sensory neurons and peripheral nerve terminals. *Journal of Neuroscience: Official Journal of the Society for Neuroscience*, *26*(48), 12512–12525.

Marfurt, D. F., Cox, J., Deek, S., & Dvorscak, L. (2010). Anatomy of the human corneal innervation. *Experimental Eye Research*, *90*(4), 478–492.

McKemy, D. D., Neuhausser, W. M., & Julius, D. (2002). Identification of a cold receptor reveals a general role for TRP channels in thermosensation. *Nature*, *416*(6876), 52–58.

Meng, I. D., & Kurose, M. (2013). The role of corneal afferent neurons in regulating tears under normal and dry eye conditions. *Experimental Eye Research*, *117*, 79–87.

Morenilla-Palao, C., Luis, E., Fernandez-Pena, C., Quintero, E., Weaver, J. L., Bayliss, D. A., & Viana, F. (2014). Ion channel profile of TRPM8 cold receptors reveals a role of TASK-3 potassium channels in thermosensation. *Cell Reports*, *8*(5), 1571–1582.

Namer, B., Barta, B., Orstavik, K., Schmidt, R., Carr, R., Schmelz, M., & Handwerker, H. O. (2009). Microneurographic assessment of C-fibre function in aged healthy subjects. *Journal of Physiology*, *587*(2), 419–428.

Nolano, M., Provitera, V., Caporaso, G., Stancanelli, A., Leandri, M., Biasiotta, A., … Truini, A. (2013). Cutaneous innervation of the human face as assessed by skin biopsy. *Journal of Anatomy*, *222*(2), 161–169.

Olivares, E., Salgado, S., Maidana, J. P., Herrera, G., Campos, M., Madrid, R., & Orio, P. (2015). TRPM8-dependent dynamic response in a mathematical model of cold thermoreceptor. *PLoS One*, *10*, e0139314.

Palkar, R., Lippoldt, E. K., & McKemy, D. D. (2015). The molecular and cellular basis of thermosensation in mammals. *Current Opinion in Neurobiology*, *34*, 14–19.

Parissi, M., Karanis, G., Randjelovic, S., Germundsson, J., Poletti, E., Ruggeri, A., … Lagali, N. (2013). Standardized baseline human corneal subbasal nerve density for clinical investigations with laser-scanning in vivo confocal microscopy. *Investigative Ophthalmology & Visual Science*, *54*(10), 7091–7102.

Parra, A., Madrid, R., Echevarria, D., del Olmo, S., Morenilla-Palao, C., Acosta, M. C., … Belmonte, C. (2010). Ocular surface wetness is regulated by TRPM8-dependent cold thermoreceptors of the cornea. *Nature Medicine*, *16*(12), 1396–1399.

Peier, A. M., Moqrich, A., Hergarden, A. C., Reeve, A. J., Andersson, D. A., Story, G. M., … Patapoutian, A. (2002). A TRP channel that senses cold stimuli and menthol. *Cell*, *108*(5), 705–715.

Quallo, T., Vastani, N., Horridge, E., Gentry, C., Parra, A., Moss, S., … Bevan, S. (2015). TRPM8 is a neuronal osmosensor that regulates eye blinking in mice. *Nature Communications*, *6*, 7150.

Reichard, M., Weiss, H., Poletti, E., Ruggeri, A., Guthoff, R. F., Stachs, O., & Baltrusch, S. (2016). Age-related changes in murine corneal nerves. *Current Eye Research*, *41*(8), 1021–1028.

Robbins, A., Kurose, M., Winterson, B. J., & Meng, I. D. (2012). Menthol activation of corneal cool cells induces TRPM8-mediated lacrimation but not nociceptive responses in rodents. *Investigative Opthalmology & Visual Science*, *53*(11), 7034–7042.

Stern, M. E., Gao, J., Siemasko, K. F., Beuerman, R. W., & Pflugfelder, S. C. (2004). The role of the lacrimal functional unit in the pathophysiology of dry eye. *Experimental Eye Research*, *78*(3), 409–416.

Sousa, P. C., Pinto, P., Leite, E., & Cunha-Vaz, J. G. (1993). Morphological and/or functional imagiology diagnosis of epiphora. *Documenta Ophthalmologica. Advances in Ophthalmology*, *83*(4), 337–348.

Takashima, Y., Daniels, R. L., Knowlton, W., Teng, J., Liman, E. R., & McKemy, D. D. (2007). Diversity in the neural circuitry of cold sensing revealed by genetic axonal labeling of transient receptor potential

melastatin 8 neurons. *Journal of Neuroscience: Official Journal of the Society for Neuroscience*, *27*(51), 14147–14157.

Teichert, R. W., Raghuraman, S., Memon, T., Cox, J. L., Foulkes, T., Rivier, J. E., & Olivera, B. M. (2012). Characterization of two neuronal subclasses through constellation pharmacology. *Proceedings of the National Academy of Science USA*, *109*(31), 12758–12763.

Viana, F., de la Pena, E., & Belmonte, C. (2002). Specificity of cold thermotransduction is determined by differential ionic channel expression. *Nature Neuroscience*, *5*(3), 254–260.

Wang, S., & Albers, K. M. (2009). Behavioral and cellular level changes in the aging somatosensory system. *Annals of the New York Academy of Sciences*, *1170*, 745–749.

Xing, H., Ling, J., Chen, M., & Gu, J. G. (2006). Chemical and cold sensitivity of two distinct populations of TRPM8-expressing somatosensory neurons. *Journal of Neurophysiology*, *95*(2), 1221–1230.

How to cite this article: Alcalde I, Íñigo-Portugués A, González-González O, et al. Morphological and functional changes in TRPM8-expressing corneal cold thermoreceptor neurons during aging and their impact on tearing in mice. *J Comp Neurol*. 2018;526:1859–1874. https://doi.org/10.1002/cne.24454

Functional and Morphologic Alterations in Mechanical, Polymodal, and Cold Sensory Nerve Fibers of the Cornea Following Photorefractive Keratectomy

Federico Bech,[1] Omar González-González,[1] Enol Artime,[1] Joana Serrano,[1] Ignacio Alcalde,[1] Juana Gallar,[2] Jesús Merayo-Lloves,[1] and Carlos Belmonte[1,2]

[1]Instituto Universitario Fernández-Vega, Universidad de Oviedo & Fundación de Investigación Oftalmológica, Oviedo, Spain
[2]Instituto de Neurociencias, Universidad Miguel Hernández-CSIC, San Juan de Alicante, Spain

Correspondence: Carlos Belmonte, Instituto de Neurociencias, UMH-CSIC, Avenida Santiago Ramón y Cajal, San Juan de Alicante, 203550, Spain;
carlos.belmonte@umh.es.

FB and OG-G contributed equally to the work presented here and should therefore be regarded as equivalent authors.

Submitted: February 5, 2018
Accepted: April 4, 2018

Citation: Bech F, González-González O, Artime E, et al. Functional and morphologic alterations in mechanical, polymodal, and cold sensory nerve fibers of the cornea following photorefractive keratectomy. *Invest Ophthalmol Vis Sci.* 2018;59:2281–2292. https://doi.org/10.1167/iovs.18-24007

Purpose. To define the characteristics and time course of the morphologic and functional changes experienced by corneal sensory nerves after photorefractive keratectomy (PRK).

Methods. Unilateral corneal excimer laser photoablation was performed in 54 anesthetized 3- to 6-month-old mice; 11 naïve animals served as control. Mice were killed 0, 3, 7, 15, and 30 days after PRK. Excised eyes were placed in a recording chamber superfused at 34°C. Electrical nerve impulse activity of single sensory terminals was recorded with a micropipette applied onto the corneal surface. Spontaneous and stimulus-evoked (cold, heat, mechanical, and chemical stimuli) nerve terminal impulse (NTI) activity was analyzed. Corneas were fixed and stained with anti–β-Tubulin III antibody to measure nerve density and number of epithelial nerve penetration points of regenerating subbasal leashes.

Results. Nerve fibers and NTI activity were absent in the injured area between 0 and 7 days after PRK, when sparse regenerating nerve sprouts appear. On day 15, subbasal nerve density reached half the control value and abnormally responding cold-sensitive terminals were recorded inside the lesion. Thirty days after PRK, nerve density was almost restored, active cold thermoreceptors were abundant, and polymodal nociceptor activity first reappeared.

Conclusions. Morphologic regeneration of subbasal corneal nerves started shortly after PRK ablation and was substantially completed 30 days later. Functional recovery appears faster in cold terminals than polymodal terminals, possibly reflecting an incomplete damage of the more extensively branched cold-sensitive axon terminals. Evolution of postsurgical discomfort sensations quality may be associated with the variable regeneration pattern of each fiber type.

Keywords: nerve regeneration, photorefractive keratectomy, cold thermoreceptors, polymodal nociceptors, dysesthesia

Photorefractive surgery (PRK) is usually accompanied by decreased corneal sensitivity, transitory tear deficiency, and symptoms of dry eye.[1–4] These disturbances are due in a large extent to damage of corneal sensory nerves. Peripheral nerve injury alters sensory input to the somatosensory cortex and to brainstem centers responsible for corneal sensation, blinking, and reflex parasympathetic stimulation of lacrimal gland secretion.[5,6] This results in dysesthesias, reduced blinking rate, and decreased basal production of the aqueous component of the tear film.[7–10]

During the first 24 hours after PRK, a local inflammatory reaction develops in the injured cornea.[11] Macrophages, monocytes, T cells, and polymorphonuclear cells infiltrate and remove damaged epithelium debris.[12] Release of cytokines, chemokines, and growth factors by injured epithelial cells and keratocytes of the anterior stroma, and by resident and migrating inflammatory cells, rapidly activates repair processes including migration and mitosis of healthy epithelial cells, nerve regrowth, and stromal healing.[13,14] Regeneration of corneal nerves after PRK occurs as a biphasic process. First, branches of the subepithelial nerve plexus at the margin of the injury site reconstruct a transient subbasal plexus composed by fine neurites that run centrally with migrating cells. In a second stage, this plexus degenerates and is replaced by nerves originating from the underlying stroma.[15,16] However, the recovery of subbasal nerve density is gradual and not complete until 2 to 3 years after surgery.[17,18]

Trigeminal ganglion sensory neurons innervating the cornea are functionally heterogeneous and have been classified as polymodal nociceptor, mechano-nociceptor, and cold thermoreceptor neurons, on the basis of intensity and form of energy (mechanical, thermal, chemical) that activates preferentially their peripheral corneal terminals.[19,20] Each functional class of corneal neuron evokes qualitatively distinct conscious sensations[21,22] and contributes differently to the modulation of tearing and blinking.[20,23,24] Experimental evidence suggests that mechano-nociceptors are important in evoking acute pricking pain when the cornea is mechanically stimulated, while activation of polymodal nociceptors by mechanical, thermal, or chemical noxious stimuli evokes burning pain, hyperalgesia, and neurogenic inflammation. Excitation of both types of nociceptor fibers elicits reflex blinking and irritative tearing.[13,25] In contrast, cold thermoreceptors mediate sensations of ocular surface cooling and drying[22,26] and play an

important role in the modulation of basal tearing and blinking rates associated with the homeostasis of eye surface wetness.[24,27] Surgical injury acutely affects the different classes of sensory axons innervating the ocular surface.[28] However, the degree of residual functional impairment in mechano-nociceptor, polymodal nociceptor, and cold thermoreceptor fibers following PRK, leading eventually to dysesthesias and reflex autonomic disturbances in operated eyes, is still poorly known.

In the present work, we analyzed the changes in spontaneous and stimulus-evoked nerve impulse activity experienced by corneal sensory terminals, immediately and at different times up to 30 days after PRK, while observing the parallel evolution of corneal nerve architecture within and around the wounded area. We discovered that cold-sensitive endings regenerate early albeit a fraction of them, located both in the injured and in the intact peripheral cornea, exhibit an abnormal impulse activity attributable to the incomplete branching of regenerating cold thermoreceptor nerve axons. Polymodal nociceptors and mechano-nociceptors required longer times to recover the normal responsiveness to their natural stimuli.

Methods

Animals

Male, 3- to 6-month-old C57BL/6 mice were purchased from Charles River Laboratory (L'Arbresle Cedex, France). Animals were handled and housed according to the ARVO Statement for the Use of Animals in Ophthalmic and Vision Research and the applicable guidelines of the European Union (2010/63/EU) and the Spanish Government (RD 53/2013). The ethics committee of the University of Oviedo approved all procedures.

Corneal Nerve Injury Through Photorefractive Keratectomy (PRK)

Surgical corneal injury was performed by using a VISX Star S2 excimer laser (VISX, Inc., Santa Clara, CA, USA) as previously described.[29–31] Right eyes were subjected to PRK surgery with the following parameters: a 1.5-mm^2 circular area, 45 μm of depth. The procedure included simultaneous ablation in a single step of the epithelium (using a defined epithelial thickness profile of 25 μm centrally) and 20 μm of the anterior stroma (representing approximately 20% of the total stromal thickness), removing all subbasal nerve fibers and intraepithelial terminals of the treated area.

Before surgery, mice were deeply anesthetized by intraperitoneal injection of a mixture of ketamine hydrochloride (80 mg/kg, Imalgene 1000; Merial Laboratorios S.A., Barcelona, Spain) and xylazine hydrochloride (5 mg/kg, Rompun; Bayer Hispania S.L., Barcelona, Spain) followed by topical application of 0.5% tetracaine chlorhydrate and 1 mg oxybuprocaine (Colircusí Anestésico Doble; Alcon S.A., Barcelona, Spain).

In Vivo Evaluation of Epithelial Wound Healing

Fluorescein staining was used to define the area (mm^2) of the corneal epithelial defect, which was measured under a Leica S6D stereoscopic microscope equipped with an EC3 digital camera (Leica Microsystems, Wetzlar, Germany) and using a fixed magnification of ×12.5. Observations were made immediately after surgery (day 0) and at 3, 7, 15, and 30 days after PRK surgery (T0, T3, T7, T15, and T30, respectively). These time points were selected because they correspond to the moment of important events in the wound-healing process.[29–32] FIJI image analysis software (ImageJ; http://imagej.nih.gov/ij/; provided in the public domain by the National Institutes of Health, Bethesda, MD, USA) was applied to measure the area of fluorescein-impregnated cornea. This was manually lined with the freehand selection tool of FIJI; the software calculated automatically the area inside the selection.

Whole-Mounted Cornea Immunohistochemistry

To obtain the enucleated eyes, animals were deeply anesthetized by intraperitoneal injection with a mixture of ketamine hydrochloride (80 mg/kg) and xylazine hydrochloride (5 mg/kg) and killed by cervical dislocation.

Immunofluorescence

Freshly isolated eyeballs from mice were dissected and fixed 1 hour at room temperature (RT) in methanol and dimethyl sulfoxide (4:1), then were postfixed for 5 minutes in methanol at −21°C. Afterwards, corneas were rehydrated in graded methanol and washed in 0.1 M PBS pH 7.4 (PBS). They were blocked (blocking serum solution) for 1 hour with 5% BSA, 5% goat serum, 0.2% sodium azide, and 0.3% Triton X-100 in PBS (PBS-Triton). After rinsing, corneas were incubated for 24 hours at RT against rabbit anti–neuronal class III β-Tubulin (1:250; Cell Signaling Technology, Boston, MA, USA) in blocking serum solution. After three rinses with 0.2% BSA (washing solution), 0.2% goat serum, 0.2% sodium azide, and PBS-Triton, corneas were incubated in blocking serum solution for 24 hours at RT with secondary antibody against anti-rabbit IgG Alexa Fluor 594 (1:500; Molecular Probes, Eugene, OR, USA). Afterwards, corneas were rinsed three times with washing solution, followed by incubation for 10 minutes at RT with 4′,6-diamidino-2-phenylindole (DAPI, 2 μg/mL; Molecular Probes). Finally, corneas were mounted in slides with fluorescent mounting medium (DAKO, Glostrup, Denmark).

Image Acquisition

Fluorescence images were obtained with a Leica TCS SP8 confocal microscope (Leica Microsystems). For whole-mounted corneas, a mosaic of images was obtained at magnification of ×200 by using tile scan utility of LASX and confocal z stacks, spaced 3.5 μm in the Z-axis.

Morphologic Data Analysis

Images were analyzed by using also the image analysis software FIJI. Whole-mounted corneas were divided in five areas of study (Supplementary Fig. S1): four peripheral zones, which were defined each as two 0.25 mm^2 square regions (a 500 × 500-μm box) whose peripheral borders were approximately 200 μm away from the limbus border and were separated approximately 500 μm from each other; and a fifth area, defined as the injured area in the center of the cornea, which was determined by the absence of DAPI staining in injured corneas (mean injured area, 1.46 ± 0.13 mm^2). This circular area was divided in three concentric circles (Supplementary Fig. S1), with the first and biggest circle corresponding to the border of the injury in PRK-ablated corneas. For comparison, in uninjured corneas the central corneal area was also divided into three similar concentric circular areas of 1.5, 1.0, and 0.5 mm^2.

Subbasal nerves were quantified in the periphery by counting the number of nerves intersecting a line drawn inside the square area (parallel to the limbus; see Supplementary Fig. S1). In the central cornea of both injured and control eyes, subbasal nerves were quantified as the number of nerves intersecting the circumferences defining each of the concen-

tric circles (Supplementary Fig. S1). Nerve density was calculated as the mean number of subbasal nerve fibers per mm^2 entering each circle.

Penetration sites of subepithelial bundles through the epithelial basal lamina were counted within the total area of the cornea. The total number of penetration points, that is, the number of points where axon bundles transverse the basal lamina of corneal epithelium, was counted both outside and inside the largest, 1.5-mm^2 circle by using z-stack images of injured and uninjured corneas, and expressed as number of penetrations per mm^2 in the periphery (outside the circle) and central cornea, respectively.

Electrophysiology

For electrophysiological studies, recordings of single corneal nerve terminals in vitro were performed as previously described.[24] In brief, mice were killed by cervical dislocation and eyes were excised and placed in a physiological saline solution similar to tear fluid (in mM: NaCl [128], KCl [5], NaH_2PO_4 [1], $NaHCO_3$ [26], $CaCl_2$ [2.4], $MgCl_2$ [1.3], and glucose [10]) and bubbled with carbogen gas (5% CO_2 and 95% O_2). The eye was then placed in a recording chamber and was continuously superfused with the same physiological saline solution. Temperature during the experiment was controlled with a homemade Peltier device.

Extracellular electrical activity of single sensory nerve endings of the corneal surface was recorded with a borosilicate glass microelectrode with tip diameter of approximately 50 µm that was filled with saline solution. An Ag/AgCl wire located in the bath serves as indifferent electrode. With the aid of a micromanipulator, the recording pipette was placed on the corneal surface with slight suction at different points both in the injured area and in the periphery (mean of 15 seals per cornea, 10 in injured area and 5 in periphery), searching for nerve terminal impulse (NTI) activity. NTIs were amplified with an AC amplifier (Neurolog NL104; Digitimer, Welwyn, UK) and stored at 10 kHz into a computer, using a CED micro 1401 interface and Spike 2 software (both from Cambridge Electronic Design, Cambridge, UK).

Only recordings containing NTIs originating from a well-defined single nerve terminal were analyzed. In these recordings NTIs were clearly distinguished from noise (~10 µV peak-to-peak) and had similar amplitudes and waveforms, indicating that they originated from the same sensory nerve ending. To minimize deterioration of the preparation with time, the total duration of the experiment was limited to a maximum of 120 minutes per eye (30 minutes for preparation; 90 minutes for recording). Percentage of successful attempts refers to the number of seals made on the cornea in which nerve terminal activity was recorded.

Experimental Protocol

The recording pipette was placed at regularly aligned points on the corneal surface, separated by an approximate distance of 0.2 mm. First, one half of the cornea was explored starting in the center and descending to the periphery; then, the eye was rotated and the opposite side of the cornea was explored.[33] After 90 minutes of recording attempts, the eye was fixed and prepared for morphologic studies.

Cold stimulation was performed by decreasing the background temperature of the perfusing solution (from ~34°C to ~14°C or ~5°C, in cold thermoreceptors or polymodal nociceptors and mechano-nociceptors, respectively), generating a cooling ramp at mean cooling rate of 0.6°C·s^{-1}; when the peak temperature of ~14°C or ~5°C was attained, warming was applied at a similar speed to return to the basal temperature. Following a resting period of 120 seconds, mechanical stimulation was performed by moving forward the pipette with a controlled displacement of the micromanipulator. Pressure with the pipette was maintained for 2 seconds. Two minutes later, a heating ramp (from 34°C to ~52°C at 0.5°C·s^{-1}, ~30 seconds' duration) was applied, returning to the initial control value of 34°C when the peak temperature was reached.

Analysis of NTI Activity

Success percentage indicates the percentage of successful attempts at recording a nerve terminal activity in relation to the total number of attempts. Background activity is defined as the mean basal ongoing frequency in impulses per second (imp·s^{-1}) at the basal temperature (33.9°C ± 0.07°C) measured during the 60-second period that preceded the onset of a stimulus.

The following parameters of the NTI activity were analyzed in the different terminal types.

Cold Thermoreceptor Terminals. *Cooling Threshold.* Temperature (°C) during a cooling ramp at which NTI frequency increased to a value that was the mean NTI frequency measured during the 10-second period preceding the onset of a cooling ramp plus three times its standard deviation.

Cooling Response. Expressed as the mean in NTI frequency between the cooling threshold and the peak response frequency values during the cooling ramp.

Polymodal and Mechano-nociceptor Terminals. *Response to Cooling.* The total number of spikes during the 45 seconds following the onset of the cooling ramp was compared with the total number of spikes during 45 seconds immediately before the cooling ramp.

Response to Heating. The total number of spikes during the 30 seconds following the onset of the heating ramp was compared with the total number of spikes during 30 seconds immediately before the heating ramp.

Response to Mechanical Force. The total number of NTIs during the 10 seconds following the onset of mechanical stimulation was compared with the total number of NTIs during the 10-second period immediately before applying the mechanical stimulus.

Statistical Analysis

Statistical comparisons were performed by using Microsoft Excel 2010 (Microsoft Corporation, Redmond, CA, USA), Origin 8 (OriginLab Corporation, Northampton, MA, USA), and InStat 3 (GraphPad Software, Inc., La Jolla, CA, USA). Data are expressed as mean ± SD. For electrophysiology data unpaired Student's *t*-test was used. The morphologic measurements were compared by using 1-way ANOVA with Tukey-Kramer multiple comparisons post hoc test. Significance threshold was set at $P < 0.05$.

Results

Sixty-five mice were used in this study. PRK was performed in a total of 54 mice. Immediately after laser ablation, fluorescein staining in seven mice delimited in the cornea a circular area of epithelial damage of 2.2 ± 0.1 mm^2. Twenty-four hours later, the size of the injured area in the same animals had decreased to 0.46 ± 0.22 mm^2. The injury was not visible after 2 days in four of the seven mice and was very small in the remaining three (0.05 ± 0.08 mm^2). On the third day, no fluorescein staining was apparent in any of the eyes. PRK caused initially a

Investigative Ophthalmology & Visual Science

marked opacity that reversed progressively with time. Still, 28% of the corneas continued to show light opacity spots 30 days after surgery.

From the 54 operated animals, 26 corneas (at T0, $n = 5$; T3, $n = 4$; T7, $n = 6$; T15, $n = 5$; T30, $n = 6$) and six corneas of intact mice were studied morphologically (Fig. 1A). Electrophysiological recordings were performed in 43 eyes at various times after PRK (T0, $n = 5$; T3, $n = 5$; T7, $n = 15$; T15, $n = 10$; T30, $n = 8$) and in five control eyes where the cornea was intact. The corneas of 15 eyes previously used for electrophysiological recordings were also studied morphologically. In total, electrical activity was recorded from 117 corneal nerve terminals: 66 with receptive fields located within the central area, in the region where the wound was performed, and 51 terminals located in the surrounding peripheral area.

In all recording experiments, the search for nerve terminal impulse activity started by placing the recording electrode on the corneal surface at different pre-established points defined both in the central area where the injury was made and in the intact periphery. From previous studies in intact mice corneas,[33] we defined the fraction of the nerve terminals of the intact cornea responding only to mechanical force as mechano-nociceptors and those activated by heat and mechanical force as polymodal nociceptors. Finally, cold thermoreceptors, initially defined by their responsiveness to cooling, were subclassified by the value of their spontaneous firing at 34°C and the temperature threshold required to increase their firing rate with a cooling ramp[33] as high-background ($\geq$1.5 NTI·s^{-1}), low-threshold ($\geq$30.5°C) cold thermoreceptors (HB-LT), or low-background ($<$1.5 NTI·s^{-1}) high-threshold ($<$30.5°C) cold thermoreceptors (LB-HT). Altogether, in the central cornea 54.1% of the terminals were identified as cold thermoreceptors, 26.7% as polymodal nociceptors, and 10% as mechano-nociceptors. In the peripheral area, 46.7% were cold thermoreceptors; 26.7%, polymodal nociceptors; and 10%, mechano-nociceptors. The remaining units recorded at the central and peripheral cornea could not be accurately classified.

Nerve Terminal Impulse Activity Was Absent From the PRK-Injured Area at Early Stages of Corneal Nerve Regeneration

At day 0, immediately after laser ablation, the corneal epithelium had disappeared and the normal innervation of the central cornea was virtually absent. Only midstromal nerve trunks, often terminating abruptly, could be identified in the stroma, while subepithelial and subbasal plexuses were lost (Figs. 1B, 2B, 3A), and no nerve penetration points were identified in the wounded area (Table). In accordance with this morphologic observation, electrical activity was undetectable within the lesioned area in the animals studied immediately after PRK (Fig. 3A).

In the peripheral cornea surrounding the wounded area, the density of nerve fibers measured after surgery and the number of nerve penetration points in the basal lamina per mm^2 was slightly lower in day 0 corneas than in the same area of the corneas of control mice (Fig. 3B; Table). At this time, the incidence of NTI activity in the peripheral area surrounding the wound was similar in operated and intact corneas (32.4% $\pm$ 9.3%, $n = 5$ at T0 versus 39.1% $\pm$ 7.7%, $n = 5$ in intact corneas; Fig. 3B).

At day 3, regenerating individual rectilinear axons, sprouting from some of the cut subbasal nerves, started to enter the injured region (Figs. 1C, 2C), although most appeared abruptly interrupted at the wound border. The overall density of these regenerating fibers within the damaged area was only 14.3% $\pm$ 3.6% of the density values at the central cornea of intact mice ($P < 0.001$; Fig. 3A, Table). At this time, NTI activity was still undetectable in the wounded area (Fig. 3A).

In the peripheral cornea surrounding the wound, the density of nerve fibers at T3 was significantly lower than in control corneas (Fig. 3B; Table). Likewise, the probability of finding an active nerve terminal at day 3 in the noninjured peripheral cornea was also lower (13.9% $\pm$ 7.9%, $n = 5$; Fig. 3B). Moreover, cold thermosensory terminals exhibiting abnormal low background activity combined with a low cooling threshold, never observed in uninjured corneas, were recorded at the periphery for the first time (Fig. 4).

At day 7 an incipient process of remodeling of the stromal nerves below the wounded area was evident, leading to new basal lamina nerve penetration points that reached near-normal numbers (Table). Entering subepithelial axons were short, tortuous, and ramified (Figs. 1D, 2D). However, at T7 most of the axons present in the ablated area originated from peripheral stumps of subbasal leashes that were growing centrally, but the nerve density remained significantly lower ($P < 0.001$) than in control mice, with nerve density values 51.7% $\pm$ 4.9% of control values (Table). The first nerve terminal electrical activity within the injured corneal area was recorded at this time point and only in 7 of the 13 explored corneas, with the probability of finding an active unit being significantly lower than for the control value (Fig. 3A). Ten active terminals were clearly identified as cold-sensitive. One active terminal with low background activity (0.03 imp·s^{-1}) responded only to mechanical stimulus (from 0 imp/10 s to 71 imp/10 s). In addition, there were three sites with low-amplitude NTIs that could not be identified functionally.

In the peripheral cornea, the mean nerve density increased slightly at T7. In addition, the percentage of points where NTI activity was recorded over the total number of attempts increased to 23.1% $\pm$ 6.5% (Fig. 3B). Six of ten terminals were classified as cold thermoreceptors, while the rest were low-amplitude, functionally unidentifiable terminals.

One Month After PRK, a Subset of the Corneal Endings Exhibited Abnormal Activity Despite the Apparent Morphologic Recovery of the Innervation

At day 15 after injury, the overall density of nerve fibers in the injured area became greater than in the periphery (Table). This was due to a higher number of stromal nerve penetrations (Table) and the incorporation of nerve fibers spreading from the periphery of the wound, forming tortuous and ramified arborizations (Figs. 1E, 2E), although nerve density was still lower (58.9% $\pm$ 3.2%, $P < 0.05$) than in control eyes. At this time, active terminals were found in 6 of 10 corneas, with a higher probability of finding active recording points than at T7 (Fig. 3A). Six of the identified terminals were characterized as cold-sensitive and one as a mechano-nociceptor. In six instances, units with spontaneous activity were observed that had a low amplitude, which decreased further with cooling, preventing reliable identification of their function.

In the peripheral cornea, nerve density continued to increase at T15 in comparison with earlier stages of the study, and the probability of finding NTIs also increased (Fig. 3B; Table), reaching values near those in the periphery of intact corneas. Four active terminals responded clearly to cold stimuli, while four others presented a low amplitude that prevented a reliable functional identification. Another terminal showed the characteristics of a mechanoreceptor (background activity of 0.05 imp·s^{-1}, and 0 imp/10 s before and 14 imp/10 s after mechanical stimulation). One polymodal nociceptor

Investigative Ophthalmology & Visual Science

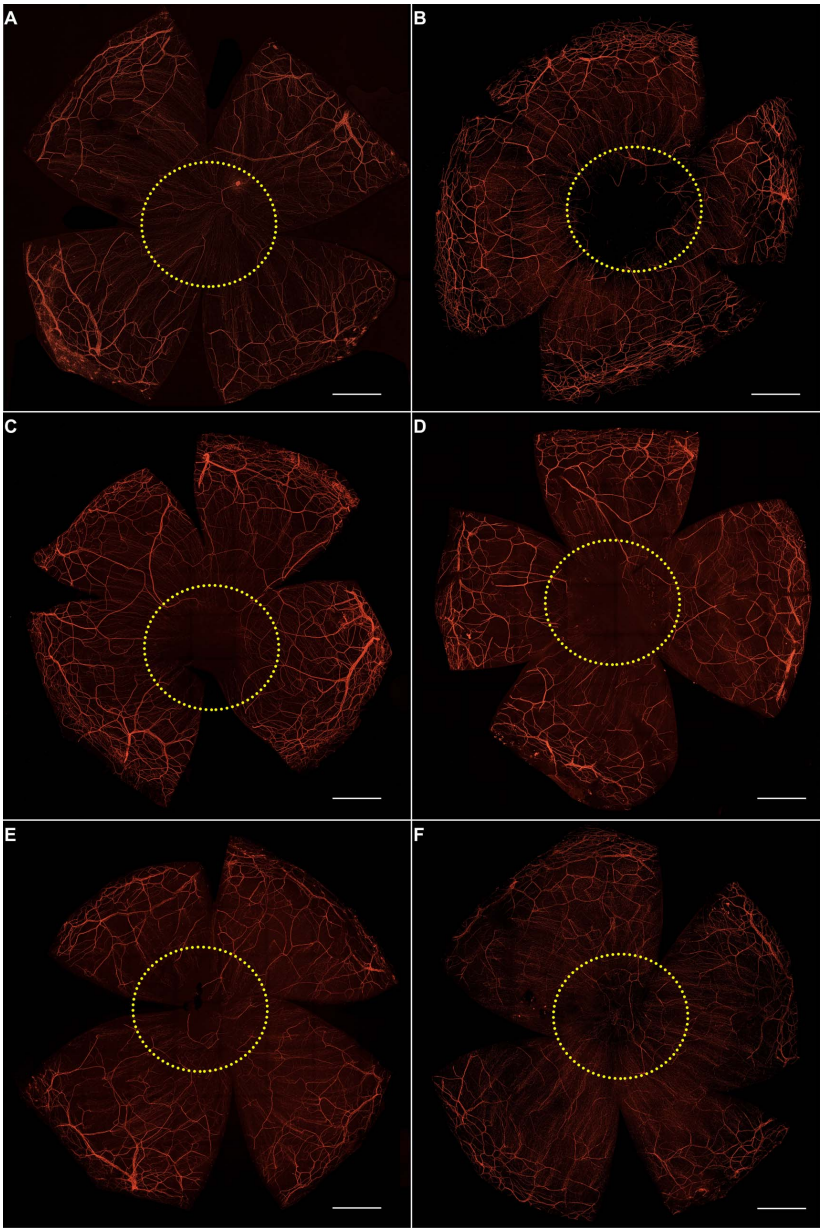

Figure 1. Subbasal and stromal corneal nerves at different times after PRK. Whole-mount corneas showing at low magnification (×200) the entire corneal innervation by stromal and subbasal corneal nerves, stained against β-Tubulin III (*red*). (**A**) An intact cornea with the area in which the PRK wound is performed has been marked with a *circle*. (**B–F**) Corneas excised and stained at different times after PRK (T0, T3, T7, T15, and T30, respectively). The *circle* indicates in each case the extension of the initial PRK-injured area. *Scale bars*: 500 μm.

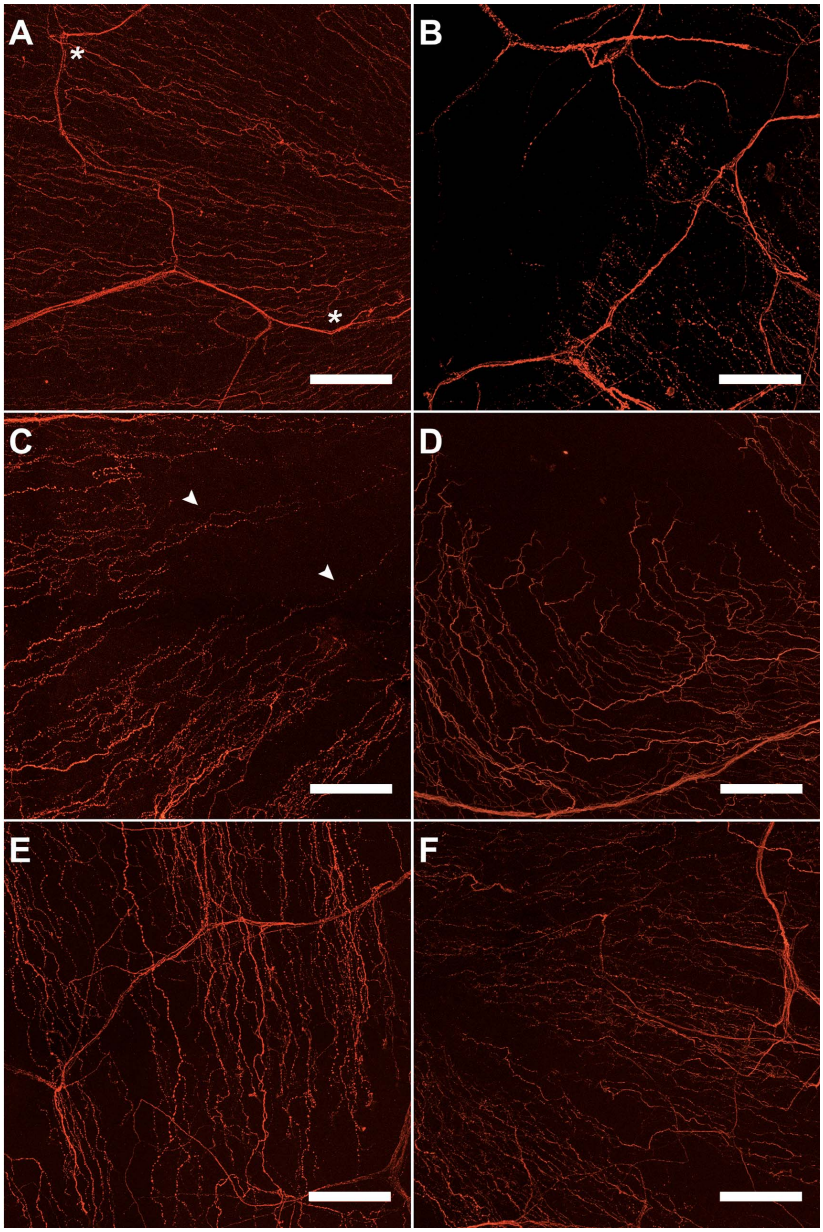

Figure 2. Subbasal and stromal corneal nerves at different times after PRK. z-stack images of whole-mount corneas stained against β-Tubulin III (*red*). Images from an intact cornea (**A**) and PRK-operated corneas at different times after PRK ([**B–F**]: T0, T3, T7, T15, and T30, respectively) are shown. *Asterisks* mark the penetration points. No subbasal nerves were observed immediately after PRK (**B**). Three days after ablation, some sprouting subbasal nerves started entering the injured area (*arrowheads*, [**C**]). *Scale bars*: 100 µm.

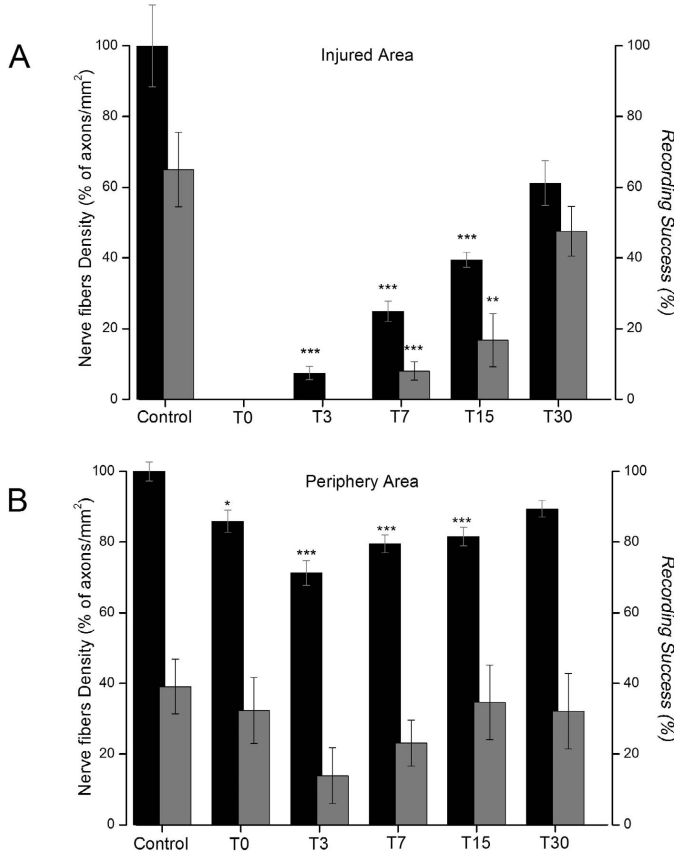

Figure 3. Density of subbasal nerve fibers (*left axis*, *black bars*) and percentage of successful attempts at recording a terminal (*right axis*, *gray bars*) in control eyes and at the different time points after PRK, in the injured area (**A**) and the peripheral, uninjured area (**B**). Nerve density is expressed as percentage of the mean number of axons/mm^2 measured in control corneas in the central (**A**) or the peripheral (**B**) cornea. Successful recording is expressed as percentage of electrophysiological recording attempts where an active corneal unit is found. Statistical analysis compared differences with control group values: **P* value < 0.05, ***P* value < 0.01, ****P* value < 0.001.

Table. Subbasal Nerve and Epithelial Penetration Point Density Values in the Injured and Peripheral Areas at Different Time Points Post PRK and in Intact Corneas (Control)

	Nerve Density, Axons/mm^2		Penetration Point Density, Points/mm^2	
Experimental Groups	**Injured Area**	**Periphery Area**	**Injured Area**	**Periphery Area**
Control, $n = 6$	574.5 ± 66.5	233.1 ± 6.3	9.9 ± 1.0	8.4 ± 0.4
T0, $n = 5$	0.0 ± 0.0*	200.0 ± 7.2†	0.0 ± 0.0*	8.1 ± 0.4
T3, $n = 4$	42.9 ± 11.0*	166.1 ± 8.2*	0.8 ± 0.5†	7.3 ± 0.3‡
T7, $n = 6$	143.0 ± 16.3*	185.4 ± 5.9*	7.9 ± 1.5	7.1 ± 0.6
T15, $n = 5$	266.5 ± 12.5*	190.0 ± 6.2*	10.0 ± 0.9	8.1 ± 0.4
T30, $n = 6$	351.6 ± 36.1‡	208.5 ± 5.4	9.4 ± 0.4	9.0 ± 0.4

Corneas were processed at 0, 3, 7, 15, and 30 days after surgery (T0, T3, T7, T15, and T30, respectively).
* *P* value < 0.001.
† *P* value < 0.05.
‡ *P* value < 0.01.

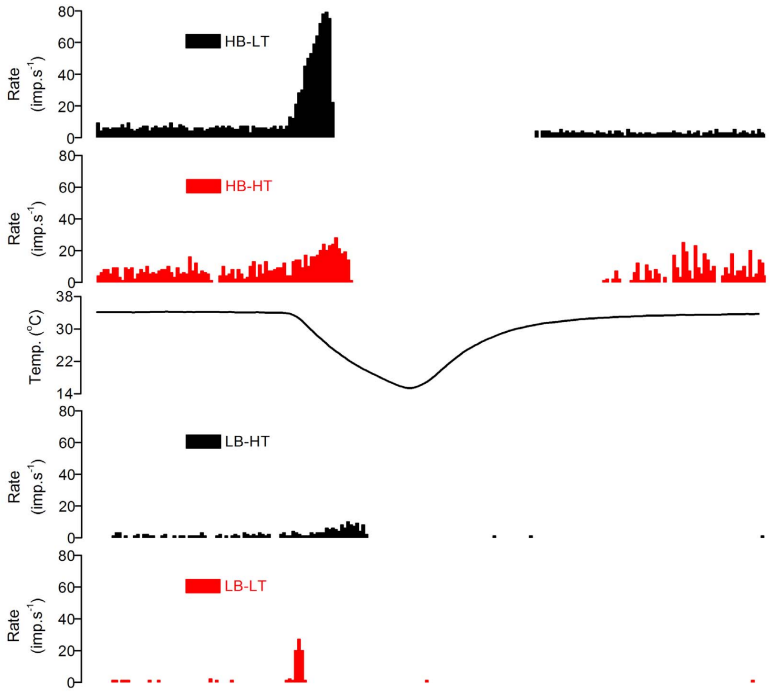

FIGURE 4. Examples of the NTI firing rate recorded in the different subclasses of cold thermoreceptor terminals at 34°C and during application of a cooling ramp down to 15°C. Traces of HB-LT and LB-HT terminals were obtained from control, uninjured mice corneas. Sample recordings of terminals exhibiting abnormal properties (high-background, high-threshold [HB-HT] and low-background, low-threshold [LB-LT] terminals, represented in *red*) were obtained from 30 days post PRK-operated corneas. Middle trace represents the perfusion solution temperature, in °C.

terminal that responded to mechanical stimulation and heat was also found.

At day 30, the overall density of subbasal nerve fibers in the injured area remained significantly lower (75.7% ± 4.1% of control corneas, $P < 0.05$) than in the central region of intact corneas (Figs. 1F, 2F, 3A; Table). Most of the nerve fibers started to organize, forming a vortex in the apex of the cornea. Nonetheless, a low number of axons still showed an erratic distribution. For the first time in the study, NTI activity was present in the injured area of all corneas tested ($n = 8$). The probability that the recording at defined points contained an active terminal was 47.5% ± 7% ($n = 8$), still below the values found in the central cornea of control eyes (65% ± 10.5%, $n = 5$) (Fig. 3A). Of the 27 active terminals found in operated corneas at T30, 5 were defined as polymodal nociceptors and 7 as cold thermoreceptors. At the remaining 15 recording sites the NTIs had a low amplitude and could not be accurately categorized.

In the corneal periphery surrounding the wounded area, the mean nerve density at T30 was similar to the same area in the intact corneas. At this time the probability of finding sites with nerve activity was 32.1% ± 10.1% (Fig. 3B; Table). Of the eight units recorded, two were characterized as cold thermoreceptors, one as polymodal, and one as a mechano-nociceptor. The remaining four units had low-amplitude NTIs, preventing reliable functional identification.

A Fraction of Cold Thermoreceptor Endings Remain Functionally Altered 30 Days After PRK

Collectively, at all times after injury, the firing of high-background cold thermoreceptor terminals found in the injured area was abnormal. HB-LT cold thermoreceptor terminals found in the injured area had on the average lower background activity and cooling response values than those of the same area seen in the healthy cornea (background activity: 3.4 ± 0.5 versus 6.1 ± 0.7 imp·s^{-1}, $P < 0.05$; cooling response: 21.5 ± 4.2 versus 34.2 ± 2.3 imp·s^{-1}, $P < 0.01$; injured, $n = 20$ versus healthy, $n = 10$). LB-HT terminals also responded less to cooling (3.3 ± 0.9 versus 6.1 ± 0.7 imp·s^{-1}, $P < 0.05$; injured, $n = 6$ versus healthy, $n = 6$). Moreover, in the injured and also in the surrounding undamaged area, we frequently observed terminals exhibiting low background activity (<1.5 imp·s^{-1} at 34°C), but combined with an abnormally low cold threshold (LB-LT). These units were observed first in the uninjured area at T3 and in the injured and uninjured area since T7. Conversely, other terminals had a high background frequency at 34°C (>1.5 imp·s^{-1}) but a cooling threshold below 30.5°C (HB-HT). Figure 4 shows an example of the firing pattern of these abnormal cold thermoreceptor terminal types. The overall incidence of abnormal units decreased during the healing period, from 37.5% 1 week after injury to approximately 22.2% 1 month later.

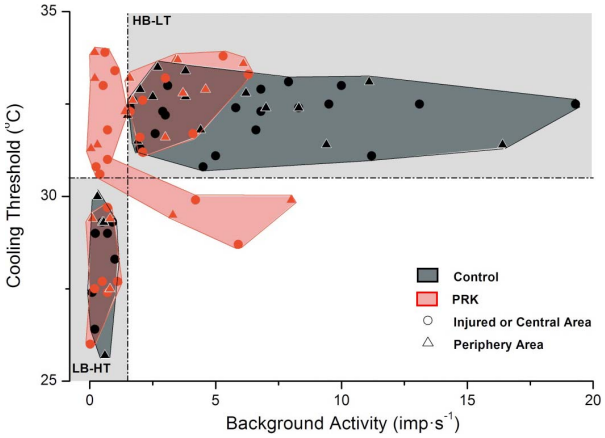

Figure 5. Distribution of corneal cold thermoreceptor terminals attendant on thermal threshold and background firing frequency. Terminals from intact, control corneas are represented with *black symbols* (*circles*, central area; *triangles*, peripheral area). Terminals recorded in PRK-operated corneas (3–30 days after surgery) are represented with *red symbols* (*circles*, terminals in the central, injured area; *triangles*, terminals of the uninjured periphery). The *horizontal* and *vertical interrupted lines* delimit respectively the values of threshold and background activity used to define terminals as HB-LT and LB-HT cold thermoreceptor types (*gray quadrants*). Some terminals of PRK-operated corneas located outside the gray quadrants of the graph possess mixed firing characteristics (high background, high threshold [HB-HT] and low background, low threshold [LB-LT]).

In Figure 5, the whole population of corneal cold thermoreceptor terminals recorded in intact corneas and in injured cornea at all postinjury days is plotted, grouped by their mean background NTI frequency at 34°C and the cooling threshold during a cooling ramp. This representation segregates clearly the canonical HB-LT thermoreceptor terminals from the LB-HT thermoreceptors, the two functional types found in intact corneas (Figs. 4, 5, shown in black). This representation also highlights the presence in PRK-treated corneas of a fraction of terminals (red symbols) that maintain the firing characteristics of typical HB-LT and LB-HT cold thermoreceptor terminals, although as indicated earlier, they present on average lower values of background activity than those of intact corneas. Figure 5 also delimits the well-defined population of abnormal cold-sensitive terminals, displaying mixed firing characteristics found in the injured and the intact area of PRK-treated corneas.

Activity of Polymodal Nociceptors in the Injured Area Reappears Only 30 Days After PRK

Endings with low background activity or silent at rest but activated by heat and mechanical stimulation were absent in the recordings performed in the injured cornea until T30. In eight corneas studied at this time, 5 of the 27 active terminals were classified as polymodal nociceptors. They presented a low background activity of 0.5 ± 0.2 imp·s^{-1} ($n = 5$). As occurs with polymodal nociceptors of the intact cornea, this background activity decreased during a cooling ramp so that the total number of impulses fired during the 45-second period before cooling (mean, 25 ± 11.8 NTIs; $n = 5$) decreased during the 45-second cooling ramp to 16.4 ± 5.4 NTIs ($n = 5$). Conversely, polymodal terminals responded clearly to heating (7.3 ± 1.9 imp/30 s before and 37.8 ± 10.7 imp/30 s during a heating ramp, $n = 5$) and clearly increased their firing rate in response to mechanical stimulation (2.8 ± 0.4 NTIs/10 s before and 22 ± 13.8 imp/10 s during mechanical stimulation).

In the periphery, polymodal nociceptor activity was also practically absent until T7, with only one terminal responding to heat and to mechanical stimulation at T3. Terminals presenting the characteristics of polymodal nociceptors were identified at T15 and T30; altogether, their incidence was lower, around 10% in lesioned versus 27% in intact corneas.

Discussion

The present work confirms the occurrence of extensive morphologic and functional damage to corneal nerves after application of the photoablation procedure used in refractive surgery, and uncovers the marked differences in time course required by corneal sensory nerve fibers of different modality (polymodal nociceptors, mechano-nociceptors, and cold thermoreceptors) to regenerate, and to recover, albeit partially, their normal responsiveness to natural stimuli. Our study additionally revealed that the functional disturbances caused by injury affect also nerve terminals outside the directly wounded area, especially in cold thermoreceptors, possibly reflecting damage by PRK to some terminal branches of parent axons that entered the wound area but that predominantly had their sensory nerve terminals in the noninjured parts of the cornea.

PRK is a procedure that completely removes the epithelium and approximately 20 μm of the anterior stroma of treated corneas, thus affecting the small and medium-sized nerve bundles running in the anterior stromal plexus, particularly its more anterior, dense part, the subepithelial plexus.[34] The laser beam directly destroys the more superficial nerve branches in the treated area, while the distal segments of axons running in a large extent outside the lesion, but affected by the laser beam, degenerate rapidly. Our work confirms previous studies reporting that within hours after PRK, nerves are totally absent from the injured area and those in the surrounding periphery are reduced in number.[16]

Investigative Ophthalmology & Visual Science

In human patients, nerve regeneration is slow. Subbasal nerve fiber bundles visualized with tandem scanning confocal microscopy are present only in 17% of the corneas 1 month after PRK, and the density of these nerve fibers is 98% less than preoperatively. After approximately 3 months, no branched nerve fibers can be seen in the center of the ablation zone; mean subbasal nerve density remains reduced by 59% at 1 year, when compared with preoperative values.[18,35] By 2 years, subbasal nerve density after PRK is similar but morphologic alterations are still present even 5 years after PRK.[36] Despite the timescale differences in regeneration speed between mice and humans, our study showed that recovery of nerve fiber density in the cornea of mice following PRK is also slow, and 1 month later has not fully reestablished the original architecture of corneal innervation.

Maintenance and remodeling of mature axons depend under normal circumstances on extrinsic signals from the environment, which activate their translational machinery, inducing the synthesis of proteins involved in the dynamic regulation of the cytoskeleton.[37] Nerve injury locally generates a cascade of retrograde signaling events that ultimately activate the transcription of genes required for axon survival and regrowth after axotomy.[38–40] Extrinsic signals acting on growth cones of the damaged axons shape the outgrowth pattern regulating the local synthesis of positive and negative regulators of cytoskeletal dynamics, thereby defining the trajectory and length of the growing fibers.[40] In addition to chemotropic cues, mechanical forces exerted by the extruding basal cells during epithelial cell proliferation accompanying corneal wound healing may also influence axonal growth. These forces are transmitted to the subbasal axons and to the reassembling epithelial basement membrane, likely affecting adhesion between epithelial cells, basement membrane, and subbasal axons and thereby, the navigation of regenerating axons.[41] Considering the numerous positive and negative regulators influencing the final trajectory and elongation of axons after injury, the slow and incomplete recovery of the prelesion innervation architecture after PRK is not surprising.[42]

Our study revealed that the appearance of sprouting axons within the injured area does not imply an immediate and parallel recovery of their function. In fact, we observed that corneal sensory terminals of different modality required variable times to recuperate responsiveness to their natural stimuli. Cold thermoreceptor terminals began to respond 1 week after surgery as occurs with mechano-nociceptors, while the first recordings of identifiable polymodal units in the injured area were obtained only 3 weeks later. It is well established that sensory ganglion neurons underlying the various somatosensory modalities possess different genetic signatures, immunocytochemical characteristics, and functional properties.[43,44] The longer time required by polymodal nociceptor neurons to restore their peripheral membrane excitability and transduction properties after PRK may reflect a distinct responsiveness of these nociceptors to the injury-triggered molecular signals responsible for rebuilding the ionic mechanisms required for the transduction and coding of specific stimuli during the regeneration process.[45] Moreover, corneal polymodal nociceptor axons are sparsely branched, generally with simple or ramifying epithelial endings.[46,47] It is therefore possible that in most cases destruction of polymodal axons by PRK affects most if not all the branches of a parent axon within the epithelium and subepithelium, thus requiring a longer time to regenerate. In contrast, cold thermoreceptor corneal axons branch very extensively and form predominantly complex endings,[24,47] a part of which may be spared from injury, thus facilitating regeneration. Still, 30 days after PRK, NTI activity of cold thermoreceptor endings within the treated area is often abnormal, suggesting that the recovery of electrophysiological properties at this time is still incomplete.

Background firing rate and dynamic sensitivity to cold of intact cold thermoreceptors depend on the level of expression of cold-activated TRPM8 channels and the modulation of their terminals' excitability by Kv and HCN channels.[48–50] It has been postulated that action potential firing of cold thermoreceptors originates within a single spatially restricted region of the nerve terminal arbor of the parent axon, where each separate branch encodes individual action potentials autonomously.[51–53]

Altered architecture of cold terminals and abnormal expression of ion channels involved in cold transduction and coding after injury likely decrease both the transducing membrane surface and the number of membrane points at which propagated impulses may generate. Both circumstances are expected to contribute to the lower background frequency and abnormal firing observed in cold thermoreceptor terminals of the injured cornea after PRK.

Notably, abnormal background activity and altered cooling responses were also observed in some of the cold thermoreceptor endings recorded into the intact cornea surrounding the PRK wound. We hypothesize that these terminals belong to cold thermoreceptor parent axons that had originally some branches extending into the operated area. Their loss after PRK reduced the total number of branches at which NTIs originate, thereby decreasing background frequency and responsiveness to cold. The same abnormal firing has been reported in cold thermoreceptor axons of very old mice, where axonal terminal branching is drastically reduced.[54]

Tearing disturbances and dryness sensation in humans appear often after PRK.[1,2] Acute, strong pain usually disappears a few days after surgery, coincident with corneal re-epithelization, which protects the intact and injured terminals against direct exposure to environmental challenges. However, sensations described as "sharp pains," "eyelid sticking to the eyeball," or "soreness of the eyelid to touch" occur 6 or more months after surgery in 5% to 25% of patients, while nearly 50% report feelings of "dryness."[55] Corneal cold thermoreceptor fibers are implicated in the regulation of basal tearing rate and have been proposed also as the source of the unpleasant dryness sensation associated with dry eye disease.[13,20,24,26] The differences in time course and characteristics of disturbances in corneal nerve activity observed in mice after PRK confirm the important role played by aberrant impulse activity in axotomized nerves for the appearance of dysesthesias following PRK[56] and lend support to the proposal that, among the different functional subclasses of corneal nerves, cold thermoreceptors are major players in the development of phantom unpleasant dryness sensation after photorefractive surgery procedures.

Acknowledgments

The authors thank the contribution of Rodolfo Madrid and James A. Brock for critical reading of the manuscript.

Supported by FC-15-GRUPIN14-141 (Consejería de Economía y Empleo, Asturias, Spain); SAF2014-54518-C3-1-R, SAF2014-54518-C3-2-R, SAF2017-83674-C2-1-R, and SAF2017-83674-C2-2-R (Ministerio de Economía, Industria y Competitividad, Spain, and European Regional Development Funds, European Union), and the Spanish "Severo Ochoa" Program for Centers of Excellence in R&D (SEV-2013-0317). Funding from Fundación Ramón Areces and Caja Rural de Asturias, Spain, and European Commission H2020 GA No. 667400 are also acknowledged.

Disclosure: **F. Bech**, None; **O. González-González**, None; **E. Artime**, None; **J. Serrano**, None; **I. Alcalde**, None; **J. Gallar**, None; **J. Merayo-Lloves**, None; **C. Belmonte**, None

References

1. Tuunanen TH, Tervo TM. Schirmer test values and the outcome of photorefractive keratectomy. *J Cataract Refract Surg*. 1996;22:702–708.
2. Ang RT, Dartt DA, Tsubota K. Dry eye after refractive surgery. *Curr Opin Ophthalmol*. 2001;12:318–322.
3. Nejima R, Miyata K, Tanabe T, et al. Corneal barrier function, tear film stability, and corneal sensation after photorefractive keratectomy and laser in situ keratomileusis. *Am J Ophthalmol*. 2005;139:64–71.
4. Kymionis GD, Tsiklis NS, Ginis H, Diakonis VF, Pallikaris I. Dry eye after photorefractive keratectomy with adjuvant mitomycin C. *J Refract Surg*. 2006;22:511–513.
5. Okamoto K, Tashiro A, Thompson R, Nishida Y, Bereiter DA. Trigeminal interpolaris/caudalis transition neurons mediate reflex lacrimation evoked by bright light in the rat. *Eur J Neurosci*. 2012;36:3492–3499.
6. Katagiri A, Thompson R, Rahman M, Okamoto K, Bereiter DA. Evidence for TRPA1 involvement in central neural mechanisms in a rat model of dry eye. *Neuroscience*. 2015;290:204–213.
7. Gallar J, Acosta MC, Moilanen JA, Holopainen JM, Belmonte C, Tervo TM. Recovery of corneal sensitivity to mechanical and chemical stimulation after laser in situ keratomileusis. *J Refract Surg*. 2004;20:229–235.
8. Nettune GR, Pflugfelder SC. Post-LASIK tear dysfunction and dysesthesia. *Ocul Surf*. 2010;8:135–145.
9. Ambrosio R Jr, Tervo T, Wilson SE. LASIK-associated dry eye and neurotrophic epitheliopathy: pathophysiology and strategies for prevention and treatment. *J Refract Surg*. 2008;24:396–407.
10. Kaminer J, Powers AS, Horn KG, Hui C, Evinger C. Characterizing the spontaneous blink generator: an animal model. *J Neurosci*. 2011;31:11256–11267.
11. Gartry DS, Muir MG, Lohmann CP, Marshall J. The effect of topical corticosteroids on refractive outcome and corneal haze after photorefractive keratectomy: a prospective, randomized, double-blind trial. *Arch Ophthalmol*. 1992;110:944–952.
12. Kirveskari J, Helinto M, Saaren-Seppala H, Renkonen R, Tervo T. Leukocyte rolling and extravasation in surgical inflammation after mechanical and laser-induced trauma in human patients. *Exp Eye Res*. 2003;77:387–390.
13. Belmonte C, Acosta MC, Merayo-Lloves J, Gallar J. What causes eye pain? *Curr Ophthalmol Rep*. 2015;3:111–121.
14. Torricelli AA, Santhanam A, Wu J, Singh V, Wilson SE. The corneal fibrosis response to epithelial-stromal injury. *Exp Eye Res*. 2016;142:110–118.
15. Rozsa AJ, Guss RB, Beuerman RW. Neural remodeling following experimental surgery of the rabbit cornea. *Invest Ophthalmol Vis Sci*. 1983;24:1033–1051.
16. Tervo K, Latvala TM, Tervo TM. Recovery of corneal innervation following photorefractive keratoablation. *Arch Ophthalmol*. 1994;112:1466–1470.
17. Erie JC. Corneal wound healing after photorefractive keratectomy: a 3-year confocal microscopy study. *Trans Am Ophthalmol Soc*. 2003;101:293–333.
18. Erie JC, McLaren JW, Hodge DO, Bourne WM. Recovery of corneal subbasal nerve density after PRK and LASIK. *Am J Ophthalmol*. 2005;140:1059–1064.
19. Belmonte C, Aracil A, Acosta MC, Luna C, Gallar J. Nerves and sensations from the eye surface. *Ocul Surf*. 2004;2:248–253.
20. Belmonte C, Nichols JJ, Cox SM, et al. TFOS DEWS II pain and sensation report. *Ocul Surf*. 2017;15:404–437.
21. Acosta MC, Tan ME, Belmonte C, Gallar J. Sensations evoked by selective mechanical, chemical, and thermal stimulation of the conjunctiva and cornea. *Invest Ophthalmol Vis Sci*. 2001;42:2063–2067.
22. Acosta MC, Belmonte C, Gallar J. Sensory experiences in humans and single-unit activity in cats evoked by polymodal stimulation of the cornea. *J Physiol*. 2001;534:511–525.
23. Acosta MC, Peral A, Luna C, Pintor J, Belmonte C, Gallar J. Tear secretion induced by selective stimulation of corneal and conjunctival sensory nerve fibers. *Invest Ophthalmol Vis Sci*. 2004;45:2333–2336.
24. Parra A, Madrid R, Echevarria D, et al. Ocular surface wetness is regulated by TRPM8-dependent cold thermoreceptors of the cornea. *Nat Med*. 2010;16:1396–1399.
25. Belmonte C, Tervo T, Gallar J. Sensory innervation of the eye. In: Levin L, Nilsson S, Ver Hoeve J, Wu S, Kaufman P, Alm A, eds. *Adler's Physiology of the Eye*. Saunders Elsevier; 2011:363–384.
26. Kovacs I, Luna C, Quirce S, et al. Abnormal activity of corneal cold thermoreceptors underlies the unpleasant sensations in dry eye disease. *Pain*. 2016;157:399–417.
27. Quallo T, Vastani N, Horridge E, et al. TRPM8 is a neuronal osmosensor that regulates eye blinking in mice. *Nat Commun*. 2015;6:7150.
28. Gallar J, Acosta MC, Gutierrez AR, Belmonte C. Impulse activity in corneal sensory nerve fibers after photorefractive keratectomy. *Invest Ophthalmol Vis Sci*. 2007;48:4033–4037.
29. Anitua E, Sanchez M, Merayo-Lloves J, De la Fuente M, Muruzabal F, Orive G. Plasma rich in growth factors (PRGF-Endoret) stimulates proliferation and migration of primary keratocytes and conjunctival fibroblasts and inhibits and reverts TGF-beta1-induced myodifferentiation. *Invest Ophthalmol Vis Sci*. 2011;52:6066–6073.
30. Alcalde I, Inigo-Portugues A, Carreno N, Riestra AC, Merayo-Lloves JM. Effects of new biomimetic regenerating agents on corneal wound healing in an experimental model of post-surgical corneal ulcers. *Arch Soc Esp Oftalmol*. 2015;90:467–474.
31. Reimondez-Troitino S, Alcalde I, Csaba N, et al. Polymeric nanocapsules: a potential new therapy for corneal wound healing. *Drug Deliv Transl Res*. 2016;6:708–721.
32. Martinez-Garcia MC, Merayo-Lloves J, Blanco-Mezquita T, Mar-Sardana S. Wound healing following refractive surgery in hens. *Exp Eye Res*. 2006;83:728–735.
33. Gonzalez-Gonzalez O, Bech F, Gallar J, Merayo-Lloves J, Belmonte C. Functional properties of sensory nerve terminals of the mouse cornea. *Invest Ophthalmol Vis Sci*. 2017;58:404–415.
34. Marfurt CF, Cox J, Deek S, Dvorscak L. Anatomy of the human corneal innervation. *Exp Eye Res*. 2010;90:478–492.
35. Erie EA, McLaren JW, Kittleson KM, Patel SV, Erie JC, Bourne WM. Corneal subbasal nerve density: a comparison of two confocal microscopes. *Eye Contact Lens*. 2008;34:322–325.
36. Moilanen JA, Vesaluoma MH, Müller LJ, Tervo TM. Long-term corneal morphology after PRK by in vivo confocal microscopy. *Invest Ophthalmol Vis Sci*. 2003;44:1064–1069.
37. Michaelevski I, Segal-Ruder Y, Rozenbaum M, et al. Signaling to transcription networks in the neuronal retrograde injury response. *Sci Signal*. 2010;3:ra53.
38. Vogelaar CF, Gervasi NM, Gumy LF, et al. Axonal mRNAs: characterisation and role in the growth and regeneration of dorsal root ganglion axons and growth cones. *Mol Cell Neurosci*. 2009;42:102–115.
39. Gumy LF, Tan CL, Fawcett JW. The role of local protein synthesis and degradation in axon regeneration. *Exp Neurol*. 2010;223:28–37.
40. Jung H, Yoon BC, Holt CE. Axonal mRNA localization and local protein synthesis in nervous system assembly, maintenance and repair. *Nat Rev Neurosci*. 2012;13:308–324.

41. Pal-Ghosh S, Pajoohesh-Ganji A, Tadvalkar G, et al. Topical Mitomycin-C enhances subbasal nerve regeneration and reduces erosion frequency in the debridement wounded mouse cornea. *Exp Eye Res*. 2016;146:361–369.
42. Namavari A, Chaudhary S, Sarkar J, et al. In vivo serial imaging of regenerating corneal nerves after surgical transection in transgenic thy1-YFP mice. *Invest Ophthalmol Vis Sci*. 2011; 52:8025–8032.
43. Lallemend F, Ernfors P. Molecular interactions underlying the specification of sensory neurons. *Trends Neurosci*. 2012;35: 373–381.
44. Usoskin D, Furlan A, Islam S, et al. Unbiased classification of sensory neuron types by large-scale single-cell RNA sequencing. *Nat Neurosci*. 2015;18:145–153.
45. Hu G, Huang K, Hu Y, et al. Single-cell RNA-seq reveals distinct injury responses in different types of DRG sensory neurons. *J Neurosci*. 2016;6:31851.
46. Alamri A, Bron R, Brock JA, Ivanusic JJ. Transient receptor potential cation channel subfamily V member 1 expressing corneal sensory neurons can be subdivided into at least three subpopulations. *Front Neuroanat*. 2015;9:71.
47. Ivanusic JJ, Wood RJ, Brock JA. Sensory and sympathetic innervation of the mouse and guinea pig corneal epithelium. *J Comp Neurol*. 2013;521:877–893.
48. Viana F, de la Pena E, Belmonte C. Specificity of cold thermotransduction is determined by differential ionic channel expression. *Nat Neurosci*. 2002;5:254–260.
49. Madrid R, de la Peña E, Donovan-Rodriguez T, Belmonte C, Viana F. Variable threshold of trigeminal cold-thermosensitive neurons is determined by a balance between TRPM8 and Kv1 potassium channels. *J Neurosci*. 2009;29:3120–3131.
50. Orio P, Parra A, Madrid R, Gonzalez O, Belmonte C, Viana F. Role of Ih in the firing pattern of mammalian cold thermoreceptor endings. *J Neurophysiol*. 2012;108:3009–3023.
51. Brock JA, Pianova S, Belmonte C. Differences between nerve terminal impulses of polymodal nociceptors and cold sensory receptors of the guinea-pig cornea. *J Physiol*. 2001;533:493–501.
52. Carr RW, Pianova S, Fernandez J, Fallon JB, Belmonte C, Brock JA. Effects of heating and cooling on nerve terminal impulses recorded from cold-sensitive receptors in the guinea-pig cornea. *J Gen Physiol*. 2003;121:427–439.
53. Carr RW, Pianova S, McKemy DD, Brock JA. Action potential initiation in the peripheral terminals of cold-sensitive neurones innervating the guinea-pig cornea. *J Physiol*. 2009;587:1249–1264.
54. Alcalde I, Íñigo-Portugués A, González-González O, et al. Morphological and functional changes in TRPM8-expressing corneal cold thermoreceptor neurons during aging and their impact on tearing in mice [published online ahead of print April 17, 2018]. *J Comp Neurol*. doi:10.1002/cne.24454.
55. Hovanesian JA, Shah SS, Maloney RK. Symptoms of dry eye and recurrent erosion syndrome after refractive surgery. *J Cataract Refract Surg*. 2001;27:577–584.
56. Belmonte C. Eye dryness sensations after refractive surgery: impaired tear secretion or "phantom" cornea? *J Refract Surg*. 2007;23:598–602.

Investigative Ophthalmology & Visual Science

Cellular/Molecular

The Immunosuppressant Macrolide Tacrolimus Activates Cold-Sensing TRPM8 Channels

José Miguel Arcas,[1] Alejandro González,[1] Katharina Gers-Barlag,[1] Omar González-González,[1,2] Federico Bech,[1,2] Lusine Demirkhanyan,[3] Eleonora Zakharian,[3] Carlos Belmonte,[1,2] Ana Gomis,[1] and Félix Viana[1]

[1]Instituto de Neurociencias de Alicante, Universidad Miguel Hernández-CSIC, 03550 San Juan de Alicante, Spain, [2]Instituto Universitario Fernández-Vega, Universidad de Oviedo & Fundación de Investigación Oftalmológica, Oviedo, Spain, and [3]Department of Cancer Biology and Pharmacology, University of Illinois College of Medicine, 1 Illini Drive, Peoria, Illinois 61605

TRPM8 is a polymodal, nonselective cation channel activated by cold temperature and cooling agents that plays a critical role in the detection of environmental cold. We found that TRPM8 is a pharmacological target of tacrolimus (FK506), a macrolide immunosuppressant with several clinical uses, including the treatment of organ rejection following transplants, treatment of atopic dermatitis, and dry eye disease. Tacrolimus is an inhibitor of the phosphatase calcineurin, an action shared with cyclosporine. Tacrolimus activates TRPM8 channels in different species, including humans, and sensitizes their response to cold temperature by inducing a leftward shift in the voltage-dependent activation curve. The effects of tacrolimus on purified TRPM8 in lipid bilayers demonstrates conclusively that it has a direct gating effect. Moreover, the lack of effect of cyclosporine rules out the canonical signaling pathway involving the phosphatase calcineurin. Menthol (TRPM8-Y745H)- and icilin (TRPM8-N799A)-insensitive mutants were also activated by tacrolimus, suggesting a different binding site. In cultured mouse DRG neurons, tacrolimus evokes an increase in intracellular calcium almost exclusively in cold-sensitive neurons, and these responses were drastically blunted in *Trpm8 KO* mice or after the application of TRPM8 antagonists. Cutaneous and corneal cold thermoreceptor endings are also activated by tacrolimus, and tacrolimus solutions trigger blinking and cold-evoked behaviors. Together, our results identify TRPM8 channels in sensory neurons as molecular targets of the immunosuppressant tacrolimus. The actions of tacrolimus on TRPM8 resemble those of menthol but likely involve interactions with other channel residues.

Key words: **cornea; neuroimmune; pain; thermoreceptor; trigeminal; TRP channel**

Significance Statement

TRPM8 is a polymodal TRP channel involved in cold temperature sensing, thermoregulation, and cold pain. TRPM8 is also involved in the pathophysiology of dry eye disease, and TRPM8 activation has antiallodynic and antipruritic effects, making it a prime therapeutic target in several cutaneous and neural diseases. We report the direct agonist effect of tacrolimus, a potent natural immunosuppressant with multiple clinical applications, on TRPM8 activity. This interaction represents a novel neuroimmune interface. The identification of a clinically approved drug with agonist activity on TRPM8 channels could be used experimentally to probe the function of TRPM8 in humans. Our findings may explain some of the sensory and anti-inflammatory effects described for this drug in the skin and the eye surface.

Introduction

Macrolide immunosuppressants are a class of natural compounds sharing a macrolide-like structure and potent immunosuppressive activity *in vitro* and *in vivo*. Tacrolimus (TAC), also known as FK506, is the best-known drug in this group. Originally isolated from the bacteria *Streptomyces tsukubaensis*, TAC binds

Received July 4, 2018; revised Nov. 2, 2018; accepted Nov. 18, 2018.

Author contributions: J.M.A., A. González, K.G.-B., E.Z., C.B., A. Gomis, and F.V. designed research; J.M.A., A. González, K.G.-B., O.G.-G., F.B., and L.D. performed research; J.M.A., A. González, O.G.-G., F.B., L.D., and F.V. analyzed data; J.M.A. wrote the first draft of the paper; J.M.A., A. González, K.G.-B., O.G.-G., F.B., L.D., E.Z., C.B., and A. Gomis edited the paper; F.V. wrote the paper.

This work was supported by Project SAF2016-77233-R and cofinanced by the European Regional Development Fund and the Severo Ochoa Programme for Centres of Excellence in R&D SEV- 2013-0317. J.M.A. was supported by Spanish Ministry of Education and Science predoctoral fellowships. K.G.-B. was supported by the International PhD Fellowships Program La Caixa-Severo Ochoa, Call 2015. We thank Ardem Patapoutian and Ajay Dhaka for providing the *Trpm8*^{EGFPf} mouse line; Carolina Roza, Katharina Zimmermann, and Francina Agosti for generous advice on setting up the mouse skin-nerve preparation; Salvador Sala and Jorge Fernández Trillo for help with the kinetic analysis; and Mireille Tora for excellent technical assistance.

The authors declare no competing financial interests.

Correspondence should be addressed to Félix Viana at felix.viana@umh.es.

https://doi.org/10.1523/JNEUROSCI.1726-18.2018

 0270-6474/19/390949-21$15.00/0

to FKBP12, a protein of the immunophilin family, and this complex acts as a potent calcineurin inhibitor, a calcium/calmodulin-dependent Ser/Thr phosphatase. Calcineurin inhibition results in the block of T-cell activation and differentiation, thus inhibiting the release of inflammatory cytokines (for review, see Rusnak and Mertz, 2000). TAC is widely used for the prevention of transplant/graft rejection. Cyclosporine is a fungal cyclic undecapeptide, structurally unrelated to TAC but sharing similar inhibitory effects on the calcineurin pathway, and also used in preventing organ rejection. Other clinical applications of TAC include their topical use in several skin disorders, including atopic dermatitis, psoriasis, and pruritus (Beck, 2005; Stull et al., 2016), and in ophthalmology for the treatment of various diseases, including Sjögren's syndrome, allergic conjunctivitis, and dry-eye disease (DED) symptoms (Fukushima et al., 2014; Wan and Dimov, 2014).

In addition to its immunosuppressive actions, previous studies suggested possible direct effects of TAC on sensory nerve endings (Senba et al., 2004). Another study postulated the activation and subsequent desensitization of TRPV1 channels by TAC (Pereira et al., 2010). Nevertheless, the mechanisms involved in TAC effectiveness for the treatment of cutaneous disorders and DED, and its molecular targets in these tissues, are presently unclear.

Here we describe the agonistic effect of TAC, but not cyclosporine, on the cold- and menthol-activated TRPM8 channel (McKemy et al., 2002; Peier et al., 2002). This polymodal, nonselective cation channel is expressed in the soma of a subset of small-diameter primary sensory neurons and their peripheral terminals (Takashima et al., 2007; Dhaka et al., 2008). Apart from cold and cooling compounds (e.g., menthol and icilin) (McKemy et al., 2002; Bödding et al., 2007; Zakharian et al., 2010), TRPM8 is also activated by the membrane lipid phosphatidylinositol 4,5-bisphosphate (PIP_2) (Liu and Qin, 2005; Rohács et al., 2005).

In addition to its well-established role in the activation of low-threshold thermoreceptors, responsible for the sensation of innocuous cold (Bautista et al., 2007; Dhaka et al., 2007), other studies showed the involvement of TRPM8 channels in noxious cold sensations and cold allodynia (for review, see Almaraz et al., 2014). TRPM8 channels also play a major role in the electrical activity of cold-sensitive corneal endings and have been implicated in the mechanisms of tearing and blinking (Parra et al., 2010; Robbins et al., 2012; Quallo et al., 2015), important players in the pathophysiology of DED (Belmonte et al., 2017). Other studies demonstrated the role of TRPM8 in menthol-induced analgesia during acute and inflammatory pain (Liu et al., 2013). A functional, truncated isoform of TRPM8 is expressed in endoplasmic reticulum of skin keratinocytes where it plays an important role in epidermal homeostasis (Bidaux et al., 2015). Recently, TRPM8 activation was shown to evoke intense itch relief in patients and animal models of chronic itch (Ständer et al., 2017; Palkar et al., 2018).

The involvement of TRPM8 in these and other common pathologies, including migraine, has made it a relevant therapeutic target, triggering major efforts in the identification of novel small-molecule modulators of TRPM8 channels (Moran and Szallasi, 2018). The list of selective antagonists has grown rapidly (for review, see Almaraz et al., 2014), and some have shown clinical efficacy in humans (Andrews et al., 2015). After the identification of menthol, several compounds where shown to have agonist activity on TRPM8, but most of them display cross pharmacology with other ion channels, especially with other members of the TRP family (Macpherson et al., 2006).

Here, we identified TAC, a clinically approved drug, as a TRPM8 agonist with direct gating of the channel. In addition, our characterization of TAC effects on TRPM8 mutants revealed important differences in its agonist effects compared with the canonical activator menthol, illuminating some novel aspects of TRPM8 function as a polymodal sensory receptor.

Materials and Methods

Animals. Studies were performed on young adult (1–4 months old) mice of either sex. Mice were bred at the Universidad Miguel Hernández Animal Research Facilities (ES-119-002001) and kept in a barrier facility under 12 h:12 h light/dark cycle with food and water *ad libitum*. WT animals were of the C56Bl6/J strain. All experimental procedures were performed according to the Spanish Royal Decree 1201/2005 and the European Community Council directive 2010/63/EU, regulating the use of animals in research.

Two transgenic mouse lines were used for calcium imaging experiments and electrophysiological recordings on DRG cultures. In *Trpm8*^{BAC}-EYFP mice, the fluorescent protein YFP is expressed under the *Trpm8* promoter (Morenilla-Palao et al., 2014). For experiments with *Trpm8 KO* mice, we used a transgenic knockin line, *Trpm8*^{EGFPf}, in which the *Trpm8* locus was disrupted and EGFP was inserted in frame with the *Trpm8* start codon (Dhaka et al., 2007). Homozygous mice (*Trpm8*$^{EGFPf/EGFPf}$) are null for TRPM8. As previously described, to enhance EGFPf expression, the lox-P-flanked neomycin selection cassette introduced into the *Trpm8* locus during the generation of the transgene was excised (Dhaka et al., 2008). Both transgenic lines allowed the identification of TRPM8-expressing cells by the expression of YFP or GFP fluorescence. Moreover, *Trpm8*$^{EGFPf/+}$ (i.e., hemizygous) allowed recordings from GFP(+) neurons with one functional copy of TRPM8. The genotype of transgenic mice was established by PCR.

Culture and transfection of mammalian cell lines. Human embryonic kidney 293 cells (HEK293) were maintained in DMEM plus Glutamax, supplemented with 10% FBS and 1% penicillin/streptomycin, incubated at 37°C in a 5% CO_2 atmosphere. HEK293 cells were plated in 24-well dishes at 2×10^5 cells/well and transiently transfected with Lipofectamine 2000 (Thermo Fisher Scientific). When necessary, we cotransfect the cells with 1 μg of TRPM8 channel plasmid (from different species) and 0.5 μg of GFP plasmid. For the transfection, 2 μl of Lipofectamine 2000 was mixed with the DNA in 100 μl of OptiMem (Thermo Fisher Scientific), a reduced serum media. Electrophysiological and calcium imaging recordings took place 24–36 h after transfection. The evening before the experiment, cells were trypsinized (0.25% trypsin-EGTA) and reseeded at lower density in 12-mm-diameter glass coverslips previously treated with poly-L-lysine.

The expression vectors used and their source were as follows: mouse TRPM8 (NM_134252) in pcDNA5, kindly provided by Ardem Patapoutian (Scripps Research Institute), was used as a WT TRPM8. A menthol-insensitive mutant (Y745H) and an icilin-insensitive mutant (N799A) were obtained by site-directed mutagenesis from this WT construct as described previously (Mälkiä et al., 2009). Point mutations were confirmed by sequencing of the plasmids and posterior analysis with Lasergene software (DNASTAR). Human TRPM8 in pcDNA3 (Veit Flockerzi, Saarland University), human TRPA1 in pCMV6-AC-GFP vector (Viktorie Vlachova, Czech Academy of Sciences), mouse mycTRPM3-IRES-GFP (Stefan Phillip, Saarland University), and rat TRPV1 in pcDNA3 (Davis Julius, University of California–San Francisco) were also transiently transfect in HEK293 cells using the same techniques.

HEK293 cells stably expressing rat TRPM8 channels (CR#1 cells) (Brauchi et al., 2004) were cultured in DMEM containing 10% of FBS, 1% penicillin/streptomycin, and 450 μg/ml geneticin (G418).

DRG cultures. Adult mice of either sex (1–4 months) were anesthetized with isoflurane and decapitated. The spinal cord was isolated, and DRGs were dissected out from all spinal segments and maintained in ice-cold HBSS solution. After isolation, DRGs were incubated with collagenase Type XI (Sigma-Aldrich) and dispase II for 30–45 min in Ca^{2+}- and Mg^{2+}-free HBSS medium at 37°C in 5% CO_2. Thereafter, DRGs were mechanically dissociated by passing 15–20 times through a 1 ml pipette

tip and filtered through a 70 μm nylon filter. Neurons were harvested by centrifugation at 1200 rpm during 5 min. The resultant pellet was resuspended in MEM supplemented with 10% FBS, 1% MEM-vit, and 1% penicillin/streptomycin and plated on poly-L-lysine-coated glass coverslips. Electrophysiological and calcium-imaging recordings were performed after 12–36 h in culture.

Fluorescence Ca^{2+} imaging. Ratiometric calcium imaging experiments were conducted with the fluorescent indicator fura-2 (Thermo Fisher Scientific). DRG neurons or HEK293 cells were incubated with 5 μM fura-2 AM and 0.2% pluronic (Thermo Fisher Scientific) for 45 min at 37°C in standard extracellular solution. Fluorescence measurements were obtained on an inverted microscope (Leica Microsystems) fitted with an Imago-QE Sensicam camera (PCO). Fura-2 was excited at 340 and 380 nm (excitation time 60 ms) with a rapid switching monochromator (TILL Photonics) or an LED-based system (Lambda OBC, Sutter Instruments). Mean fluorescence intensity ratios (F340/F380) were displayed online with TillVision software (TILL Photonics) every 2 s. The standard bath solution contained the following (in mM): 140 NaCl, 3 KCl, 2.4 $CaCl_2$, 1.3 $MgCl_2$, 10 HEPES, and 10 glucose, and was adjusted to a pH of 7.4 with NaOH (290 mOsm/kg). Calcium imaging and electrophysiological recordings were performed at a basal temperature of 33 ± 1°C. Before the start of the experiment, an image of the microscopic field was obtained with transmitted light and under 460 nm excitation wavelength, to identify fluorescent cells.

Responses to agonists were calculated by measuring the peak ratio values, after subtracting the mean baseline fluorescence ratio during the 15 s previous to agonist application. Responses were scored as positive if the increase in fluorescence (Δfura-2 ratio) was >0.08.

Electrophysiology in cultured cells. Whole-cell voltage- and current-clamp recordings were obtained from mice DRG neurons or transiently transfected HEK293 cells with borosilicate glass patch-pipettes (Sutter Instruments, 4–8 MΩ resistance) and were performed simultaneously with temperature recordings. Signals were recorded with an Axopatch 200B patch-clamp amplifier (Molecular Devices) and digitized through a Digidata 1322A (Molecular Devices). Stimulus delivery and data acquisition were performed using pCLAMP9 software (Molecular Devices).

For neuronal recordings, we used the standard bath solution (see above) at a basal temperature of 33°C. The intracellular solution contained the following (in mM): 115 K-gluconate, 25 KCl, 9 NaCl, 10 HEPES, 0.2 EGTA, 1 MgCl, 1 Na_2GTP, and 3 K_2ATP, adjusted to pH 7.35 with KOH (280 mOsm/kg). In voltage-clamp recordings, amplifier gain was set at ×1, sampling rate was set to 10 kHz, and the signal was filtered at 2 kHz. Neurons were voltage-clamped at a potential of −60 mV. For current-clamp recordings, gain was set at ×10, acquisition rate was 50 kHz, and the signal was filtered at 10 kHz. Once in the whole-cell configuration, resting membrane potential was measured. In neurons that fired action potentials at rest, a small DC current was injected to bring the cell to ~−55 mV.

For electrophysiological experiments in HEK293 cells, to minimize desensitization of TRPM8 responses, a calcium-free extracellular solution was used (in mM as follows): 144.8 NaCl, 3 KCl, 1 EGTA, 1.3 $MgCl_2$, 10 HEPES, and 10 glucose (290 mOsm/kg, pH adjusted to 7.4 with NaOH). The intracellular solution for HEK293 recordings was (in mM as follows): 135 CsCl, 2 $MgCl_2$, 10 HEPES, 1 EGTA, 5 Na_2ATP, and 0.1 NaGTP, adjusted to pH 7.4 with CsOH (280 mOsm/kg). Recordings were performed at a basal temperature of 33 ± 1°C, except for the experiments in which opening and inactivation kinetics were studied in which temperature was set at 23 ± 1°C.

After a Giga-ohm seal was formed, and the whole-cell configuration was established, cells were voltage-clamped at a potential of −60 mV, and voltage ramps from −100 to 150 mV (0.62 mV/ms) were applied at 3 s intervals (0.33 Hz). For the experiments examining the opening and inactivation kinetics, 100 ms duration voltage steps were applied (from −80 to 240 mV) from a holding potential of −80 mV. The currents were acquired at 10 kHz, filtered at 2 kHz, The ramps were analyzed with WinASCD software package (Prof. G. Droogmans, Laboratory of Physiology, KU Leuven).

Temperature stimulation. Glass coverslip pieces with cultured cells were placed in a microchamber and continuously perfused with solutions warmed at 32°C-34°C. The temperature was adjusted with a Peltier device (CoolSolutions) placed at the inlet of the chamber, and controlled by a feedback device (Reid et al., 2001). Cold sensitivity was investigated with a temperature drop to ~18°C. The bath temperature was monitored with an IT-18 T-thermocouple connected to a Physitemp BAT-12 microprobe thermometer (Physitemp Instruments) and digitized with an Axon Digidata 1322A AD converter running Clampex 9 software (Molecular Devices).

Preparation and purification of the TRPM8 protein from HEK293 cells. HEK293 cells stably expressing rat myc-tagged TRPM8 were grown to 70%–80% confluence, washed, and collected with PBS. Cells were harvested and resuspended in NCB buffer, containing 500 mM NaCl, 50 mM NaH_2PO_4, 20 mM HEPES, 10% glycerol, pH 7.5, with addition of 1 mM of protease-inhibitor PMSF, 5 mM β-mercaptoethanol. Thereafter, cells were lysed by the freeze-thawing method and centrifuged at low speed to remove cell debris and DNA. The supernatant was further centrifuged at 40,000 × *g* for 2.5 h, and the pellet resuspended in NCB buffer with addition of a protease inhibitor mixture (Roche Diagnostics), 0.1% Nonidet P40 (Roche Diagnostics), and 0.5% dodecyl-maltoside (DDM) (Calbiochem). The suspension was incubated overnight at 4°C on a shaker with gentle agitation and then centrifuged for 1 h. at 40,000 × *g*. Further, the TRPM8 protein was purified by immunoprecipitation with anti-Myc-IgG conjugated to A/G-protein magnetic beads (Thermo Fisher Scientific), following the procedure provided by the manufacturer. All steps of purification were performed at 4°C. For the planar lipid bilayers experiments, the protein was eluted with NCB-elution buffer, containing 0.03% lauryl maltose neopentyl glycol (LMNG) and Myc-peptide (150 μg/ml).

Planar lipid bilayer measurements. Planar lipid bilayers measurements were performed as previously described (Zakharian et al., 2010; Asuthkar et al., 2015). Planar lipid bilayers were formed from a solution of synthetic 1-palmitoyl-2-oleoyl-glycero-3-phosphocholine and 1-palmitoyl-2-oleoyl-glycero-3-phosphoethanolaminein (Avanti Polar Lipids) in a 3:1 ratio in n-decane (Sigma-Aldrich). The solution was used to paint a bilayer in an aperture of ~150 μm diameter in a Delrin cup (Warner Instruments) between symmetric aqueous bathing solutions of 150 mM KCl, 0.2 mM $MgCl_2$, 1 μM $CaCl_2$, 20 mM HEPES, pH 7.4, at 22°C. All lipid bilayer experiments were performed in the presence of PIP_2, unless specifically omitted as indicated: 2.5 μM DiC8-PIP_2 (Cayman Chemical) dissolved in water was added to both compartments. All salts were ultrapure (>99%) (Sigma-Aldrich). Bilayer capacitances were in the range of 50–75 pF. After the bilayers had been formed, the TRPM8 protein from the micellar suspension (20 ng/ml) was added by painting to both compartments. Unitary currents were recorded with an integrating patch-clamp amplifier (Axopatch 200B, Molecular Devices). The trans solution (voltage command side) was connected to the CV 201A head stage input, and the *cis*-solution was held at virtual ground via a pair of matched Ag-AgCl electrodes. Currents through the voltage-clamped bilayers (background conductance < 1 pS) were filtered at the amplifier output (low pass, −3 dB at 10 kHz, 8-pole Bessel response). Data were secondarily filtered at 100 Hz through an 8-pole Bessel filter (950 TAF, Frequency Devices) and digitized at 1 kHz using an analog-to-digital converter (Digidata 1322A, Molecular Devices), controlled by pClamp10.3 software (Molecular Devices). Single-channel conductance events, all points' histograms, open probability, and other parameters were identified and analyzed using the Clampfit10.3 software (Molecular Devices).

Isolated skin nerve preparation. Extracellular recordings from single cutaneous primary afferent axons in an isolated mouse skin-saphenous nerve preparation were obtained following previously published procedures (Roza et al., 2006; Zimmermann et al., 2009). In brief, adult male C57BL/6J mice were killed by cervical dislocation, and the hairy skin from either hindpaw, with the saphenous nerve attached, was dissected free from underlying muscles and placed in a custom made Teflon recording chamber with the corium side up (Zimmermann et al., 2009).

The chamber containing the preparation was continuously superfused at a rate of 4 ml/min with oxygenated external solution consisting of the following (in mM): 107.8 NaCl, 26.2 $NaHCO_3$, 9.64 sodium gluconate, 7.6 sucrose, 5.55 glucose, 3.5 KCl, 1.67 NaH_2PO_4, 1.53 $CaCl_2$, and 0.69

$MgSO_4$, which was adjusted to pH 7.4 by continuously gassing with 95% oxygen/5% CO_2. Temperature of the solution was maintained ~34°C with a SC-20 in-line heater/cooler system, driven by a CL-100 bipolar temperature controller (Warner Instruments).

After pulling back the perineurum with Dumont #5SF forceps, a small bundle of fibers was aspirated into a patch-pipette connected to a high gain AC differential amplifier (model DAM 80; World Precision Instruments). A reference electrode was positioned inside the chamber. Input signals were amplified, digitized (CED Micro1401-3; Cambridge Electronic Design) at 25 kHz and stored in the hard drive of a PC for off-line analysis. For recording and off-line analysis, the Spike 2 software package was used (Cambridge Electronic Design).

A small, cone-shaped piece of frozen external solution was moved slowly over the corium side of the skin and used to identify cold spots: brisk thermoreceptor fiber activity was evoked by the ice cone when in the immediate vicinity of the receptive field, and this activity stopped shortly after removing the stimulus. Cold spots identified in this way where then isolated from the surrounding tissue with a small ABS thermoplastic ring, and delivery of the subsequent cold and chemical stimuli was restricted to a circular area (5 mm diameter) of the skin. Cold stimuli were performed with solutions flowing through a Peltier system custom-designed to deliver a small volume of solution inside the ring isolating the skin area. Starting from a baseline temperature of 34°C–35°C, the temperature reached ~12°C in ~50 s.

In control conditions, at the baseline temperature of 34°C–35°C, cold thermoreceptors were silent, firing action potentials during the cooling ramp. The cold threshold was defined as the temperature corresponding to the first spike during a cooling ramp. When chemical sensitization led to the appearance of ongoing activity already at basal temperature, cold threshold was taken as the mean temperature during the 60 s preceding the start of the cooling ramp. Chemical sensitivity of single fibers was tested with consecutive applications of TAC (30 μM), followed by menthol (50 μM) after a period of wash. Chemical sensitivity during recordings at 34°C was defined as the presence of at least 20 spikes during a period of 2 min before the cooling ramp. To explore their effects on cold sensitivity, a cold temperature ramp was also applied in the presence of TAC or menthol.

Extracellular recording of corneal nerve terminals. Adult C57BL/6J mice (3–6 months old; $n = 10$) were killed by cervical dislocation, their eyes extracted, mounted in a small chamber, and continuously perfused with an oxygenated solution (~310 mOsm/kg) of the following composition (in mM): 128 NaCl, 5 KCl, 1 NaH_2PO_4, 26 $NaHCO_3$, 2.4 $CaCl_2$, 1.3 $MgCl_2$, and 10 D-glucose. The solution was bubbled with carbogen gas (5% CO_2 and 95% O_2) and maintained at the desired temperature with a Peltier device.

A broken patch-pipette, mounted on a micromanipulator and connected to a high-gain amplifier (Neurolog NL104, Digitimer), was gently pressed against the corneal surface to obtain extracellular recordings of single cold-sensitive corneal nerve terminals *in vitro*, as described previously (Parra et al., 2010; González-González et al., 2017). Recordings were digitized at 10 kHz and stored in a computer using a CED micro 1401 interface and Spike 2 software (both from Cambridge Electronic Design).

The corneal surface was systematically explored with the recording microelectrode until the isolation of spontaneous activity. Starting from a basal temperature of 34°C, the bath temperature was lowered in a staircase fashion to 30°C and 25°C and maintained at each level for ~3 min. After returning to 34°C, the eye was bathed in 30 μM TAC and the staircase of low temperatures repeated. Each cornea was only exposed once to the drug.

Behavioral assessment of temperature sensitivity. Male C57BL/6J mice (2–3 months old) were obtained from The Jackson Laboratory and bred in house. The TRPM8 KO line was the same used in the cellular studies and kept on a C57BL/6J background (Dhaka et al., 2007). Mice were housed in large cages (1290D Eurostandard Type III) with food and water *ad libitum*. Animals were tested between 8:30 A.M. and 11:00 A.M. Before testing, animals were acclimatized to handling and being held in a lightly restrained position for 30 s on a flat surface at room temperature. For baseline measurements, each hindpaw was placed individually in contact with the surface of a Peltier-regulated metal plate (Bioseb cold/hot plate) set to 10°C, and the withdrawal latency was measured with a cutoff time of 30 s (Menéndez et al., 2002). The mean of the two paws was calculated and taken as the baseline (i.e., naive) value for each mouse. Thereafter, each mouse received vehicle (8% ethanol, 2% Cremophor in saline) in one of their paws and either menthol (1%) or TAC (1%) in the other one. Solutions were injected intraplantarly in a volume of 25 μl. Animals were returned to their cages, and each paw was tested again 20 min after injections. In TRPM8 KO mice, the experiments were identical, except that menthol was not injected in these animals. In all cases, the experimenter was blind to the treatment when doing the measurements.

Behavioral assessment of blinking. Adult male C57BL/6J or *Trpm8*$^{-/-}$ (Dhaka et al., 2008) mice were lightly restrained, and 5 μl of saline, vehicle (8% ethanol, 2% Cremophor in saline), TAC (1%), or an hyperosmolar (785 mOsm/kg) solution of saline supplemented with NaCl was applied to one eye from the tip of a graduated micropipette (Gilson Pipetman P20). The blinking of that particular eye was recorded using a Logitech HD webcam camera at 30 frames per second. The solutions were then removed and the mice returned to their home cages and left undisturbed for at least 5 h between each experiment. Each animal was tested in morning and afternoon sessions, alternating the left and right eyes. Recordings were replayed at slow motion on a computer screen, and the number of blinks was counted over a 2 min period. Counting started 3 s after the application, as there were always some blinks associated with the application of the drop. Quantification of the number of blinks was performed independently by 2 observers on 100 videos. The correlation coefficient (r) for both measurements was 0.996.

Behavioral assessment of tearing. Adult male C57BL/6J mice ($n = 10$) were anesthetized by intraperitoneal injection of a mixture of ketamine hydrochloride (80 mg/kg, Imalgene 1000; Merial Laboratorios) and xylazine hydrochloride (5 mg/kg, Rompun; Bayer Hispania). Basal tear flow was measured in both eyes, after consecutive applications of a drop (2 μl), using a graduated micropipette (Gilson Pipetman P2), of either saline, vehicle (8% ethanol, 2% Cremophor in saline), and TAC (1%), in this order, using phenol red threads (Zone-Quick, Menicon Pharma). Each solution was applied for 2 min. Thereafter, excess fluid was removed using a sterile absorbent swap (Sugi Eyespear pointed tip, Kettencach). After a rest period of 5 min, a phenol red thread was gently placed between the lower lid and the bulbar conjunctiva at the nasal angle during 1 min. To quantify the staining of the threads, the wetted length was measured under a stereomicroscope. After 2 additional minutes, a new solution was applied. One week later, the protocol was repeated in some of the same animals ($n = 5$) but applying saline solution in the three consecutive tests.

Chemicals. TAC, also known as FK506 (LC Laboratories) was prepared in a DMSO stock (50 mM) and was dissolved in prewarmed (50°C) control solution. When TAC was added to the external solution, a white cloud of precipitation appeared and gentle shaking was applied until total dissolution was obtained. Due to its poor solubility in water, a solution of 30 μM TAC was the highest concentration tested. The stock of cyclosporine (LC Laboratories) was also 50 mM in DMSO. Menthol (Scharlau), BCTC (4-(3-chloro-2-pyridinyl)-*N*-[4-(1,1-dimethylethyl)phenyl]-1-piperazinecarboxamide; Tocris Bioscience), AMTB (*N*-(3-aminopropyl)-2-[(3-methylphenyl)methoxy]-*N*-(2-thienylmethyl)benzamide hydrochloride; Tocris Bioscience), M8-B (*N*-(2-aminoethyl)-*N*-[[3-methoxy-4-(phenylmethoxy)phenyl] methyl]-2-thiophenecarboxamide hydrochloride), pregnenolone sulfate (Tocris Bioscience), allyl isocyanate (AITC; Sigma-Aldrich), and capsaicin (8-methyl-*N*-vanillyl-*trans*-6-nonenamide; Sigma-Aldrich) were prepared as stocks and stored at −20°C. For *in vivo* experiments, a 10% (100 mg/ml) stock of TAC was prepared in 80% ethanol, 20% Cremophor in PEG-60 Hydrogenated Castor Oil (BASF), and diluted to 1% in saline on the day of the experiment. The final solution had a homogeneous milky white color without precipitations.

Experimental design and statistical analysis. To estimate shifts in the voltage dependence of TRPM8 activation, current-voltage (I–V) relationships obtained from repetitive (0.33 Hz) voltage ramps (−100 to 150

mV, 400 ms duration) were fitted with a function that combines a linear conductance multiplied by a Boltzmann activation term as follows:

$$I = G \times (V - E_{rev})/(1 + \exp((V_{1/2} - V)/dx))$$

where G is the whole-cell conductance, E_{rev} is the reversal potential of the current, $V_{1/2}$ is the potential for half-maximal activation, and dx is the slope factor. The G value obtained for a high menthol concentration (800 μM) was taken as G_{max} and was used for the representation of G/G_{max} curves.

For the fitting of G/G_{max} curves extracted from the voltage pulses protocol, a Boltzmann equation was used as follows:

$$G/G_{max} = A2 + (A1 - A2)/(1 + \exp((V_m - V_{1/2})/dx))$$

where A2 is the maximal normalized conductance, A1 is the minimal normalized conductance, V_m is the test potential, $V_{1/2}$ is the potential for half-maximal activation and dx is the slope factor.

Conductance-voltage (*G–V*) curves were constructed from the *I–V* curves of individual cells by dividing the evoked current by the driving force, according to the following equation:

$$G = I/(V_m - V_{rev})$$

where V_m is the testing potential and V_{rev} is the reversal potential of the current.

The threshold temperatures were estimated as the first point at which the measured signal (F340/F380 or current) deviated by at least 4 times the SD of its baseline. All fittings were performed with the Levenberg–Marquardt method implemented in the Origin 8.0 software. Data are reported as mean ± SEM. When comparing two means, statistical significance ($p < 0.05$) was assessed by Student's two-tailed *t* test. For multiple comparisons of means, one-way ANOVAs were performed, followed by Bonferroni's *post hoc* analysis, using Prism version 4.00 for Windows (GraphPad Software).

Results

TAC activates recombinant TRPM8 channels

To evaluate the agonist effect of TAC on TRPM8, we performed intracellular Ca^{2+} imaging experiments on HEK293 cells stably expressing rat TRPM8 channels. As shown in Figure 1*A*, *B*, TAC produced a dose-dependent activation of TRPM8, with an estimated EC_{50} of 14.1 ± 25.9 μM ($n = 105$ cells). Due to its poor solubility in aqueous solutions, it was not possible to test TAC at higher concentrations. At low concentrations, the calcium response evoked by TAC was sustained, whereas at higher concentrations there was some desensitization during agonist application, similar to the results observed with other chemical agonists of TRPM8 (e.g., menthol) (Rohács et al., 2005). No changes in Ca^{2+} levels were observed when TAC was applied in the absence of external Ca^{2+} (data not shown), indicating that Ca^{2+} influx rather than Ca^{2+} release is responsible for TAC-induced elevation in cytosolic Ca^{2+}.

TRPM8 is activated by cold temperature (McKemy et al., 2002; Peier et al., 2002), and menthol potentiates responses to cold (Voets et al., 2004; Mälkiä et al., 2007). Similarly, TAC produced a dose-dependent potentiation of cold-evoked responses in mouse TRPM8, with effects evident at 1 μM and saturation at ~10 μM (Fig. 1*C*,*D*). At 10 μM, peak amplitude of cold-evoked responses increased approximately fourfold with respect to responses in control ($p < 0.005$) (Fig. 1*D*). A closer inspection of TRPM8-evoked $[Ca^{2+}]_i$ responses during cooling pulses revealed that TAC, at concentrations of 10–30 μM, produced a marked shift in the threshold for cold-evoked responses toward warmer temperatures. The average shift was ~7°C for the highest concentration tested, changing from 21.9 ± 0.9°C in control solution to 29.1 ± 0.5°C in 30 μM TAC ($n = 15$, $p < 0.005$).

We also explored the sensitivity of human TRPM8 to TAC. As shown in Figure 1*E*, TAC (30 μM) produced $[Ca^{2+}]_i$ elevations in HEK293 cells transiently expressing hTRPM8, and this activation was not observed in untransfected cells (Fig. 1*E*). A summary of the effects of TAC, menthol, and cold on hTRPM8 is shown in Figure 1*F*.

In contrast to the effects of TAC, cyclosporine (30 μM), a structurally unrelated calcineurin inhibitor, had no effect on HEK293 cells stably expressing rat TRPM8 channels (Fig. 1*G*,*H*).

Together, these results indicate that the immunosuppressant TAC acts like a potent cold-mimetic compound on TRPM8 channels of different mammalian species by a mechanism independent of its canonical signaling pathway.

TAC activates TRPM8 currents

In whole-cell patch-clamp recordings, application of 30 μM TAC activated robust whole-cell currents in HEK293 cells expressing mouse TRPM8 (Fig. 2*A*). The *I–V* relationship of the TAC-activated current showed strong outward rectification and a reversal potential close to 0 mV, in line with the previously described properties of TRPM8 (Fig. 2*B*) (Voets et al., 2004; Mälkiä et al., 2007). Confirming the results obtained in calcium imaging experiments, cold-evoked inward and outward currents were strongly potentiated in the presence of TAC (Fig. 2*A*,*B*), leading to large inward (−8.3 ± 1.7 pA/pF cold vs −101.2 ± 30.9 pA/pF TAC plus cold) and outward currents (437 ± 47 pA/pF cold vs 597 ± 59 pA/pF TAC plus cold) ($n = 7$, $p < 0.01$) (Fig. 2*C*). Similar results were observed in HEK293 cells transfected with human TRPM8. In cells expressing hTRPM8, TAC (30 μM) activated a rectifying nonselective current, and cold-evoked currents were strongly potentiated by TAC: −78.7 ± 13.4 pA/pF versus −121.9 ± 18.3 pA/pF at −100 mV ($n = 8$, $p < 0.0001$) and 493 ± 26.2 pA/pF versus 594.3 ± 55.5 pA/pF at 100 mV ($n = 8$, $p = 0.0159$).

To confirm the agonism of TAC on TRPM8 channels, we tested the effect of AMTB, a selective TRPM8 antagonist. As shown in Figure 2*D*, the responses to TAC were fully suppressed by 10 μM AMTB (352 ± 55 pA/pF in TAC vs 16 ± 3 pA/pF in TAC plus AMTB) ($n = 6$, $p < 0.01$). AMTB also reduced the voltage-dependent activation of TRPM8 at the baseline temperature of 33°C. During combined application of cooling and TAC, the blocking effect of AMTB was only partial (Fig. 2*D–F*).

Biophysical characterization of TAC effects on TRPM8 gating

Previous studies showed that low temperature and menthol activate TRPM8 channels by producing a shift in the voltage dependence of activation toward more negative potentials (Brauchi et al., 2004; Voets et al., 2004), whereas antagonists have the opposite effect (Mälkiä et al., 2007). Recently, Janssens et al. (2016) applied kinetic analysis to describe the mechanisms whereby chemical ligands impact on TRPM8 channel gating, and differentiated between two types of agonists: those stabilizing the open channel (e.g., menthol) and those that cause a destabilization of the closed state (e.g., AITC). We used mouse TRPM8 heterologously expressed in HEK293 to characterize the effects of TAC (30 μM) on voltage dependence and channel gating and compared the effects of TAC, menthol, and AITC. Whole-cell recordings during steps from −80 to 240 mV were obtained at room temperature (23 ± 1°C), leading to substantial baseline activation of TRPM8. Menthol was applied at 10 μM, TAC at 30 μM, and AITC at 10 mM, concentrations that gave rise to similar steady-state TRPM8 current amplitudes. Following the sequential application of the three agonists, the voltage protocol was

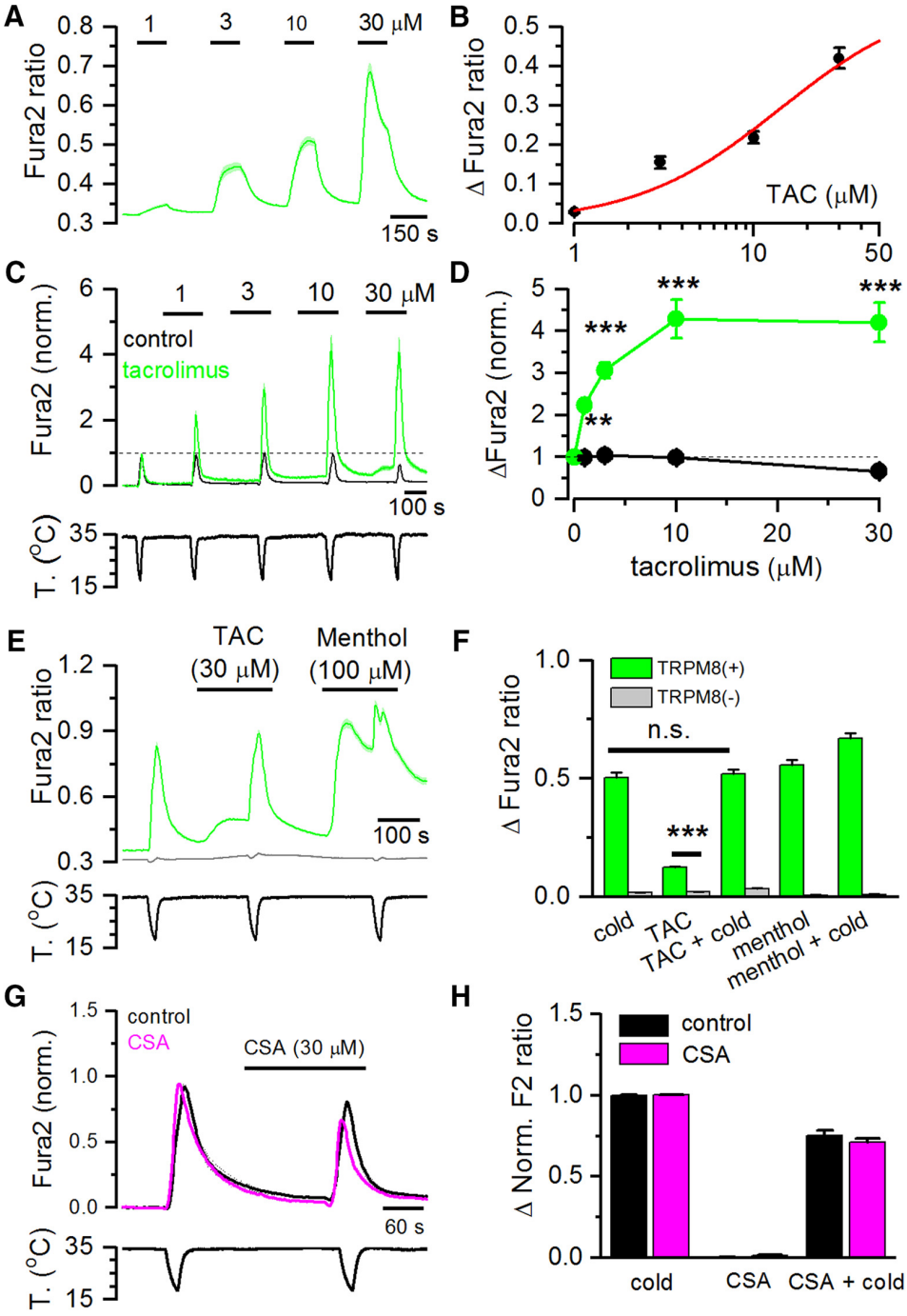

Figure 1. TAC activates recombinant TRPM8 channels and potentiates cold-evoked responses. ***A***, Average ± SEM fura-2 ratio changes in HEK293 cells stably expressing rat TRPM8 during sequential application of TAC at different concentrations ($n = 105$). ***B***, Dose–response curve of TAC effects on TRPM8-expressing cells. Data have been fitted with a logistic function ($EC_{50} = 14.1 \pm 25.9\ \mu M$). ***C***, Average ± SEM time course of fura-2 ratio in HEK293-expressing mouse TRPM8 during consecutive application of cold pulses in control solution (black trace, $n = 15$) or in the presence of increasing TAC concentrations (green trace, $n = 16$). Bottom, Time course of the corresponding temperature ramps. In the absence of TAC, the response to cold was relatively stable, whereas in the presence of TAC, the response to cold was strongly sensitized. Responses in individual cells have been normalized to their response to the first cooling pulse. ***D***, Summary plot of the effect of different doses of TAC on the amplitude of cold-evoked responses in mTRPM8 cells. $^{**}p < 0.01$ (ANOVA test in combination with Bonferroni's *post hoc* test). $^{***}p < 0.001$ (ANOVA test in combination with Bonferroni's *post hoc* test). ***E***, Average ± SEM fura-2 ratio responses to cold, TAC (30 μM), and menthol (100 μM) in HEK293 cells transiently transfected with human TRPM8 and GFP. Green represents GFP(+) cells ($n = 132$). Gray represents GFP(−) cells ($n = 87$). ***F***, Summary of mean responses in cells transfected with hTRPM8 (green bars) to the different agonists. Gray represents the responses of untransfected, GFP(−) cells. TAC produced a significant activation of hTRPM8 ($^{***}p < 0.001$; unpaired Student's *t* test). ***G***, Average ± SEM fura-2 ratio changes in HEK293 cells stably expressing rat TRPM8 during application of two cooling ramps. For the black traces ($n = 25$), cooling ramps were delivered in control solution. For the pink traces ($n = 107$), the second cooling ramp was applied in the presence of 30 μM cyclosporine (CSA). ***H***, Histogram summarizing the effects of cyclosporine on cold-evoked calcium responses during the protocol shown in ***G***. No significant differences were found between the cells perfused with control solution or cyclosporine (unpaired Student's *t* test).

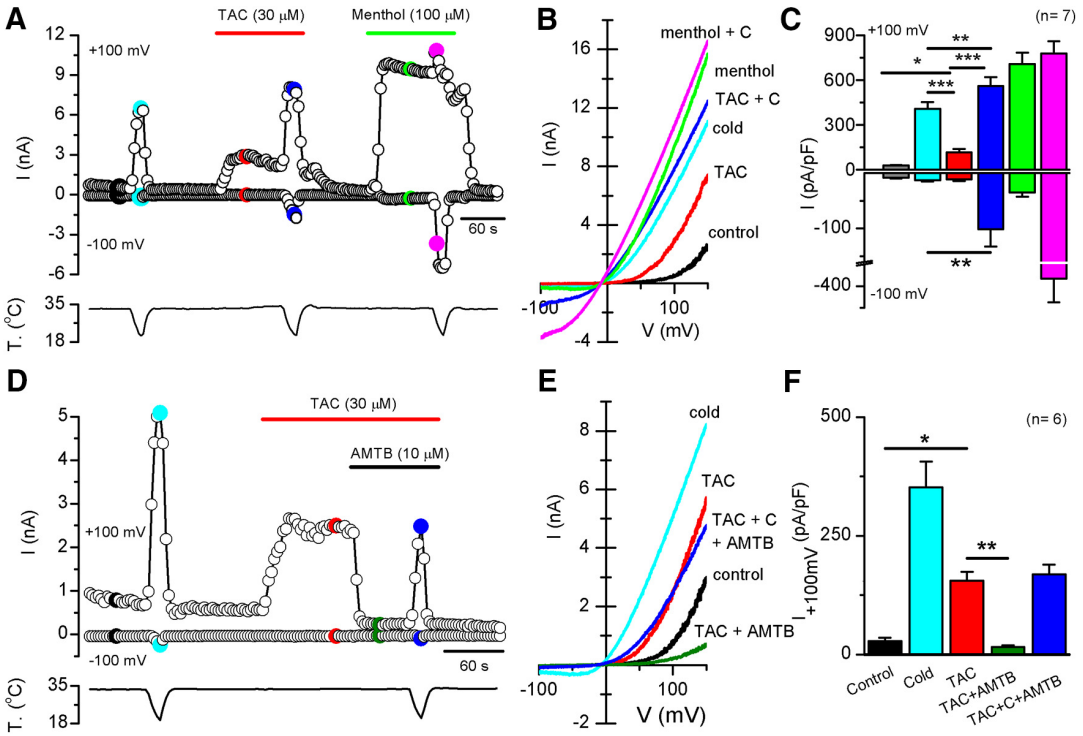

Figure 2. TAC activates TRPM8-mediated whole-cell currents in HEK293 cells. ***A***, Representative time course of whole-cell currents at −100 and 100 mV in HEK293 cell transiently transfected with mTRPM8 during application of agonists. Bottom, Simultaneous recording of the bath temperature during the experiment. ***B***, *I–V* relationship of responses shown in ***A***, obtained with a 400 ms voltage ramp from −100 to 150 mV. The color of individual traces matches the color at each particular time point in ***A***. TAC evokes a nonselective cationic current with typical TRPM8 features and potentiates the cold-evoked response. ***C***, Bar histogram summarizing the mean current density values at 100 and −100 mV to the different stimuli shown in ***A***, with the same color code. Statistical differences were evaluated by a one-way ANOVA, followed by Bonferroni's *post hoc* test. ***D***, Representative time course of whole-cell currents at −100 and 100 mV during a protocol in which the effect of AMTB was studied. AMTB 10 μM totally abolished TAC-evoked currents. Bottom, Simultaneous recording of the bath temperature during the experiment. ***E***, *I–V* relationship of responses shown in ***D***. The color of the *I–V* curves matches the colored time points in ***D***. AMTB also blocks the voltage-dependent activation of TRPM8 at basal temperature. ***F***, Bar histogram summarizing the mean current density values at 100 mV to the different stimuli applied in ***D***. Statistical differences were evaluated by a one-way ANOVA, followed by Bonferroni's *post hoc* test. *$p < 0.05$, **$p < 0.01$, ***$p < 0.001$.

repeated in the presence of 800 μM menthol, a saturating concentration, to obtain a G_{max} value for TRPM8 activity.

Figure 3*A* shows a representative example of a family of currents recorded in a cell expressing mTRPM8 during 100 ms voltage steps ranging from −80 to 240 mV. The average steady-state *I–V* and *G–V* curves for the different conditions are shown in Figure 3*B* and Figure 3*C*, respectively. Analysis of these curves revealed a strong leftward shift of the activation curve in the presence of the three agonists, with a change in the voltage for half-maximal activation ($V_{1/2}$) from 153 ± 7 mV in control to 106 ± 10 mV in the presence of TAC (calculated from *G–V*) (Fig. 3*D*). The shift in $V_{1/2}$ with respect to control conditions was highly significant ($p < 0.0001$). Menthol (10 μM) and AITC (10 mM) had similar effects on $V_{1/2}$ (Fig. 3*D*).

To characterize the effect of the different agonists on TRPM8 gating kinetics, we studied the changes in the time course of current activation during voltage steps to 120 mV (Fig. 3*E*) and their relaxation upon return to −80 mV (Fig. 3*F*). For a better comparison, currents were normalized to their steady-state values. Both menthol and TAC produced a clear slowing of the gating kinetics during depolarization to 120 mV and after the return to −80 mV. In contrast, AITC clearly accelerates the activation kinetics (Fig. 3*E*), without affecting the current relaxation kinetics upon repolarization to −80 mV (Fig. 3*F*). Currents in control or during AITC application were adequately fitted with a single exponential (data not shown). In contrast, the currents in TAC or menthol required a double exponential. To quantify the differences in kinetics produced by the three chemical agonists in more detail, we compared the rise time to 95% of the initial value. These results are shown in Figure 3*G*, *H* for the activation and deactivation time course, respectively.

These results show that the mechanism of action of TAC on TRPM8 gating resemble those of menthol and are different of the AITC gating mechanism (Janssens et al., 2016).

Gating of TRPM8 by TAC in planar lipid bilayers

To test the possible direct action of TAC on TRPM8 gating, we evaluated channel activity in a reconstituted system. The myc-tagged rat TRPM8 protein was purified from HEK293 cells stably expressing the channels using immunoprecipitation, and incorporated into planar lipid bilayers as previously described (Zakharian et al., 2010). Similarly to other TRPM8 agonists (Zakharian et al., 2010; Asuthkar et al., 2015), TAC led to TRPM8 channel openings only in the presence of its prime gating factor, PIP_2. Incubation of TRPM8 with TAC alone (30 μM) for a few hours (2–3 h of testing) was insufficient to activate the channel (data not shown). Similarly, PIP_2 alone (2.5 μM) did not induce channel openings at RT (data not shown). However, TRPM8 opened promptly soon after the addition of 2.5 μM PIP_2 to TAC (Fig. 4*A*). In the presence of TAC, TRPM8 exhibited outward currents with a mean slope conductance of ~31 pS, and inward conductance of ~20 pS. The TAC-induced TRPM8 channel openings also dem-

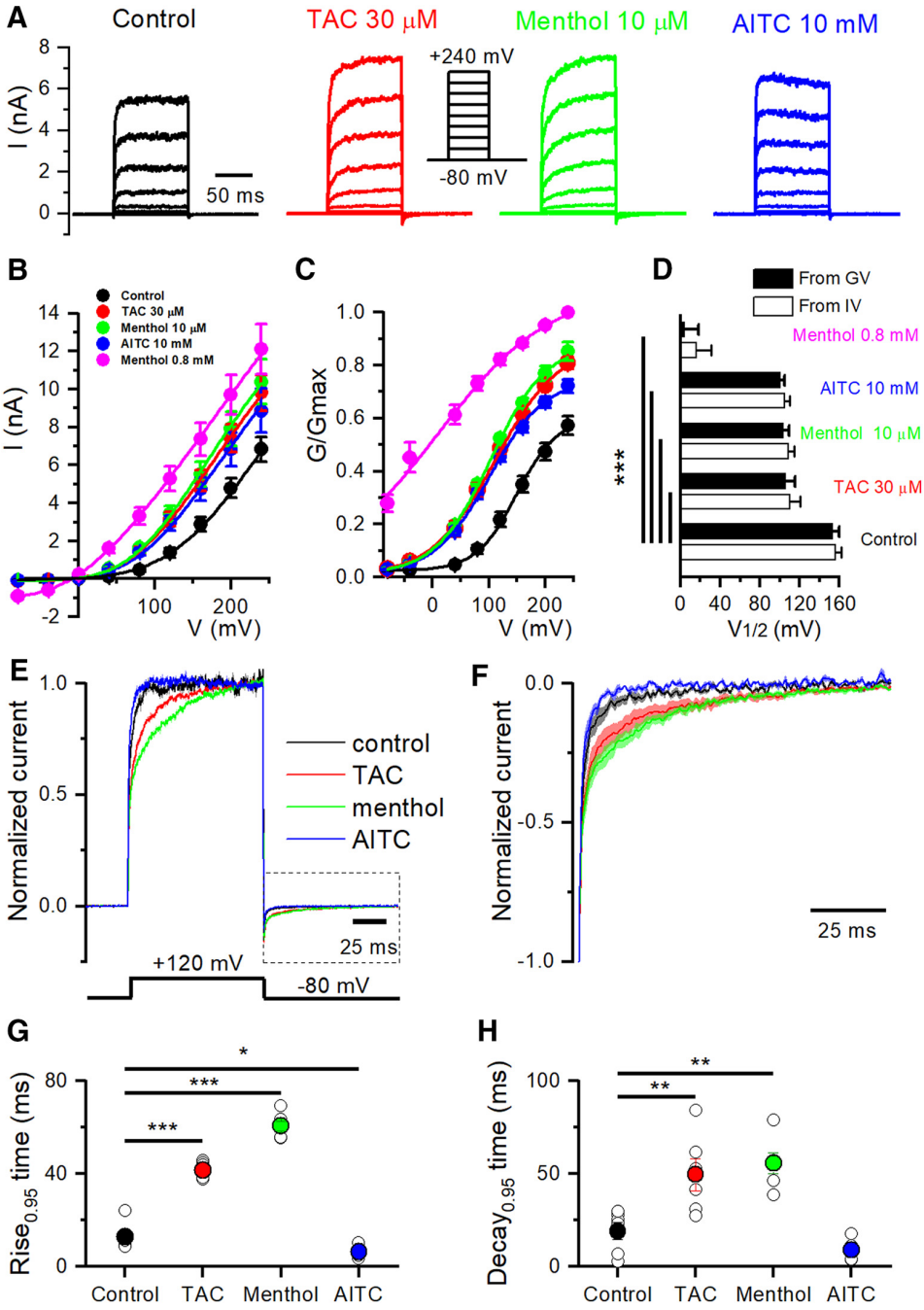

Figure 3. Biophysical characterization of TAC effects on TRPM8 gating. ***A***, Whole-cell TRPM8 currents in response to the indicated voltage step protocol (from −80 to 240 mV, Δv = 40 mV) in control conditions and in the presence of TAC (30 μM), menthol (10 μM), and AITC (10 mM) at 24°C. Note the variable effect of agonists on activation kinetics. ***B***, Averaged ($n = 6$) steady-state *I–V* curves extracted from individual cells after application of Protocol A. The lines indicate the fitting to a linearized Boltzmann equation (see Materials and Methods). ***C***, Averaged ($n = 6$) voltage dependence activation curves in control conditions and in the presence of the different agonists. Conductance (G) was calculated as the steady-state current divided by the driving force (Driving force $= V_{test} - E_{rev}$), and normalized to the estimated maximal conductance (G_{max}), which was the G value at 240 mV in the presence of 0.8 mM menthol. ***D***, Mean ($n = 6$) $V_{1/2}$ values calculated from fitting the individual *I–V* curves to the linearized Boltzmann equation (white bars) or the individual G/G_{max}–*V* curves fitted to the Boltzmann equation (black bars). All three agonists produced similar shifts in $V_{1/2}$ values at the indicated concentrations. Statistical differences were evaluated by a one-way ANOVA, followed by Bonferroni's *post hoc* test. ***E***, Averaged TRPM8 current during a voltage step from −80 to 120 mV, in control condition and in the presence of the different agonists. Currents were normalized to their steady-state amplitude after baseline subtraction. ***F***, Averaged ± SEM TRPM8 deactivation kinetics at −80 mV obtained from current tails after a voltage step to 120 mV (box bounded by dotted line in ***E***), in control condition and in the presence of the different agonists. The current was normalized to the maximum value, and baseline was subtracted. ***G***, Mean values of the current activation time course, measured from baseline to 95% amplitude, for voltage steps to 120 mV. ***H***, Mean values of current deactivation time course at −80 mV, measured from baseline to 95% amplitude, following a voltage step to 120 mV. ***F***, ***G***, Statistical differences were evaluated with a one-way ANOVA, followed by Bonferroni's *post hoc* test. *$p < 0.05$, **$p < 0.01$, ***$p < 0.001$.

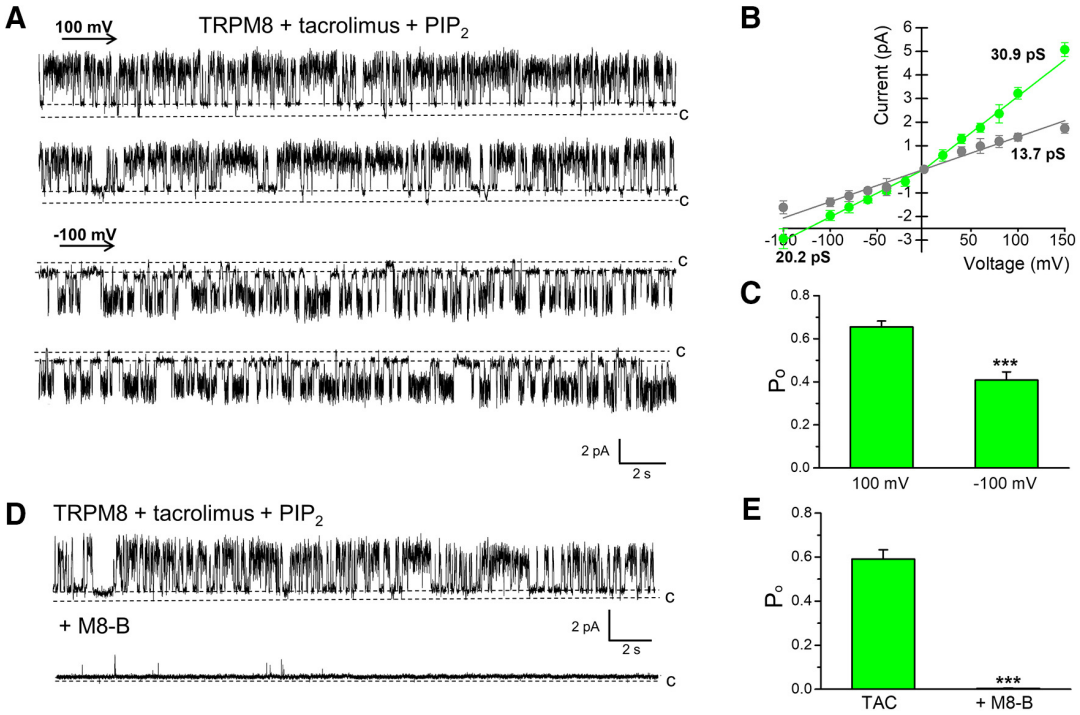

Figure 4. TAC activates purified TRPM8 in planar lipid bilayers. ***A***, Representative single-channel recordings of TRPM8 obtained at 100 mV and −100 mV showing the activation with 30 μM TAC in the presence of 2.5 μM PIP_2. ***B***, *I–V* curve of TRPM8 single-channel current during TAC activation at different membrane potentials, showing the main conductance of outward and inward currents (green trace), and a lower subconductance state (gray trace). ***C***, Bar graph represents open probability (Po) values at 100 and −100 mV in the presence of TAC and PIP_2. Data represent mean ± SEM from 13 experiments; number of events = 28,935. Po was significantly higher at 100 mV (***$p < 0.001$, paired Student's *t* test). ***D***, Representative current traces demonstrating inhibition of TAC-induced TRPM8 activity with M8-B (20 μM). TRPM8 was activated with 30 μM TAC in the presence of 2.5 μM PIP_2. Traces were obtained at 100 mV. ***E***, Bar graph summarizing the inhibition produced by M8-B on Po. Data represent mean ± SEM from four experiments (***$p < 0.001$, paired Student's *t* test).

onstrated a distinct subconductance state of ~14 pS (Fig. 4*A*,*B*). In addition to the differences in conductance for currents flowing in the inward or outward direction, an outward rectification was also evident in open probability (P_o) (Fig. 4*C*). Next, we tested the effect of a specific TRPM8 antagonist on TAC-induced channel activity. As shown in Figure 4*D*, *E*, the TRPM8 inhibitor M8-B essentially eliminated channel openings. Together, these results establish a direct agonistic action of TAC on TRPM8 channels, and also demonstrate the requirement of its activity on PIP_2.

TAC activates the menthol-insensitive TRPM8-Y745H mutant but fails to potentiate its cold response

A single tyrosine residue (Y745), located on transmembrane segment 1 according to recent Cryo-EM structural analysis (Yin et al., 2018), is essential for the activating actions of menthol on TRPM8 channels (Bandell et al., 2006; Mälkiä et al., 2009). These mutant channels are completely insensitive to menthol but retain the normal responsiveness to cold and voltage exhibited by WT channels.

Using calcium imaging, we found that TAC activates mouse TRPM8-Y745H (Fig. 5*A*,*B*). On average, the amplitude of the $[Ca^{2+}]_i$ elevation after application of 30 μM TAC, normalized to the response to a cold ramp in control conditions, was 0.20 ± 0.008 in WT channels ($n = 66$) compared with 0.17 ± 0.007 in TRPM8-Y745H ($n = 38$, $p < 0.05$). Remarkably, despite a normal response to cold or TAC, the TRPM8-Y745H mutant showed no potentiation of the cold response by TAC (ratio of TAC plus cold/cold = 1.09 ± 0.05). In contrast, the WT channel showed a strong potentiation (1.4 ± 0.08) (Fig. 5*B*, $p < 0.01$).

To confirm these differences, we examined the effects of TAC on whole-cell currents in WT and mutant channels (Fig. 5*C*). The current generated by TAC was normalized to the cold response evoked in control conditions in the same cell, at a potential of 100 mV. On average, TAC current was 0.27 ± 0.04 in WT channels and 0.30 ± 0.04 in the Y745H mutant, confirming that the TRPM8-Y745H mutants maintain their normal sensitivity to TAC. In the same cells, menthol (100 μM) had no effect, as expected for the Y745H mutant (data not shown). Moreover, whole-cell recordings confirmed that the potentiation of the cold-evoked response by TAC was absent in the Y745H mutant (WT ratio = 1.39 ± 0.05 vs TRPM8-Y745H ratio = 0.83 ± 0.09) (Fig. 5*D*).

Next, we explored TAC sensitivity in the TRPM8-N799A mutant. This residue was shown to mediate responses to icilin, a different TRPM8 agonist (Chuang et al., 2004). TRPM8-N799A mutants behaved like TRPM8 WT channels, with normal responses to TAC and the potentiation of the cold response (Fig. 5*C*,*D*), suggesting that the effects of TAC on TRPM8 do not involve the icilin-binding site.

These results suggest a mode of action of TAC independent of the putative menthol and icilin binding sites and unveil the importance of the Y745 residue in the allosteric coupling between cold and TAC activation of TRPM8.

Effects of TAC on other thermoTRP channels

Next, we tested the effects of TAC on other thermally sensitive TRP channels (Dhaka et al., 2006). As shown in Figure 6*A*, TAC (30 μM) had no activating effect on rat TRPV1 or mouse TRPM3.

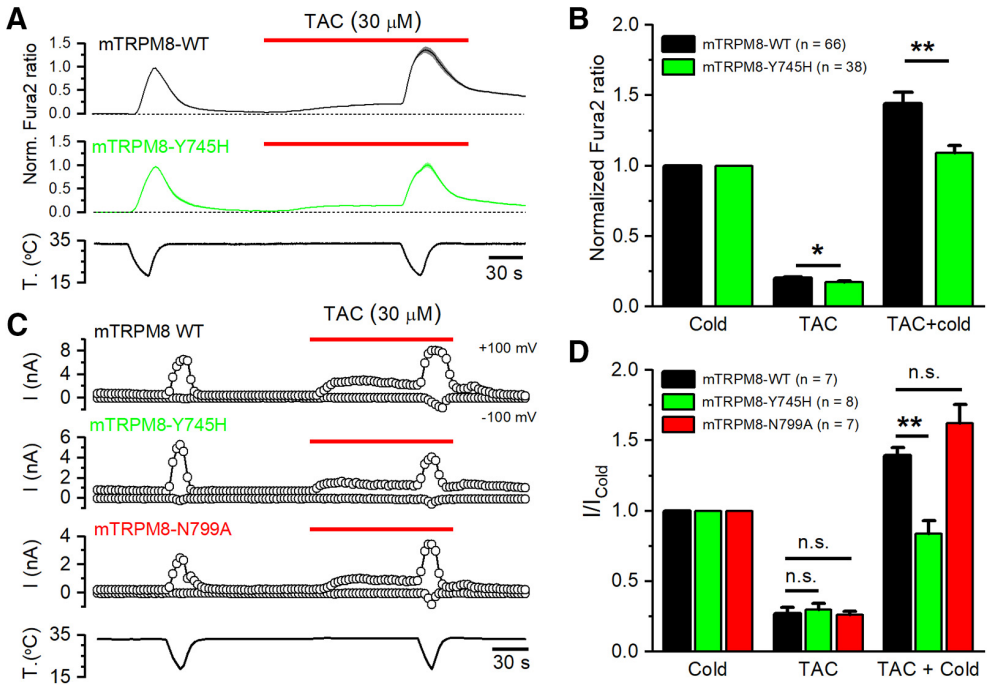

Figure 5. TAC activates the menthol- and the icilin-insensitive TRPM8 mutants. ***A***, Averaged ± SEM fura-2 ratio fluorescence of mouse TRPM8-transfected HEK293 cells during cooling, TAC (30 μM) and the combined application of TAC and cooling. Records have been baseline-subtracted and the average trace normalized to the initial response to cold. Top to bottom, Calcium responses of WT TRPM8, the menthol-insensitive TRPM8 –Y745H mutant, and a representative recording of the temperature time course in the chamber during the recording. ***B***, Histogram of mean response amplitudes to the different stimuli, normalized to the initial cold response. Note the lack of potentiation of the cold-evoked response by TAC in the menthol-insensitive mutant. Statistical differences were evaluated by an unpaired Student's *t* test. ***C***, Representative traces of whole-cell recordings exploring the effect of cold and TAC in two different TRPM8 mutants. Top to bottom, Currents, measured at −100 and 100 mV, in WT mouse TRPM8, the menthol-insensitive TRPM8 –Y745H mutant, and the icilin-insensitive TRPM8 –N799A mutant. Bottom, Representative recording of the temperature change in the chamber during the protocol. ***D***, Histogram of the average current values to the different agonists in TRPM8 WT and the different mutants during the protocol shown in ***C***. For each cell, current responses were normalized to the initial cold-evoked response. Statistical differences for the response to each agonist in the different TRPM8 constructs were evaluated with a one-way ANOVA, followed by Bonferroni's *post hoc* test. *$p < 0.05$, **$p < 0.01$.

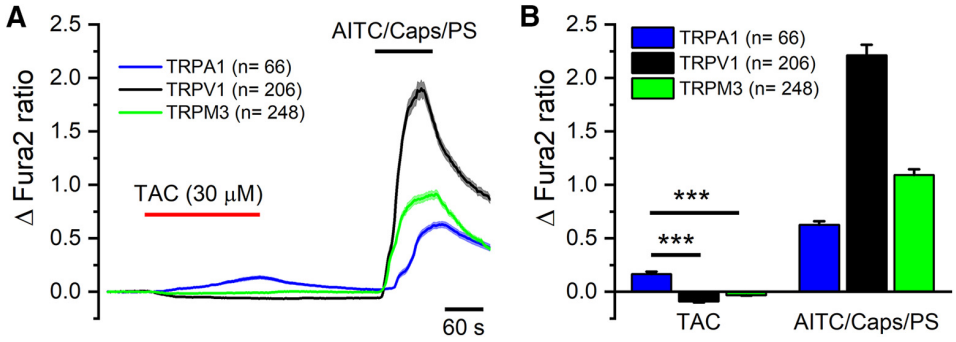

Figure 6. TAC activates human TRPA1 channels. ***A***, Averaged ± SEM fura-2 fluorescence ratio of HEK292 cells transfected with human TRPA1 (blue trace), rat TRPV1 (black trace), or mouse TRPM3 (green trace) during applications of TAC (30 μM) and their canonical agonists capsaicin (100 nM), AITC (50 μM), and pregnenolone sulfate (PS, 50 μM). ***B***, Bar histogram summarizing the effect of TAC or the canonical agonists, capsaicin, AITC, or PS, on fura-2 fluorescence ratio. Individual records have been baseline-subtracted. TAC produced a significant elevation in $[Ca^{2+}]_i$ in TRPA1-transfected cells compared with TRPV1- or TRPM3-transfected cells (***$p < 0.001$, one-way ANOVA followed by Bonferroni's *post hoc* test). ***$p < 0.001$.

In contrast, the same concentration of TAC activated human TRPA1, with a slowly rising $[Ca^{2+}]_i$ response. The activating effects of TAC on TRPA1 were more modest than those produced by its canonical agonist AITC (Fig. 6*B*). We noticed that application of TAC produced a modest inhibition of basal calcium levels in cells expressing TRPV1 or TRPM3, suggesting some inhibitory effect on background activity at this temperature (i.e., 34°C). The effects of TAC on recombinant TRPM8 and TRPA1 channels motivated a deeper characterization of its action on primary sensory neurons.

TAC activates TRPM8-expressing cold-sensitive neurons and potentiates their cold response

TRPM8-expressing neurons represent only a small fraction of all DRG neurons (McKemy et al., 2002; Takashima et al., 2007; Dhaka et al., 2008). We used a BAC-transgenic mouse expressing enhanced YFP under the *Trpm8* promoter, *Trpm8*^{BAC}-EYFP (Morenilla-Palao et al., 2014) and intracellular Ca^{2+} imaging to identify TRPM8-expressing neurons in DRG cultures. Confirming our previous finding in this transgenic mouse line (Morenilla-Palao et al., 2014), most YFP(+) neurons were

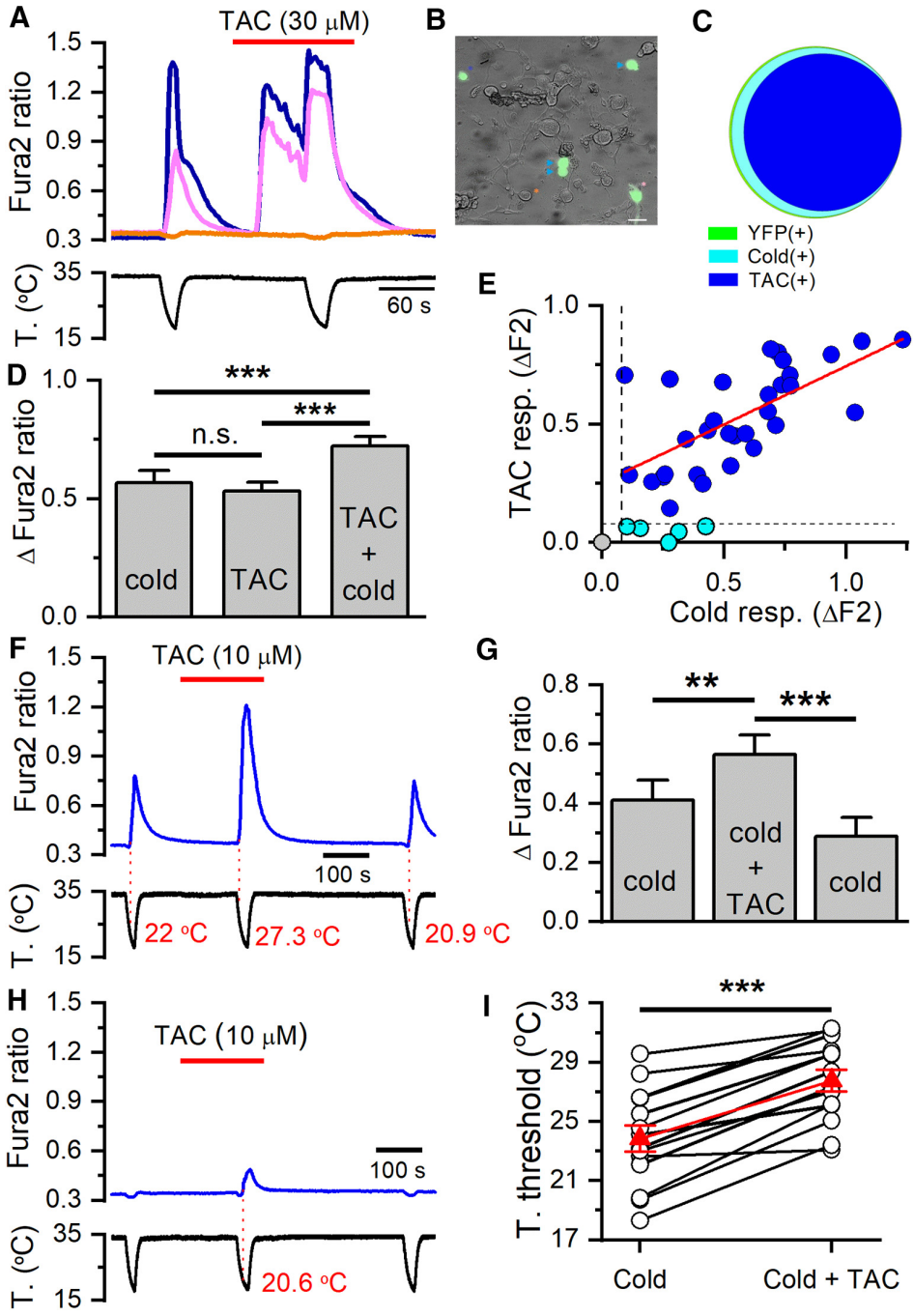

Figure 7. TAC activates cold-sensitive neurons selectively. ***A***, Ratiometric [Ca^{2+}] measurement from fura-2 loaded cultured DRG neurons in *Trpm8*^{BAC}-EYFP mice. Two cold-sensitive neurons (blue and magenta traces) increased their [Ca^{2+}] level during the cooling ramp. The same neurons also responded to 30 μM TAC, and their response to cold was potentiated. The cold-insensitive neuron (orange trace) did not respond to any of these stimuli. ***B***, Representative image of a DRG culture from a *Trpm8*^{BAC}-EYFP mouse. ***A***, Traces correspond to the neurons marked with the same colored asterisk: orange for YFP(−), blue and magenta for YFP(+). Three additional YFP(+) neurons, marked with blue arrowheads, also responded to cold and TAC. Scale bar, 20 μm. ***C***, Venn diagram showing the strong overlap between YFP(+) neurons (green, $n = 37$), the response to cooling (cyan, $n = 36$), and the response to TAC (blue, $n = 31$). In this sample, none of the YFP(−) neurons ($n = 130$) responded to TAC. ***D***, Bar histogram showing the average amplitude of the responses to cold, to TAC, and to cold in the presence of TAC. Amplitudes were similar for cold and TAC, whereas the responses to cold were significantly higher in the presence of TAC. One-way ANOVA for repeated measures followed by Bonferroni's *post hoc* test. ***E***, Correlation between amplitude of cold- and TAC-evoked responses in individual DRG neurons. Black dotted lines indicate the threshold amplitude established for considering a positive response. Blue points represent the neurons that responded to cold and TAC ($n = 31$). Cyan points represent the neurons that responded to cold but did not respond to TAC ($n = 5$). Note the small cold-evoked response in neurons unresponsive to TAC. Gray point represents the single YFP(+) neuron that did not respond to cold or TAC. The linear fit to the blue points (red line) yielded a correlation coefficient (r^2) of 0.42. ***F***, Representative trace of fura-2 ratio fluorescence in a DRG neuron during three consecutive cooling ramps. Note the strong, reversible potentiation of the cold-evoked response in the presence of 10 μM TAC. Red numbers indicate the temperature at which the measured signal (F340/F380) deviated by at least 4 times the SD of its baseline (i.e., temperature threshold). ***G***, Bar histogram summarizing the effect of 10 μM TAC on the amplitude of the cold-evoked response. One-way ANOVA for repeated measures followed by Bonferroni's *post hoc* test. ***H***, Time course of fura-2 ratio in a YFP(+), which was not activated in control conditions (i.e., cold insensitive) but was recruited in the presence of 10 μM TAC. ***I***, Temperature threshold of individual YFP(+) neurons to cold or cold plus 10 μM TAC. The mean temperature threshold (red triangles) shifted from 23.9 ± 0.9°C in control solution to 27.8 ± 0.8°C in the presence of 10 μM TAC ($p < 0.001$, $n = 14$, paired Student's *t* test). $^{**}p < 0.01$, $^{***}p < 0.001$.

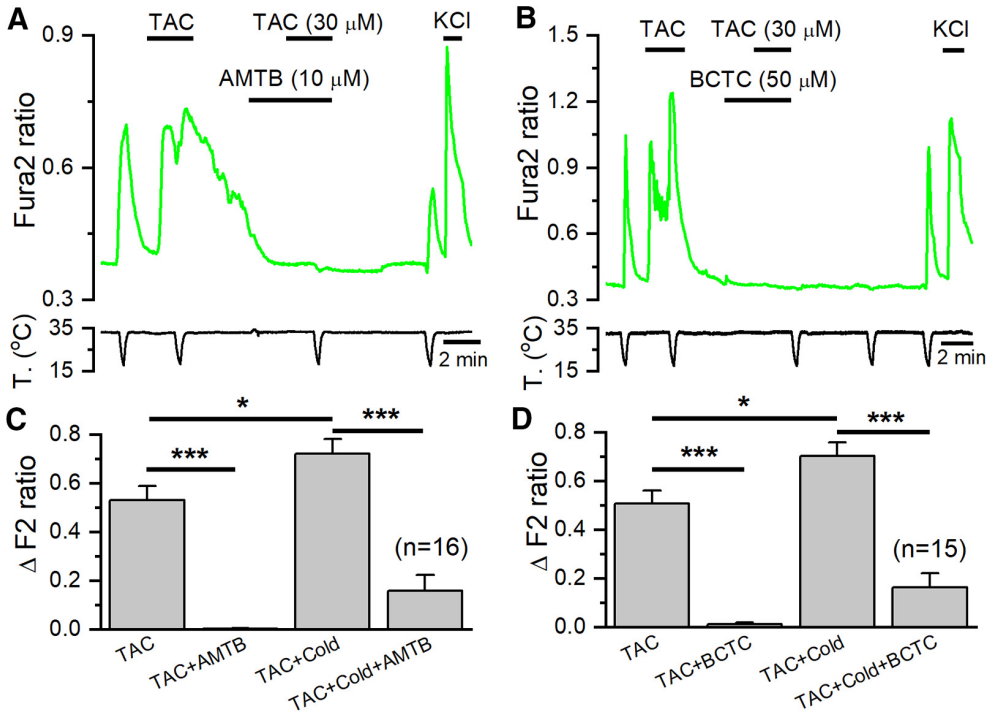

Figure 8. TRPM8 antagonists block the excitatory effects of TAC on mice DRG neurons. ***A***, Ratiometric [Ca^{2+}] levels in a fura-2 AM-loaded cultured DRG neuron from a *Trpm8*^{BAC}-EYFP mouse, showing the response to cold and TAC in control conditions and in the presence of the TRPM8 blocker AMTB (10 μM). ***B***, A similar protocol in the presence of BCTC (50 μM), a different, structurally unrelated, TRPM8 blocker. ***C***, Bar histograms summarizing the effects of AMTB ($n = 16$), and (***D***) BCTC ($n = 15$) on cold- and TAC-evoked responses. Statistical differences evaluated with one-way ANOVA followed by Bonferroni *post hoc* test. *$p < 0.05$, ***$p < 0.001$.

activated by cold (36 of 37), but only 1 in 130 YFP(−) was cold-sensitive, suggesting a very good match between YFP fluorescence and TRPM8 expression (Fig. 7*B*,*C*).

Application of 30 μM TAC activated the majority of TRPM8-expressing thermoreceptor neurons (31 of 36), identified by the expression of YFP and by their response to a cold temperature ramp (Fig. 7*A*,*C*). In the presence of 30 μM TAC, the amplitude of cold-evoked responses also increased significantly in YFP(+) neurons (Fig. 7*D*). TAC and cold produced a similar activation of individual neurons, and the amplitude of both responses was strongly correlated ($r^2 = 0.42$) (Fig. 7*E*). In contrast, none (0 of 130) of the YFP(−) neurons (i.e., those not expressing TRPM8) were activated by 30 μM TAC, although they showed normal responses to 30 mM KCl (data not shown).

We also examined the effects of lower concentration of TAC on DRG neurons. As shown in Figure 7*F*, at 10 μM, the effects of TAC on [Ca^{2+}] levels on a YFP(+) neuron were negligible. However, we found that this concentration of TAC sensitized the response of TRPM8-expressing neurons to cold in a reversible manner. This is a similar effect to that described for other chemical agonists of TRPM8 (McKemy et al., 2002; Voets et al., 2004). On average, the [Ca^{2+}] response to cold increased from 0.41 ± 0.07 during the first cold ramp to 0.57 ± 0.06 during a second cold ramp, in the presence of TAC ($p < 0.01$, $n = 14$) (Fig. 7*G*). The larger amplitude in the cold-evoked response was accompanied by a shift in the response threshold of individual neurons toward warmer temperatures (Fig. 7*F*,*I*). On average, the threshold shifted by ~4°C, from a mean of 23.8 ± 0.9°C in control to 27.8 ± 0.7°C in the presence of 10 μM TAC ($p < 0.001$, $n = 14$). In addition, one YFP(+) neuron initially insensitive to cold became cold sensitive during the application of this TAC concentration, and this activation was reversible (Fig. 7*H*).

In agreement with the observations obtained in TRPM8-transfected HEK293 cells, cyclosporine (30 μM) failed to activate YFP(+) DRG neurons (0 of 37), or sensitize their responses to cold: the increase in cold-evoked fura-2 ratio was 0.72 ± 0.13 in the presence of vehicle ($n = 16$), compared with 0.63 ± 0.06 in the presence of cyclosporine ($n = 37$) ($p = 0.40$, unpaired Student's *t* test).

Collectively, these results indicate that TAC excites cold-sensitive neurons that express TRPM8, and potentiates their cold response by shifting the threshold temperature to warmer temperatures.

TRPM8 mediates TAC responses in DRG neurons

Next, we explored whether TAC responses in cold-sensitive DRG neurons were mediated by TRPM8 activation. To this end, we combined two experimental strategies: a pharmacological approach using two different TRPM8 blockers and a genetic approximation, characterizing responses in TRPM8 KO mice. If TAC responses were mediated by TRPM8 activation, they should be sensitive to TRPM8 antagonists. As shown in Figure 8*A*, *B*, this prediction was fulfilled; the responses to TAC in cold-sensitive DRG neurons were completely blocked by AMTB (10 μM) and BCTC (50 μM), two structurally unrelated TRPM8 antagonists (Almaraz et al., 2014). A summary of these results is shown in Figures 8*C*, *D*. Moreover, the $[Ca^{2+}]_i$ elevation during cold ramps in the presence of TAC were also greatly reduced by these two antagonists ($p < 0.001$).

To confirm the effects of TAC on native TRPM8 channels, we examined responses to TAC in DRG cultures from a transgenic mouse line in which a farnesylated eGFP is expressed from the *Trpm8* locus (*TRPM8*^{EGFPf}) in replacement of TRPM8, allowing the identification of putative TRPM8-expressing neurons

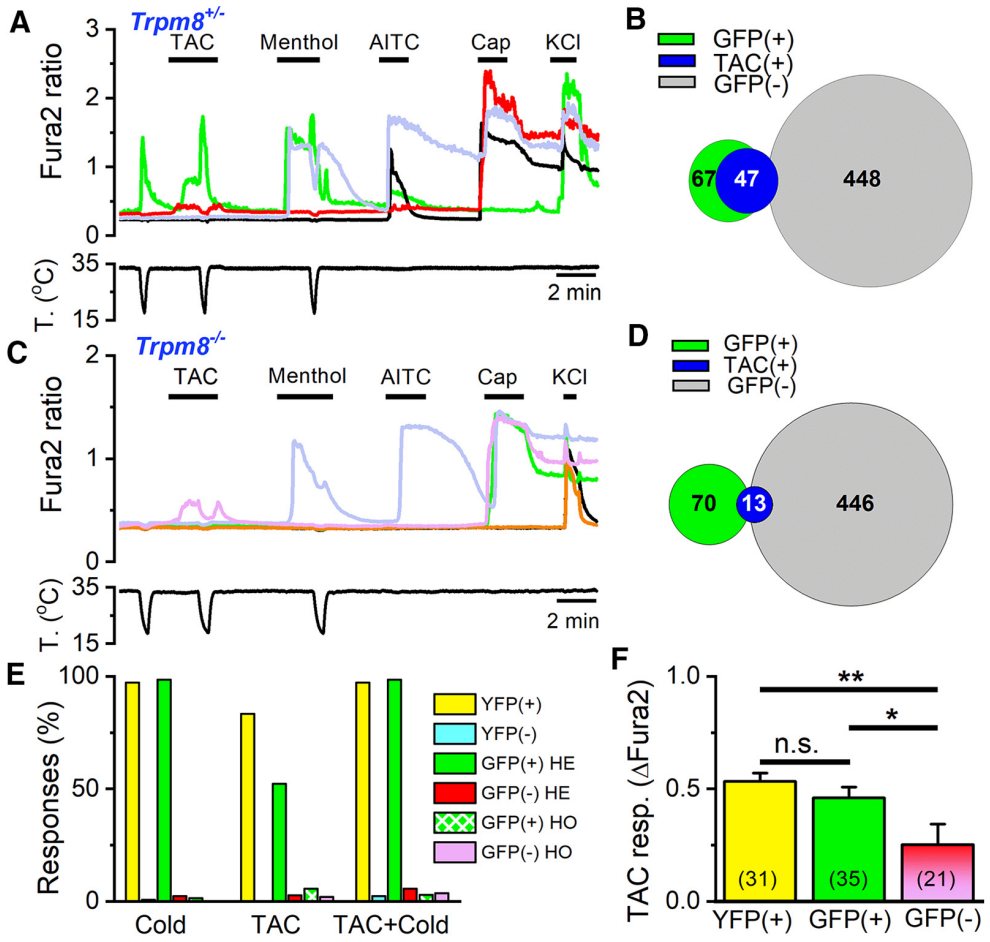

Figure 9. TRPM8 is the principal mediator of the excitatory effects of TAC on DRG neurons. ***A***, Representative traces of fura-2 ratio fluorescence in a *Trpm8*$^{EGFPf/+}$ DRG culture. Consecutive applications of cold, TAC (30 μM), menthol (100 μM), AITC (100 μM), capsaicin (100 nM), and high K^+ (30 mM) were used to define the phenotype of each neuron. The GFP(+) neuron (green trace) is activated by cold, TAC, and menthol. A GFP(−) neuron (red trace) is not activated by cold or menthol but shows a small response to TAC; typically, these neurons are activated by capsaicin. ***B***, Venn diagram summarizing the responses to TAC in GFP(+) and GFP(−) neurons in *Trpm8*$^{EGFPf/+}$ mice. ***C***, Representative traces of fura-2 ratio fluorescence in cultured DRG neurons from a *Trpm8* KO mouse. Same protocol as in ***A***. Note the inhibition of the small TAC response by cooling in a GFP(−) neuron (pink trace). A GFP(+) neuron (green trace) does not respond to cold or menthol but responds to capsaicin. ***D***, Venn diagram summarizing the responses to TAC in GFP(+) and GFP(−) neurons in *Trpm8* KO mice. ***E***, Summary of responses (in percentage of total neurons) to cold, TAC, and TAC plus cold in *Trpm8*^{BAC}-EYFP, *Trpm8*$^{EGFPf/+}$, and *Trpm8*$^{EGFPf/EGFPf}$ mice. For each mouse line, neurons have been separated as fluorescent or nonfluorescent. ***F***, Mean amplitude of TAC responses in fluorescent (TRPM8^{BAC}-EYFP and *Trpm8*$^{EGFPf/+}$) and nonfluorescent neurons (*Trpm8*$^{EGFPf/+}$ and *Trpm8*$^{EGFPf/EGFPf}$). Differences in amplitude between fluorescent and nonfluorescent neurons were statistically significant (one-way ANOVA). *$p < 0.05$, **$p < 0.01$.

(Dhaka et al., 2007). We compared responses in cultures from *Trpm8*$^{EGFPf/+}$ mice, which maintain one copy of TRPM8, with those in *Trpm8*$^{EGFPf/EGFPf}$ animals, thus null for TRPM8.

In *Trpm8*$^{EGFPf/+}$ DRG cultures, 13% (67 of 515) of the neurons were fluorescent and practically all of them (66 of 67) were activated by cold or menthol, consistent with their expression of TRPM8 (Fig. 9*A*). Moreover, approximately half of the green fluorescent neurons were activated by TAC (35 of 67). In the presence of TAC, or menthol, cold responses were potentiated (Fig. 9*A*, green trace), consistent with an effect on TRPM8. The phenotype of GFP(−) neurons was very different: very few (2.4%) were cold-sensitive, and only 2.7% (12 of 448) were activated by TAC (Fig. 9*A*, red trace), a significantly lower percentage ($p < 0.001$, *Z* test). A Venn diagram of these results is shown in Figure 9*B*. In summary, in agreement with the results observed in *Trpm8*^{BAC}-EYFP mice, there is a high correlation between expression of TRPM8 and responses to TAC.

The responses to TAC in *Trpm8*$^{EGFPf/EGFPf}$ (i.e., *Trpm8* KO) mice were very infrequent, albeit detectable in some neurons (Fig. 9*C*, pink trace). In total, only 13 of 516 (2.9%) DRG neurons responded to 30 μM TAC in *Trpm8* KO animals (4 were GFP(+) and 9 were GFP(−)). The main reduction occurred in GFP(+) neurons, in parallel with a near suppression of their responses to cold or menthol (Fig. 9*C*, green trace). As summarized in Figure 9*D*, of 70 GFP(+) neurons tested, only 4 (5.7%) responded to TAC, a drastic reduction from the responses observed in GFP(+) neurons in *Trpm8*$^{EGFPf/+}$ mice ($p < 0.001$, *Z* test). Figure 9*E* summarizes the responses to TAC and cold in fluorescent and nonfluorescent cells of the two transgenic mouse lines. It is evident that expression of TRPM8 is highly correlated with responses to TAC.

Finally, in GFP(−) neurons of *Trpm8*$^{EGFPf/EGFPf}$ mice, only 2% (9 of 446) responded to TAC, a very similar percentage to that observed in GFP(−) neurons of *Trpm8*$^{EGFPf/+}$ mice. The responses to TAC in GFP(−) neurons had some distinct characteristics: because the results were similar in *Trpm8*$^{EGFPf/+}$ and *Trpm8*$^{EGFPf/EGFPf}$ animals, we pooled them together. In GFP(−) neurons, the amplitude of TAC responses was smaller ($p <$

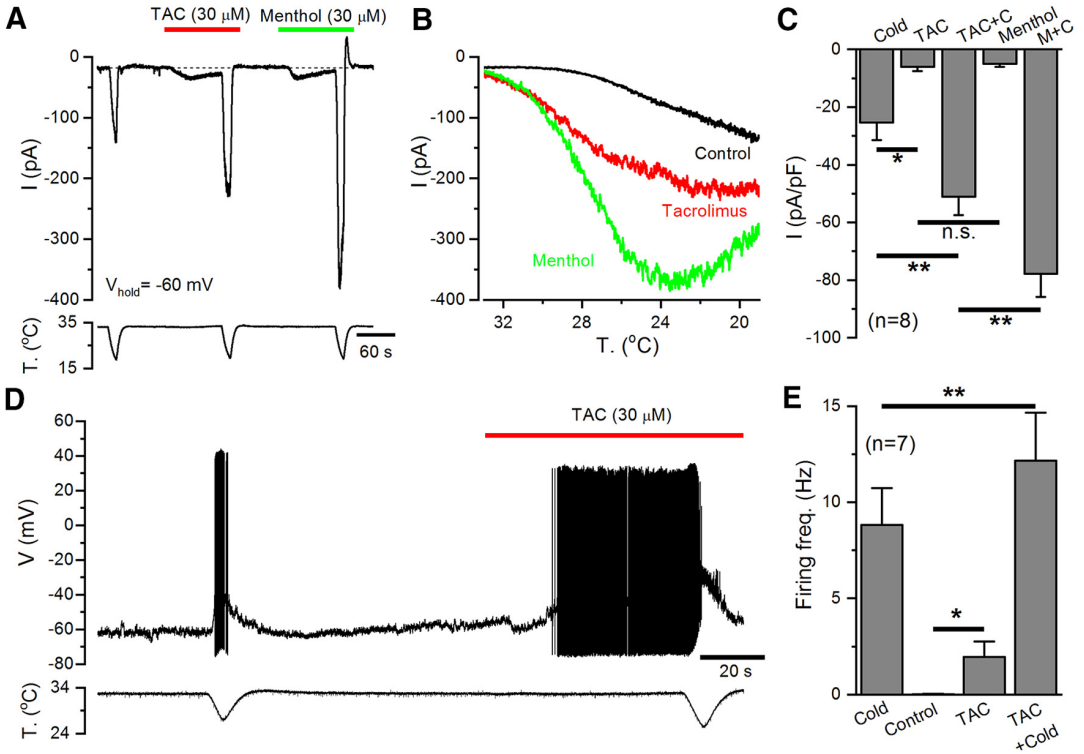

Figure 10. TAC increases the excitability of cold-sensitive DRG neurons. ***A***, Representative whole-cell recording in the voltage-clamp configuration ($V_{hold} = -60$ mV) of a TRPM8-expressing, cold-sensitive DRG neuron identified by the expression of EYFP. TAC (30 μM) evoked an inward current similar in amplitude to that elicited by menthol (30 μM). Both TAC and menthol strongly potentiate the response to cold. Bottom, Simultaneous recording of bath temperature during the recording. ***B***, Current-temperature relationships for the same neuron in control (black trace) and in the presence of 30 μM TAC (red trace) or 30 μM menthol (green trace). Note the marked shift in temperature threshold. ***C***, Bar histogram summarizing the effects of agonists on the amplitude of inward currents during the protocol shown in ***A***. The statistical analysis consisted of a one-way ANOVA followed by Bonferroni's *post hoc* test (*$p < 0.05$, **$p < 0.01$). ***D***, Representative recording of a cold-sensitive DRG neuron in the whole-cell current-clamp configuration showing responses to cold and to the application of TAC (30 μM). TAC evoked AP firing at 33°C and greatly enhanced the firing frequency during a cold ramp. Bottom, Simultaneous recording of bath temperature. ***E***, Bar histogram summarizing the mean responses, measured as average firing frequency, during the different stimuli applied. Firing frequency for cold was averaged from the first to the last spike during the cooling ramp. Firing frequency in control condition was calculated during the minute preceding TAC application (only 3 of 7 neurons fired action potentials in control conditions). TAC-evoked firing was calculated from the first spike during TAC application to the start of the cold ramp. The analysis consisted of a paired *t* test for cold versus TAC plus cold (**$p = 0.009$) and control vs TAC (*$p = 0.048$).

0.001) compared with responses in fluorescent neurons of *Trpm8*$^{EGFPf/+}$ mice or *Trpm8*^{BAC}-EYFP mice (Fig. 9*F*), and they were nearly abolished during the cooling ramp (Fig. 9*A*,*C*). None of these neurons was cold-sensitive (Fig. 9*A*, red trace). Interestingly, of the 21 GFP(−) neurons activated by TAC, 18 also responded to capsaicin (100 nM) and 11 responded to AITC (50 μM). These characteristics are consistent with a possible effect of TAC on TRPV1. However, we note that in these cultures 43.8% (452 of 1031) of the neurons responded to capsaicin, but only 22 of these 452 (4.9%) responded to TAC.

Together, the results obtained with pharmacological blockers and after genetic inactivation of TRPM8 indicate that the main excitatory action of TAC in DRG neurons is mediated by activation of TRPM8 channels in cold-sensitive neurons, with some weaker effects on capsaicin-sensitive neurons, presumably though TRPV1.

TAC activates inward currents and elicit AP firing in cold thermoreceptors

The effect of TAC on the excitability of cold thermoreceptors was further evaluated by performing electrophysiological recordings in cultured DRG neurons from *Trpm8*^{BAC}-EYFP mice. As shown in Figure 10*A*, in whole-cell patch-clamp recordings, TAC (30 μM) activated an inward current and potentiated the currents evoked by cold temperature in all the YFP(+) neurons tested. This potentiation was accompanied by a clear shift in the activation of cold-evoked currents to warmer temperatures (Fig. 10*B*). In the same neurons, application of menthol (30 μM) produced similar effects to TAC, although its potentiating effect on cold-evoked currents was stronger. A summary of these results is shown in Figure 10*C*.

Recordings in the current-clamp configuration of TRPM8-expressing cold thermoreceptors, at a holding temperature of 33°C, showed that TAC application induced the firing of action potentials and strongly potentiated cold-evoked firing (Fig. 10*D*). These results are summarized in Figure 10*E*.

These data confirm that TAC activates a depolarizing inward current similar to the TRPM8-dependent I_{Cold} current, increasing the excitability of cold-sensitive neurons.

TAC activates cold-sensitive corneal afferents

The corneal surface is densely innervated by cold-sensitive nerve endings that express TRPM8 channels (Parra et al., 2010; Alamri et al., 2018; Alcalde et al., 2018). We used extracellular recordings of these terminals in a mouse *in vitro* preparation to investigate the effects of TAC on sensory nerve endings.

Corneal cold-sensitive nerve endings are characterized by their spontaneous, low-frequency, background activity at 34°C with a sharp increase in firing rate, often organized in the form of bursts, during cooling (Fig. 11*A*,*C*) (Carr et al., 2003; Parra et al.,

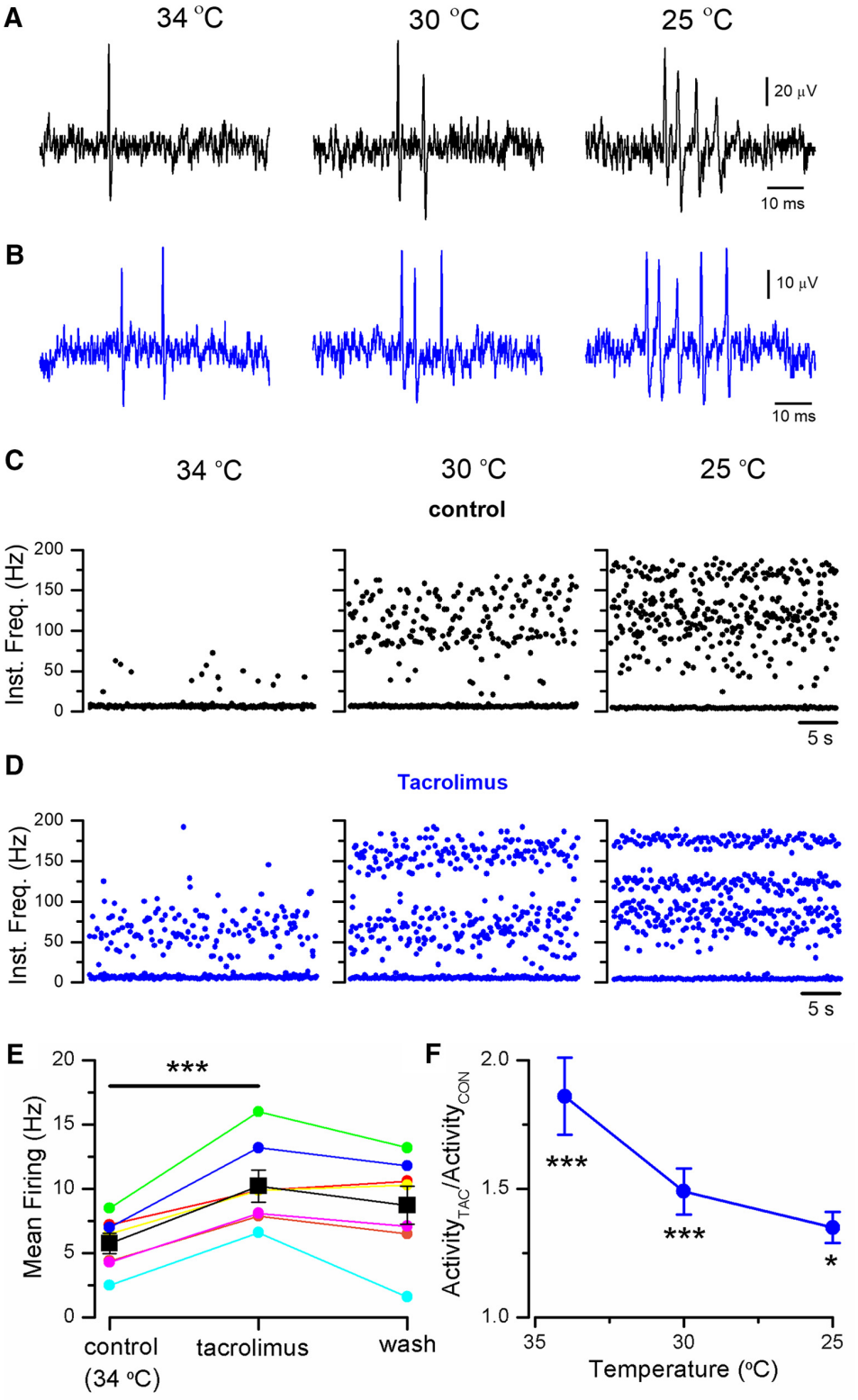

Figure 11. TAC activates corneal cold thermoreceptor endings. ***A***, Representative example of nerve terminal impulses recorded from a mouse corneal ending in control solution, at three different temperatures. ***B***, Recordings from the same ending during application of 30 μM TAC. ***C***, Instantaneous firing frequency from the same ending as in ***A*** (control solution), and ***D***, as in ***B*** (in TAC). Note the regular firing in bursts during cooling. ***E***, Summary of the effects of 30 μM TAC on spontaneous firing in 7 individual endings at the basal temperature of 34°C. The increase in firing was statistically significant (***$p < 0.001$, paired Student's *t* test). ***F***, Mean firing rate in TAC at three different temperatures in 7 cold thermoreceptor endings. Activity at each temperature has been normalized to the value obtained in control solution. Statistical differences evaluated by one-way ANOVA for repeated measures followed by Bonferroni *post hoc* test. (*$p < 0.05$, ***$p < 0.001$.)

2010; Orio et al., 2012). At a baseline temperature of 34°C, exposure to 30 μM TAC produced clear excitatory effects (Fig. 11*B*,*D*, left), with an increase in the basal firing rate, from 5.8 ± 0.8 Hz in control to 10.2 ± 1.6 Hz in TAC ($n = 7$, $p < 0.001$; paired Student's *t* test). The firing rate increases during cooling in the presence of TAC (Fig. 11*B–D*, middle, right). Figure 11*E* shows a summary of the effects of TAC on basal firing rate for individual cold-sensitive endings at 34°C. The excitatory effect of TAC was also evident on the steady-state firing rate at lower temperatures, with an elevation in mean firing frequency and the increase in the number of spikes per burst (Fig. 11*B*). The potentiation of activity mediated by TAC at the different temperatures is shown in Figure 11*F*. The washout of TAC effects was only partial, probably explained by the long application times required to examine the effects of TAC at different temperatures and the lipophilic nature of the compound (Fig. 11*E*).

These results show that the excitatory effects of TAC on cold thermoreceptor activity are maintained at peripheral nerve endings, the physiological site for chemotransduction and thermotransduction in these neurons.

TAC sensitizes cutaneous cold thermoreceptors

To further characterize the effects of TAC on cold thermoreceptor endings, we used a mouse skin-nerve preparation. We focused our efforts on unimodal cutaneous cold receptors (i.e., cold-activated fibers insensitive to mechanical stimuli) because it is well known that TRPM8 plays an essential role in their cold-evoked activity (Toro et al., 2015; Winter et al., 2017). We identified 9 fibers in the saphenous nerve with the aforesaid characteristics. These fibers were silent at the baseline temperature of 34°C–35°C but were activated when cold solution was delivered to their isolated receptive field (Fig. 12*A*,*B*), with a mean cold threshold of 30.4 ± 1°C ($n = 9$) (Fig. 12*C*). During application of TAC (30 μM), none of the fibers presented activity at the basal temperature of 34°C. However, their cold-evoked activity was clearly modified in the presence of TAC (Fig. 12*A*,*B*). In 6 of these 9 fibers, TAC shifted their cold threshold to warmer temperatures (mean temperature threshold displacement of 2.1 ± 0.5°C, $n = 9$) and shifted their stimulus response function to warmer temperatures (Fig. 12*C*). As in the cornea, the washout of TAC effects was only partial (Fig. 12*B*,*C*). In these endings, menthol (50 μM) produced qualitatively similar excitatory effects, although more intense. Thus, menthol produced an increase in spontaneous activity at the basal temperature of 34°C–35°C in 5 of 9 endings tested (Fig. 12*B*). In addition, menthol shifted their temperature threshold, by at least 1°C, to warmer values in all of them ($n = 9$). The mean temperature threshold displacement produced by menthol was 3.3 ± 0.7°C (Fig. 12*C*), and their overall firing was more pronounced and shifted to warmer temperatures (Fig. 12*D*). Collectively, these results indicate that TAC sensitizes a population of cutaneous TRPM8-expressing thermoreceptor endings to cold temperature.

TAC evokes TRPM8-dependent cold hypersensitivity

Agonists of TRPM8 channels can lead to cold-evoked avoidance behaviors (Rossi et al., 2006; Klein et al., 2010). Thus, we examined the possible influence of TAC on cold-evoked behaviors in mice. In adult WT mice, intraplantar injection of 1% TAC decreased the latency of paw withdrawal from a cold plate set at 10°C. The reduction was significant ($p < 0.01$, one-way ANOVA) compared with the injection of vehicle or the latency observed in naive paws (Fig. 13*A*, left). Injection of 1% menthol, the canonical agonist of TRPM8 channels, also caused a significant reduction in withdrawal latency (Fig. 13*A*). To test for the role of TRPM8 in the cold hypersensitivity produced by TAC, we examined the withdrawal latency in *Trpm8* KO mice. As shown in Figure 13*A* (right), in these mice, TAC failed to sensitize their response to cold (one-way ANOVA), and their withdrawal latency was significantly longer compared with results obtained in WT ($p < 0.01$, unpaired *t* test).

These results confirm the role of TRPM8 channels in the cold hypersensitivity produced by TAC at peripheral nerve endings.

TAC triggers tearing and blinking

Afferent discharge from different classes of corneal sensory fibers, including cold receptors and polymodal nociceptors, participates in the neural mechanisms of basal and reflex-evoked tearing (Belmonte and Gallar, 2011; Meng and Kurose, 2013). We examined the effect of TAC solutions on tearing in anesthetized WT mice. We applied, sequentially, a small drop of saline, vehicle, or TAC (1%) to both eyes and measured the tearing after a rest period of 5 min. As shown in Figure 13*B*, TAC produced a significant increase in tearing compared with saline ($p < 0.01$) or vehicle ($p < 0.05$; one-way ANOVA). To control for possible sensitization effects produced by repeated applications of solutions to the corneal surface, we designed a control experiment, consisting of 3 consecutive applications of saline, which resulted in very similar mean values of tearing for each of them (Fig. 13*C*).

A previous study identified the critical role of TRPM8 channels in eye blinking in mice following application of hyperosmolar solutions (Quallo et al., 2015). Thus, we decided to investigate the effects of TAC solutions applied to the corneal surface. We counted the number of blinks observed after unilateral application of solutions with 1% TAC to the eyes of WT ($n = 8$) and *Trpm8*$^{-/-}$ mice ($n = 17$). Application of saline (315 mOsm/kg) or vehicle had only a small effect on blinking. In contrast, as shown in Figure 13*D* (left), 1% TAC triggered a large increase in the number of blinks in WT mice. In agreement with previous findings (Quallo et al., 2015), hyperosmotic solutions (785 mOsm/kg) also triggered a marked increase in eye blinking, similar to that observed with TAC.

Repeating the tests in *Trpm8* KO mice confirmed a reduction in blinking, compared with WT ($p < 0.01$, unpaired *t* test), produced by hyperosmolar solutions reported previously. In contrast, the blinks produced by 1% TAC in *Trpm8* KO mice were very variable, but they were not different from those observed in WT mice (Fig. 13*D*, right). These results suggest that 1% TAC has effects on blinking that are in independent of TRPM8 activity.

Discussion

Natural products remain an important source for the development of pharmaceutical drugs (Newman and Cragg, 2016), and have also played a fundamental role in the discovery and characterization of TRP channels (Julius, 2005; Nilius and Appendino, 2011; Meotti et al., 2014). However, despite major drug discovery efforts, the number of chemical agonists reported for TRPM8 channels is still very modest (Bödding et al., 2007; Almaraz et al., 2014; LeGay et al., 2016; Moran and Szallasi, 2018). Moreover, many of these agonists show cross-sensitivity with other TRP channels (Macpherson et al., 2006). We have identified TAC, a clinically relevant macrolide immunosuppressant produced by soil microorganisms, as a novel agonist of TRPM8 channels. These findings highlight a novel neuroimmune interface in peripheral tissues with several potential applications. First, it expands the current arsenal of drugs targeting TRPM8 and provides

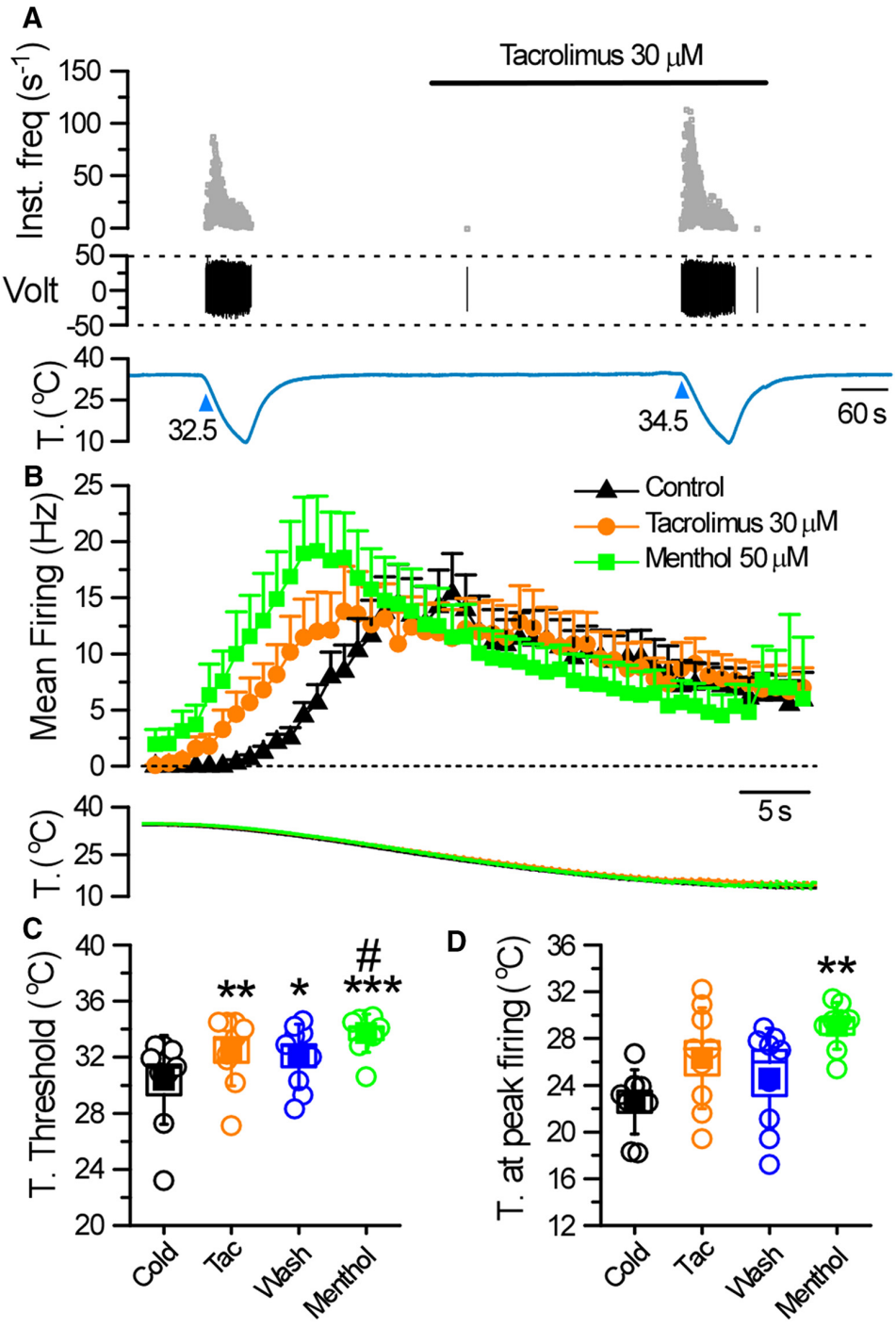

Figure 12. TAC activates cutaneous cold thermoreceptors. ***A***, Representative recording showing the response of a cold fiber to a decrease in the temperature of the isolated receptive field, before and after treatment with 30 μM TAC. Top to bottom, Instantaneous firing frequency, the voltage signal, and the temperature of the receptive field. ***B***, Histogram showing the averaged cold-evoked response of cold fibers from C57BL/6J mice in control solution (black triangles), in the presence of 30 μM TAC (orange circles), and in 50 μM menthol (green squares). Average discharge rates are represented in bins of 2 s. Bottom, The temperature ramp for each of the datasets. ***C***, Temperature threshold for activation of impulse discharge. ***D***, Temperature for reaching the maximal discharge rate. Squares represent mean values. Boxes represent SEM. Error bars indicate standard deviation (SD). In ***C*** and ***D***, $^{*}p < 0.05$, $^{**}p < 0.01$, $^{***}p < 0.001$ (one-way ANOVA with Bonferroni's post hoc correction). The asterisks compare significance with respect to cold. The $^{\#}(p < 0.05)$ compares significance with respect to wash.

new clues about its activation mechanism. Second, the effects of TAC on TRPM8 could be used as an experimental tool to investigate the functional activity of this polymodal ion channel in humans, for example, as a new surrogate model of cold allodynia and hyperalgesia (Andersen et al., 2014).

In contrast to TAC, cyclosporine, a cyclic undecapeptide also targeting calcineurin signaling, had no effect on TRPM8 or cold-evoked responses in DRG neurons. This result excludes this pathway as the one involved in the effects of TAC. Moreover, the activation of reconstituted TRPM8 by TAC in planar lipid bilay-

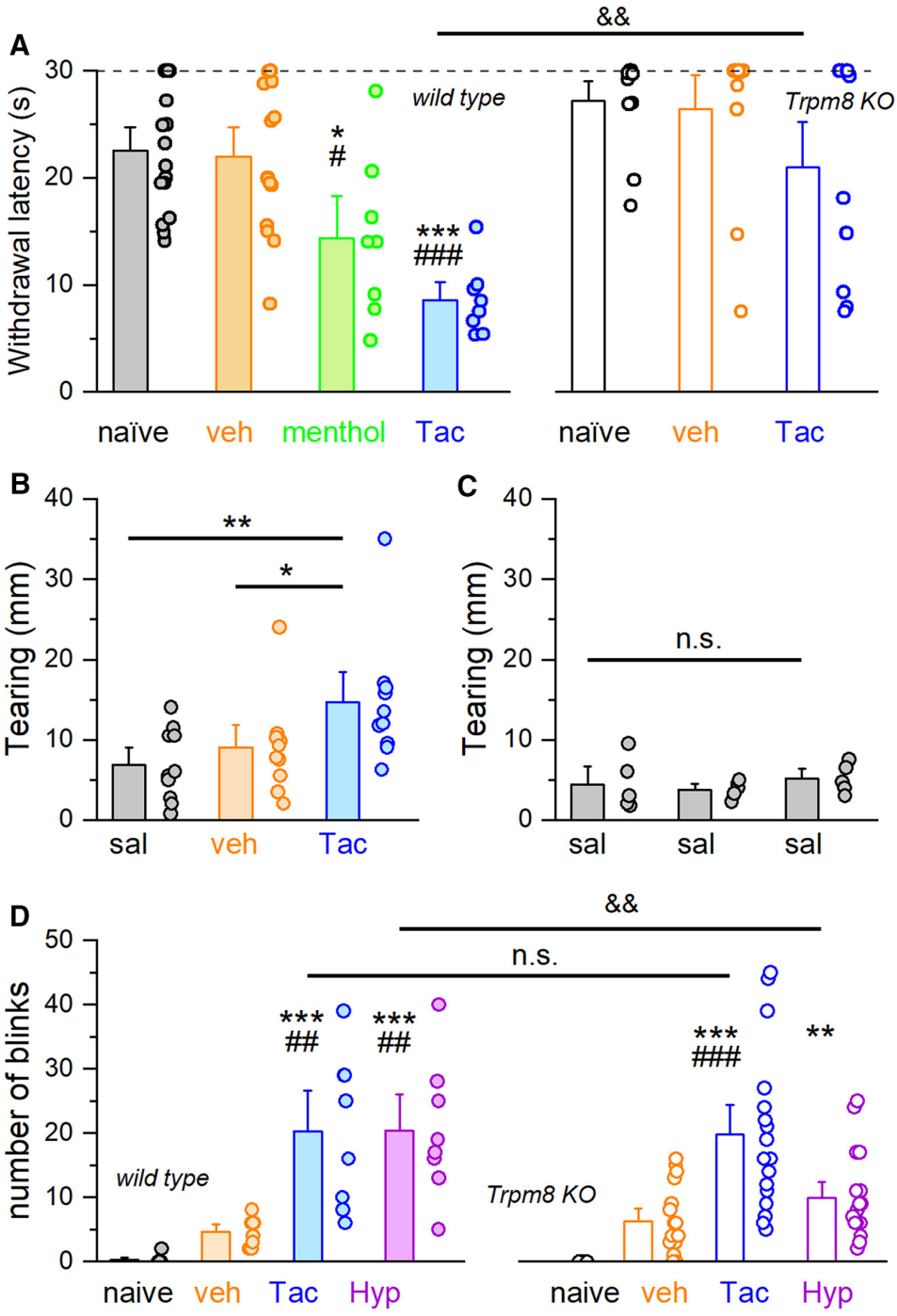

Figure 13. TAC sensitizes cold-evoked responses and triggers eye blinking and tearing. ***A***, Withdrawal latencies for hindpaws placed in contact with a cold metal plate set at 10°C. Individual and mean ± SEM values in WT (filled bars) mice for different conditions: naive mice, after the injection of vehicle, 1% menthol, and 1% TAC. Right, Open bars represent the same experiment in *Trpm8* KO mice. Differences with respect to naive (*), to vehicle (#) (one-way ANOVA followed by Bonferroni's *post hoc* test). TAC reduces the withdrawal latency in WT mice compared with *Trpm8* KO. $^{\&\&}p < 0.01$ (unpaired Student's *t* test). ***B***, Effects of different topical solutions on basal tearing in mice. The left and the right eye received 2 μl of saline, vehicle (8% ethanol, 2% Cremophor in saline) or TAC (1%). Tearing was estimated from the length of staining in the threads. The effect of TAC was significant with respect to saline ($^{**}p < 0.01$) or vehicle ($^{*}p < 0.05$) ($n = 10$ mice; one-way ANOVA). ***C***, Three consecutive applications of saline were used as a control ($n = 5$ mice). No increment in tearing was observed in this case (one-way ANOVA). ***D***, Effects of different topical solutions (5 μl) on eye blinking, monitored over a 2 min period, in WT mice (filled bars; $n = 8$). Compared with saline (*) and vehicle (#) (see above), 1% TAC and hyperosmotic (785 mOsm/kg) solution increased the number of blinks ($^{***}p < 0.001$. $^{\#\#}p < 0.01$). In *Trpm8* KO mice (open bars; $n = 17$), TAC increased the number of blinks with respect to saline ($^{***}p < 0.001$) or the TAC vehicle ($^{\#\#\#}p < 0.001$), and Hyp increased the blinks with respect to saline ($^{**}p < 0.001$) (one-way ANOVA followed by Bonferroni's *post hoc* test). The number of blinks to Hyp were significantly reduced in *Trpm8* KO mice compared with WT. $^{\&\&}p < 0.01$ (unpaired Student's *t* test).

ers conclusively demonstrates that the interaction of TAC with the channel is direct and does not require signaling cascades. Similarly to the activation by cold and menthol, the gating of TRPM8 by TAC depended specifically on the presence of $PI(4,5)P_2$ (Zakharian et al., 2010).

Biophysical and molecular aspects of TAC agonism on TRPM8

In many aspects, the activation of TRPM8 by TAC resembles the effects of menthol on channel gating: TAC shifts the activation threshold of TRPM8 to higher temperatures and slows the activation kinetics. These characteristics fit with the description of Type I agonists introduced by Janssens et al. (2016), which include menthol, thymol, icilin, and linalool. Interestingly, the effects of TAC persisted in a menthol-insensitive mutant. Our previous characterization of antagonist effects on TRPM8 suggested a sequential model of TRPM8 gating where chemical modulators can favor (e.g., menthol) or hinder (e.g., BCTC or SKF96365) the energetics of subsequent channel opening by cold temperature or voltage from different binding sites (Mälkiä et al., 2009). This model is consistent with the actions of TAC, having an excitatory action on the menthol-insensitive Y745H mutant, but failing to facilitate the gating by cold temperature, suggesting that the actions of different chemical agonists converge from independent binding sites.

The identification of the residues critical for TAC effects should be addressed in the future; we excluded its interaction with the icilin and menthol binding sites. The recent cryostructure of the TRPM8 tetramer could facilitate their identification (Yin et al., 2018).

Specificity of TAC effects

Based on the pharmacological characterization in WT, hemizygous, and *Trpm8* null mice, we conclude that the effects of TAC on TRPM8-expressing sensory neurons is highly selective. However, this specificity is not absolute. In cultured neurons of *Trpm8* KO mice, a small effect of TAC remains that is likely mediated by TRPV1. A previous study found that TAC activated a small percentage (3.1%) of rat DRG neurons, and many of these neurons were also activated by capsaicin (Senba et al., 2004). As in our case, and consistent with a weak effect, the percentage of capsaicin-positive neurons was much higher than those responding to TAC. Surprisingly, we did not observe any effects of TAC on recombinant TRPV1 channels. In contrast, TAC also activated TRPA1 expressed heterologously, albeit less affectively than TRPM8.

The behavioral results indicate that the cold hypersensitivity produced by TAC is clearly mediated by TRPM8. The stronger effects of TAC compared with menthol, opposite to the effects observed *in vitro*, may be explained by its actions on other ion channels (Swandulla et al., 1987). Moreover, it is well known that high concentrations of topical menthol, as used here, are analgesic (Liu et al., 2013). A reported side effect of TAC treatment is the experience of chills. They could be caused by activation of TRPM8 because it is an effect observed with other TRPM8 agonists (e.g., icilin), and linked to the role of the channel in thermoregulation (Knowlton et al., 2011; Pogorzala et al., 2013; Reimúndez et al., 2018).

Topical applications of 1% TAC solutions also increased basal tearing and triggered eye blinking. However, in this last case, the effects were not reduced in TRPM8 KO mice. This result suggests that this solution has irritant effects that are independent of TRPM8 activation. Because topical TAC formulations have much higher concentrations of the drug than we could test in solution *in vitro*, it could lead to activation of other nociceptive TRP channels, explaining the transient burning sensation reported upon topical application of TAC to the eye (Fukushima et al., 2014; Abud et al., 2016) and the skin. These irritant actions are the most common side effect associated with topical application of TAC. Consistent with a possible activation of TRPA1, in a murine model of chronic contact hypersensitivity, TAC increased the number of scratch bouts, and these were significantly reduced by topical application of a TRPA1 antagonist (Wong et al., 2018). Alternatively, because a subpopulation of TRPM8-expressing primary sensory neurons have a nociceptive phenotype (Xing et al., 2006; Alcalde et al., 2018), and many also express TRPV1, their activation may contribute to the transient discomfort produced by TAC.

Therapeutic implications

TRPM8 plays a multifaceted role in cold-related pain. On one hand, it appears to participate in the mechanisms of cold hyperalgesia and allodynia (Knowlton et al., 2013). At the same time, it is the principal mechanism of menthol-induced analgesia (Liu et al., 2013), and also plays a significant role in cooling-mediated analgesia (Proudfoot et al., 2006; Knowlton et al., 2013). Activation of TRPM8 sensory pathways also reliefs the sensation of itch (Palkar et al., 2018). Moreover, TRPM8 activation has a potent anti-inflammatory role in the gut (Ramachandran et al., 2013). Therefore, TRPM8 modulators (agonists and antagonists) may offer multiple possibilities in the relief of pain and visceral inflammation (Pérez de Vega et al., 2016; Moran and Szallasi, 2018).

Because activation of TRPM8 regulates basal tearing and blinking (Parra et al., 2010; Quallo et al., 2015), it has been proposed as a possible therapy for DED (Parra et al., 2010; Belmonte and Gallar, 2011). In addition to its use as a systemic immunosuppressant in the prevention of organ rejection, TAC is also used topically in the treatment of DED symptoms (Jones et al., 2017). In clinical ophthalmology, TAC has been used in solutions at concentrations up to 0.1%. This is equivalent to 1.2 mM, suggesting that it should readily activate TRPM8 channels at corneal endings. We observed a clear effect of 1% TAC solutions on basal tearing and eye blinking, suggesting that some of the beneficial effects reported for TAC in dry-eye conditions (Abud et al., 2016) may involve activation of TRPM8 channels in trigeminal cold thermoreceptor endings. However, the fact that blinking was not reduced in TRPM8 null mice clearly indicates that other mechanisms are involved at this concentration and with this particular formulation. The activation of TRPA1, and possibly TRPV1, at these high concentrations of TAC could also explain the burning sensation reported by some patients.

We also show that TAC activates cutaneous cold thermoreceptor endings and sensitizes responses to cold temperature. The apparent potency was lower than for corneal endings. This, however, may reflect a poor accessibility of the drug in the *in vitro* preparation we used, which lacks vascularization and requires application of substances through the corium. Whether activation of TRPM8 by TAC is relevant for the treatment of atopic dermatitis is currently unclear. Nevertheless, it is becoming well established that electrical activity in peripheral sensory endings can have potent immunomodulatory effects (Chavan et al., 2017), suggesting that modulation of TRPM8 channels by TAC may play a role in its anti-inflammatory actions. At this point, this is just a hypothesis but with important implications.

In conclusion, we report the activation of cold-activated TRPM8 channels by the natural immunosuppressant TAC. The speed of the effect and the action on reconstituted channels make it incompatible with transcriptional actions. Biophysically, the effects of TAC on TRPM8 gating resemble those of menthol, although mutagenesis studies suggest and independent binding site.

References

Abud TB, Amparo F, Saboo US, Di Zazzo A, Dohlman TH, Ciolino JB, Hamrah P, Dana R (2016) A clinical trial comparing the safety and efficacy of topical tacrolimus versus methylprednisolone in ocular graft-versus-host disease. Ophthalmology 123:1449–1457. CrossRef Medline

Alamri AS, Wood RJ, Ivanusic JJ, Brock JA (2018) The neurochemistry and morphology of functionally identified corneal polymodal nociceptors and cold thermoreceptors. PLoS One 13:e0195108. CrossRef Medline

Alcalde I, Íñigo-Portugués A, González-González O, Almaraz L, Artime E, Morenilla-Palao C, Gallar J, Viana F, Merayo-Lloves J, Belmonte C (2018) Morphological and functional changes in TRPM8-expressing corneal cold thermoreceptor neurons during aging and their impact on tearing in mice. J Comp Neurol 526:1859–1874. CrossRef Medline

Almaraz L, Manenschijn JA, de la Peña E, Viana F (2014) Trpm8. Handb Exp Pharmacol 222:547–579. CrossRef Medline

Andersen HH, Olsen RV, Møller HG, Eskelund PW, Gazerani P, Arendt-Nielsen L (2014) A review of topical high-concentration L-menthol as a translational model of cold allodynia and hyperalgesia. Eur J Pain 18:315–325. CrossRef Medline

Andrews MD, Af Forselles K, Beaumont K, Galan SR, Glossop PA, Grenie M, Jessiman A, Kenyon AS, Lunn G, Maw G, Owen RM, Pryde DC, Roberts D, Tran TD (2015) Discovery of a selective TRPM8 antagonist with clinical efficacy in cold-related pain. ACS Med Chem Lett 6:419–424. CrossRef Medline

Asuthkar S, Demirkhanyan L, Sun X, Elustondo PA, Krishnan V, Baskaran P, Velpula KK, Thyagarajan B, Pavlov EV, Zakharian E (2015) The TRPM8 protein is a testosterone receptor: II. Functional evidence for an ionotropic effect of testosterone on TRPM8. J Biol Chem 290:2670–2688. CrossRef Medline

Bandell M, Dubin AE, Petrus MJ, Orth A, Mathur J, Hwang SW, Patapoutian A (2006) High-throughput random mutagenesis screen reveals TRPM8 residues specifically required for activation by menthol. Nat Neurosci 9:493–500. CrossRef Medline

Bautista DM, Siemens J, Glazer JM, Tsuruda PR, Basbaum AI, Stucky CL, Jordt SE, Julius D (2007) The menthol receptor TRPM8 is the principal detector of environmental cold. Nature 448:204–208. CrossRef Medline

Beck LA (2005) The efficacy and safety of tacrolimus ointment: a clinical review. J Am Acad Dermatol 53:S165–S170. CrossRef Medline

Belmonte C, Gallar J (2011) Cold thermoreceptors, unexpected players in tear production and ocular dryness sensations. Invest Ophthalmol Vis Sci 52:3888–3892. CrossRef Medline

Belmonte C, Nichols JJ, Cox SM, Brock JA, Begley CG, Bereiter DA, Dartt DA, Galor A, Hamrah P, Ivanusic JJ, Jacobs DS, McNamara NA, Rosenblatt MI, Stapleton F, Wolffsohn JS (2017) TFOS DEWS II pain and sensation report. Ocul Surf 15:404–437. CrossRef Medline

Bidaux G, Borowiec AS, Gordienko D, Beck B, Shapovalov GG, Lemonnier L, Flourakis M, Vandenberghe M, Slomianny C, Dewailly E, Delcourt P, Desruelles E, Ritaine A, Polakowska R, Lesage J, Chami M, Skryma R, Prevarskaya N (2015) Epidermal TRPM8 channel isoform controls the balance between keratinocyte proliferation and differentiation in a cold-dependent manner. Proc Natl Acad Sci U S A 112:E3345–E3354. CrossRef Medline

Bödding M, Wissenbach U, Flockerzi V (2007) Characterisation of TRPM8 as a pharmacophore receptor. Cell Calcium 42:618–628. CrossRef Medline

Brauchi S, Orio P, Latorre R (2004) Clues to understanding cold sensation: thermodynamics and electrophysiological analysis of the cold receptor TRPM8. Proc Natl Acad Sci U S A 101:15494–15499. CrossRef Medline

Carr RW, Pianova S, Fernandez J, Fallon JB, Belmonte C, Brock JA (2003) Effects of heating and cooling on nerve terminal impulses recorded from cold-sensitive receptors in the guinea-pig cornea. J Gen Physiol 121:427–439. CrossRef Medline

Chavan SS, Pavlov VA, Tracey KJ (2017) Mechanisms and therapeutic relevance of neuro-immune communication. Immunity 46:927–942. CrossRef Medline

Chuang HH, Neuhausser WM, Julius D (2004) The super-cooling agent icilin reveals a mechanism of coincidence detection by a temperature-sensitive TRP channel. Neuron. 43:859–869. CrossRef Medline

Dhaka A, Viswanath V, Patapoutian A (2006) Trp ion channels and temperature sensation. Annu Rev Neurosci 29:135–161. CrossRef Medline

Dhaka A, Murray AN, Mathur J, Earley TJ, Petrus MJ, Patapoutian A (2007) TRPM8 is required for cold sensation in mice. Neuron 54:371–378. CrossRef Medline

Dhaka A, Earley TJ, Watson J, Patapoutian A (2008) Visualizing cold spots: TRPM8-expressing sensory neurons and their projections. J Neurosci 28:566–575. CrossRef Medline

Fukushima A, Ohashi Y, Ebihara N, Uchio E, Okamoto S, Kumagai N, Shoji J, Takamura E, Nakagawa Y, Namba K, Fujishima H, Miyazaki D (2014) Therapeutic effects of 0.1% tacrolimus eye drops for refractory allergic ocular diseases with proliferative lesion or corneal involvement. Br J Ophthalmol 98:1023–1027. CrossRef Medline

González-González O, Bech F, Gallar J, Merayo-Lloves J, Belmonte C (2017) Functional Properties of Sensory Nerve Terminals of the Mouse Cornea. Invest Ophthalmol Vis Sci. 58:404–415. CrossRef

Janssens A, Gees M, Toth BI, Ghosh D, Mulier M, Vennekens R, Vriens J, Talavera K, Voets T (2016) Definition of two agonist types at the mammalian cold-activated channel TRPM8. Elife 5:e17240. CrossRef Medline

Jones L, Downie LE, Korb D, Benitez-Del-Castillo JM, Dana R, Deng SX, Dong PN, Geerling G, Hida RY, Liu Y, Seo KY, Tauber J, Wakamatsu TH, Xu J, Wolffsohn JS, Craig JP (2017) TFOS DEWS II management and therapy report. Ocul Surf 15:575–628. CrossRef Medline

Julius D (2005) From peppers to peppermints: natural products as probes of the pain pathway. Harvey Lect 101:89–115. Medline

Klein AH, Sawyer CM, Carstens MI, Tsagareli MG, Tsiklauri N, Carstens E (2010) Topical application of L-menthol induces heat analgesia, mechanical allodynia, and a biphasic effect on cold sensitivity in rats. Behav Brain Res 212:179–186. CrossRef Medline

Knowlton WM, Daniels RL, Palkar R, McCoy DD, McKemy DD (2011) Pharmacological blockade of TRPM8 ion channels alters cold and cold pain responses in mice. PLoS One 6:e25894. CrossRef Medline

Knowlton WM, Palkar R, Lippoldt EK, McCoy DD, Baluch F, Chen J, McKemy DD (2013) A sensory-labeled line for cold: TRPM8-expressing sensory neurons define the cellular basis for cold, cold pain, and cooling-mediated analgesia. J Neurosci 33:2837–2848. CrossRef Medline

LeGay CM, Gorobets E, Iftinca M, Ramachandran R, Altier C, Derksen DJ (2016) Natural-product-derived transient receptor potential melastatin 8 (TRPM8) channel modulators. Org Lett 18:2746–2749. CrossRef Medline

Liu B, Qin F (2005) Functional control of cold- and menthol-sensitive TRPM8 ion channels by phosphatidylinositol 4,5-bisphosphate. J Neurosci 25:1674–1681. CrossRef Medline

Liu B, Fan L, Balakrishna S, Sui A, Morris JB, Jordt SE (2013) TRPM8 is the principal mediator of menthol-induced analgesia of acute and inflammatory pain. Pain 154:2169–2177. CrossRef Medline

Macpherson LJ, Hwang SW, Miyamoto T, Dubin AE, Patapoutian A, Story GM (2006) More than cool: promiscuous relationships of menthol and other sensory compounds. Mol Cell Neurosci 32:335–343. CrossRef Medline

Mälkiä A, Madrid R, Meseguer V, de la Peña E, Valero M, Belmonte C, Viana F (2007) Bidirectional shifts of TRPM8 channel gating by temperature and chemical agents modulate the cold sensitivity of mammalian thermoreceptors. J Physiol 581:155–174. CrossRef Medline

Mälkiä A, Pertusa M, Fernández-Ballester G, Ferrer-Montiel A, Viana F (2009) Differential role of the menthol-binding residue Y745 in the antagonism of thermally gated TRPM8 channels. Mol Pain 5:62. CrossRef Medline

McKemy DD, Neuhausser WM, Julius D (2002) Identification of a cold receptor reveals a general role for TRP channels in thermosensation. Nature 416:52–58. CrossRef Medline

Menéndez L, Lastra A, Hidalgo A, Baamonde A (2002) Unilateral hot plate test: a simple and sensitive method for detecting central and peripheral hyperalgesia in mice. J Neurosci Methods 113:91–97. CrossRef Medline

Meng ID, Kurose M (2013) The role of corneal afferent neurons in regulating tears under normal and dry eye conditions. Exp Eye Res 117:79–87. CrossRef Medline

Meotti FC, Lemos de Andrade E, Calixto JB (2014) TRP modulation by natural compounds. Handb Exp Pharmacol 223:1177–1238. CrossRef Medline

Moran MM, Szallasi A (2018) Targeting nociceptive transient receptor potential channels to treat chronic pain: current state of the field. Br J Pharmacol 175:2185–2203. CrossRef Medline

Morenilla-Palao C, Luis E, Fernández-Peña C, Quintero E, Weaver JL, Bayliss DA, Viana F (2014) Ion channel profile of TRPM8 cold receptors reveals a role of TASK-3 potassium channels in thermosensation. Cell Rep 8:1571–1582. CrossRef Medline

Newman DJ, Cragg GM (2016) Natural products as sources of new drugs from 1981 to 2014. J Nat Prod 79:629–661. CrossRef Medline

Nilius B, Appendino G (2011) Tasty and healthy TR(i)Ps: the human quest for culinary pungency. EMBO Rep 12:1094–1101. CrossRef Medline

Orio P, Parra A, Madrid R, González O, Belmonte C, Viana F (2012) Role of ih in the firing pattern of mammalian cold thermoreceptor endings. J Neurophysiol 108:3009–3023. CrossRef Medline

Palkar R, Ongun S, Catich E, Li N, Borad N, Sarkisian A, McKemy DD (2018) Cooling relief of acute and chronic itch requires TRPM8 channels and neurons. J Invest Dermatol 138:1391–1399. CrossRef Medline

Parra A, Madrid R, Echevarria D, del Olmo S, Morenilla-Palao C, Acosta MC, Gallar J, Dhaka A, Viana F, Belmonte C (2010) Ocular surface wetness is regulated by TRPM8-dependent cold thermoreceptors of the cornea. Nat Med 16:1396–1399. CrossRef Medline

Peier AM, Moqrich A, Hergarden AC, Reeve AJ, Andersson DA, Story GM, Earley TJ, Dragoni I, McIntyre P, Bevan S, Patapoutian A (2002) A TRP channel that senses cold stimuli and menthol. Cell 108:705–715. CrossRef Medline

Pereira U, Boulais N, Lebonvallet N, Pennec JP, Dorange G, Misery L (2010) Mechanisms of the sensory effects of tacrolimus on the skin. Br J Dermatol 163:70–77. CrossRef Medline

Pérez de Vega MJ, Gómez-Monterrey I, Ferrer-Montiel A, González-MuñizR (2016) Transient receptor potential melastatin 8 channel (TRPM8) modulation: cool entryway for treating pain and cancer. J Med Chem 59:10006–10029. CrossRef Medline

Pogorzala LA, Mishra SK, Hoon MA (2013) The cellular code for mammalian thermosensation. J Neurosci 33:5533–5541. CrossRef Medline

Proudfoot CJ, Garry EM, Cottrell DF, Rosie R, Anderson H, Robertson DC, Fleetwood-Walker SM, Mitchell R (2006) Analgesia mediated by the TRPM8 cold receptor in chronic neuropathic pain. Curr Biol 16:1591–1605. CrossRef Medline

Quallo T, Vastani N, Horridge E, Gentry C, Parra A, Moss S, Viana F, Belmonte C, Andersson DA, Bevan S (2015) TRPM8 is a neuronal osmosensor that regulates eye blinking in mice. Nat Commun 6:7150. CrossRef Medline

Ramachandran R, Hyun E, Zhao L, Lapointe TK, Chapman K, Hirota CL, Ghosh S, McKemy DD, Vergnolle N, Beck PL, Altier C, Hollenberg MD (2013) TRPM8 activation attenuates inflammatory responses in mouse models of colitis. Proc Natl Acad Sci U S A 110:7476–7481. CrossRef Medline

Reid G, Amuzescu B, Zech E, Flonta ML (2001) A system for applying rapid warming or cooling stimuli to cells during patch clamp recording or ion imaging. J Neurosci Methods 111:1–8. CrossRef Medline

Reimúndez A, Fernández-Peña C, García G, Fernández R, Ordás P, Gallego R, Pardo-Vazquez JL, Arce V, Viana F, Señarís R (2018) Deletion of the cold thermoreceptor TRPM8 increases heat loss and food intake leading to reduced body temperature and obesity in mice. J Neurosci 38:3643–3656. CrossRef Medline

Robbins A, Kurose M, Winterson BJ, Meng ID (2012) Menthol activation of corneal cool cells induces TRPM8-mediated lacrimation but not nociceptive responses in rodents. Invest Ophthalmol Vis Sci 53:7034–7042. CrossRef Medline

Rohács T, Lopes CM, Michailidis I, Logothetis DE (2005) PI(4,5)P2 regulates the activation and desensitization of TRPM8 channels through the TRP domain. Nat Neurosci 8:626–634. CrossRef Medline

Rossi HL, Vierck CJ Jr, Caudle RM, Neubert JK (2006) Characterization of cold sensitivity and thermal preference using an operant orofacial assay. Mol Pain 2:37. CrossRef Medline

Roza C, Belmonte C, Viana F (2006) Cold sensitivity in axotomized fibers of experimental neuromas in mice. Pain 120:24–35. CrossRef Medline

Rusnak F, Mertz P (2000) Calcineurin: form and function. Physiol Rev 80:1483–1521. CrossRef Medline

Senba E, Katanosaka K, Yajima H, Mizumura K (2004) The immunosuppressant FK506 activates capsaicin- and bradykinin-sensitive DRG neurons and cutaneous C-fibers. Neurosci Res 50:257–262. CrossRef Medline

Ständer S, Augustin M, Roggenkamp D, Blome C, Heitkemper T, Worthmann AC, Neufang G (2017) Novel TRPM8 agonist cooling compound against chronic itch: results from a randomized, double-blind, controlled, pilot study in dry skin. J Eur Acad Dermatol Venereol 31:1064–1068. CrossRef Medline

Stull C, Lavery MJ, Yosipovitch G (2016) Advances in therapeutic strategies for the treatment of pruritus. Expert Opin Pharmacother 17:671–687. CrossRef Medline

Swandulla D, Carbone E, Schäfer K, Lux HD (1987) Effect of menthol on two types of Ca currents in cultured sensory neurons of vertebrates. Pflugers Arch 409:52–59. CrossRef Medline

Takashima Y, Daniels RL, Knowlton W, Teng J, Liman ER, McKemy DD (2007) Diversity in the neural circuitry of cold sensing revealed by genetic axonal labeling of transient receptor potential melastatin 8 neurons. J Neurosci 27:14147–14157. CrossRef Medline

Toro CA, Eger S, Veliz L, Sotelo-Hitschfeld P, Cabezas D, Castro MA, Zimmermann K, Brauchi S (2015) Agonist-dependent modulation of cell surface expression of the cold receptor TRPM8. J Neurosci 35:571–582. CrossRef Medline

Voets T, Droogmans G, Wissenbach U, Janssens A, Flockerzi V, Nilius B (2004) The principle of temperature-dependent gating in cold- and heat-sensitive TRP channels. Nature 430:748–754. CrossRef Medline

Wan XC, Dimov V (2014) Pharmacokinetic evaluation of topical calcineurin inhibitors for treatment of allergic conjunctivitis. Expert Opin Drug Metab Toxicol 10:543–549. CrossRef Medline

Winter Z, Gruschwitz P, Eger S, Touska F, Zimmermann K (2017) Cold temperature encoding by cutaneous TRPA1 and TRPM8-carrying fibers in the mouse. Front Mol Neurosci 10:209. CrossRef Medline

Wong LS, Otsuka A, Yamamoto Y, Nonomura Y, Nakashima C, Kitayama N, Usui K, Honda T, Kabashima K (2018) TRPA1 channel participates in tacrolimus-induced pruritus in a chronic contact hypersensitivity murine model. J Dermatol Sci 89:207–209. CrossRef Medline

Xing H, Ling J, Chen M, Gu JG (2006) Chemical and cold sensitivity of two distinct populations of TRPM8-expressing somatosensory neurons. J Neurophysiol 95:1221–1230. CrossRef Medline

Yin Y, Wu M, Zubcevic L, Borschel WF, Lander GC, Lee SY (2018) Structure of the cold- and menthol-sensing ion channel TRPM8. Science 359:237–241. CrossRef Medline

Zakharian E, Cao C, Rohács T (2010) Gating of transient receptor potential melastatin 8 (TRPM8) channels activated by cold and chemical agonists in planar lipid bilayers. J Neurosci 30:12526–12534. CrossRef Medline

Zimmermann K, Hein A, Hager U, Kaczmarek JS, Turnquist BP, Clapham DE, Reeh PW (2009) Phenotyping sensory nerve endings in vitro in the mouse. Nat Protoc 4:174–196. CrossRef Medline